

Award Number: DAMD17-03-1-0373

TITLE: Near-Infrared Fluorescence Imaging Guided Therapy: Molecular Beacon-Based Photosensitizers Triggered by Breast Cancer-Specific mRNA

PRINCIPAL INVESTIGATOR: Gang Zheng, Ph.D.  
Juan Chen  
Klara Stefflova

CONTRACTING ORGANIZATION: University of Pennsylvania  
Philadelphia, PA 19104

REPORT DATE: May 2007

TYPE OF REPORT: Final

PREPARED FOR: U.S. Army Medical Research and Materiel Command  
Fort Detrick, Maryland 21702-5012

DISTRIBUTION STATEMENT: Approved for Public Release;  
Distribution Unlimited

The views, opinions and/or findings contained in this report are those of the author(s) and should not be construed as an official Department of the Army position, policy or decision unless so designated by other documentation.

# REPORT DOCUMENTATION PAGE

*Form Approved*  
*OMB No. 0704-0188*

Public reporting burden for this collection of information is estimated to average 1 hour per response, including the time for reviewing instructions, searching existing data sources, gathering and maintaining the data needed, and completing and reviewing this collection of information. Send comments regarding this burden estimate or any other aspect of this collection of information, including suggestions for reducing this burden to Department of Defense, Washington Headquarters Services, Directorate for Information Operations and Reports (0704-0188), 1215 Jefferson Davis Highway, Suite 1204, Arlington, VA 22202-4302. Respondents should be aware that notwithstanding any other provision of law, no person shall be subject to any penalty for failing to comply with a collection of information if it does not display a currently valid OMB control number. **PLEASE DO NOT RETURN YOUR FORM TO THE ABOVE ADDRESS.**

<b>1. REPORT DATE</b> 01-05-2007			<b>2. REPORT TYPE</b> Final		<b>3. DATES COVERED</b> 1 May 2003 – 30 Apr 2007	
<b>4. TITLE AND SUBTITLE</b>  Near-Infrared Fluorescence Imaging Guided Therapy: Molecular Beacon-Based Photosensitizers Triggered by Breast Cancer-Specific mRNA					<b>5a. CONTRACT NUMBER</b>	
					<b>5b. GRANT NUMBER</b> DAMD17-03-1-0373	
					<b>5c. PROGRAM ELEMENT NUMBER</b>	
<b>6. AUTHOR(S)</b>  Gang Zheng, Ph.D. Juan Chen Klara Stefflova Email: <a href="mailto:gang.zheng@uhnres.utoronto.ca">gang.zheng@uhnres.utoronto.ca</a>					<b>5d. PROJECT NUMBER</b>	
					<b>5e. TASK NUMBER</b>	
					<b>5f. WORK UNIT NUMBER</b>	
<b>7. PERFORMING ORGANIZATION NAME(S) AND ADDRESS(ES)</b>  University of Pennsylvania Philadelphia, PA 19104					<b>8. PERFORMING ORGANIZATION REPORT NUMBER</b>	
<b>9. SPONSORING / MONITORING AGENCY NAME(S) AND ADDRESS(ES)</b> U.S. Army Medical Research and Materiel Command Fort Detrick, Maryland 21702-5012					<b>10. SPONSOR/MONITOR'S ACRONYM(S)</b>	
					<b>11. SPONSOR/MONITOR'S REPORT NUMBER(S)</b>	
<b>12. DISTRIBUTION / AVAILABILITY STATEMENT</b> Approved for Public Release; Distribution Unlimited						
<b>13. SUPPLEMENTARY NOTES</b> Original contains colored plates: ALL DTIC reproductions will be in black and white.						
<b>14. ABSTRACT</b> We have developed breast cancer-targeted photodynamic molecular beacons (PMB) using two different activation mechanisms: mRNA-triggered (openable) PMB and protease-triggered (cleavable) PMB. We have validated the core principle of PMB concept: the ability of photosensitizer (PS) to produce singlet oxygen ( $^1O_2$ ) can be precisely controlled in response to specific breast cancer-associated biomarkers. For the first time, using mouse models and on separate cells, we have shown that it is possible to limit the collateral damage to surrounding normal cells using this approach, thus achieved the unprecedented tumor selectivity for breast cancer PDT. In addition, we also demonstrated the versatility of the PMB design by developing PDT beacons with "tailored" functions such as the PDT agents with a built-in apoptosis sensor for in situ and real time monitoring of the therapeutic outcome.						
<b>15. SUBJECT TERMS</b> Photodynamic therapy, breast cancer, molecular beacon, singlet oxygen, mRNA, protease						
<b>16. SECURITY CLASSIFICATION OF:</b>				<b>17. LIMITATION OF ABSTRACT</b>	<b>18. NUMBER OF PAGES</b>	<b>19a. NAME OF RESPONSIBLE PERSON</b> USAMRMC
<b>a. REPORT</b> U	<b>b. ABSTRACT</b> U	<b>c. THIS PAGE</b> U	<b>19b. TELEPHONE NUMBER</b> (include area code)			
				UU	101	

## Table of content

Introduction .....	5
Body .....	6
<i>Task 1: To synthesize a model BChl-MB containing an AS-ON loop sequence complementary to the sequence of a well-known mRNA, a BChl based fluorophore, a CAR quencher and appropriate linkers, and to optimize the structure of BChl-MB in order to maximize the fluorescence and singlet oxygen quenching efficiency in the stem-loop form in solution.</i> .....	6
1. Synthesis of stable Bacteriochlorophyll Analogs (BChl) .....	6
2. Synthesis of Carotenoid (CAR) .....	6
3. Design and synthesis of c-raf-1 mRNA triggered PMB.....	7
4. Validation of the activation of P30C specific to c-raf-1 mRNA.....	9
5. Caspase-3-triggered PMB, characterization and solution validation.....	11
<i>Task 2: To deliver model BChl-PMBs to cells expressing mRNA and to demonstrate that these PMBs can hybridize with target mRNAs in cells</i> .....	13
1. Validation of the in vitro uptake and activation of P30C.....	13-
<i>Task 3: To identify an AS-ON loop sequence for BChl-MBs complementary to an accessible sequence in EGFRvIII mRNA.</i> .....	15
<i>Task 4: To synthesize BChl-MBs containing the EGFRvIII AS loop and demonstrate that such MBs can hybridize with EGFRvIII mRNA in solution and in cancer cells expressing EGFRvIII.</i> .....	15
<i>Task 5: To determine the in vitro photodynamic efficacy and the specificity of BChl-MBs.</i> .....	15
<i>Revised Task 4: To synthesize a PMB containing MMP7specific peptide linker and demonstrate that such PMB can be specifically activated by MMP7 in solution and in cancer cells expressing MMP7</i> .....	16-
<i>Revised Task 5: To determine the in vitro and in vivo photodynamic efficacy and specificity of MMP7-triggered PMB</i> .....	16-
1. Design and synthesis of MMP-7-triggered PMB.....	16
2. Validation of MMP7-triggered PP <sub>MMP7</sub> B activation and its corresponding <sup>1</sup> O <sub>2</sub> activation in solution.....	16-
3. Validation of MMP7-triggered PP <sub>MMP7</sub> B activation and its corresponding PDT activation in cancer cells.....	17
4. Preliminary in vivo PDT response of PP <sub>MMP7</sub> B.....	19
<i>Additional accomplishment 1: Using the <sup>1</sup>O<sub>2</sub> scavenging property of CAR in PMB to minimize photodamage to non-targeted cells</i> .....	20-

*Additional accomplishment 2: PDT agent with a built-in apoptosis sensor for evaluating its own therapeutic outcome in situ*.....21

Key research accomplishments.....22

Reportable outcomes.....23

Conclusions .....26

Reference.....26

Appendixes.....28

## Introduction

The overall objective of this project is to develop a photodynamic molecular beacon (PMB) that is targeted to and activated by a cancer signature (e.g., EGFRvIII mRNA that is expressed in breast cancer but not in nonmalignant breast tissue) and to investigate the potentially utility of this agent for near-infrared fluorescence imaging (NIRF)-guided photodynamic therapy (PDT). PDT is a cancer treatment modality involving the combination of light, a photosensitizer (PS) and molecular oxygen. Each factor is ineffective by itself, but when the PS is irradiated with light of an appropriate wavelength in the presence of oxygen, cytotoxic reactive oxygen species, mainly singlet oxygen ( $^1\text{O}_2$ ), are produced. The current limitation of PDT modality is the lack of sufficient tumor-to-tissue contrast due to the relatively non-specific nature of delivering the PS to the tumor. We have developed a new PDT concept, 'photodynamic molecular beacons (PMB)', featuring precise control of the ability of PS to produce  $^1\text{O}_2$  by responding to specific cancer-associated biomarkers. As depicted in Figure 1, a PS and a quencher (Q) are conjugated in PMB via a linker molecule and are initially kept in close proximity. When the PMB meet the target biomarker, the linker could be either cleaved or opened, and hence the quencher will be removed from the close proximity of the PS, making the PS photodynamic active. Upon the light irradiation,  $^1\text{O}_2$  will be generated to destroy the targeted cells. Thus, the PDT selectivity will no longer solely depend on how selectively the PS can be delivered to cancer cells. Rather, it will depend on how specific the choice of biomarker is to targeted cancer cells and how selective the PMB linker is to this biomarker. The application of this PMB for targeting the breast cancer-associated biomarkers will allow for the selective photodynamic treatment of breast tumors. In these four years research period, we have started from an original idea to fully validate the concept and ultimately to implement this concept for breast cancer applications. Briefly, we have synthesized a series of stable PS/quencher pairs of PMB, developed two major types of PMBs for breast cancer treatment by targeting *c-raf* kinase and matrix metalloproteinase 7 (MMP7) respectively, and confirmed that photodynamic activity of these PMBs are silenced in native state and can be specifically activated by their targets *in solution*, *in vitro* and *in vivo*. Thus, for the first time, we have shown true tumor selectivity by demonstrating that it is possible to only destroy the targeted cancer cells and to protect surrounding normal cells from PDT-induced collateral damage.

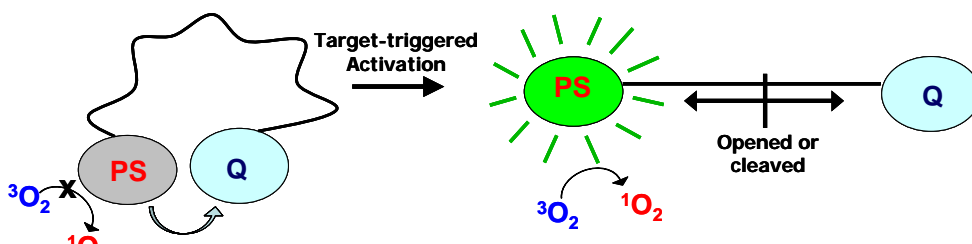


Figure 1. The activation mechanism of PMB

## Body

*Task 1:* To synthesize a model BChl-MB containing an AS-ON loop sequence complementary to the sequence of a well-known mRNA, a BChl based fluorophore, a CAR quencher and appropriate linkers, and to optimize the structure of BChl-MB in order to maximize the fluorescence and singlet oxygen quenching efficiency in the stem-loop form in solution.

In Year 1 (May 1, 2003 – April 30, 2004), we have accomplished followings: 1) designed and synthesized a few stable bacteriochlorophyll analogs as effective photosensitizers for PDT; 2) designed and synthesized a PMB for targeting c-raf-1-mRNA. This c-raf-1-mRNA triggered PMB contains an AS-ON loop with a sequence complementary to the sequence of c-raf-1 mRNA. We also designed and synthesized a model PMB featuring a caspase-3-specific cleavable peptide linker. Using this beacon, we were able to prove the first key hypothesis of this project that the PS's ability to produce  $^1\text{O}_2$  can be precisely controlled (turned on and off) in response to a biomarker.

### 1. Synthesis of stable Bacteriochlorophyll Analogs (BChl):

Bacteriochlorophyll (BChl) from *R. Sphaeroides* is an excellent near-infrared (NIR) dye for NIR imaging and photodynamic therapy (PDT) because of its favorable photophysical properties ( $^1\text{O}_2$  yield: 45%) and long activation and fluorescence emission wavelengths ( $\lambda_{\text{abs}}$  825nm;  $\lambda_{\text{em}}$  840nm)[1]. Since the native BChl is very unstable and undergoes rapid oxidation to the chlorin state (660 nm), we have synthesized many stable BChl analogs, including both chemically-modified native BChl and synthetic BChl analogs. We have also synthesized two isothiocyanate-containing BChl analogs derived from bacteriopurpurinimide (BChlPP) and bacteriochlorin  $e_6$  (BChlE6), as well as a succinimide ester-containing pyropheophorbide acid (Pyro), which was prepared from chlorophyll (Chl, the plant counterpart of BChl) extracted from *Spirulina* algae[2] (Figure 2). Introducing such amine-reactive universal groups (isothiocyanate or succinimide ester) into the BChl/Chl macrocycle allows conjugation of these NIR dyes to an oligonucleotide or a peptide by coupling to the terminal amine group.

### 2. Synthesis of Carotenoid (CAR):

Carotenoids (CARs) are well known as pro-vitamin A and antioxidant in animals and as pigments and photoprotective agents in the photosynthetic system in plants [3]. These important biofunctions are due to its ability to: A) quench chlorophyll's (or other porphyrin-based molecule's) excited triplet state, inhibiting production of harmful  $^1\text{O}_2$ , B) scavenge the already generated  $^1\text{O}_2$ , protecting the photosynthetic apparatus[4, 5], C) either absorb light around 500 nm and transfer this excitation energy to the chlorophyll as part of light harvesting or vice-versa quench the chlorophyll fluorescence as antioxidants[6], and D) quench radical species that could potentially react with various biomolecules [3]. To mimic the function of CAR in natural photosynthesis system some carotenoporphyrins were synthesized, where the carotenoid analogue was directly conjugated to either meso-tetraphenyl porphyrins[7, 8], pheophorbide[9] or hematoporphyrin[10]. These carotenoporphyrins were found to have a very good photoprotective property. Therefore, CAR is our first choice of the quencher molecules for PMB design. We have synthesized two analogues: carotenoid acid (CAR acid) and carotenoid succinimide ester (CAR-NHS) that are used in conjugation to oligonucleotide or peptide by coupling with the terminal primary amine group (Figure 3).

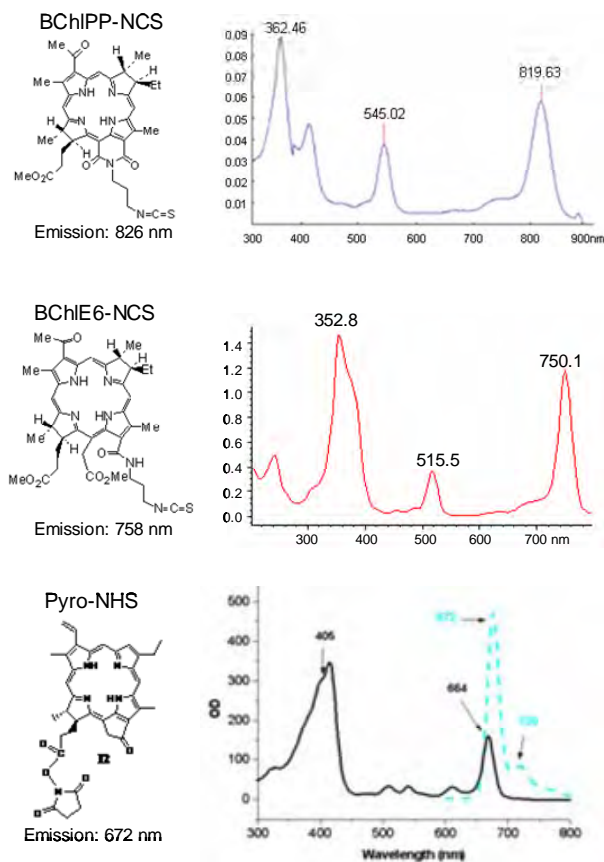


Figure 2. The structure of bacteriopurpurinimide isothiocyanate (BChlPP-NCS), bacteriochlorin  $e_6$  isothiocyanate (BChlE6-NCS) and pyropheophorbide succinimide ester (Pyro-NHS) (left) and their corresponding absorption spectra (right).

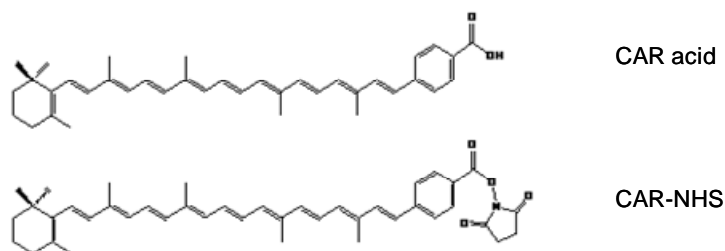


Figure 3. The structure of carotenoid acid (CAR acid) and carotenoid succinimide ester (CAR-NHS)

### 3. Design and synthesis of c-raf-1 mRNA triggered PMB

Raf-1 is a serine/threonine kinase that involved in the activation of MAP kinase pathway and directly contributes to malignant transformation, thus is a potential therapeutic target. More importantly, its antisense drug ISIS 5132, containing a synthetic, 20-base oligodeoxynucleotide that hybridizes to c-raf-1 kinase mRNA, is well known to be able to specifically suppress Raf-1 expression both *in vitro* and *in vivo*. By extending the application of this antisense sequence, we have designed and synthesized a c-raf-1 mRNA triggered PMB. This so called “P30C” beacon consists of a Pyro as the fluorescent PS, a CAR as the quencher and a 30-base single-stranded oligonucleotide,

GCGAGUCCCGCCUGUGACAUGCAUUCUCGC as a linker, in which the middle of 20-base loop sequence (without underline) is consistent to the ISIS 5132 antisense drug and the two 5-base arm sequences on each end of loop (with underline) are complementary to each other to form a loop-stem structure (Figure 4). The Pyro and CAR are attached to the end of each arm sequence respectively. We hypothesized that the stem-loop structure of linker can induce proximity of Pyro (PS) and CAR (Q), thus making the P30C photodynamic silent in native state. In the presence of the c-raf-1 mRNA, the loop antisense sequence will hybridize with the mRNA, disrupting the hydrogen bonds of the stem and making the linker opened. The CAR (Q) hence is removed from the immediate vicinity of the Pyro (PS). Upon irradiating with light, the Pyro emits fluorescence and generates cytotoxic singlet oxygen.

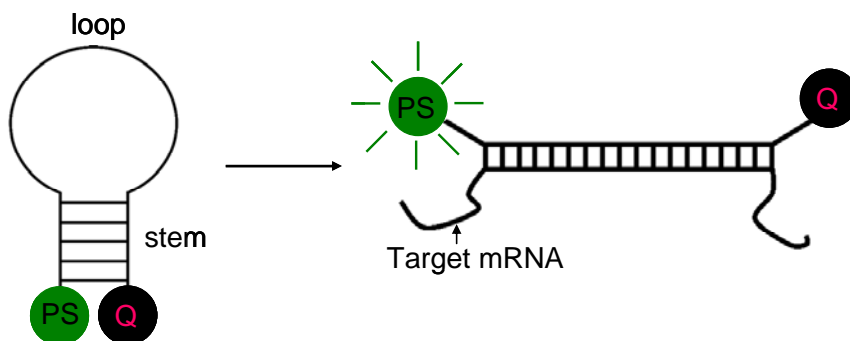


Figure 4. The concept of mRNA-triggered

Many technical obstacles were encountered during P30C synthesis. For example, the standard aqueous solution-based oligonucleotide conjugation protocol, even with the help of organic solvents (ACN), can not be used for P30C synthesis because of the high hydrophobicity of Pyro and CAR. Three different conjugation approaches were designed and used for P30C synthesis in Year 1 and we finally synthesized P30C with sufficient purity using the approach as depicted in Figure 5. Briefly, a single-stranded 30mer 2'-OMethyl RNA sequence: GCGAGUCCCGCCUGUGACAUGCAUUCUCGC was synthesized first on the 3'-phthalimidyl-modified CPG purchased from TriLink BioTechnologies (San Diego, CA) using an automatic DNA synthesizer. A 5'-Amino-modifier C6, 6-(4-monomethoxytritylamino)hexyl-(2-cyanoethyl)-(N,N-diisopropyl)-phosphoramidite, was then coupled to the 5'-end of the 30mer RNA sequence to give 5'-MMT-30mer-(phthalimidyl-CPG). During the next step, the 5'-MMT protecting group was removed by 2.5% trichloroacetic acid (TCA) in dichloromethane (DCM) to expose the free amine group, which was then conjugated with the CAR acid. This 5'-CAR conjugated CPG was treated with the concentrated ammonium hydroxide at 55°C for 17 h to remove the CPG support and to cleave the protecting groups on RNA sequence including the phthalimidyl group on 3' end of sequence to expose the 3'-NH<sub>2</sub> group. Pyro-NHS was then conjugated with 3'-NH<sub>2</sub> of the RNA to acquire 5'-CAR-30mer-Pyro-3' (P30C). The structure of the P30C beacon was confirmed by its' corresponding UV-vis spectrum, showing characteristic absorptions of Pyro(411, 664nm), CAR (472, 501nm) and oligonucleotide (260nm), as well as the MALDI-TOF mass spectrum (calculated: 11329.2, found: 11326.3).

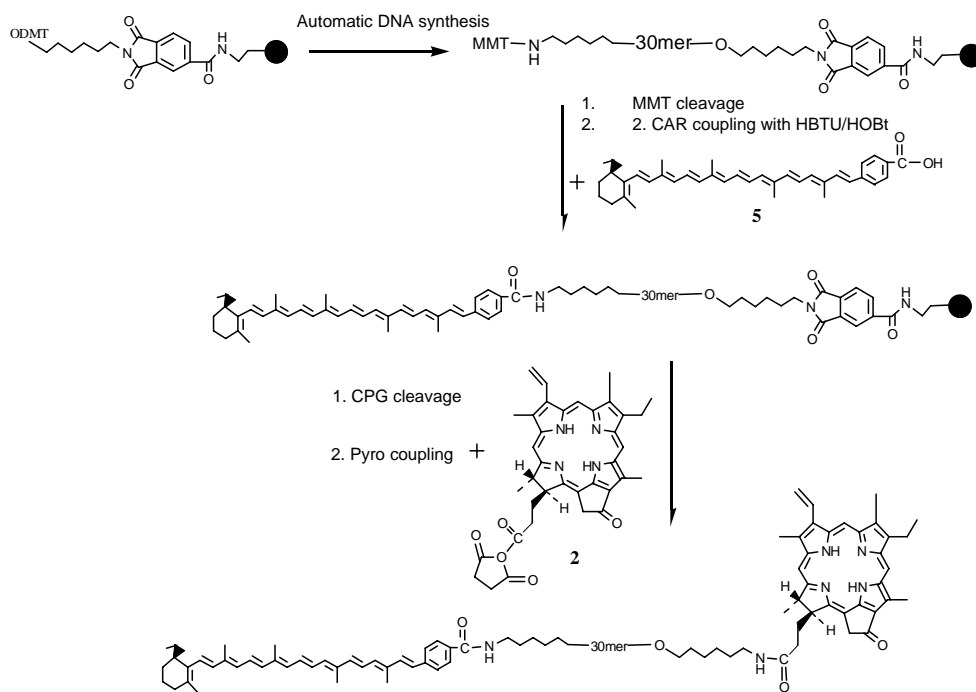


Figure 5. The synthesis protocol of P30C

#### 4. Validation of the activation of P30C specific to *c-raf-1* mRNA

After the P30C has been synthesized and characterized, we have accomplished followings in Year 2 (May 1, 2004 – April 30, 2005): 1) validated the *c-raf-1* mRNA triggered PMB concept in solution; 2) achieved efficient delivery of this P30C into the MDA-MB-231 human breast cancer cells; 3) demonstrated the selective PDT efficacy of P30C in MDA-MB-231 cells.

To test these hypotheses, P30C beacon-target hybridization studies were carried out in solution. Shown in Figure 6 are fluorescence restoration spectra of P30C hybridization with complementary target sequence and mismatched sequence (only one base mismatched in the middle of target sequence). Upon hybridization, the complementary RNA sequence gave a 13-fold fluorescence increase in P30C, while 1-mismatched sequence just gave 4-fold fluorescence increase. On the other hand, the high specificity of P30C to target was further confirmed by using a random control beacon (r-P30C), which didn't show any fluorescence increase when hybridized with a complementary target. These data confirmed that the 30mer sequence of P30C is a suitable linker for PMB as the Pyro fluorescence was effectively quenched by CAR in native P30C and is specifically activated by complementary target. Moreover, these results indicate the very high level specificity of PMB as it can distinguish mRNA target sequence at the single base level.

To test the  $^1\text{O}_2$  quenching and activation of P30C,  $^1\text{O}_2$  generation was measured directly at its 1270 nm luminescence in solution of P30C alone and P30C with complementary target sequence. In this study, Pyro-30mer (P30) alone, without the CAR

moiety, was used as a positive control. As shown in Figure 7, P30C has 15-fold less  $^1\text{O}_2$  production than P30, confirming the CAR-mediated  $^1\text{O}_2$  quenching in P30C. Moreover, addition of the target to P30C (molar ratio: 2:1, incubation time 30min) resulted in a 9-fold increase of  $^1\text{O}_2$  signal, while the target has no effect on the  $^1\text{O}_2$  production of P30. These data suggest that adding the complementary target RNA to P30C induces the separation of the CAR from the immediate vicinity of the Pyro that allows photoactivation of the Pyro.

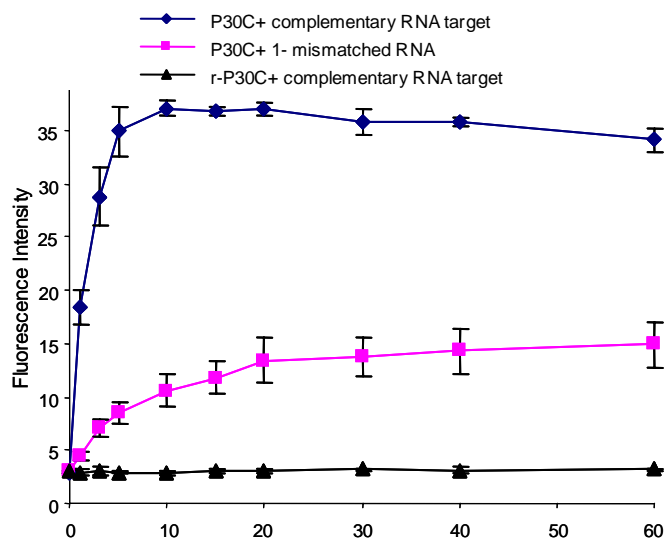


Figure 6. Time-driven fluorescence measurement was used to monitor P30C beacon-target hybridization. Data shown here was based on 4 different experiments and the results were expressed as mean  $\pm$  standard error.

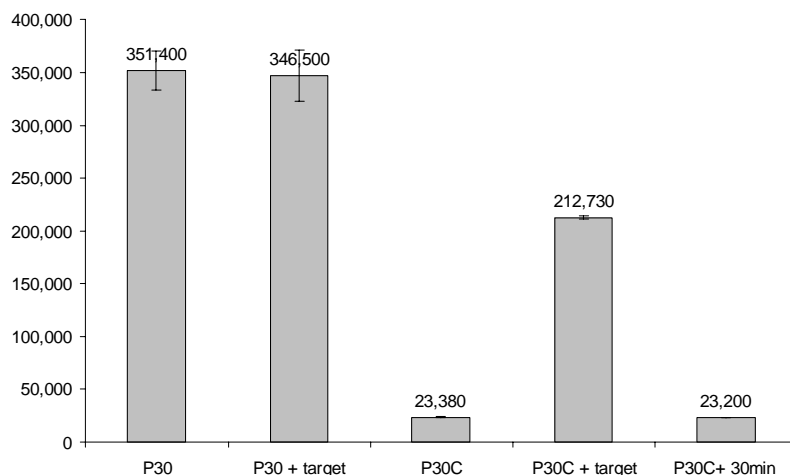


Figure 7. The total  $^1\text{O}_2$  counts of P30, P30 + complementary target RNA (P30+ target), P30C, P30C + complementary target RNA (P30C+ target), P30C incubated in buffer for 30min (P30C+30min). Data shown here was based on 3 different experiments and the results were expressed as mean  $\pm$  standard error.

5. Caspase-3-triggered PMB: synthesis, characterization and solution validation (see Appendix 1 for details).

While we were overcoming numerous technical challenges associated with the chemical synthesis of mRNA-triggered PMB, we decided to develop a model PMB based a caspase-3-specific peptide linker. Using this beacon, our plan was to prove the first key hypothesis of this project that the PS's ability to produce  $^1\text{O}_2$  can be turned on and off in response to a biomarker.

To build this model construct, a cleavable caspase-3 substrate GDEVDGSGK (recognition site underlined) was chosen as the peptide sequence, for which there is a well-established assay for the caspase-3-specific fluorogenic substrate. Pyro and CAR were used as the PS and Q moieties. To synthesize the Pyro-Peptide-CAR (PPC) beacon, a GDEVDGSGK peptide was synthesized (Figure 8A). Pyro was coupled to the N-terminal glycine of peptide on solid support. This conjugate was then cleaved from the solid support and deprotected. CAR conjugation was then carried out in solution, since it is acid-labile.

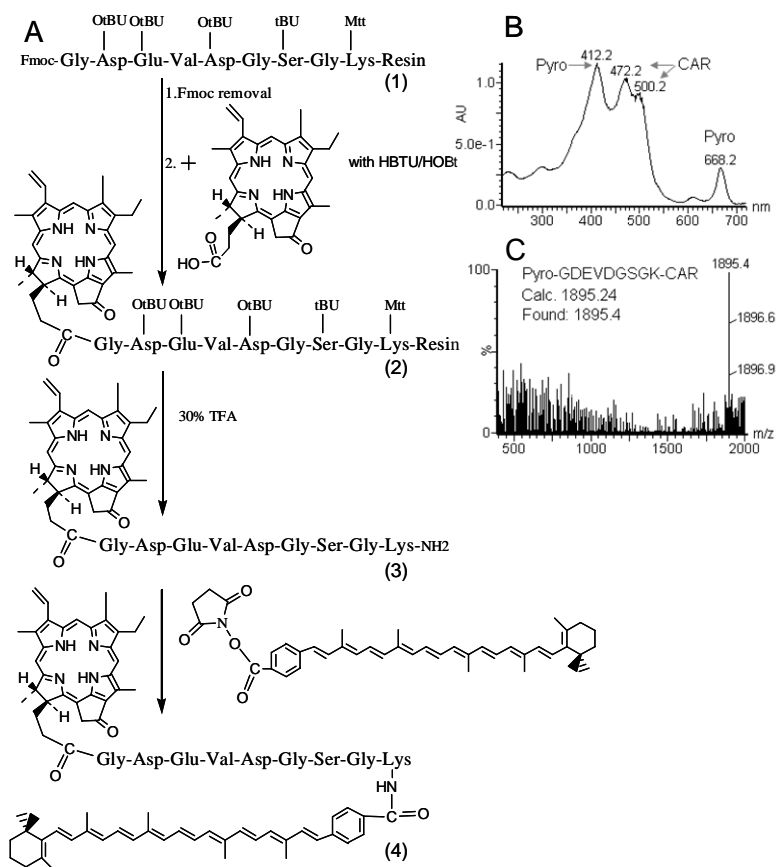


Figure8. Synthesis and characterization of Pyro-GDEVDGSGK-CAR (PPC): A) Synthesis of PPC, B) The UV-vis spectrum of PPC and C) The ESI-MS spectrum of PPC.

Purification of this product was achieved by HPLC. The structure of PPC was confirmed by MALDI-TOF (Figure 8C) (calculated: 1895.24, found 1896.03). The presence of all three structural components in PPC was further confirmed by UV-vis, which shows characteristic peaks of the Pyro (420, 663 nm) and CAR (472, 501 nm) moieties (Figure 8B).

The HPLC-purified PPC was then used to test the caspase-3 cleavage. It was incubated in buffer for 3 h either alone, with the addition of caspase-3 or with caspase-3 plus inhibitor (caspase-3: PPC: inhibitor =1:100:2400), then analyzed by HPLC coupled to UV-Vis spectroscopy and ESI-MS. As shown in Figure 9, caspase-3 cleaved 80% of PPC (HPLC retention time: RT=14.70min) into two fragments corresponding, respectively, to a Pyro moiety (RT=7.64min) and a CAR moiety (RT=11.95min) based on their absorption characteristics. Importantly, this specific cleavage was further confirmed by ESI-MS: the two fragments were identified as Pyro-GDEVD-COO<sup>-</sup> (Calc.1050.12, found 1050.7) and NH<sub>2</sub>-GSGK-CAR (Calc. 862.54, found 862.8). On the other hand, no detectable cleavage was observed in PPC only or in PPC+caspase-3+inhibitor. These data demonstrate that caspase-3 specifically cleaves PPC at the caspase-3-specific cleavage site between D and G[11].

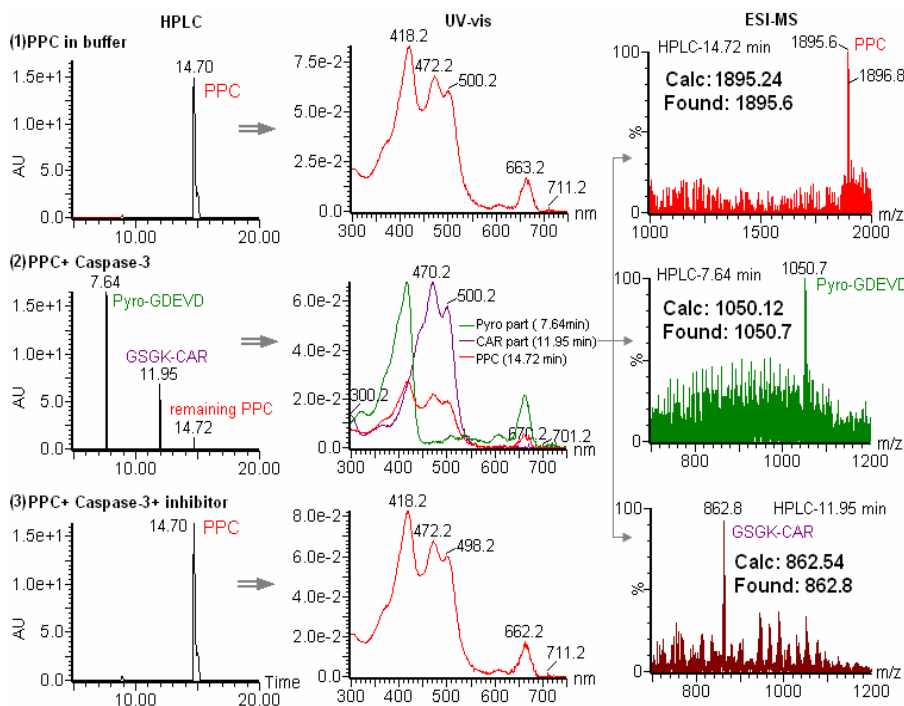


Figure 9. Validation of PPC specific cleavage by caspase-3. First column: HPLC chromatography of (1) PPC alone, (2) PPC+ caspase-3 and (3) PPC+ caspase-3 +inhibitor after 3 h incubation; Second column: the corresponding UV-vis spectra of each HPLC peaks in PPC alone (top), PPC+ caspase-3 (middle) and PPC+ caspase-3 +inhibitor (bottom); third column: ESI-MS spectra of the HPLC peaks in PPC +caspase-3 with retention times 14.72 min (top), 7.64 min (middle) and 11.95 min(bottom).

To test the caspase-3-mediated  $^1\text{O}_2$  control,  $^1\text{O}_2$  was measured directly in solutions of PPC alone, PPC incubated with caspase-3 and PPC incubated with caspase-3 plus a caspase-3 inhibitor. Pyro-peptide (PP) alone, without the CAR moiety, was used as a positive control. As shown in Figure 10, caspase-3 and its inhibitor have no effect on the  $^1\text{O}_2$  production of PP, and PPC itself has eight-fold less  $^1\text{O}_2$  production than PP. Thus, the  $^1\text{O}_2$  quenching in PPC is due to the presence of CAR. Moreover, addition of caspase-3 to the PPC (molar ratio: 1:60; incubation time: 1 h) resulted in a four-fold increase in  $^1\text{O}_2$  signal, an effect that was completely prevented by co-incubation with the caspase-3 inhibitor (8 x PPC concentration with the same incubation time). The two-fold difference in  $^1\text{O}_2$  luminescence as well as  $^1\text{O}_2$  lifetime between the PP and PPC+caspase-3 is probably due to the presence of free CAR quenchers in solution after cleavage. This effect will likely be less in vivo since there will be less free CARs available. The difference in  $^1\text{O}_2$  luminescence between PPC alone and PPC+caspase-3 is likely due to both photosensitizer triplet-state quenching and  $^1\text{O}_2$  scavenging by CAR. These data demonstrate that  $^1\text{O}_2$  production is effectively inhibited by the CAR quencher and that caspase-3-induced separation of the Q and the PS molecules allows photoactivation of the latter.

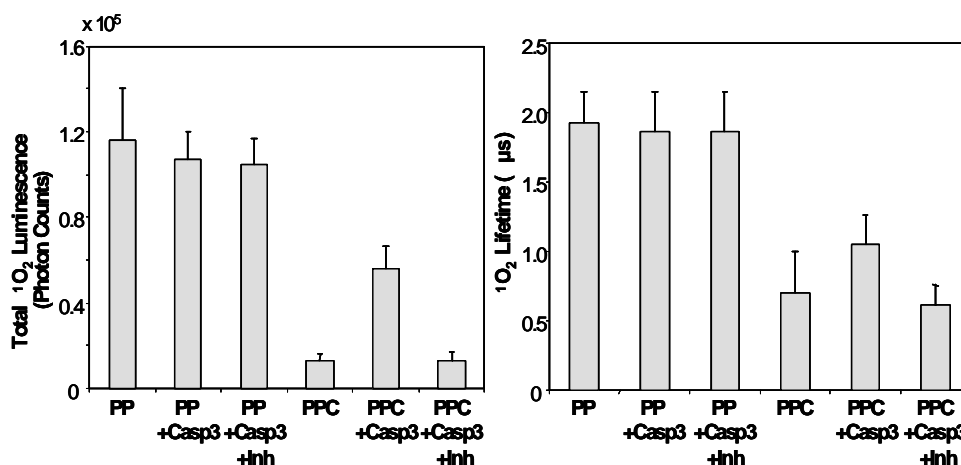


Figure 10. Total  $^1\text{O}_2$  luminescence counts and lifetime for PP, PP+caspase-3, PP+caspase-3+inhibitor, PPC, PPC+caspase-3, PPC+caspase-3+inhibitor.

*Task 2: To deliver model BChl-PMBs to cells expressing mRNA and to demonstrate that these PMBs can hybridize with target mRNAs in cells in vitro.*

### 1. Validation of the in vitro uptake and activation of P30C

The effective delivery of oligonucleotides inside cells is a well known technical challenge. Somewhat to our surprise, we found that P30C and P30 efficiently enter inside cells without the use of transfect agents. As the confocal images shown in Figure 11, MDA-MB-231 cells (overexpress *c-raf-1* mRNA) alone do not have any Pyro's fluorescence background (Ex. 633nm, Em. 650-750nm), whereas cells incubated with 100 $\mu\text{M}$  of P30C for 4 h clearly show Pyro's fluorescence and its fluorescence intensity is

similar to that of P30 (positive control). These images suggest that both P30 and P30C constructs were taken up into cells without transfect agents, and most importantly, P30C was activated in cells overexpressing *c-raf-1* mRNA.

This self-driven cell uptake of P30C beacon is attributed to the Pyro's ability to serve as a delivery vehicle for PMB, a property we and others have recently discovered. In order to clarify this issue, we synthesized a FRET-based beacon, F30B, containing a fluorescein molecule (FAM) conjugated with a black hole quencher 1 (BHQ1) through a similar oligonucleotide linker as P30C. As shown in Figure 12, the cells incubated with 10  $\mu\text{M}$  of F30B didn't show any FAM's fluorescence (Ex. 488nm, Em. 500-750nm), whereas the cells co-incubated with 10  $\mu\text{M}$  of F30B and 0.05g/L of Lipofectamine TM2000 (a well known transfect agent) showed significant fluorescence in cell plasma. This demonstrated that F30B can only uptake in cells with the aid of transfect agent and its activation is offered inside cells overexpressing *c-raf-1* mRNA. Moreover, these data underlines an important finding that Pyro can serves both as the PS and as the delivery vehicle for the PMB, thus alleviate the beacon delivery hurdle.



Figure 11. The confocal images of MDA-MB-231 cells: 1) alone, 2) incubated with 100 $\mu\text{M}$  of P30 for 4 h and 3) incubated with 100 $\mu\text{M}$  of P30C for 4 h. The numbers refer to each pair of images, with the fluorescence image (left) and the bright field image (right) shown.

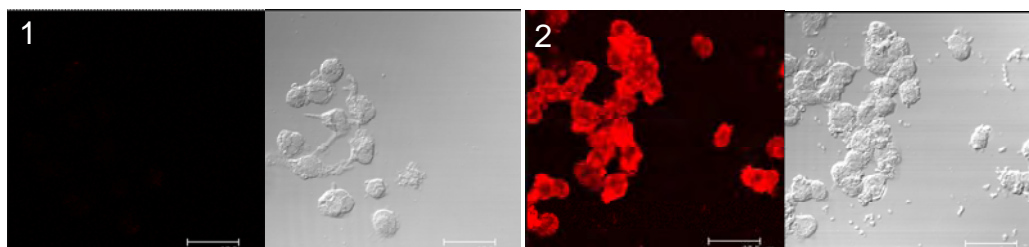


Figure 12. The confocal images of MDA-MB-231 cells : 1) incubated with 10  $\mu\text{M}$  of F30B for 4 h and 2) co-incubated with 10  $\mu\text{M}$  of F30B and 0.05g/L of Lipofectamine TM2000 for 4 h.

To verify P30C is an effective PDT agent in the presence of *c-raf-1* mRNA, cell viability (MTT assay) was measured in MDA-MB-231 (overexpressing *c-raf-1*) cells before and after the PDT treatment. As shown in Figure 13, 1) none of P30C, P30 (positive control) or r-P30C (negative control) had noticeable dark toxicity in experimental condition, the viability of cells incubated with 2 $\mu\text{M}$  of P30C, P30 or r-P30C without light being the same as that of control cells without drug and light; 2) upon 5 J/  $\text{cm}^2$  of PDT treatment, 2  $\mu\text{M}$  of P30C induced significant cell death (38% cells viability), which is similar to that the positive control P30 did (34% cells viability), while negative control r-P30C showed less cell death (78% cells viability). These data confirmed that P30C is an effective PDT agent in the cells overexpressing *c-raf-1* mRNA.

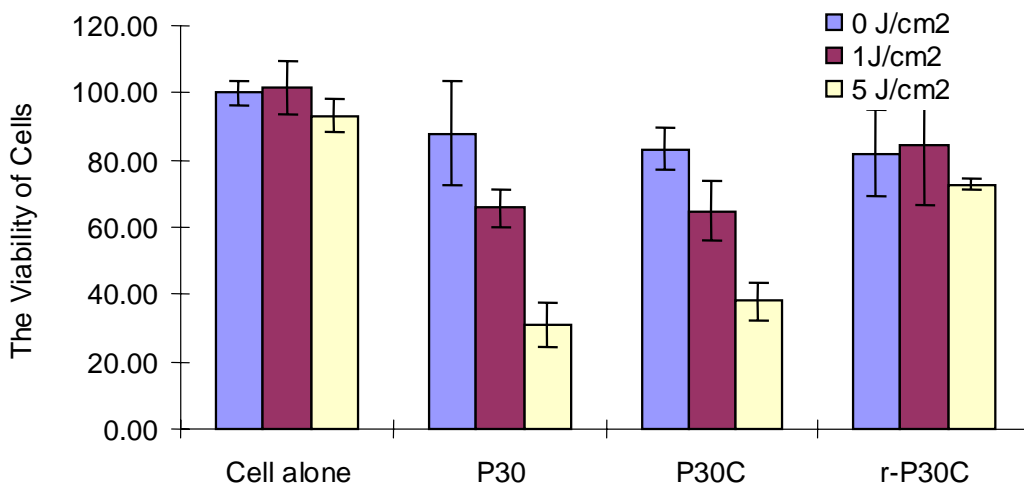


Figure 13. The viability of cells after PDT treatment with different light dose. MDA-MB-231 cells were incubated with 2 $\mu$ M of P30 (positive control), 2 $\mu$ M of P30C and 2 $\mu$ M of r-P30C (negative control).

*Task 3: To identify an AS-ON loop sequence for BChl-MBs complementary to an accessible sequence in EGFRvIII mRNA.*

*Task 4: To synthesize BChl-MBs containing the EGFRvIII AS loop and demonstrate that such MBs can hybridize with EGFRvIII mRNA in solution and in cancer cells expressing EGFRvIII*

*Task 5: To determine the in vitro photodynamic efficacy and the specificity of BChl-MBs*

After two years efforts, we have demonstrated the core principle of mRNA-triggered PMB that the control of the PS's ability to produce  $^1\text{O}_2$  in response to sequence-specific mRNA. However, major challenges were encountered to further evaluate the selective PDT-induced cell death *in vitro* and *in vivo*. First, the current technique does not allow us to validate the specificity of mRNA triggered P30C activation *in vitro* (cell culture) and *in vivo* (animal) because there is no cell line available to serve as the c-raf-1 mRNA negative control (cells not expressing c-raf-1). Secondly, the *in vitro* PDT efficacy and specificity of P30C is modest: 62% reduction of cell viability for P30C vs 27% for r-P30C (negative control), presumably due to the non-sequence specific opening or enzyme-mediated nucleic acid backbone cleavage of the beacons, processes that compete with the hybridization of the beacons with target mRNA.

***Facing these considerable hurdles associated with the mRNA-triggered PMB and recognizing the early success we have had with the PMB featuring protease-cleavable linker, we decided to focus on the “Big Picture” and revised our tasks from developing a breast cancer-specific mRNA-triggered PMB to a breast cancer-specific protease-triggered PMB in order to achieve the ultimate PDT selectivity for breast cancer treatment. We have selected matrix metalloproteinase 7 (MMP7) as our target because MMP7 mRNA was detected in most neoplastic epithelial tumor cells of breast adenocarcinomas and MMP7 protein is highly overexpressed in these cells.***

*Revised Task 4: To synthesize a PMB containing MMP7specific peptide linker and demonstrate that such PMB can be specifically activated by MMP7 in solution and in cancer cells expressing MMP7 (see Appendix 2 for details).*

*Revised Task 5: To determine the in vitro and in vivo photodynamic efficacy and specificity of MMP7-triggered PMB (see Appendix 2 for details)*

### 1. Design and synthesis of MMP7-triggered PMB

In the year 3, our study focused on developing a MMP7-triggered PMB,  $PP_{MMP7B}$ , using: 1) Pyro as the PS, 2) a black hole quencher 3 (BHQ3) as dual fluorescence[12] and  $^1O_2$  quencher[13] and 3) a short peptide sequence, *GPLGLARK*, as the MMP7-cleavable linker, with the cleavage site between G and L and recognition site as indicated by italics[14, 15]. As depicted in Figure 14, Pyro and BHQ3 are conjugated to the opposite ends of the peptide linker to keep them in close proximity, enabling FRET and  $^1O_2$  quenching to make this construct not only optically silent but also photodynamically inactive. We postulate that when the beacon enters MMP7-expressing cells, MMP7 should induce specific cleavage of the peptide linker and remove the Pyro from the vicinity of BHQ3, restoring its fluorescence and photoreactivity. Subsequently, upon light irradiation, the targeted cells should be fluorescent and produce cytotoxic  $^1O_2$ , while leaving normal cells undetectable and unharmed.

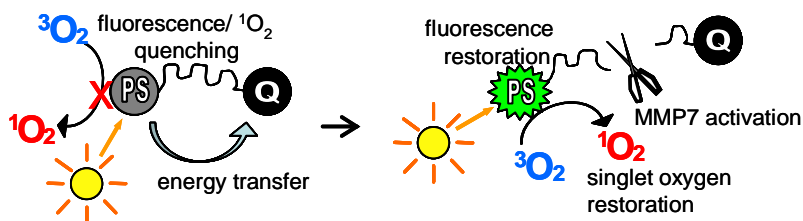


Figure 14. The concept of MMP7 triggered PMB

$PP_{MMP7B}$  (Pyro-*GPLGLARK*-BHQ3), was synthesized and its structure was confirmed by UV-vis spectroscopy (Pyro-specific absorbance was found at 414 nm and BHQ3-specific absorbance at 676 nm) and MALDI-ToF (Calc. 1856.29, found 1855.76).  $PP_{MMP7}$  (Pyro-*GPLGLARK*- $\epsilon$ NH<sub>2</sub>) was used as positive control.

### 2. Validation of MMP7-triggered $PP_{MMP7B}$ activation and its corresponding $^1O_2$ activation in solution

In order to evaluate the efficiency of  $^1O_2$  and fluorescence quenching in intact  $PP_{MMP7B}$  and the specificity of its activation by target MMP7, fluorescence and  $^1O_2$  near-infrared (1270nm) luminescence were measured respectively in solutions of  $PP_{MMP7}$ ,  $PP_{MMP7}+BHQ3$  (1:1 molar ratio),  $PP_{MMP7B}$ ,  $PP_{MMP7B}+MMP7$  and  $PP_{MMP7B}+MMP7+MMP7$  inhibitor. As shown in Figure 15, comparing with  $PP_{MMP7}$ , 13-fold less of fluorescence and 18-fold less of  $^1O_2$  production were observed in  $PP_{MMP7B}$ , while physical mixture of BHQ3 and  $PP_{MMP7}$  did not show noticeable fluorescence and

$^1\text{O}_2$  quenching, confirming that the close proximity of Pyro and BHQ3 by the MMP7 associated peptide (GPLGLARK) effectively inhibits both  $^1\text{O}_2$  and fluorescence production of Pyro. Moreover, adding MMP7 to the  $\text{PP}_{\text{MMP7B}}$  (molar ratio: 1: 60; 3h incubation) restored the quenched  $^1\text{O}_2$  and fluorescence by 19-fold and 12-fold respectively and these restoration were completely blocked by co-incubation with the MMP7 inhibitor (molar ratio: 1:60:1200 for MMP7:  $\text{PP}_{\text{MMP7B}}$ : inhibitor), confirming that MMP7-induced separation of Pyro and BHQ3 allows the photoactivation of Pyro.

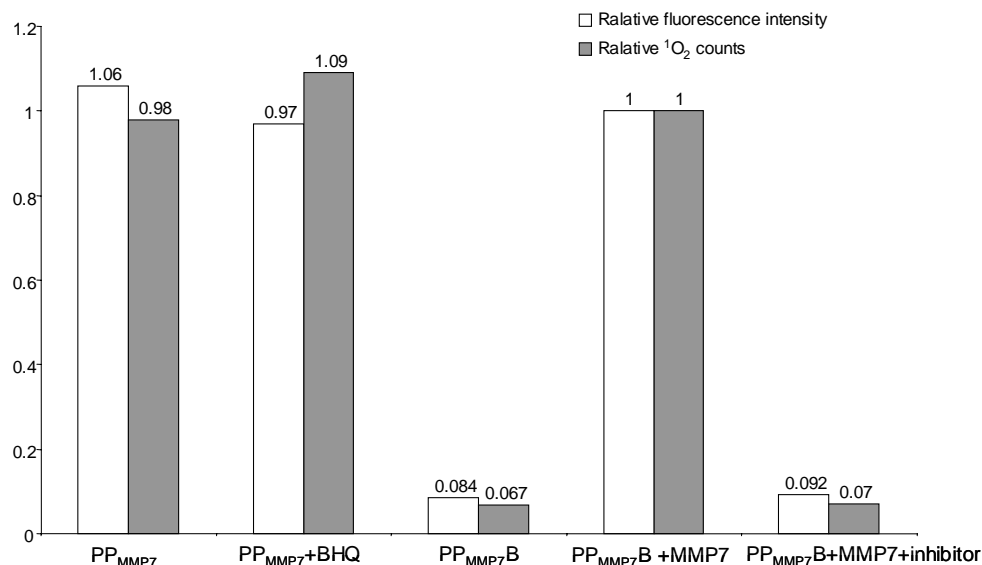


Figure 15. The relative fluorescence intensity and  $^1\text{O}_2$  luminescence counts of  $\text{PP}_{\text{MMP7}}$ ,  $\text{PP}_{\text{MMP7+BHQ}}$ ,  $\text{PP}_{\text{MMP7B}}$ ,  $\text{PP}_{\text{MMP7B+MMP7}}$  and  $\text{PP}_{\text{MMP7B+MMP7+inhibitor}}$ .

### 3. Validation of MMP7-triggered $\text{PP}_{\text{MMP7B}}$ activation and its corresponding PDT activation in cancer cells

After we validated the MMP7-triggered  $\text{PP}_{\text{MMP7B}}$  activation in solution, we further evaluated the  $\text{PP}_{\text{MMP7B}}$  activation in cancer cells. As the confocal images shown in Figure 16, a strong fluorescence signal was observed in KB cells (MMP7 positive,  $\text{MMP7}^+$ ) incubated with 60  $\mu\text{M}$   $\text{PP}_{\text{MMP7B}}$  for 4 h (Figure 16C), whereas BT20 cells (MMP7 negative,  $\text{MMP7}^-$ ) incubated with 60  $\mu\text{M}$   $\text{PP}_{\text{MMP7B}}$  for 4 h showed minimal fluorescence (Figure 16D). Further evidence was obtained by the HPLC analysis of cell media collected at the end of drug incubation. As shown in Figure 17A,  $\text{PP}_{\text{MMP7B}}$  (at 26min) was cleaved by MMP7 in KB medium, generating two fragments associated respectively with a Pyro moiety (at 36min) and a BHQ3 moiety (at 14min) based on their absorption characteristics (Figure 17C). This was further confirmed by MALDI-TOF as the two fragments were identified as Pyro-GPLG-COO $^-$  (Calc.857.44, found 857.26) and BHQ3 NH $_2$ -LARK(BHQ3) (Calc.1014.62, found 1013.13). In addition, no cleavages were found in BT20 medium of  $\text{PP}_{\text{MMP7B}}$  (Figure 17B). These data clearly demonstrated that the cleavage of  $\text{PP}_{\text{MMP7B}}$  was specifically mediated by MMP7 at the known MMP7 cleavage site between G and L [16, 17].

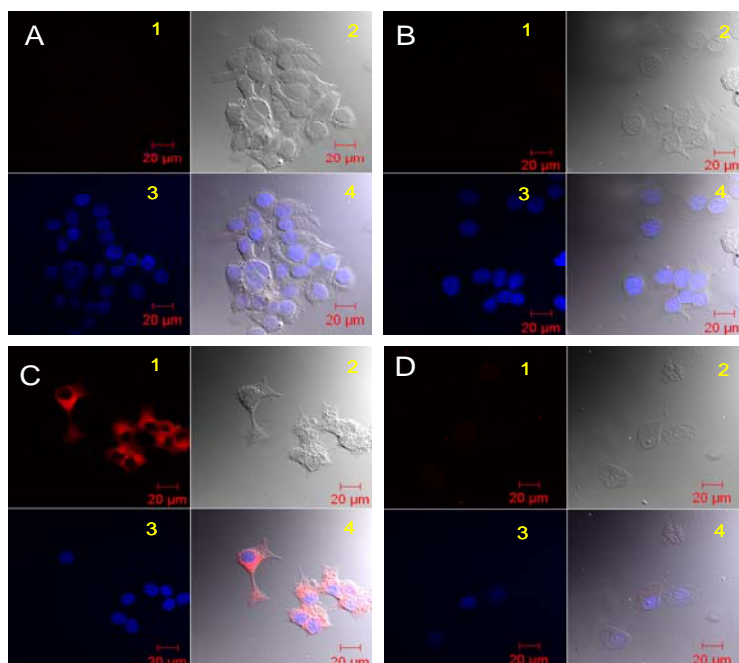


Figure 16. Confocal microscopy images of PP<sub>MMP7B</sub> in KB (MMP7<sup>+</sup>) and BT20 (MMP7<sup>-</sup>) cells. The numbers refer to each pair of images, with 1) fluorescence images, 2) bright field images, 3) DAPI imaging, and 4) overlaid images. **A)** KB cell alone, **B)** BT20 cell alone, **C)** KB cells+60 μM PP<sub>MMP7B</sub>, **D)** BT20 cells+60 μM PP<sub>MMP7B</sub>.

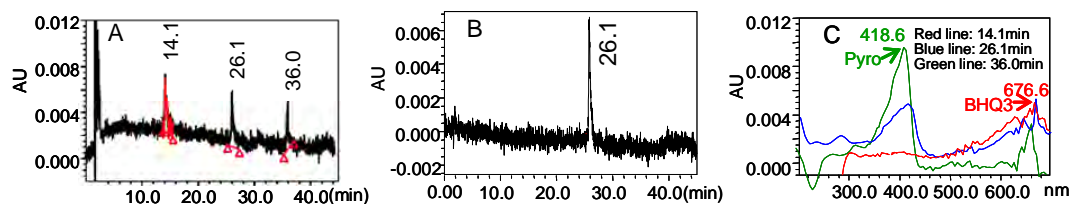


Figure 17. HPLC spectra of 1) the KB cells medium incubated with PP<sub>MMP7B</sub> for 4 h, 2) the HT1080 cells medium incubated with PP<sub>MMP7B</sub> for 4 h and 3) the corresponding UV-vis spectrum of the HPLC peaks shown different retention time.

In order to verify that <sup>1</sup>O<sub>2</sub> production of PP<sub>MMP7B</sub> can be specifically activated by MMP7 *in vitro*, cell viability (MTT assay) was measured in KB (MMP7<sup>+</sup>) and BT20 (MMP7<sup>-</sup>) cells before and after the PDT treatment, normalized to the viability of cells not treated with drug or light. As shown in Figure 18, 1) PP<sub>MMP7B</sub> didn't shown any noticeable dark toxicity to KB and BT20 cells in the range of concentrations used; 2) upon PDT treatment, PP<sub>MMP7B</sub> reduced the viability of only KB cells (MMP7<sup>+</sup>) and its efficacy is drug and light doses dependent. At a high light dose of 7.5J/cm<sup>2</sup>, PP<sub>MMP7B</sub> is effective against KB cells at 0.5μM, whereas it did not induce any photodynamic cytotoxicity to BT20 cells (MMP7<sup>-</sup>) even at 4μM. Taken together, PP<sub>MMP7B</sub> is specifically photoactivated by MMP7 and its photodynamic cytotoxicity is MMP7 sequence specific.

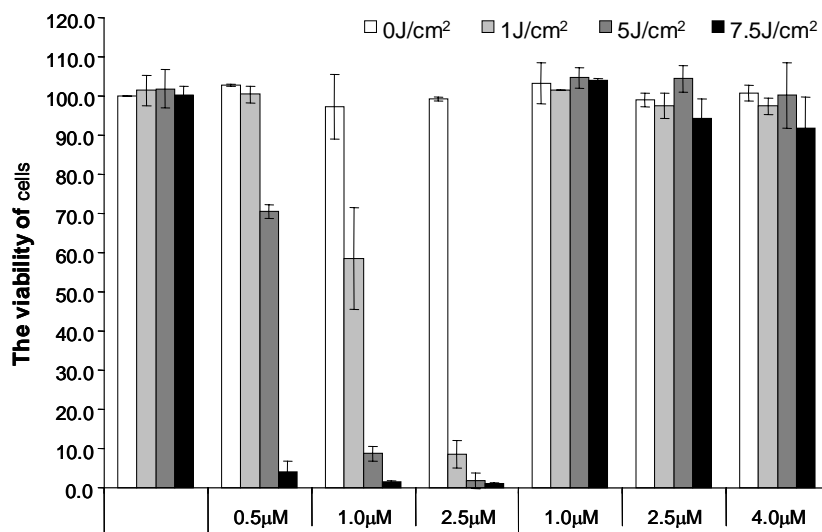


Figure 18. Photodynamic cytotoxicity determined by cell viability (MTT) assay. Viability of KB (MMP7<sup>+</sup>) and BT20 (MMP7<sup>-</sup>) cells after incubated with PP<sub>MMP7B</sub> at different concentration and with different PDT light doses (1, 5, 7.5 J/cm<sup>2</sup>) compared with cell alone that serve as the 100% viable reference. Data shown here was based on 3 different experiments and the results were expressed as mean ± standard error.

#### 4. Preliminary *in vivo* PDT response of PP<sub>MMP7B</sub>

To evaluate the PDT efficacy of the PP<sub>MMP7B</sub> *in vivo*, the mouse bearing two KB tumors (one on each flank) was injected with 80 nmol of PP<sub>MMP7B</sub> intravenously via the tail vein, while the second mouse was kept as a drug-free control. The activation of PP<sub>MMP7B</sub> in the first mouse was continuously monitored by *in vivo* fluorescence imaging. As shown in Figure 19, immediately after injection (Figure 19-2), no fluorescence increase was observed anywhere compared to the “pre-scan” images (Figure 19-1) or the drug-free mouse (Figure 19-7). This confirmed that PP<sub>MMP7B</sub> is optically silent in its native state due to fluorescence quenching by BHQ3. However, fluorescence signals started to increase in KB tumors 20min after injection and reached the highest level at 3h (Figure 19-3), clearly indicating PP<sub>MMP7B</sub> activation by MMP7. At this time point, the PDT treatment was given to the tumor on the left flank, whereas the tumor on the opposite side served as a dark control. The drug-free mouse was treated in the same way. One hour after PDT treatment (4 h post injection) (Figure 19-4), the treated tumor in the drugged animal became edematous, while the untreated tumor in the drugged animal and both tumors in the drug-free mouse showed no changes in size or fluorescence signal. Three days post-PDT, the treated tumor in the drugged mouse was reduced in size and became necrotic (Figure 19-5). Thirty days post-PDT, this treated tumor was not visible and did not reappear (Figure 19-6), while the untreated tumor (Figure 19-6) and both the treated and untreated tumors in the drug-free mouse (Figure 19-8) continued to grow. These data clearly demonstrate that PP<sub>MMP7B</sub> accumulates and can be photodynamically activated in MMP7<sup>+</sup> tumors.

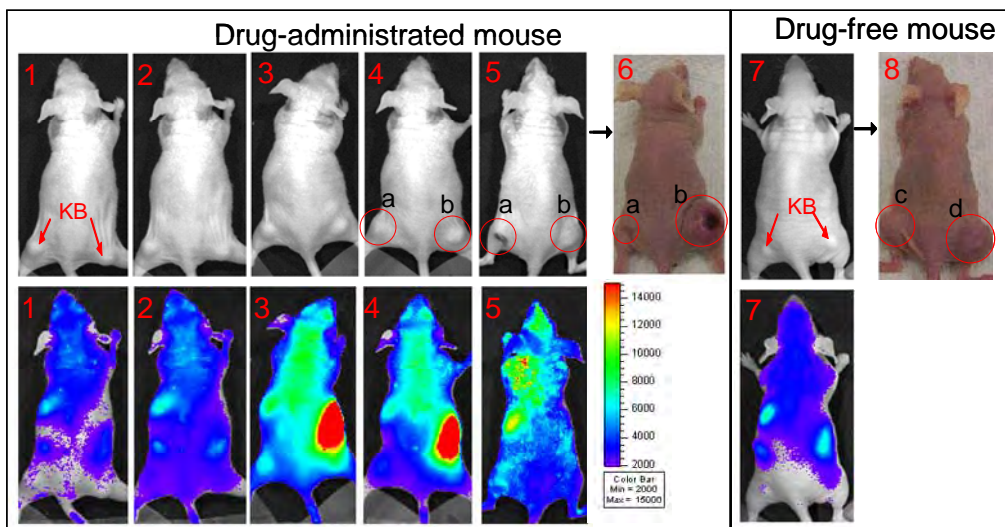


Figure 19. *In vivo* images of mice showing bright field (top) and fluorescence (bottom). 1-5: PP<sub>MMP7B</sub>-administered mouse (1: pre-scan, 2: 10min post i.v. injection, 3: 3h post i.v. injection, 4: 5 h post i.v. injection and 1 h post PDT, 5: 3 d post PDT). 6: Photograph of PP<sub>MMP7B</sub>-administered mouse (30 d post PDT). Tumors were marked by circle in images 4, 5, 6 with the letters corresponding to: a=light treated tumor and b=non-light treated tumor. 7: Drug-free mouse (pre-scan). 8: Photograph of drug free mouse (30 d post PDT) with light treated tumor marked as “c” and non-light treated tumor as “d”.

***In conclusion, we have validated the PMB concept for the first time in vitro using MMP7 triggered PP<sub>MMP7B</sub> on KB (MMP7 positive) and BT20 cells (MMP7 negative), confirming that the PDT activity of the beacon can be specifically triggered by a breast cancer signature (MMP7), allowing the selectively destruction the target cancer cells while leave the non-targeted cells unharmed. In addition, we have also obtained the first in vivo evidence of the PMB concept in mice bearing KB tumors (MMP7 positive).***

***Additional accomplishment 1: Using the <sup>1</sup>O<sub>2</sub> scavenging property of CAR in PMB to minimize photodamage to non-targeted cells (see Appendix 3 for details).***

One of the ways to optimize the PMB selectivity is to maximize the <sup>1</sup>O<sub>2</sub> quenching efficiency before it interacts with targeted biomarkers. Since <sup>1</sup>O<sub>2</sub> is produced by energy transfer from the triplet state of a PS, generated by an intersystem crossing from the PS excited singlet state, <sup>1</sup>O<sub>2</sub> quenching could be potentially achieved by: 1) direct scavenging <sup>1</sup>O<sub>2</sub>, 2) quenching PS triplet excited state and 3) quenching PS singlet excited state. Their relative importance depends on the choice of PS-quencher pair. From our early studies (Appendix 1), we already demonstrated that CAR has dual quenching modes and PS excited states deactivation is more dominant than the <sup>1</sup>O<sub>2</sub> scavenging. Here, we want to study whether its <sup>1</sup>O<sub>2</sub> scavenging properties can be used to minimize the photodamage of intact PMBs to non-targeted cells. To evaluate the effects of intact PPC towards non-targeted cells, caspase-3 was selected as the trigger because it is a well-known cell apoptosis marker and is not expressed in viable cells, thus eliminating the potential cleavage of PPC in non-targeted cells. As shown in Figure 20, cells incubated with either

PP or PPC without light treatment showed similar viability as control cells (no drug/ no light), demonstrating minimal dark cytotoxicity of PP and PPC for the given concentrations. With a light exposure of  $7.5\text{J}/\text{cm}^2$ ,  $0.5\mu\text{M}$  PP reduced the cell viability to less than 10% and this reduction is drug-dose dependent. However, PPC did not induce any measurable cell phototoxicity even at 30-fold greater concentrations ( $15\mu\text{M}$ ). This ultra-high level of photoprotective property of PPC offers its potential application for leading to a high PDT selectivity of targeted cancer cells while leaving normal cells unharmed. In conclusion, we have validated that CAR, as a quencher molecule in PMB, turned off the  $^1\text{O}_2$  production of Pyro by both quenching the PS excited states and directly scavenging  $^1\text{O}_2$ . As a result, it could lose some PDT potency of PPC toward targeted cells. However, as a “trade off”, it should lead to a very high level of “protection” for non-targeted cells. Thus, using CAR for PMB could potentially improve the PDT selectivity.

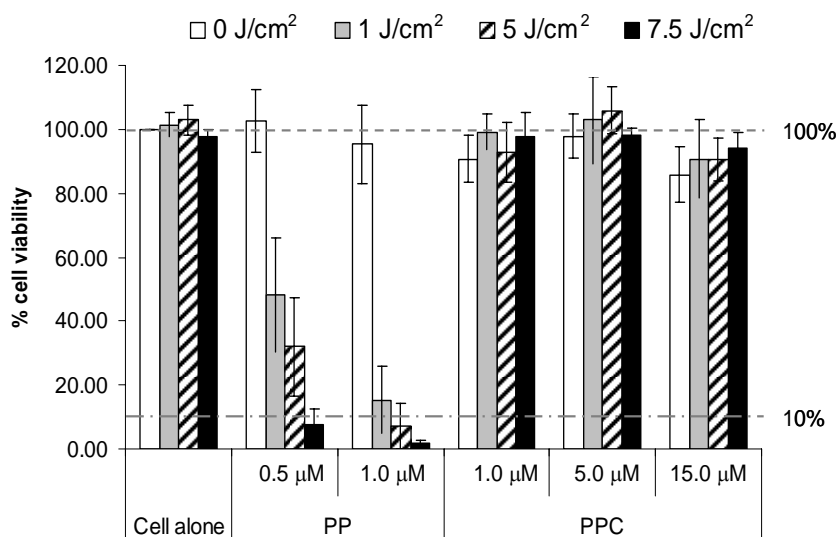


Figure 20. Post-PDT viability of HepG<sub>2</sub> cells incubated with PP or PPC and treated with no ( $0\text{ J}/\text{cm}^2$ ) or 1, 5, and  $7.5\text{ J}/\text{cm}^2$  light dose. The viability of cells incubated with PP is reduced below 10% of the drug-free and light-free control cells (100% viability) using only  $0.5\mu\text{M}$  drug and  $7.5\text{ J}/\text{cm}^2$  light dose, while PPC, even at  $15\mu\text{M}$  and  $7.5\text{ J}/\text{cm}^2$  does not kill the cells, suggesting that CAR induced an excellent photoprotective capability of PPC.

*Additional accomplishment 2: PDT agent with a built-in apoptosis sensor for evaluating its own therapeutic outcome in situ (see Appendices 4 and 5 for details).*

As described above, we have developed a series of PMBs with different short peptide sequences linking PS and Q moieties. During our investigations, we found that when a BHQ3 quencher is used, the  $^1\text{O}_2$  quenching efficiency of the PMB is determined primarily by the peptide sequences. In the case of MMP7-cleavable peptide (GPLGLARK), both fluorescence and  $^1\text{O}_2$  quenching are complete (> 18-fold). On the contrary, in the case of caspase-3-cleavable peptide (GDEVDSGK), we observed

**complete** fluorescence quenching (>15-fold) but only **partial**  $^1\text{O}_2$  quenching (~6-fold). These observations led to the development of a novel beacon, called PDT agent with a built-in apoptosis sensor (PDT-BIAS).

The PDT-BIAS contains a Pyro connected to a BHQ3 by a caspase-3 cleavable peptide linker (GDEVDSGSK). Due to the fact that BHQ3 only partially quenches Pyro's ability to produce  $^1\text{O}_2$ , once activated by PDT, Pyro moiety of such beacons will generate sufficient  $^1\text{O}_2$  to compromise the mitochondrial membrane. If a sufficient number of mitochondria are destroyed to the point where the cell cannot compensate for this loss, the cell will die. If this damage is not drastic enough to lead to cell disintegration *via* necrosis, the release of cytochrome c from the mitochondrial membrane triggers an apoptotic cascade, which ultimately leads to caspase-3 activation. Once activated, caspase-3 cleaves the GDEVDSGSK peptide linker between Pyro and BHQ3 and restores the fluorescence, identifying those cells dying by this apoptosis process. This fluorescence increase is not observed for light-only or drug-only control cells (i.e. when the cells are not killed) or in the case of cells incubated with a beacon containing a scrambled sequence (not cleavable by caspase-3) and treated with light.

Attachment of a tumor homing molecule (folate) increases the specificity of the PDT-BIAS to enable its *in vivo* applications and also shows that incorporation of delivery component does not impair the PDT-BIAS's function. Triggering and reporting apoptosis was demonstrated both *in vitro* and *in vivo*. Although the main obstacle in widely applying this approach remains the partial  $^1\text{O}_2$  quenching, nevertheless, this beacon can be used as a valuable tool for elucidating the true PDT mechanism.

### **Key research accomplishments:**

We have fully developed the concept of photodynamic molecular beacon (PMB) featuring the precise control of the ability of PS to produce  $^1\text{O}_2$  by responding to specific cancer-associated biomarkers.

- We have evaluated two “on-and-off” triggering mechanisms to silence the PMB activity in non-targeted cells and to activate PMB in targeted cancer cells. The first one operates an “openable” oligonucleotide linker that can hybridize with a tumor-specific mRNA. The second one uses a “cleavable” peptide linker for specific tumor-associated protease.
- For the proposed tumor mRNA-triggered PMB, we have developed a c-raf-1 mRNA-triggered PMB (P30C) for breast cancer treatment and have demonstrated that its photoactivity is silenced in the native state and can be specifically activated by c-raf-1 mRNA.
- We have also developed a MMP7-triggered PMB ( $\text{PP}_{\text{MMP7B}}$ ) for breast cancer treatment. Using this  $\text{PP}_{\text{MMP7B}}$ , we firstly confirmed that the PDT activity of the beacon can be specifically activated by a breast cancer signature (MMP7), allowing the selective damage of the target cancer cells (KB,  $\text{MMP7}^+$ ) while leave the non-targeted cells (BT20,  $\text{MMP7}^-$ ) unharmed. In addition, we demonstrate *in vivo* that  $\text{PP}_{\text{MMP7B}}$  accumulates and can be photodynamically activated in  $\text{MMP7}^+$

tumors. *Therefore, for the first time, we have accomplished true tumor selectivity for PDT as proposed.*

- We have developed the PDT agent with built-in apoptosis sensor for in vivo real time NIRF of tumor apoptosis triggered by its photosensitization in situ.

### **Reportable outcomes:**

#### ***Research Papers:***

- *Appendix #1:* Chen J, Stefflova K, Neidre M, Wilson B, Chance B, Glickson JD, Zheng G. Protease-Triggered Photosensitizing Beacon Based on Singlet Oxygen Quenching and Activation. *J. Am. Chem. Soc.*, **2004**, 126(37), 11450-11451.
- *Appendix #2:* Zheng G, Chen J, Stefflova K, Jarvi M, Wilson. Photodynamic Molecular Beacon as an Activatable Photosensitizer Based on Protease Controlled Singlet Oxygen Quenching and Activation, *Proc. Natl. Acad. Sci. USA*, **2007**, 104:8989-8994.
- *Appendix #3:* Chen J, Lo G, Jarvi, M, Stefflova K, Wilson B, Zheng G, Using singlet oxygen scavenging properties of Carotenoid in photodynamic molecular beacons to minimize Photodamage to non-targeted cells, *Photochem. Photobiol. Sci.*, **2007**, submitted (invited contribution).
- *Appendix #4:* Stefflova K, Chen J, Marotta D, Li H, Zheng G, Photodynamic therapy agent with a built-in apoptosis sensor for evaluating its own therapeutic outcome *in situ*, *J. Med. Chem.* **2006**, 49:3850-3856.
- *Appendix #5:* Stefflova K, Chen J, Li H, Zheng G, Targeted Photodynamic Therapy Agent with a Built-in Apoptosis Sensor for *In Vivo* Near-infrared Imaging of Tumor Apoptosis Triggered by its Photosensitization In Situ, *Molecular Imaging*, **2006**, 5:520-532.
- *Appendix #6:* Stefflova K, Li H, Chen J, Zheng G, Peptide-based pharmacomodulation of a cancer-targeted optical imaging and photodynamic therapy agent, *Bioconjugate Chem.*, **2007**, 18:379-388.
- *Appendix #7:* Stefflova K, Chen J, Zheng G, Killer beacons for combined near-infrared fluorescence imaging and photodynamic therapy, *Curr Med Chem*, **2007**, 14:1893-1910.
- *Manuscript #8:* Stefflova K, Chen J, Zheng G, Using molecular beacons for cancer imaging and treatment, *Frontiers in Bioscience*, **2007**, 12: 4709-4721.
- *Manuscript #9:* Chen J, Stefflova K, Kim S, Li H, Marotta D, Chance B, Glickson J, Zheng G, Molecular Beacon-Based Photodynamic Therapy. *Proc. SPIE*, **2004**, 5630, 16-25.
- *Manuscript #10:* Zheng G, Chen Y, Intes X, Chance B, Glickson, J. Contrast-Enhanced Near-Infrared (NIR) Optical Imaging for Subsurface Cancer Detection. *J. Porphyrins and Phthalocyanines*, **2004**, 8: 1106-1117.

- *Manuscript #11*: Chen J, Stefflov K, Warren M, Bu J, Wilson B, Zheng G, Rational Design of a Receptor-Targeted Photodynamic Molecular Beacon for the Multi-level Control of Singlet Oxygen production and PDT Activity in Cancer Cells. *Proc. SPIE*, **2007**, 6449, 61-69.
- *Manuscript #12*: Chen J, Lo P-C, Warren M, Stefflova K, Cheng JD, Wilson BC, and Zheng G. New linker design for biomarker-triggered photodynamic molecular beacons, *Proc. SPIE*, **2007**, accepted.

### ***Patent Applications:***

Zheng G, Glickson J, Chance B, Delikatny EJ, Stefflova K and Chen J: Activatable Photodynamic Therapy Agents, International patent applications: PCT/US2005/048944, June 2, 2005; PCT/US2004/038024, November 15, 2004 and US Provisional Patent applications: No. 60/695,156, June 29, 2005); No. 60/558,501, April 1, 2004 and No. 60/519,794, November 14, 2003.

### ***Abstracts:***

1. Chen J, Stefflova K, Niedre M, Wilson, Zheng G. Near-Infrared Fluorescence Imaging Guided Therapy: Molecular Beacon Based Photosensitizers Triggered by Breast Cancer-Specific mRNA. *Molecular Imaging* **2004**, 3(3), 277.
2. Stefflova K, Chen J, Marotta D, Li H and Zheng G. Photodynamic Therapy Agents with Built-in Apoptosis Reporters (PDT-BIAR). *Molecular Imaging* **2004**, 3(3), 277.
3. Zheng G, Chen J, Stefflova K, Niedre M, Wilson B, Chance B and Glickson JD. New Photodynamic Therapy Concept Based On Singlet Oxygen Quenching and Activation. *Molecular Imaging* **2004**, 3(3), 235.
4. Zheng G, Wilson B, Glickson JD and Chance B. Cancer Detection, Photodynamic Therapy and Mitochondrial Damage Assessment. *Molecular Imaging* **2004**, 3(3), 204.
5. Chen J, Stefflova K, Kim S, Niedre M, Wilson B, Chance B, Glickson JD and Zheng G. Peptide beacons as novel photodynamic therapy (PDT) agents. *ABSTRACTS OF PAPERS OF THE AMERICAN CHEMICAL SOCIETY* **2004**, 228: MEDI-115
6. Stefflova K, Chen J and Zheng G. Photodynamic therapy (PDT) agent with a built-in apoptosis sensor. *ABSTRACTS OF PAPERS OF THE AMERICAN CHEMICAL SOCIETY* **2004**, 228: MEDI-116
7. Kim S, Qi C, Chen Y, Li H, Chance B, Glickson JD and Zheng G. Synthesis of novel bacteriochlorophyll analogs as targeted contrast agents for cancer detection

and treatment. *ABSTRACTS OF PAPERS OF THE AMERICAN CHEMICAL SOCIETY 2004*, 228: MEDI-119

8. Zheng G, Chen J, Stefflova K, Niedre M, Wilson B: Near-infrared fluorescence imaging guided therapy: molecular beacon-based photosensitizers triggered by c-raf-1 mRNA. *Proceedings of Era of Hope Department of Defense Breast Cancer Research Program Meeting* June 2005.
9. Stefflova K, Chen J, Li H, Marotta D, Zheng G: Targeted PDT Agent with Built-in Apoptosis Reporter Designed for Assessing Therapeutic Outcome In Vivo, *4th Annual Meeting of the Society for Molecular Imaging*, September 2005.
10. Stefflova K, Chen J, Li H, Zheng G: Targeted Photodynamic Therapy Agent with a Built-in Apoptosis Sensor for *In Vivo* Near-infrared Imaging of Tumor Apoptosis Triggered by its Photosensitization *In Situ*. *5th Annual Meeting of the Society for Molecular Imaging*, September 2006, Waikoloa, Hawaii.
11. Stefflova K, Chen J, Li H, Zheng G: Modular Peptide-conjugated Fluorescent Photosensitizer for targeted *In Vivo* Near-infrared Imaging and Photodynamic Therapy of Cancer. *5th Annual Meeting of the Society for Molecular Imaging*, September 2006, Waikoloa, Hawaii.
12. Chen J, Stefflok, Li H, Warren M, Zheng G: Matrix Metalloproteinase-7 Activatable Fluorescence Sensor-Guided Photodynamic Therapy Agent. *5th Annual Meeting of the Society for Molecular Imaging*, September 2006, Waikoloa, Hawaii.
13. Chen J, Stefflov K, Warren M, Bu J, Wilson B, Zheng G: Novel Molecular Beacons for Cancer Imaging and Treatment. *Photonic West*, January 2007, San Jose, CA.
14. Zheng G, Chen J, Stefflova K, Wilson B: Photodynamic Molecular Beacons. *11th World Congress of International Photodynamic Association*, March 2007, Shanghai, China
15. Chen J, Corbin I, Zheng G: Novel Targeting and Activation Strategies for Photodynamic Therapy. *Light-Activated Tissue Regeneration and Therapy II*, ECI, June 2007, Tomar, Portugal.
16. Zheng G, Chen J, Stefflova K, Jarvi M, Wilson B: Detection and treatment of cancers using photodynamic molecular beacons. *European Conference of Biomedical Optics*, June 2007, Munich, Germany.

## **Conclusions:**

We have synthesized breast cancer-targeted photodynamic molecular beacon (PMB) using two different activation mechanisms: mRNA-triggered (openable) PMB and protease-triggered (cleavable) PMB. We have validated the core principle of PMB concept: the ability of photosensitizer (PS) to produce singlet oxygen ( $^1\text{O}_2$ ) can be precisely controlled in response to specific breast cancer-associated biomarkers. For the first time, using mouse models and on separate cells, we have shown that it is possible to limit the collateral damage to surrounding normal cells using this approach, thus achieved the unprecedented tumor selectivity for breast cancer PDT. In addition, we also demonstrated the versatility of the PMB design by developing PDT beacons with “tailored” functions such as the PDT agents with a built-in apoptosis sensor for *in situ* and real time monitoring of the therapeutic outcome.

## Reference

- [1] Henderson, B. W.; Sumlin, A. B.; Owczarczak, B. L.; Dougherty, T. J. *J Photochem Photobiol B*, **1991**, *10*, 303-13.
- [2] Zheng, G.; Potter, W. R.; Camacho, S. H.; Missert, J. R.; Wang, G.; Bellnier, D. A.; Henderson, B. W.; Rodgers, M. A.; Dougherty, T. J.; Pandey, R. K. *J Med Chem*, **2001**, *44*, 1540-59.
- [3] Edge, R.; McGarvey, D. J.; Truscott, T. G. *J Photochem Photobiol B*, **1997**, *41*, 189-200.
- [4] Foote, C. S.; Chang, Y. C.; Denny, R. W. *J Am Chem Soc*, **1970**, *92*, 5218-9.
- [5] Telfer, A.; Dhimi, S.; Bishop, S. M.; Phillips, D.; Barber, J. *Biochemistry*, **1994**, *33*, 14469-74.
- [6] Young, A. J.; Frank, H. A. *J Photochem Photobiol B*, **1996**, *36*, 3-15.
- [7] Moore A. L., J. A., Tom R., Gust D., Moore T. A., Bensasson R. A. and Land E. *J. Science*, **1982**, *216*, 982-984.
- [8] Reddi E., S. A., Jori G., Kerrigan P.K., Liddell P.A., Moore A.L., Moore T.A. and Gust D. *Br J Cancer*, **1994**, *69*.
- [9] Gurfinkel, M.; Thompson, A. B.; Ralston, W.; Troy, T. L.; Moore, A. L.; Moore, T. A.; Gust, J. D.; Tatman, D.; Reynolds, J. S.; Muggenburg, B.; Nikula, K.; Pandey, R.; Mayer, R. H.; Hawrysz, D. J.; Sevcik-Muraca, E. M. *Photochem Photobiol*, **2000**, *72*, 94-102.
- [10] Tatman, D.; Liddell, P. A.; Moore, T. A.; Gust, D.; Moore, A. L. *Photochem Photobiol*, **1998**, *68*, 459-66.
- [11] Pham W., W. R. a. T. C.-H. *Angew. Chem.*, **2002**, *114*, 3811-3813.

- [12] Stefflova, K.; Chen, J.; Marotta, D.; Li, H.; Zheng, G. *J Med Chem*, **2006**, *49*, 3850-6.
- [13] Clo, E.; Snyder, J. W.; Voigt, N. V.; Ogilby, P. R.; Gothelf, K. V. *J Am Chem Soc*, **2006**, *128*, 4200-1.
- [14] Knight, C. G.; Willenbrock, F.; Murphy, G. *FEBS Lett*, **1992**, *296*, 263-6.
- [15] Smith, M. M.; Shi, L.; Navre, M. *J Biol Chem*, **1995**, *270*, 6440-9.
- [16] Weingarten, H.; Feder, J. *Anal Biochem*, **1985**, *147*, 437-40.
- [17] Weingarten, H.; Martin, R.; Feder, J. *Biochemistry*, **1985**, *24*, 6730-4.

## Protease-Triggered Photosensitizing Beacon Based on Singlet Oxygen Quenching and Activation

Juan Chen,<sup>†</sup> Klara Stefflova,<sup>‡</sup> Mark J. Niedre,<sup>§</sup> Brian C. Wilson,<sup>§</sup> Britton Chance,<sup>||</sup>  
Jerry D. Glickson,<sup>†</sup> and Gang Zheng<sup>\*†</sup>

Departments of Radiology, Chemistry, Biochemistry, and Biophysics, University of Pennsylvania, Philadelphia, Pennsylvania 19104, and Department of Medical Physics, Ontario Cancer Institute/University of Toronto, Toronto, Ontario M5G 2M9, Canada

Received May 4, 2004; E-mail: Gang.Zheng@uphs.upenn.edu

In type-II photosensitization the singlet oxygen,  $^1\text{O}_2$ , is generated by energy transfer from the triplet state of a photosensitizer molecule (PS), following intersystem crossing of the PS from its photoexcited singlet to triplet state.<sup>1</sup>  $^1\text{O}_2$  is widely believed to be the major cytotoxic agent involved in photodynamic therapy.<sup>1</sup>

In 1990, Matayoshi et al.<sup>2</sup> first used fluorescence resonance energy transfer (FRET) to design activated probes for imaging retroviral proteases. FRET-based imaging probes ("molecular beacons") have since been used in many applications,<sup>3,4</sup> including protease-activated near-infrared (NIR) fluorescent probes developed by Weissleder and colleagues for cancer imaging.<sup>5</sup> These yield high tumor-to-background ratios, since they are nonfluorescent in the native state.

Here we combine these two concepts, i.e., type-II photosensitization and molecular beacons, to design a photosensitizing beacon (PS-beacon) comprising a disease-specific linker, a PS, and a  $^1\text{O}_2$  quencher/scavenger, such that there is no photosensitization until the linker interacts with a specific target molecule, such as a tumor-specific enzyme.

As proof-of-principle of this approach, we designed a protease-triggered PS-beacon, depicted in Figure 1A. This molecule consists of a short peptide sequence specific to a protease that is over-expressed in cancer cells. A PS and a  $^1\text{O}_2$  quencher/scavenger (Q) are conjugated to the opposite ends of this sequence. Proximity of PS and Q can quench  $^1\text{O}_2$  generation through PS triplet-state energy transfer and/or can scavenge the  $^1\text{O}_2$  that has been generated. We hypothesize that, in the presence of tumor-specific enzyme, the substrate sequence will be cleaved and PS and Q will separate so that the PS can be photoactivated.

To build the model construct, a cleavable caspase-3 substrate, GDEVDGSGK (recognition site underlined), was chosen as the peptide sequence, for which there is a well-established assay for the caspase-3-specific fluorogenic substrate.<sup>6</sup> Pyropheophorbide *a* (Pyro) was used as the PS. This is a chlorophyll analogue that has long-wavelength absorption at 667 nm and is an efficient  $^1\text{O}_2$  producer with a quantum yield  $>50\%$ .<sup>7</sup> A carotenoid (CAR) was selected as the Q moiety, since CARs are well known both to quench triplet excited states and also to scavenge singlet oxygen.<sup>8</sup> Hence, when the CAR moiety is held in close proximity to the PS by the short peptide sequence, it should efficiently decrease  $^1\text{O}_2$  generation and lifetime.

To synthesize the Pyro-peptide-CAR (PPC) PS-beacon (Figure 1B), a GDEVDGSGK peptide was synthesized. Pyro was coupled to the N-terminal glycine of peptide on solid support. This conjugate was then cleaved from the support and deprotected. CAR conjugation was then carried out in solution, since it is acid-labile.

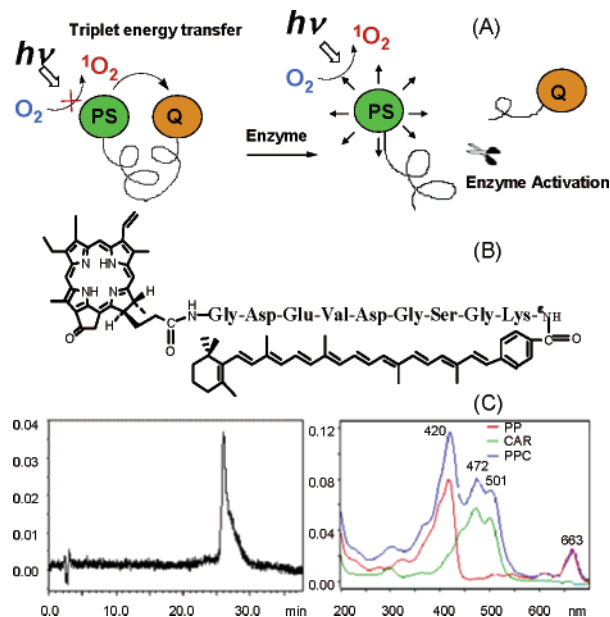


**Figure 1.** (A) Concept of  $^1\text{O}_2$  quenching/scavenging and activation. (B) Structure of caspase-3 activatable PPC beacon. (C) HPLC retention time<sup>9</sup> of PPC and the corresponding absorption spectra of PPC compared to Pyropheophorbide (PP) and CAR.

Purification of this product was achieved by using two connected Diol and C18 Sep-pak columns and confirmed by HPLC (Figure 1C). The structure of PPC was confirmed by MALDI-TOF (calculated 1895.24, found 1896.03). The presence of all three structural components in PPC was further confirmed by UV-vis (Figure 1C), which shows characteristic peaks of the Pyro (420, 663 nm) and CAR (472, 501 nm) moieties.

The PPC was then tested for caspase-3 cleavage using HPLC. As shown in Figure 2A, addition of caspase-3 clearly induced cleavage, as demonstrated by the diminishing PPC peak at 26.7 min and the rise of Pyro and CAR residues at 12.4 and 20.7 min, respectively. The cleavage was proved to be caspase-3-specific by using a caspase-3-specific inhibitor (Ac-DEVD-CHO) that completely blocked the enzyme activity.<sup>6</sup> The stability of both Pyro and CAR upon caspase-3 cleavage was demonstrated by the fact that their absorption spectra remain unchanged (Figure 2B).

To test this concept,  $^1\text{O}_2$  was measured directly in solutions of PPC alone, PPC incubated with caspase-3, and PPC incubated with caspase-3 plus a caspase-3 inhibitor. Pyro-peptide (PP) alone, without the CAR moiety, was used as a positive control.  $^1\text{O}_2$  generation was quantified by measuring its NIR luminescence at 1270 nm, using an instrument that has been described previously.<sup>10</sup> Briefly, a 10 ns pulsed 523 nm laser (75 mW/cm<sup>2</sup>) excites the solution and the luminescence spectrum is sampled, after rejection

<sup>†</sup> University of Pennsylvania Radiology.

<sup>‡</sup> University of Pennsylvania Chemistry.

<sup>§</sup> Ontario Cancer Institute/University of Toronto.

<sup>||</sup> University of Pennsylvania Biochemistry/Biophysics.

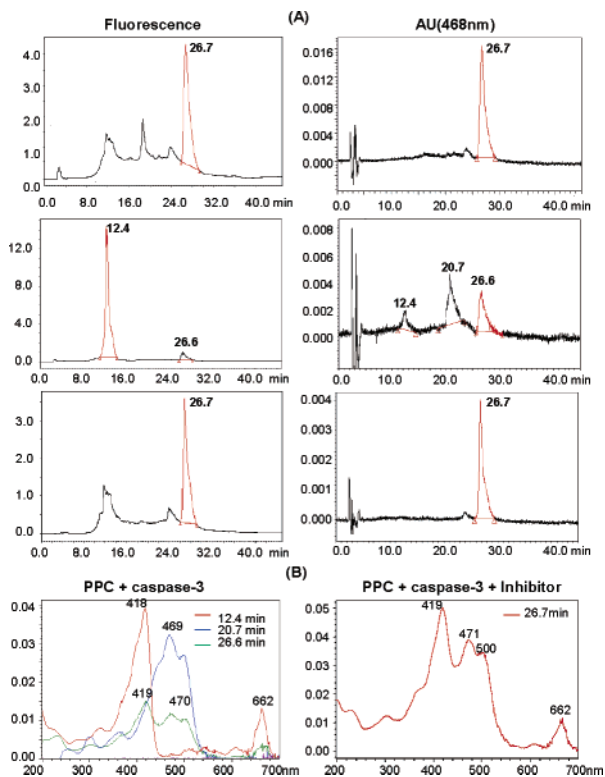


**Figure 2.** (A) HPLC chromatograms monitoring caspase-3 cleavage by Pyro fluorescence (left) and CAR absorption (right): PPC alone (first row), PPC + caspase-3 (second row), and PPC + caspase-3 + inhibitor (third row). (B) Absorption spectra corresponding to the dominant HPLC peaks for PPC + caspase-3 (left) and PPC + caspase-3 + inhibitor (right).

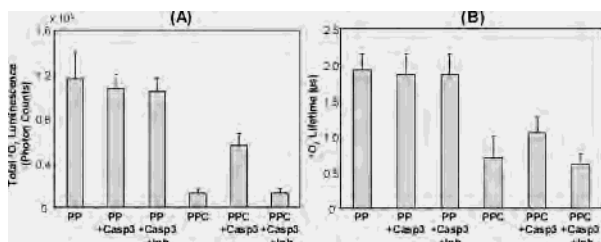


**Figure 3.** (A) Total <sup>1</sup>O<sub>2</sub> luminescence counts for PP, PP + caspase-3, PP + caspase-3 + inhibitor, PPC, PPC + caspase-3, and PPC + caspase-3 + inhibitor. (B) Corresponding <sup>1</sup>O<sub>2</sub> lifetime.

of PS fluorescence, using a set of interference filters and a high-sensitivity NIR photomultiplier tube operating in the time-resolved single-photon counting mode.

As shown in Figure 3, caspase-3 and its inhibitor have no effect on the <sup>1</sup>O<sub>2</sub> production of PP, and PPC itself has 8-fold less <sup>1</sup>O<sub>2</sub> production than PP. Thus, the <sup>1</sup>O<sub>2</sub> quenching in PPC is due to the presence of CAR. Moreover, addition of caspase-3 to the PPC (molar ratio 1:60; incubation time 1 h) resulted in a 4-fold increase in <sup>1</sup>O<sub>2</sub> signal, an effect that was completely prevented by co-incubation with the caspase-3 inhibitor (8 × PPC concentration with the same incubation time). The 2-fold difference in <sup>1</sup>O<sub>2</sub> luminescence as well as <sup>1</sup>O<sub>2</sub> lifetime between the PP and PPC + caspase-3 is probably due to the presence of free CAR quenchers

in solution after cleavage. This effect will likely be less in vivo since there will be less free CARs available. The difference in <sup>1</sup>O<sub>2</sub> luminescence between PPC alone and PPC + caspase-3 is likely due to both photosensitizer triplet-state quenching and <sup>1</sup>O<sub>2</sub> scavenging by CAR. These data demonstrate that <sup>1</sup>O<sub>2</sub> generation is effectively inhibited by the CAR quencher and that caspase-3-induced separation of the quencher and the photosensitizer molecules allows photoactivation of the latter.

In addition, the ratio of the PPC to PPC + caspase-3 in <sup>1</sup>O<sub>2</sub> lifetime (Figure 3B) is 3:4, whereas this ratio in total <sup>1</sup>O<sub>2</sub> (Figure 3A) is 1:4. Since <sup>1</sup>O<sub>2</sub> luminescence is directly proportional to <sup>1</sup>O<sub>2</sub> lifetime, Pyro triplet state quenching by CAR seems to be more important for the intact PPC molecule than <sup>1</sup>O<sub>2</sub> scavenging. This is consistent with the fact that the requirement for efficient triplet state quenching is less rigid than the direct <sup>1</sup>O<sub>2</sub> quenching (five double bonds in CAR required for the former but nine required for the latter).<sup>11</sup>

All of the above experiments were repeated at least in triplicate and were statistically significant ( $p < 0.04$ ).

In conclusion, a new photosensitization concept has been developed, based on <sup>1</sup>O<sub>2</sub> quenching and activation, and the first PS-beacon designed using this concept has been validated in solution by direct <sup>1</sup>O<sub>2</sub> luminescence and lifetime measurements. It is planned to test this next in cancer cells in vitro and in vivo with a tumor-specific peptide linker<sup>5</sup> and to extend the concept to other activation mechanisms, such as the use of tumor-specific antisense linker.<sup>12</sup>

**Acknowledgment.** This work was supported by DOD DAMD17-03-1-0373 (G.Z.), NIH R21-CA95330 (G.Z.), the Oncologic Foundation of Buffalo (G.Z.), and the National Cancer Institute of Canada (B.W., M.N.). Partial support from NIH R24-CA83105 (J.D.G.) is also acknowledged.

## References

- (1) Dougherty, T. J.; Gomer, C. J.; Henderson, B. W.; Jori, G.; Kessel, D.; Korbek, M.; Moan, J.; Peng, Q. *J. Natl. Cancer Inst.* **1998**, *90*, 889–905.
- (2) Matayoshi, E. D.; Wang, G. T.; Krafft, G. A.; Erickson, J. *Science* **1990**, *247*, 954–958.
- (3) Zhang, J.; Campbell, R. E.; Ting, A. Y.; Tsien, R. Y. *Nat. Rev. Mol. Cell Biol.* **2002**, *3*, 906–918.
- (4) Tyagi, S.; Kramer, F. R. *Nat. Biotech.* **1996**, *14*, 303–308.
- (5) Weissleder, R.; Tung, C. H.; Mahmood, U.; Bogdanov, A. *Nat. Biotech.* **1999**, *17*, 375–378.
- (6) Nicholson, D. W.; Ali, A.; Thornberry, N. A.; Vaillancourt, J. P.; Ding, C. K.; Gallant, M.; Gareau, Y.; Griffin, P. R.; Labelle, M.; Lazebnik, Y. A.; Munday, N. A.; Raju, S. M.; Smulson, M. E.; Yamin, T.; Yu, V. L.; Miller, D. K. *Nature* **1998**, *17*, 1295–1304.
- (7) Zhang, M.; Zhang, Z. H.; Blessington, D.; Li, H.; Busch, T. M.; Madrak, V.; Miles, J.; Chance, B.; Glickson, J. D.; Zheng, G. *Bioconjugate Chem.* **2003**, *14*, 709–714.
- (8) Gust, D.; Moore, T. A.; Moore, A. L.; Jori, G.; Reddi, E. *Ann. N.Y. Acad. Sci.* **1993**, *691*, 32–47.
- (9) HPLC method: column, RP C8 300 Å; solvents, A = 0.1% TFA in water, B = CH<sub>3</sub>CN, C = MeOH; gradient, 60% A and 40% B to 10% A and 90% B in the first 20 min, then to 90% B and 10% C for another 10 min, finally to 80% B and 20% C for 10 min.
- (10) Niedre, M.; Secord, A. J.; Patterson, M. S.; Wilson, B. C. *Cancer Res.* **2003**, *63*, 7986–7994.
- (11) Foote, C. S.; Chang, Y. C.; Denny, R. W. *J. Am. Chem. Soc.* **1970**, *92*, 5216–5218.
- (12) Sokol, D. L.; Zhang, X.; Lu, P.; Gewirtz, A. M. *Proc. Natl. Acad. Sci. U.S.A.* **1998**, *95*, 11538–11543.

JA047392K

# Photodynamic molecular beacon as an activatable photosensitizer based on protease-controlled singlet oxygen quenching and activation

Gang Zheng<sup>\*†‡§</sup>, Juan Chen<sup>\*†‡</sup>, Klara Stefflova<sup>¶</sup>, Mark Jarvi<sup>\*†</sup>, Hui Li<sup>‡</sup>, and Brian C. Wilson<sup>\*†</sup>

<sup>\*</sup>Department of Medical Biophysics, University of Toronto, Toronto, ON, Canada M5G 1L7; <sup>†</sup>Division of Biophysics and Bioimaging, Ontario Cancer Institute, Toronto, ON, Canada M5G 1L7; and Departments of <sup>‡</sup>Radiology and <sup>¶</sup>Chemistry, University of Pennsylvania, Philadelphia, PA 19104

Edited by Britton Chance, University of Pennsylvania School of Medicine, Philadelphia, PA, and approved April 11, 2007 (received for review December 15, 2006)

Molecular beacons are FRET-based target-activatable probes. They offer control of fluorescence emission in response to specific cancer targets, thus are useful tools for *in vivo* cancer imaging. Photodynamic therapy (PDT) is a cell-killing process by light activation of a photosensitizer (PS) in the presence of oxygen. The key cytotoxic agent is singlet oxygen ( $^1O_2$ ). By combining these two principles (FRET and PDT), we have introduced a concept of photodynamic molecular beacons (PMB) for controlling the PS's ability to generate  $^1O_2$  and, ultimately, for controlling its PDT activity. The PMB comprises a disease-specific linker, a PS, and a  $^1O_2$  quencher, so that the PS's photoactivity is silenced until the linker interacts with a target molecule, such as a tumor-associated protease. Here, we report the full implementation of this concept by synthesizing a matrix metalloproteinase-7 (MMP7)-triggered PMB and achieving not only MMP7-triggered production of  $^1O_2$  in solution but also MMP7-mediated photodynamic cytotoxicity in cancer cells. Preliminary *in vivo* studies also reveal the MMP7-activated PDT efficacy of this PMB. This study validates the core principle of the PMB concept that selective PDT-induced cell death can be achieved by exerting precise control of the PS's ability to produce  $^1O_2$  by responding to specific cancer-associated biomarkers. Thus, PDT selectivity will no longer depend solely on how selectively the PS can be delivered to cancer cells. Rather, it will depend on how selective a biomarker is to cancer cells, and how selective the interaction of PMB is to this biomarker.

activation | image-guided therapy | photodynamic therapy | matrix metalloproteinases | quencher

Photodynamic therapy (PDT) is an emerging cancer treatment modality involving the combination of light, a photosensitizer (PS), and molecular oxygen (1). It offers unique control in the PS's action, because the key cytotoxic agent, singlet oxygen ( $^1O_2$ ), is produced only *in situ* upon irradiation. Therefore, PDT selectivity can be controlled at three different levels. The first level is to control how light is delivered to the disease tissue. This approach is the easiest to implement, because light can be readily manipulated and positioned, particularly through the judicious use of advanced fiber optics (e.g., prostate interstitial fibers) (2). However, it cannot achieve a high level of selectivity because of the limited tumor localization of existing PDT agents, which in turn cause treatment-related toxicity to surrounding normal tissues as well as sunlight-induced skin toxicity. The second level is to control how the PS is delivered to the tumor tissue. This approach has been actively pursued by many research groups, including ours, and has resulted in improvement of PDT selectivity (3–7). However, it is still vulnerable to collateral damage to surrounding normal tissues. A new direction is to exert control of the PS's ability to produce  $^1O_2$  (9–14). This third level control has the potential to achieve ultimate PDT selectivity to cancer cells while leaving normal cells unharmed.

We introduced the concept of photodynamic molecular beacons (PMB) that are capable of controlling  $^1O_2$  production that

responds specifically to certain cancer biomarkers (9). This approach is an extension of the well known molecular beacons (MB) (15) that use the FRET principle for controlling fluorescence emission in response to target activation. By combining MB with PDT, we seek to enable cancer biomarker-controlled  $^1O_2$  production to achieve unprecedented PDT selectivity. The PMB comprises a disease-specific linker, a PS, and a  $^1O_2$  quencher, so that the PS's photoactivity is silenced until the linker interacts with a target molecule, such as a tumor-associated protease. In that initial study, a pyropheophorbide [(Pyro) as PS] and a carotenoid (as  $^1O_2$  quencher) were kept in close proximity by the self-folding of a caspase-3 specific peptide sequence, resulting in effective  $^1O_2$  quenching. Upon caspase-3-induced cleavage, the  $^1O_2$  production increased markedly in solution, as evidenced by direct  $^1O_2$  near-infrared (NIR) luminescence intensity and lifetime measurements. However, because caspase-3 is a cell apoptosis marker (16), it is difficult to further validate the concept in cancer cells by using this particular PMB, because of the difficulty of distinguishing PDT-induced toxicity in apoptotic cells. Hence, finding a specific cleavable peptide linker to target tumor-associated proteases is necessary.

Matrix metalloproteinases (MMPs) are known to be important in normal tissue remodeling but also play critical roles in many diseases (17), such as atherosclerosis, lung pulmonary fibrosis, and cancer. The presence of extracellular and membrane-bound MMPs in tumors not only aids the degradation of extracellular matrix by the neoplastic cells but also facilitates their motility and directs cell invasion (18). Thus, MMPs have long been of interest as pharmaceutical targets (17). Among these, matrix metalloproteinase-7 (MMP7) has been a particularly important target, because of its epithelial origin and its high expression in pancreatic, colon, breast, and nonsmall-cell lung cancer (19, 20).

In this report, we describe the synthesis and characterization of an MMP7-triggered PMB, PP<sub>MMP7</sub>B, using: (i) Pyro as the PS, because of its excellent  $^1O_2$  quantum yield, NIR fluorescence emission, and high tumor affinity (21); (ii) black hole quencher

Author contributions: G.Z. and J.C. designed research; J.C., K.S., M.J., and H.L. performed research; J.C., K.S., and M.J. contributed new reagents/analytic tools; G.Z., J.C., K.S., M.J., H.L., and B.C.W. analyzed data; and G.Z., J.C., and B.C.W. wrote the paper.

The authors declare no conflict of interest.

This article is a PNAS Direct Submission.

Freely available online through the PNAS open access option.

Abbreviations: PDT, photodynamic therapy; PMB, photodynamic molecular beacons; NIR, near-infrared; PS, photosensitizer;  $^1O_2$ , singlet oxygen; Pyro, pyropheophorbide a; BHQ3, black hole quencher 3; MMP7, matrix metalloproteinase-7; PP<sub>MMP7</sub>B, MMP7-triggered PMB; C-PPB, control Pyro-Peptide-BHQ3; MTT, 3-(4,5-dimethylthiazol-2-yl)-2,5-diphenyltetrazolium bromide; UV-vis, UV-visible; KB, human nasopharyngeal epidermoid carcinoma cells; BT20, human breast carcinoma cells.

<sup>§</sup>To whom correspondence should be addressed. E-mail: gang.zheng@uhnres.utoronto.ca.

© 2007 by The National Academy of Sciences of the USA



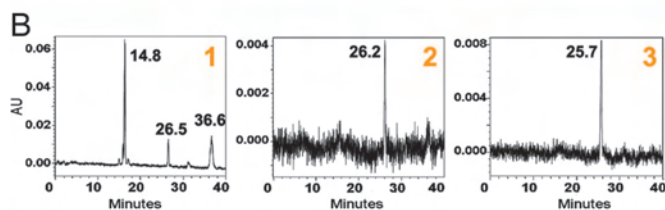
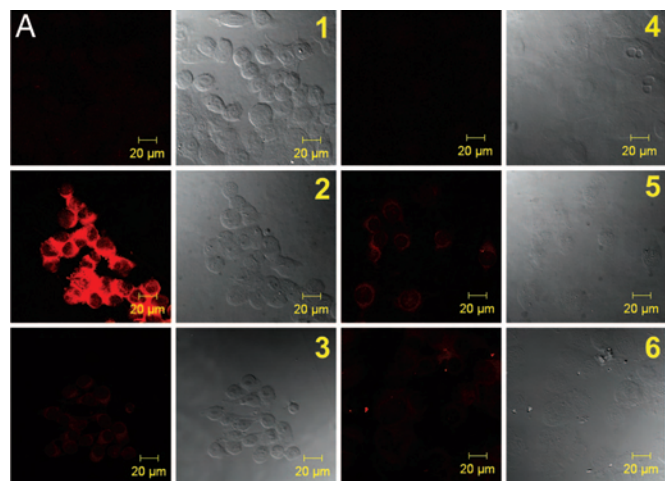


**Fig. 3.** *In vitro* validation of MMP7-specific activation. (A) Confocal images of PP<sub>MMP7B</sub> and control C-PPB in KB (MMP7<sup>+</sup>) and BT20 (MMP7<sup>-</sup>) cells showing fluorescence (Left) and bright field (Right) in each case. (1) KB cells alone, (2) KB cells plus 60 μM PP<sub>MMP7B</sub>, (3) KB cells plus 60 μM C-PPB, (4) BT20 cells alone, (5) BT20 cells plus 60 μM PP<sub>MMP7B</sub>, and (6) BT20 cells plus 60 μM C-PPB. (B) HPLC spectra of cell incubation media after 5-h incubation: (1) KB cells + PP<sub>MMP7B</sub>, (2) BT20 cells + PP<sub>MMP7B</sub>, and (3) KB cells + C-PPB.

two fragments associated, respectively, with a Pyro moiety (at 36 min) and a BHQ3 moiety (at 14 min), based on their absorption characteristics (Fig. 2B2). This was further confirmed by MALDI-TOF, because the two fragments were identified as Pyro-GPLG-COO<sup>-</sup> (calculated, 857.44; found, 857.26) and NH<sub>2</sub>-LARK(BHQ3) (calculated, 1,014.62; found, 1,013.13). In addition, no cleavage was observed in the solution of PP<sub>MMP7B</sub>+MMP2 (Fig. 2B3) or C-PPB+MMP7 (Fig. 2B4). Taken together, these data demonstrate that the MMP7 specifically induced PP<sub>MMP7B</sub> cleavage at the known MMP7 cleavage site between G and L (24, 25).

To evaluate the efficiency of <sup>1</sup>O<sub>2</sub> quenching in intact PP<sub>MMP7B</sub> and the specificity of its <sup>1</sup>O<sub>2</sub> activation by MMP7, <sup>1</sup>O<sub>2</sub> NIR (1,270 nm) luminescence was measured directly in solutions of PP<sub>MMP7B</sub>+BHQ3 (1:1 molar ratio), PP<sub>MMP7B</sub>, PP<sub>MMP7B</sub>+MMP7, and PP<sub>MMP7B</sub>+MMP7+MMP7 inhibitor. PP<sub>MMP7B</sub> alone was used as a positive control. As shown in Fig. 2C, compared with PP<sub>MMP7B</sub>, 18-fold lower <sup>1</sup>O<sub>2</sub> production was observed in PP<sub>MMP7B</sub>, whereas a similar <sup>1</sup>O<sub>2</sub> production was found in the same concentration of PP<sub>MMP7B</sub>+BHQ3, confirming that the close proximity of Pyro and BHQ3 by the self folding of the MMP7-cleavable peptide effectively inhibits the <sup>1</sup>O<sub>2</sub> production of Pyro. Moreover, adding MMP7 to the PP<sub>MMP7B</sub> (molar ratio: 1: 60; 3 h incubation) restored the quenched <sup>1</sup>O<sub>2</sub> production by 19-fold, an effect completely blocked by coinubation with the MMP7 inhibitor (molar ratio, 1:60:1,200 for MMP7; PP<sub>MMP7B</sub>, inhibitor), confirming that MMP7-induced separation of Pyro and BHQ3 allows the photoactivation of Pyro. All of the above experiments were repeated in triplicate and the <sup>1</sup>O<sub>2</sub> production of PP<sub>MMP7B</sub>, PP<sub>MMP7B</sub>+BHQ3, and PP<sub>MMP7B</sub>+MMP7 are all statistically different from that of PP<sub>MMP7B</sub> (*P* < 0.05), whereas none of those three is statistically different from the other.

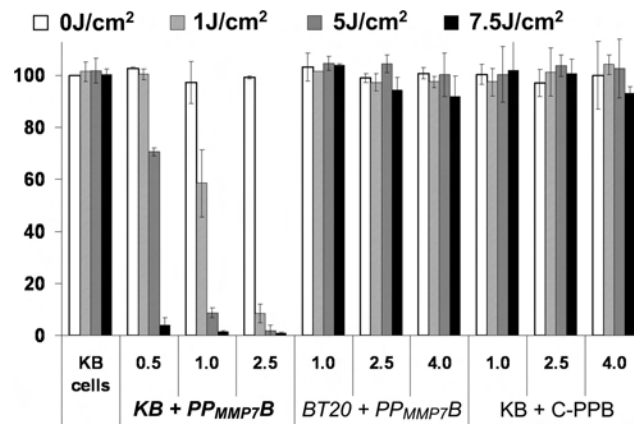


**Fig. 4.** Photodynamic cytotoxicity determined by MTT assay as a function of PS and light doses, compared with untreated cells; means ± standard errors for triplicate experiments.

#### Validation of MMP7-Triggered PP<sub>MMP7B</sub> Activation and Its Corresponding PDT Activation in Cancer Cells.

After we validated the MMP7-triggered PP<sub>MMP7B</sub> activation in solution, we evaluated this in cancer cells. To prove that PP<sub>MMP7B</sub> can be specifically activated by MMP7 *in vitro*, confocal fluorescence microscopy studies were performed on KB (MMP7<sup>+</sup>) and BT20 (MMP7<sup>-</sup>) (26) cells incubated with either PP<sub>MMP7B</sub> or the control C-PPB, with 633 nm excitation and >650 nm detection. As expected, confocal images showed a strong fluorescence signal in KB cells (MMP7<sup>+</sup>) incubated with PP<sub>MMP7B</sub> (Fig. 3A2), whereas control experiments yielded the following results: (i) BT20 cells (MMP7<sup>-</sup>) incubated with PP<sub>MMP7B</sub> showed minimal fluorescence (Fig. 3A5), and (ii) both KB and BT20 cells showed minimal fluorescence when incubated with C-PPB (Figs. 3A3 and 6). Further evidence was obtained by HPLC analysis of cell media collected at the end of drug incubation. Fig. 3B1 shows that PP<sub>MMP7B</sub> was cleaved by MMP7 in KB medium, generating two fragments consistent with the solution studies, whereas no cleavages were found in BT20 medium of PP<sub>MMP7B</sub> (Fig. 3B2) and KB medium of C-PPB (Fig. 3B3). These data clearly demonstrated that PP<sub>MMP7B</sub> can enter cells directly, and its cleavage was specifically mediated by MMP7 in cancer cells. Pyro serves in this case as a multifunctional module: (i) as a fluorescent dye, (ii) as a PS, and (iii) as a delivery vehicle, as shown (22).

To verify that <sup>1</sup>O<sub>2</sub> production of PP<sub>MMP7B</sub> can be specifically activated by MMP7 *in vitro*, cell viability (MTT assay) was measured in KB (MMP7<sup>+</sup>) and BT20 (MMP7<sup>-</sup>) cells before and after PDT treatment, normalized to the viability of cells not treated with drug or light. Fig. 4 shows the following: (i) Neither PP<sub>MMP7B</sub> nor C-PPB (negative control) had noticeable dark toxicity in the range of concentrations used, the viability of cells incubated with even the highest PP<sub>MMP7B</sub> and C-PPB concentrations (4 μM) without light being the same as that of control cells without drug and light. (ii) Upon PDT treatment, PP<sub>MMP7B</sub> reduced the viability of only the KB cells (MMP7<sup>+</sup>), and its efficacy was drug- and light-dose-dependent. At a high light dose of 7.5 J/cm<sup>2</sup>, PP<sub>MMP7B</sub> was effective against KB cells at 0.5 μM, whereas it did not induce any photodynamic cytotoxicity in BT20 cells (MMP7<sup>-</sup>) even at 4 μM. (iii) At the same dose (4 μM, 7.5 J/cm<sup>2</sup>), C-PPB also did not reduce the cell viability of KB cells (MMP7<sup>+</sup>). Taken together, PP<sub>MMP7B</sub> is specifically photoactivated by MMP7 and its photodynamic cytotoxicity is MMP7 sequence-specific.

To determine the subcellular localization of the PP<sub>MMP7B</sub>, MitoTracker Green FM (Invitrogen, Carlsbad, CA) was used to stain the mitochondria of the KB cells incubated with PP<sub>MMP7B</sub>.

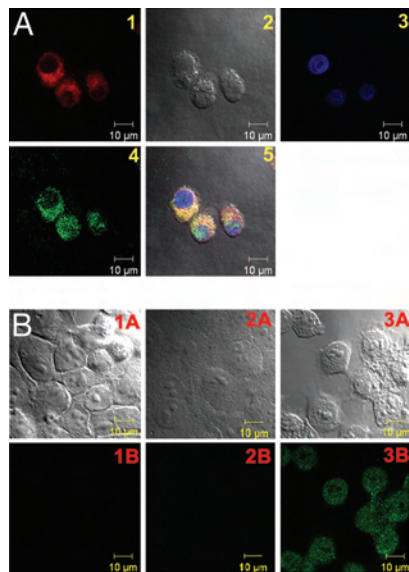


**Fig. 5.** Confocal images showing PP<sub>MMP7</sub>B localization and PP<sub>MMP7</sub>B-induced apoptosis. (A) Confocal images of KB cells stained with 100 nM of MitoTracker Green FM for 30 min after 4-h incubation with 20  $\mu$ M PP<sub>MMP7</sub>B: (1) Pyro image, (2) differential interference contrast image, (3) DAPI image, (4) MitoTracker image, and (5) overlaid image. (B) Confocal images showing fluorescence at 488 nm (Lower) and bright field (Upper). (1) KB cells stained with Apoptag; (2) KB cells incubated with 2  $\mu$ M PP<sub>MMP7</sub>B for 3 h, kept in the dark for 3 h, and stained with Apoptag; (3) KB cells incubated with 2  $\mu$ M PP<sub>MMP7</sub>B for 3 h, treated with PDT (5 J/cm<sup>2</sup>), and stained with Apoptag 3 h after PDT.

Confocal microscopy showed a high degree of colocalization for Pyro and MitoTracker fluorescence (Fig. 5A), demonstrating that PP<sub>MMP7</sub>B was cleaved by MMP7 and that the Pyro fragment was internalized in the cells within or nearby mitochondria but was absent from the nucleus. This indicates that PP<sub>MMP7</sub>B could be a potent PDT agent, because mitochondria are known as effective targets for PDT damage (27).

To determine whether the PP<sub>MMP7</sub>B-induced photodynamic cytotoxicity to KB cells is related to apoptosis, the Apoptag Plus *in situ* fluorescein detection kit S7111 (Chemicon, Temecula, CA) was used to stain KB cells in accordance with the manu-

facturer's protocol. As shown in Fig. 5B3, KB cells incubated with 2  $\mu$ M PP<sub>MMP7</sub>B for 3 h, followed by PDT treatment (5 J/cm<sup>2</sup>), produced a strong apoptosis signal 3 h after PDT, as the cells lit up in the Apoptag fluorescein channel (excitation wavelength, 488 nm; emission wavelength, 497–580 nm), whereas KB cells incubated with the same concentration of PP<sub>MMP7</sub>B in the absence of light did not show any significant apoptosis (Fig. 5B2). This observation, together with the evidence of mitochondrial localization of the PMB, suggests that apoptosis is likely the primary mechanism of cell death.

**Preliminary *in Vivo* PDT Response of PP<sub>MMP7</sub>B.** To evaluate the PDT efficacy of the PP<sub>MMP7</sub>B *in vivo*, the mouse bearing two KB tumors (one on each flank) was injected with 80 nmol PP<sub>MMP7</sub>B intravenously by the tail vein, whereas the second mouse was kept as a drug-free control. The activation of PP<sub>MMP7</sub>B in the first mouse was continuously monitored by *in vivo* fluorescence imaging. As shown in Fig. 6, immediately after injection (Fig. 6B and b), no fluorescence increase was observed anywhere compared with the “prescan” images (Fig. 6A and a) or the drug-free mouse (Fig. 6G and g). This confirmed that PP<sub>MMP7</sub>B is optically silent in its native state because of fluorescence quenching by BHQ3. However, fluorescence signals started to increase in KB tumors 20 min after injection and reached the highest level at 3 h (Fig. 6C and c), clearly indicating PP<sub>MMP7</sub>B activation presumably by MMP7. At this time point, the PDT treatment was given to the tumor on the left flank, whereas the tumor on the opposite side served as a dark control. The drug-free mouse was treated in the same way. One hour after PDT treatment (4 h after injection) (Fig. 6D and d), the treated tumor in the drugged animal became edematous, whereas the untreated tumor in the drugged animal and both tumors in the drug-free mouse showed no changes in size or fluorescence signal. Three days after PDT, the treated tumor in the drugged mouse was reduced in size (Fig. 6E and e), and 30 days after PDT, it completely regressed without any sign of regrowth (Fig. 6F), whereas the untreated tumor (Fig. 6F) and both tumors in the drug-free mouse (Fig. 6H) continued to grow. These data clearly demonstrate that PP<sub>MMP7</sub>B accumulates and can be photodynamically activated in MMP7<sup>+</sup> tumors.

## Discussion

The present report describes the full implementation of the PMB concept, including detailed synthesis of a MMP7-specific PMB

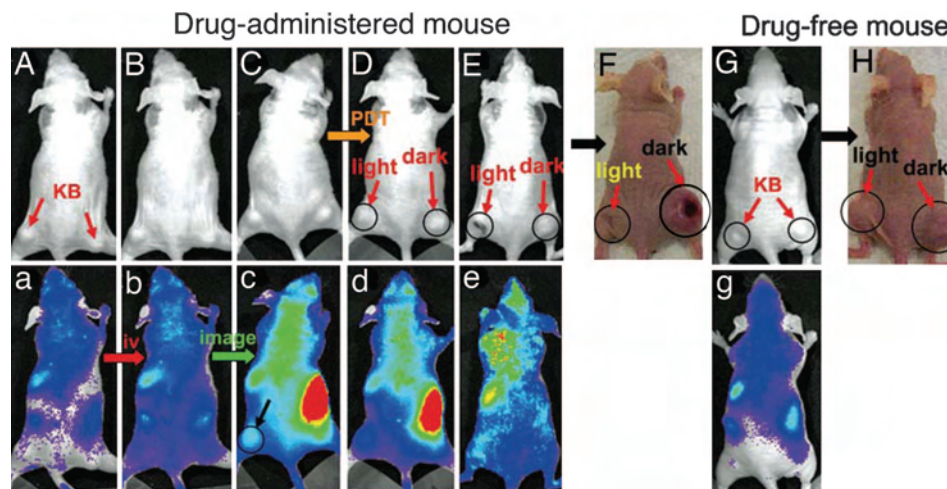


**Fig. 6.** *In vivo* images of mice showing bright field (A–H) and fluorescence (a–e and g). (A–E) PP<sub>MMP7</sub>B-administered mouse (A, prescan; B, 10 min after i.v. injection; C, 3 h after i.v. injection; D, 5 h after i.v. injection and 1 h after PDT; E, 3 d after PDT). (F) Photograph of PP<sub>MMP7</sub>B-administered mouse (30 d after PDT). Light-treated tumors are marked as “light” and nonlight-treated tumors as “dark.” (G) Drug-free mouse (prescan). (H) Photograph of drug-free mouse (30 d after PDT) with light-treated tumor marked as “light” and nonlight-treated tumor as “dark.”

(PP<sub>MMP7B</sub>), the systematic validation of its utility as an activatable PDT agent *in vitro*, and the initial demonstration of its feasibility *in vivo*. We have validated this PP<sub>MMP7B</sub> construct, because keeping Pyro and BHQ3 in close proximity using the self folding of an MMP7-specific peptide linker results in effective <sup>1</sup>O<sub>2</sub> quenching (94%), whereas the same concentration of PP<sub>MMP7</sub> mixed with free BHQ3 (1:1 molar ratio) did not show any <sup>1</sup>O<sub>2</sub> quenching. Furthermore, when the peptide linker was specifically cleaved by MMP7, the quenched <sup>1</sup>O<sub>2</sub> was completely restored, and the <sup>1</sup>O<sub>2</sub> production was similar to that of mixture of PP<sub>MMP7</sub> and BHQ3. Thus, this PMB provided a very high degree of control of the PS's ability to produce <sup>1</sup>O<sub>2</sub> in response specifically to activation by a cancer-associated biomarker (MMP7).

While this manuscript was under preparation, Choi *et al.* (28) reported that a chlorin *e*<sub>6</sub>-containing polymer sensitive to cathepsin B can be used for controlling <sup>1</sup>O<sub>2</sub> and PDT activity. However, this was not the first time that a protease-specific molecule has been used to control <sup>1</sup>O<sub>2</sub> (9), and the approach is distinctively different from ours in that it used PS self quenching to control <sup>1</sup>O<sub>2</sub> production, with both the <sup>1</sup>O<sub>2</sub> quenching and activation efficiencies inversely depending on the degree of PS substitution on the poly-L-lysine sequence. Thus, the higher degree of PS substitution leads to the higher <sup>1</sup>O<sub>2</sub> quenching efficiency. Meanwhile, the higher degree of PS substitution will also decrease the <sup>1</sup>O<sub>2</sub> activation efficiency, because it decreases the availability of the cathepsin B recognition sites.

NIR fluorescence imaging (NIRF) and PDT have become effective components in the armamentarium of cancer imaging and therapies, and their utility could be greatly increased if techniques can be devised to enhance the specificity of delivery of the dyes to the tumor tissue and to activate them, particularly in the NIR wavelength range, to treat deep-seated tumors. Our work is intended to achieve both goals by using a sequence-specific peptide as the triggering device for activating the NIRF and PDT only in targeted cells, thus significantly enhancing the tumor-to-tissue contrast of NIRF and potentially improving the therapeutic ratio of PDT. Thereby, the tumor selectivity of PDT treatment will no longer depend solely on how selectively the PS can be delivered to cancer cells. Rather, it will be based on how selective a specific biomarker is to cancer cells, and how selective the interaction of the PMB is to this biomarker.

The PMB described here is activated specifically by MMP7, a tumor-associated protease. However, the same principle could be applied to other activation schemes that could separate the PS from its quencher. For example, this concept could be applied to nucleic acid-based molecular beacons, in which a tumor-specific mRNA can hybridize with the complementary DNA sequence between the PS and a <sup>1</sup>O<sub>2</sub> quencher to trigger PDT-induced cell kill.<sup>11</sup> It also could be applied to DNA sequence-controlled on-and-off switchable <sup>1</sup>O<sub>2</sub> sensitizers (10), in which a PS and a <sup>1</sup>O<sub>2</sub> quencher are kept in close contact in the "off-state" by DNA-programmed assembly, and the PS will be activated after releasing from the quencher through a process of competitive DNA hybridization. Alternatively, it could be applied to a phospholipase-activated optical probe, in which a tumor-associated phospholipase is used as the triggering device.<sup>\*\*</sup> Hence, this approach could have potential to generate a wide range of clinically useful strategies to enhance the specificity and efficacy of PDT to treat cancer and, by analogy, also other pathologies. In addition, our approach of achieving the high tumor selectivity of PDT treatment through controlling the PS's ability to produce <sup>1</sup>O<sub>2</sub> could significantly minimize PDT complications by protecting adjacent nontargeted tissues from pho-

todamage, making PDT a safer and more selective clinical technique.

## Materials and Methods

UV-vis and fluorescence spectra were recorded on a PerkinElmer (Boston, MA) Lambda 20 spectrophotometer and LS-50B spectrofluorometer, respectively. MALDI-TOF mass spectroscopy was performed on an Applied Biosystems (Foster City, CA) Voyager DE system. Reverse-phase analytical HPLC was performed on a Zorbax 300SB-C8 column using a Waters (Milford, MA) 600 Controller with a 2996 photodiode array detector (HPLC method; solvent A, 0.1% TFA and water; solvent B, acetonitrile; gradient, from 80% of A and 20% of B to 100% of B over 40 min; flow rate, 1.0 ml/min). Confocal microscopy images were acquired by using a Zeiss (Heidelberg, Germany) LSM510 META laser-scanning confocal microscope, and *in vivo* fluorescence images were acquired on a Xenogen IVIS imager (Hopkinton, MA).

The peptide synthesis reagents for activation, 1-hydroxybenzotriazole and *O*-(benzotriazol-1-yl)-*N,N,N',N'*-tetramethyluronium hexafluorophosphate, were purchased from ACROS (Morris Plains, NJ) and Sigma (St. Louis, MO), respectively. Sieber amide resins, and all of the *N*- $\alpha$ -Fmoc-protected amino acids were purchased from Novabiochem (San Diego, CA).

### Synthesis of PP<sub>MMP7B</sub> (Fig. 1B). Fmoc-GPLGLAR(Pbf)K(Mtt)-Sieber resin

(1). A peptide of Fmoc-GPLGLAR(Pbf)K(Mtt)-Sieber resin (1) was synthesized by manual Fmoc solid-phase peptide synthesis protocol by using commercially available *N*- $\alpha$ -Fmoc-protected amino acids, Sieber amide resin as a solid support, and *O*-(benzotriazol-1-yl)-*N,N,N',N'*-tetramethyluronium hexafluorophosphate/1-hydroxybenzotriazole as a carboxyl-group activating agent.

**Pyro-GPLGLAR(Pbf)K(Mtt)-Sieber resin (2).** After the last Fmoc group was removed from the peptide-resin (1) with 20% piperidine in *N,N*-dimethylformamide, the resin was washed with 1-methyl-2-pyrrolidinone and pyropheophorbide  $\alpha$  acid was coupled to the *N*-terminal glycine of the peptide-resin [Pyro acid/1-hydroxybenzotriazole/*O*-(benzotriazol-1-yl)-*N,N,N',N'*-tetramethyluronium hexafluorophosphate/peptide 3:3:3:1]. The reaction was shaken under argon overnight at room temperature, after which the green resin was washed and dried to give Pyro-GPLGLAR(Pbf)K(Mtt)-Sieber resin (2).

**Pyro-GPLGLAR(Pbf)K( $\epsilon$ -NH<sub>2</sub>) (3).** This peptide resin (2) was treated with 3% TFA and 5% triisopropylsilane (Tis) in dichloromethane for 1 h at room temperature to cleave the peptide sequence from the Sieber resin and deprotect the Mtt group on the C-terminal of lysine. After removing the cleaved solid resin by filtration, the filtrate was concentrated and precipitated by adding anhydrous ether to give Pyro-GPLGLAR(Pbf)K( $\epsilon$ -NH<sub>2</sub>) (3). It was further washed by ether and dried under high vacuum. A part of Pyro-GPLGLAR(Pbf)K( $\epsilon$ -NH<sub>2</sub>) (3) was treated by 95% TFA and 5% Tis to remove the Pbf-protected group on arginine and was afterward purified by HPLC to obtain Pyro-GPLGLARK( $\epsilon$ -NH<sub>2</sub>) (PP<sub>MMP7</sub>), which was used as positive control (without quencher moiety).

**Pyro-GPLGLARK(BHQ3) (4).** The Pyro peptide (3) (10 mg, 6  $\mu$ mol) was dissolved in 200  $\mu$ l of anhydrous DMSO with 1% of *N,N*-diisopropylethyl amine and reacted with BHQ3-NHS (4.7 mg, 6  $\mu$ mol, Biosearch Technologies, Novato, CA) for 3 h under argon. The reaction was stopped by precipitation with 2 ml of ether to give Pyro-GPLGLAR(Pbf)K(BHQ3). This peptide was treated by 95% TFA and 5% triisopropylsilane to remove the Pbf-protected group on arginine and was afterward purified by HPLC to obtain Pyro-GPLGLARK(BHQ3) (PP<sub>MMP7B</sub>) (4).

**PP<sub>MMP7B</sub> Activation by MMP7 in Buffer.** An MMP7 fluorescence assay kit, containing the active form of human MMP7 enzyme ( $M_r$  = 20,400), MMP7 inhibitor NNGH (8) ( $M_r$  = 316.4), and MMP7 fluorogenic substrate Ac-PLG-[2-mercapto-4-methyl-pentanoyl]-

<sup>1</sup>Chen, J., Stefflova, K., Niedra, M.J., Wilson, B.C., Zheng, G. (2004) *Mol Imag* 3:277 (abstr).

<sup>\*\*</sup>Mawn, T.M., Popov, A.V., Milkevitch, M., Kim, S., Zheng, G., Delikatny, E.J. (2006) *Mol Imag* 5:315 (abstr).

LG-OC<sub>2</sub>H<sub>5</sub> (23), was purchased from Biomol (Plymouth Meeting, PA). The buffer used for cleavage contains 50 mM Hepes, 10 mM CaCl<sub>2</sub>, 0.05% Brij 35, pH 7.5. Before each cleavage study, the activity of MMP7 was confirmed by its ability to cleave the fluorogenic substrate Ac-PLG-[2-mercapto-4-methyl-pentanoyl]-LG-OC<sub>2</sub>H<sub>5</sub>. The PP<sub>MMP7</sub>B sample was prepared as 5 ml of 0.4 μM stock solution in the buffer. The composition of each sample was as follows: (i) PP<sub>MMP7</sub>B+MMP7: 1 ml of PP<sub>MMP7</sub>B stock solution with 1 μl of MMP7 (0.45 g/liter); (ii) PP<sub>MMP7</sub>B+MMP7+inhibitor: 1 ml of PP<sub>MMP7</sub>B stock solution with 2 μl of inhibitor (2 g/liter) and 1 μl of MMP7 (0.45 g/liter) (the molar ratio of PP<sub>MMP7</sub>B: MMP7: inhibitor was 50:1:1,500); (iii) PP<sub>MMP7</sub>B+MMP2: 1 ml of PP<sub>MMP7</sub>B stock solution with 1 μl of MMP2 (0.50 g/liter); and (iv) C-PPB+MMP7: 1 ml of 0.4 μM control C-PPB with 1 μl of MMP7 (0.45 g/liter). The fluorescence of these four solutions was monitored in real time by fluorescence spectroscopy at 37°C with an excitation wavelength of 660 nm and emission at 674 nm. After 2 h, the cleavage solutions were analyzed by HPLC to collect the cleaved fragments for identification by using MALDI-TOF.

**<sup>1</sup>O<sub>2</sub> Measurement.** PDT-generated <sup>1</sup>O<sub>2</sub> was quantified in solutions of PP<sub>MMP7</sub>, PP<sub>MMP7</sub>+BHQ3, PP<sub>MMP7</sub>B, PP<sub>MMP7</sub>B+MMP7, and PP<sub>MMP7</sub>B+MMP7+MMP7 inhibitor, by directly measuring its NIR luminescence at 1,270 nm by using an instrument and technique that have been described (29). Briefly, a 10 ns pulsed 523-nm laser excited the solution, and the luminescence spectrum was sampled, after rejection of PS fluorescence, by using a set of interference filters and a high-sensitivity NIR photomultiplier tube operating in the time-resolved single photon-counting mode.

**Cell Lines.** KB cells (human nasopharyngeal epidermoid carcinoma cells, high MMP7 expression, MMP7<sup>+</sup>) and BT20 cells (a human breast cancer cell line, lack of MMP7 expression, MMP7<sup>-</sup>) (26) were purchased from American Type Culture Collection (Manassas, VA). Both KB and BT-20 cells were cultured in MEM supplemented with 2 mM L-glutamine/17.9 mM sodium bicarbonate/0.1 mM nonessential amino acids/1.0 mM sodium pyruvate/10% FBS. All cells were grown at 37°C in a humidified atmosphere containing 5% CO<sub>2</sub>.

**Confocal Microscopy.** KB and BT20 cells were grown for 2 d in four-well Lab-Tek (Naperville, IL) chamber slides. MEM containing 60 μM PP<sub>MMP7</sub>B or control C-PPB was added, and the cells were incubated for 5 h at 37°C. The incubation medium was removed and run on HPLC, while the cells were washed five

times with ice-cold PBS and then fixed for 20 min with 1% formaldehyde in PBS at room temperature. The chamber slides were then imaged by confocal microscopy with 633 nm excitation and >650 nm detection.

**MTT Assay.** KB and BT20 cells were grown for 2 d in 96-well plates. Experiments were started, after one quick wash with ice-cold PBS buffer, by addition of 100 μl of cell growth medium containing the indicated amounts of PP<sub>MMP7</sub>B and control C-PPB. After 16 h incubation at 37°C with 5% CO<sub>2</sub>, the cells were washed twice with ice-cold PBS buffer, and then 100 μl of cell growth medium was added. PDT treatment was performed by using a 670-nm continuous wavelength laser with one of three different light fluences (1, 5, or 7.5 J/cm<sup>2</sup>). The cells were allowed to continue growth for 24 h, at which time the MTT tracer, 3-(4,5-dimethylthiazol-2-yl)-2,5-diphenyltetrazolium bromide (Invitrogen) was added to the medium at 0.5 mg/ml. Two hours later, the medium was removed and replaced with 150 μl of 1:1 DMSO/70% isopropanol in 0.1 M HCl. The absorbance at 570 nm was measured on a Bio-Tek ELx model 800 (MTX Lab System, Vienna, VA).

**In Vivo Imaging and PDT Treatment.** Two nude mice were inoculated with 10<sup>7</sup> KB cells on both left and right flanks, and the tumors were grown for 5 d with the mice maintained on a low-fluorescence diet. “Prescan” images were obtained on the Xenogen (Hopkinton, MA) imager with a Cy 5.5 filter (λ<sub>ex</sub> = 615–665 nm, λ<sub>em</sub> = 695–770 nm). One mouse was anesthetized afterward and injected intravenously with 80 nmol PP<sub>MMP7</sub>B by tail vein, whereas the other was kept as a drug-free control. The former was then continually scanned to monitor the increase of fluorescence in tumor over time. Very strong fluorescence was observed in the KB tumor after 3 h. At this time, the left tumor on both the drug-administered and drug-free mice was treated by using surface irradiation (1.2 cm<sup>2</sup>) from a 670 nm laser to a light dose of 135 J/cm<sup>2</sup> over 30 min, whereas the right tumors were kept as dark controls. The mice were then monitored daily in the fluorescence imager over 30 d.

This study was supported by U.S. DOD Breast Cancer Research Program DAMD17-03-1-0373 and National Institutes of Health Grant R21-CA95330, the Oncologic Foundation of Buffalo, the Joey and Toby Tanenbaum/Brazilian Ball Chair in Prostate Cancer Research Princess Margaret Hospital (G.Z.), and the National Cancer Institute of Canada (B.C.W.).

- Dougherty TJ, Gomer CJ, Henderson BW, Jori G, Kessel D, Korbelik M, Moan J, Peng Q (1998) *J Natl Cancer Inst* 90:889–905.
- Pinthus JH, Bogaards A, Weersink R, Wilson BC, Trachtenberg J (2006) *J Urol* 175:1201–1207.
- Chen B, Pogue BW, Hasan T (2005) *Exp Opin Drug Del* 2:477–487.
- Sharman WM, van Lier JE, Allen CM (2004) *Adv Drug Del Rev* 56:53–76.
- Zhang M, Zhang Z, Blessington D, Li H, Busch TM, Madrak V, Miles J, Chance B, Glickson JD, Zheng G (2003) *Bioconjug Chem* 14:709–714.
- Zheng G, Li H, Zhang M, Lund-Katz S, Chance B, Glickson JD (2002) *Bioconjug Chem* 13:392–396.
- Stefflova K, Li H, Chen J, Zheng G (2007) *Bioconjug Chem* 18:379–388.
- MacPherson LJ, Bayburt EK, Capparelli MP, Carroll BJ, Goldstein R, Justice MR, Zhu L, Hu S, Melton RA, Fryer L, et al. (1997) *J Med Chem* 40:2525–2532.
- Chen J, Stefflova K, Niedre MJ, Wilson BC, Chance B, Glickson JD, Zheng G (2004) *J Am Chem Soc* 126:11450–11451.
- Clo E, Snyder JW, Voigt NV, Ogilby PR, Gothelf KV (2006) *J Am Chem Soc* 128:4200–4201.
- Hirakawa K, Kawanishi S, Hirano T (2005) *Chem Res Toxicol* 18:1545–1552.
- McCarthy JR, Perez JM, Bruckner C, Weissleder R (2005) *Nano Lett* 5:2552–2556.
- McDonnell SO, Hall MJ, Allen LT, Byrne A, Gallagher WM, O’Shea DF (2005) *J Am Chem Soc* 127:16360–16361.
- Snyder JW, Lambert JD, Ogilby PR (2006) *Photochem Photobiol* 82:177–184.
- Matayoshi ED, Wang GT, Krafft GA, Erickson J (1990) *Science* 247:954–958.
- Thornberry NA, Lazebnik Y (1998) *Science* 281:1312–1316.
- Overall CM, Kleinfeld O (2006) *Nat Rev* 6:227–239.
- Brooks PC, Stromblad S, Sanders LC, von Schalscha TL, Aimes RT, Stetler-Stevenson WG, Quigley JP, Cheresch DA (1996) *Cell* 85:683–693.
- Shiomi T, Okada Y (2003) *Cancer Metast Rev* 22:145–152.
- Leinonen T, Pirinen R, Bohm J, Johansson R, Ropponen K, Kosma VM (2006) *Lung Cancer* 51:313–321.
- MacDonald IJ, Morgan J, Bellnier DA, Paszkiewicz GM, Whitaker JE, Litchfield DJ, Dougherty TJ (1999) *Photochem Photobiol* 70:789–797.
- Stefflova K, Chen J, Marotta D, Li H, Zheng G (2006) *J Med Chem* 49:3850–3856.
- Knight CG, Willenbrock F, Murphy G (1992) *FEBS Lett* 296:263–266.
- Weingarten H, Feder J (1985) *Anal Biochem* 147:437–440.
- Weingarten H, Martin R, Feder J (1985) *Biochemistry* 24:6730–6734.
- Giambardi TA, Grant GM, Taylor GP, Hay RJ, Maher VM, McCormick JJ, Klebe RJ (1998) *Matrix Biol* 16:483–496.
- Kessel D, Luguya R, Vicente MG (2003) *Photochem Photobiol* 78:431–435.
- Choi Y, Weissleder R, Tung CH (2006) *Cancer Res* 66:7225–7229.
- Niedre MJ, Secord AJ, Patterson MS, Wilson BC (2003) *Cancer Res* 63:7986–7994.

# Using the Singlet Oxygen Scavenging Property of Carotenoid in Photodynamic Molecular Beacons to Minimize Photodamage to Non-targeted Cells

Juan Chen<sup>1,2</sup>, Mark Jarvi<sup>1</sup>, Pui-chi Lo<sup>1</sup>, Klara Stefflova<sup>3</sup>, Brian C. Wilson<sup>1</sup> and Gang  
Zheng<sup>1,2,3</sup>

<sup>1</sup>Department of Medical Biophysics, Ontario Cancer Institute and University of  
Toronto, Toronto, ON, M5G 1L7, Canada, <sup>2</sup>Departments of Radiology, <sup>3</sup>Chemistry,  
University of Pennsylvania, Philadelphia, PA, 19104, USA

<sup>3</sup>Correspondence addressed to: Dr. Gang Zheng, MaRS Center, TMDT 5-363, 101  
College St., Toronto, ON, M5G 1L7, Canada, email: gang.zheng@uhnres.utoronto.ca

## Summary

We recently introduced the concept of photodynamic molecular beacons (PMB) for selective control of photodynamic therapy (PDT). The PMB consists of a peptide linker that is sequence specific to a cancer-associated protease. A photosensitizer (PS) and a singlet oxygen ( $^1\text{O}_2$ ) quencher are conjugated to the opposite ends of this linker. Proximity of the PS and quencher can efficiently inhibit  $^1\text{O}_2$  generation. In the presence of a targeted protease, the substrate sequence is cleaved and the PS and quencher will separate so that the PS can be photo-activated. There are two ways to optimize the PMB selectivity to cancer cells. The first is to increase the protease specificity to targeted cells and the second is to minimize the phototoxicity of intact (uncleaved) PMBs in non-targeted (normal) cells. Carotenoids (CARs) are well known in nature for their role in quenching excited states of PS and in directly scavenging  $^1\text{O}_2$ . The purpose of this study is to evaluate whether the CAR with dual quenching modes (PS excited states

deactivation and  $^1\text{O}_2$  scavenging) can be used to minimize the photodamage of intact PMBs to non-targeted cells. Thus, we synthesized a beacon (PPC) with a caspase-3 cleavable peptide linking a PS and a CAR quencher. It was confirmed that CAR deactivates the PS excited states and also directly scavenges  $^1\text{O}_2$ . Moreover, the *in vitro* PDT response showed that CAR completely shuts off the photodynamic effect in non-targeted HepG<sub>2</sub> cells, while PS without CAR (control) remains highly potent even at a much lower (30-fold) dose.

**Keywords:** Photodynamic therapy (PDT), molecular beacon, photodynamic molecular beacon (PMB), carotenoid (CAR), singlet oxygen ( $^1\text{O}_2$ ), quenching, scavenging, pyropheophorbide (Pyro)

## Introduction

Photodynamic therapy (PDT) is a cancer treatment modality involving the combination of light, a photosensitizer (PS) and molecular oxygen<sup>1</sup>. Each factor is ineffective by itself, but when the PS is irradiated with light of an appropriate wavelength in the presence of oxygen, cytotoxic reactive oxygen species, mainly singlet oxygen ( $^1\text{O}_2$ ), are produced<sup>1, 2</sup>. We recently introduced a new concept, ‘photodynamic molecular beacons (PMB)’, capable of precise control of the ability of PS to produce  $^1\text{O}_2$  by responding to specific cancer-associated biomarkers<sup>3, 4</sup>. Briefly, this PMB comprises a disease-specific peptide linker, a PS and a  $^1\text{O}_2$  quencher, so that the PS’s photodynamic toxicity is silenced until the peptide linker is cleaved by a tumor-associated protease. Thus, the PDT selectivity will no longer solely depend on how selectively the PS can be delivered to cancer cells. Rather, it will depend on how specific this protease is to

targeted cancer cells and how selective the PMB is to this protease. In addition, the PDT selectivity may also depend on how completely the PMB photoactivity is silenced, since any residual  $^1\text{O}_2$  production from intact PMB could lead to phototoxicity to non-targeted (normal) cells.

In our previous matrix metalloproteinase-7 (MMP7)-triggered PMB (PP<sub>MMP7</sub>B), a black hole quencher 3 (BHQ3) was used as the quencher molecule to inhibit the  $^1\text{O}_2$  production of pyropheophorbide (Pyro)-based PS by the deactivation of Pyro's excited singlet state, thus reducing the production of Pyro's excited triplet state and ultimately leading to lower  $^1\text{O}_2$  production. Using this PMB, we demonstrated that the MMP7-triggered production of  $^1\text{O}_2$  is both efficient and specific. More importantly, this study confirmed MMP7-mediated photodynamic cytotoxicity in targeted cancer cells *in vitro* and *in vivo*, thus validating the core principle of the PMB concept that selective PDT-induced cell death can be achieved by exerting precise control of the PS's ability to produce  $^1\text{O}_2$  in targeted cancer cells in response to specific cancer-associated biomarkers<sup>4</sup>.

In this study, we are looking for ways to further improve our current PMB design from a new angle. Specifically, we examine the role of quenchers in minimizing the photodamage of intact (uncleaved) PMB molecules to non-targeted (normal) cells due to residual  $^1\text{O}_2$  production.

Based on the  $^1\text{O}_2$  production mechanism in type-II photosensitization process,  $^1\text{O}_2$  is produced by energy transfer from the PS excited triplet state, generated by intersystem crossing from the PS excited singlet state. Thus,  $^1\text{O}_2$  quenching can be potentially achieved via three pathways: 1) by deactivating the PS singlet state, 2) by deactivating

the PS triplet state, and/or 3) by directly scavenging  $^1\text{O}_2$  (Figure 1). Carotenoids (CARs) are well known as antioxidants in animals and photoprotective agents in the photosynthetic system of plants<sup>5</sup>. These important biofunctions are due to its ability to: A) quench the excited triplet state of chlorophyll (or other porphyrin-based molecules), inhibiting production of harmful  $^1\text{O}_2$ , B) scavenge  $^1\text{O}_2$ , protecting the photosynthetic apparatus<sup>6, 7</sup>, C) absorb light around 500 nm and transfer this excitation energy to chlorophyll as part of light harvesting<sup>8</sup>, and D) quench radical species that could potentially react with various biomolecules<sup>5</sup>. In order to mimic the function of CAR in natural photosynthetic systems, carotenoporphyrins have been synthesized, in which the carotenoid analogue was directly conjugated to either meso-tetraphenyl porphyrins<sup>9, 10</sup>, pheophorbide<sup>11</sup> or hematoporphyrin<sup>12</sup>. These carotenoporphyrins were found to have very good photoprotective properties. Hence, CAR with multiple modes of  $^1\text{O}_2$  quenching could be an ideal quencher molecule for minimizing the phototoxicity of PMB to non-targeted cells.

We have synthesized a CAR-based PMB, named 'PPC', containing a CAR as the quencher, a Pyro as the PS and a caspase-3 cleavable peptide sequence, *GDEVDGSGK*, as the linker (Figure 1). In an earlier communication<sup>3</sup>, we have demonstrated in solution that PPC exerts selective control of  $^1\text{O}_2$  production in response to caspase-3-specific cleavage. Here, we report the detailed chemical synthesis, characterization and evaluation of this PPC beacon, particularly the multiple roles of the CAR quencher. More importantly, we investigated the role of CAR in minimizing the photodamage from intact (uncleaved) PMB in non-targeted (normal) cells. For this purpose, caspase-3 was selected as a model target because it is a well-known marker for cell apoptosis<sup>13</sup> and is not

expressed in viable HepG<sub>2</sub> cells, thus minimizing the potential cleavage of PPC in non-targeted cells.

## **Results and discussion**

### **Synthesis and characterization of the PPC beacon**

The PPC beacon was synthesized following the detailed protocol shown in Figure 2. The final product was purified by HPLC. Its structure was confirmed by UV/vis spectroscopy (Figure 2B), showing characteristic peaks for Pyro at 412.2, 668.2 nm and CAR at 472.2, 500.2 nm, as well as by ESI mass spectrometry (ESI-MS) (Figure 2C: calc: 1895.24, found 1895.40).

### **Validation of caspase-3-triggered cleavage of PPC**

The specific cleavage of PPC by caspase-3 has already been demonstrated previously<sup>3</sup>, although there were small “debris” peaks in the HPLC chromatography due to impurities in the PPC used. Here, an HPLC-purified PPC was used to further validate the unique cleavage of PPC by caspase-3. The HPLC-purified PPC was incubated in buffer for 3 h either alone, with the addition of caspase-3 or with caspase-3 plus inhibitor (caspase-3: PPC: inhibitor =1:100:2400). The samples were then analyzed by HPLC coupled to UV-Vis spectroscopy and ESI-MS. As shown in Figure 3Aii, caspase-3 cleaved 80% of PPC (HPLC retention time: RT=14.70min) into two fragments corresponding, respectively, to a Pyro moiety (RT=7.64min) and a CAR moiety (RT=11.95min) based on their absorption characteristics (Figure 3Bii). Importantly, this specific cleavage was further confirmed by ESI-MS: the two fragments were identified as Pyro-GDEV<sup>-</sup>D-COO<sup>-</sup> (Calc.1050.12, found 1050.7) (Figure 3Cii) and NH<sub>2</sub>-GSGK-CAR

(Calc. 862.54, found 862.8) (Figure 3Ciii). On the other hand, no detectable cleavage was observed in PPC only (Figure 3Ai) or in PPC+caspase-3+inhibitor (Figure 3Aiii). These data demonstrate that caspase-3 specifically induces PPC cleavage at the cleavage site between D and G, the known cleavage site<sup>14</sup>.

### **Validation of caspase-3-triggered <sup>1</sup>O<sub>2</sub> activation and determination of CAR quenching mechanisms**

Subsequently, the <sup>1</sup>O<sub>2</sub> near-infrared (1270 nm) luminescence of PPC in buffer, PPC+caspase-3, and PPC+caspase-3+inhibitor were measured. PP (Pyro with peptide linker but without the CAR moiety) was used as a positive control to quantify the photophysical properties of Pyro and all experimental samples were prepared at the same molar concentration of Pyro. As shown in Figure 4A, PPC produced 78% less <sup>1</sup>O<sub>2</sub> luminescence than PP, suggesting that attachment of CAR to Pyro via a short peptide linker effectively inhibited Pyro <sup>1</sup>O<sub>2</sub> production. Moreover, addition of caspase-3 to PPC (1: 100 molar ratio) resulted in a 3-fold increase of <sup>1</sup>O<sub>2</sub> production, an effect that was completely blocked by co-incubation with caspase-3 inhibitor (24-fold of PPC concentration), confirming that caspase-3 specifically activated the PPC <sup>1</sup>O<sub>2</sub> production. However, this caspase-3-induced PPC cleavage did not restore the <sup>1</sup>O<sub>2</sub> production completely. Compared with PP, PPC+caspase-3 showed a 30% decrease in <sup>1</sup>O<sub>2</sub> luminescence counts (Figure 4A). This decrease was similar to the corresponding decrease in its <sup>1</sup>O<sub>2</sub> lifetime (Figure 4B). Taken together with the result that 65% of fluorescence was quenched in intact PPC (Figure 4C), these data suggest that the <sup>1</sup>O<sub>2</sub> inhibition in PPC is caused both by deactivation of the PS excited states and by direct <sup>1</sup>O<sub>2</sub> scavenging.

In order to address how CAR acts in PPC and how importantly it serves as a  $^1\text{O}_2$  scavenger, we subsequently measured and compared the fluorescence and  $^1\text{O}_2$  luminescence of PP versus PP + free CAR at different molar ratios. As shown in Figure 4C, unlike PPC that shows 65% fluorescence quenching, adding free CAR to the PP solution had no measurable effect on the fluorescence of Pyro, even at a 10-fold higher concentration (CAR:Pyro=10:1 molar ratio), indicating that free CAR does not quench the Pyro singlet state. However, free CAR did reduce the  $^1\text{O}_2$  luminescence of PP by 30% at a 1:1 molar ratio, and this was CAR concentration dependent (Figure 4D). Furthermore, CAR concentration dependent decreases in the  $^1\text{O}_2$  lifetime (Figure 4E) and the Pyro triplet state lifetime (Figure 4F) were also observed. These findings demonstrate that free CAR acts both as a  $^1\text{O}_2$  scavenger and Pyro triplet state quencher, rather than as a Pyro singlet state quencher. This partiality in quenching is most likely related to the difference in lifetimes. The relatively short lived PS singlet state ( $\sim 10^{-9}$ s) is relatively impervious to quenching from free CAR compared to the longer lived PS triplet state and  $^1\text{O}_2$  ( $\sim 10^{-7} - 10^{-6}$  s). More importantly, PPC induced much more effective fluorescence and  $^1\text{O}_2$  quenching than the mixture of PP + free CAR, even with 10-fold higher concentration of CAR (Figure 4C, D). This indicates that CAR inhibits  $^1\text{O}_2$  production in PPC primarily through non-radiative quenching of the Pyro singlet state, with a smaller fraction due to quenching of the Pyro triplet state and scavenging of  $^1\text{O}_2$  generated from any unquenched Pyro.

As shown in Figure 4A, the  $^1\text{O}_2$  luminescence intensity from PPC +caspase-3 was similar to that of PP + free CAR (1:1 molar ratio), suggesting that after proteolytic cleavage the cleaved CAR can still quench the Pyro triplet state and scavenge  $^1\text{O}_2$ .

Consequently, in targeted tumor cells, if this cleaved CAR cannot diffuse after cleavage, it could decrease the PDT efficacy of PPC. However, this could be addressed by slightly increasing the concentration of PPC to compensate for the residual  $^1\text{O}_2$  scavenging. On the other hand, CAR-mediated  $^1\text{O}_2$  scavenging could act as an additional photoprotective role in non-targeted cells by scavenging the residual  $^1\text{O}_2$  production, thus minimizing photodamage.

All of the above experiment were repeated in triplicate and the  $^1\text{O}_2$  production of PP, PP+caspase-3 and PP +free CAR were all statistically different from PPC ( $p < 0.05$ ), whereas there was no statistically significant difference between PPC and PPC+caspase-3 +inhibitor.

### **Lack of PPC phototoxicity in non-targeted cells**

To evaluate the effects of intact PPC molecules towards non-targeted cells, caspase-3 was selected as the trigger because it is a well-known cell apoptosis marker and is not expressed in viable HepG<sub>2</sub> cells, thus eliminating the potential cleavage of PPC in non-targeted cells.

HepG<sub>2</sub> cells incubated with PP and PPC at various concentrations were subjected to PDT using different light doses and their post-PDT viability was quantified by MTT assay. As shown in Figure 5, cells incubated with either PP or PPC without light treatment showed similar viability as control cells (no drug/ no light), demonstrating minimal dark cytotoxicity of PP and PPC for the given concentrations. Upon light exposure, PP killed cells at a very low concentration and reduced the cell viability in a drug- and light-dose-dependent manner. With a light exposure of  $7.5\text{J}/\text{cm}^2$ ,  $0.5\mu\text{M}$  PP reduced the cell viability to less than 10%. However, PPC did not induce any measurable

cell phototoxicity even at 30-fold greater concentrations (15 $\mu$ M). This near 100% photoprotection of intact PPC was higher than expected based on the data obtained in solution, where PPC produced only 4.3-fold less  $^1\text{O}_2$  than PP (Figure 4). This suggests that CAR may act not only as a  $^1\text{O}_2$  quencher, but also has some other, undetermined photoprotective role(s). For example, it may quench other radical species, thus inhibiting their biomolecular reactions. This issue will be investigated in future studies.

## Conclusion

Using this caspase-3 cleavable PPC beacon, we have validated that CAR, as a quencher molecule in PMB, turned off the  $^1\text{O}_2$  production of Pyro by both quenching the PS excited states and directly scavenging  $^1\text{O}_2$ . As a result, it could lose some PDT potency of PPC toward targeted cells. However, as a “trade off”, it should lead to a very high level of “protection” for non-targeted cells. Thus, using CAR for PMB could potentially improve the PDT selectivity. It is planned to test the photoactivation of CAR-based PMB next *in vitro* and *in vivo* by targeting a tumor-associated biomarker, such as MMP7.

## Experimental

UV-vis and fluorescence spectra were recorded with the Varian Cary 50 UV/vis spectrophotometer (Lake Forest, CA, USA) and HORIBA Jobin Yvon FluoroMax®-4 spectrofluorometer (Edison, NJ, USA), respectively. Reverse-phase analytical HPLC was performed on a Zorbax 300SB-C8 column using a Waters 2695 controller with a 2996 photodiode array detector and Waters ZQ™ mass detector (HPLC method: solvent A=0.1% trifluoroacetic acid (TFA); solvent B=acetonitrile; solvent C=methanol;

gradient: from 60%A+40%B to 10%A+90%B in the first 20min, then to 90%B+10%C for another 10min, finally to 80%B+20%C for 10min; flow rate: 1.0mL/min).

The peptide synthesis reagents for activation, 1-hydroxybenzotriazole (HOBt) and *O*-(Benzotriazol-1-yl)-*N,N,N',N'*-tetramethyluronium hexafluorophosphate (HBTU), were purchased from ACROS (Morris Plains, NJ, USA) and Sigma-Aldrich (St. Louis, MO, USA) respectively. The Sieber amide resins and all of the *N*- $\alpha$ -Fmoc protected amino acids were purchased from Novabiochem (San Diego, CA, USA).

### **Synthesis of Pyropheophorbide-Peptide-Carotenoid (PPC) (Figure3)**

#### *Pyropheophorbide-Peptide-Carotenoid (PPC)*

*Fmoc-GD(Boc)E(Boc)VD(Boc)GS(Boc)GK(Mtt)-Sieber resin (1)*: A peptide of *Fmoc-GD(Boc)E(Boc)VD(Boc)GS(Boc)GK(Mtt)-Sieber resin (1)* was synthesized by a manual Fmoc solid phase peptide synthesis (SPPS) protocol using commercially available *N*- $\alpha$ -Fmoc protected amino acids, sieber amide resin as a solid support and HBTU/HOBt as a carboxyl-group activating agent.

*Pyro-GD(Boc)E(Boc)VD(Boc)GS(Boc)GK(Mtt)-Sieber (2)*: After the last Fmoc group was removed from the peptide-resin (1) with 20% piperidine in DMF, the resin was washed with 1-methy-2-pyrrolidinone (NMP), and pyropheophorbide  $\alpha$  acid (Pyro-acid) was coupled to the *N*-terminal Glycine of the peptide-resin (Pyro acid/HOBt/HBTU/peptide 3:3:3:1) in dry NMP for 17 h to give *Pyro-GD(Boc)E(Boc)VD(Boc)GS(Boc)GK(Mtt)-Sieber resin (2)*.

*Pyro-GDEVDGSGK( $\epsilon$ -NH<sub>2</sub>) (PP) (3)*: This peptide resin (2) was treated with 50% TFA and 5% triisopropylsilane (Tis) in dichloromethane (DCM) for 2 h at room temperature to cleave the peptide sequence from the Sieber resin and also deprotect the

protected group on peptide. After removing the cleaved solid resin by filtration, the filtrate was concentrated and precipitated by adding anhydrous diethyl ether, to give *Pyro-GDEV DGS GK*( $\epsilon$ -NH<sub>2</sub>) (**3**, **PP**). It was further washed by diethyl ether and dried under high vacuum. The structure was confirmed by ESI-MS (Calc. 1377.64, found 1377.5). It serves as positive control (without quencher moiety).

*Pyro-GDEV DGS GK-CAR* (**PPC**) (**4**): The PP (6.9mg, 5 $\mu$ mol) (**3**) was dissolved in 100 $\mu$ L of anhydrous dimethyl sulfoxide (DMSO) with 1% of *N,N*-diisopropylethyl amine (DIPEA) and reacted with *CAR-NHS* (3.8mg, 6 $\mu$ mol) for 5 h under argon. The reaction was stopped by precipitation with 2 mL of ether, to give *Pyro-GDEV DGS GK-CAR* (**4**, **PPC**). The product was then purified by HPLC and its structure was confirmed by UV-vis spectrum and ESI-MS (Calc. 1895.24, found 1895.4).

#### **PPC cleavage by caspase-3 in solution**

The purified PPC were tested against caspase-3, with and without caspase-3 inhibitor. The caspase-3 kit (containing the active form of caspase-3 enzyme, caspase-3 inhibitor Ac-DEVD-CHO and caspase-3 fluorogenic substrate Z-DEVD-AMC) was purchased from BD Biosciences (San Jose, CA, USA). The buffer used in all cleavage experiments contained 20mM PIPES, 100mM NaCl, 10mM DTT, 1mM EDTA, 0.1% (w/v) CHAPS, 10% sucrose, 0.3% Tween-80, pH 7.2. Prior to the PPC cleavage study, the activity of caspase-3 was confirmed by its ability to cleave the fluorogenic substrate Z-DEVD-AMC. PP, PPC and free *CAR-NHS* were prepared as stock solutions of 0.53mM in DMSO, and the caspase-3 inhibitor was prepared as 1mg/mL stock solution in DMSO. The composition of each cleavage sample was as follows: 1) PP alone (5.3 $\mu$ M): 5 $\mu$ L PP stock solution (0.53mM)+50 $\mu$ L DMSO+445 $\mu$ L buffer; 2) PPC in buffer (5.3 $\mu$ M):

5 $\mu$ L PPC stock solution (0.53mM)+50 $\mu$ L DMSO+445 $\mu$ L buffer; 3) PPC+caspase-3 (1:100 molar ratio): 5 $\mu$ L PPC stock solution (0.53mM)+50 $\mu$ L DMSO+445 $\mu$ L buffer+0.8 $\mu$ g caspase-3; 4) PPC+caspase-3+inhibitor (1:100:2400 molar ratio): 5 $\mu$ L PPC stock solution (0.53mM)+445 $\mu$ L buffer+50 $\mu$ L inhibitor (50 $\mu$ g)+0.8 $\mu$ g caspase-3; 5) PP +Free CAR (1:1 molar ratio): 5 $\mu$ L PP stock solution (0.53mM)+5 $\mu$ L Free CAR-NHS solution (0.53mM)+45 $\mu$ L DMSO+445 $\mu$ L buffer. All solutions were incubated for 3 h at 37 °C and then diluted with 3.0mL of DMSO to halt the cleavage. These solutions were then analyzed by HPLC, and the fluorescence and  $^1\text{O}_2$  production were measured.

### **$^1\text{O}_2$ generation assays in solution**

PDT-generated  $^1\text{O}_2$  was quantified in solutions of PP, PPC alone, PPC+caspase-3, PPC+caspase-3+inhibitor, and PP+free CAR, by measuring its NIR luminescence at 1270nm using an instrument that has been described before<sup>15</sup>. Briefly, a 10ns pulsed 523 nm laser excited the solution. The luminescence spectrum was sampled, after rejection of background luminescence, using a set of interference filters, with a high-sensitivity NIR photomultiplier tube module (H9170-45, Hamamatsu, USA) operating in time-resolved single photon counting mode. The  $^1\text{O}_2$  and triplet state lifetimes were determined by fitting the data to the following three parameter equation<sup>16</sup>:

$$[{}^1\text{O}_2](t) = A \frac{\tau_D}{\tau_T - \tau_D} (e^{(-t/\tau_T)} - e^{(-t/\tau_D)}),$$

where A is a constant accounting for the number of incident photons, PS extinction coefficient, PS concentration,  $^1\text{O}_2$  quantum yield  $^1\text{O}_2$  radiative lifetime and the system collection efficiency.  $\tau_D$  and  $\tau_T$  are the singlet oxygen and triplet state lifetimes, respectively. Non-linear least-squares fitting was performed with Origin software on background-corrected, time-resolved data.

## **Cell line**

Hepatoblastoma-G<sub>2</sub> (HepG<sub>2</sub>) tumor cells, which were obtained from Dr. Theo van Berkel's laboratory at University of Leiden, Netherlands, were cultured in complete DMEM containing 90% Dulbecco's modified Eagle's medium (DMEM), 10% fetal bovine serum (FBS), 2mM L-glutamine, 10mM HEPES (Hank's balanced salt solution) and 100U/mL penicillin- streptomycin. All cells were grown at 37°C in a humidified atmosphere containing 5% CO<sub>2</sub>.

## **Cell viability study (MTT assay).**

HepG<sub>2</sub> cells were seeded in clear 96-well plates at a density of 50,000cells/well and were grown for 2 days at 37°C. Cells were subsequently rinsed with HBSS and incubated with no drug or 0.5, 1 or 5µM PP or 1, 5 or 15µM PPC in 0.8% BSA medium for 20 h. Cells were then rinsed with HBSS, cultured in 100µL of complete DMEM, and treated with three different light doses by a 670 nm laser light at a fluence rate of 20mW/cm<sup>2</sup>. At 24 h post treatment, the MTT tracer, 3-(4,5-Dimethylthiazol-2-yl)-2,5-diphenyltetrazolium bromide ( ATCC, Manassas, VA) was added to the medium at 0.5mg/mL. Two hours later, the medium was removed and replaced with 150µL of 1: 1 DMSO: 70% isopropanol in 0.1M HCl. The absorbance at 570 nm was measured on a Bio-tek ELx model 800 (MTX Lab System Inc., Vienna, VA, USA). All experiments were repeated 20 times.

## **Acknowledgments**

This work was supported by DOD Breast Cancer Research Program DAMD17-03-1-0373 (GZ), NIH R21-CA95330 (GZ), the Joey and Toby Tanenbaum/Brazilian Ball Chair

in Prostate Cancer Research (GZ), and the Canadian Cancer Society/National Cancer Institute of Canada (BCW).

## Reference

1. T. J. Dougherty, C. J. Gomer, B. W. Henderson, G. Jori, D. Kessel, M. Korbelik, J. Moan and Q. Peng, *J Natl Cancer Inst*, 1998, **90**, 889-905.
2. B. C. Wilson and M. S. Patterson, *Phys Med Biol*, 1986, **31**, 327-360.
3. J. Chen, K. Stefflova, M. J. Niedre, B. C. Wilson, B. Chance, J. D. Glickson and G. Zheng, *J Am Chem Soc*, 2004, **126**, 11450-11451.
4. G. Zheng, J. Chen, K. Stefflova, M. Jarvi, H. Li and B. C. Wilson, *Proceedings of the National Academic of Science, USA*, 2007, in press.
5. R. Edge, D. J. McGarvey and T. G. Truscott, *J Photochem Photobiol B*, 1997, **41**, 189-200.
6. C. S. Foote, Y. C. Chang and R. W. Denny, *J Am Chem Soc*, 1970, **92**, 5218-5219.
7. A. Telfer, S. Dhami, S. M. Bishop, D. Phillips and J. Barber, *Biochemistry*, 1994, **33**, 14469-14474.
8. A. J. Young and H. A. Frank, *J Photochem Photobiol B*, 1996, **36**, 3-15.
9. J. A. Moore A. L., Tom R., Gust D., Moore T. A., Bensasson R. A. and Land E. J., *Science*, 1982, **216**, 982-984.
10. S. A. Reddi E., Jori G., Kerrigan P.K., Liddell P.A., Moore A.L., Moore T.A. and Gust D., *Br J Cancer*, 1994, **69**, 5.
11. M. Gurfinkel, A. B. Thompson, W. Ralston, T. L. Troy, A. L. Moore, T. A. Moore, J. D. Gust, D. Tatman, J. S. Reynolds, B. Muggenburg, K. Nikula, R. Pandey, R. H. Mayer, D. J. Hawrysz and E. M. Sevick-Muraca, *Photochem Photobiol*, 2000, **72**, 94-102.
12. D. Tatman, P. A. Liddell, T. A. Moore, D. Gust and A. L. Moore, *Photochem Photobiol*, 1998, **68**, 459-466.
13. N. A. Thornberry and Y. Lazebnik, *Science*, 1998, **281**, 1312-1316.
14. W. R. a. T. C.-H. Pham W., *Angew. Chem.*, 2002, **114**, 3811-3813.
15. M. J. Niedre, A. J. Secord, M. S. Patterson and B. C. Wilson, *Cancer Res*, 2003, **63**, 7986-7994.
16. M. Niedre, M. S. Patterson and B. C. Wilson, *Photochem Photobiol*, 2002, **75**, 382-391.

## Figure Legends

Figure 1: Concept of protease-controlled  $^1\text{O}_2$  quenching and activation (reproduced with permission from ref 3).

Figure 2. Synthesis and characterization of PPC: A) Synthesis protocol for Pyro-GDEVDGSGK-CAR (PPC). B) The UV-vis spectrum of PPC and C) The ESI-MS spectrum of PPC.

Figure 3. Validation of PPC specific cleavage by caspase-3: A) HPLC chromatography of (i) PPC alone, (ii) PPC+ caspase-3 and (iii) PPC+ caspase-3 +inhibitor after 3 hours incubation; B) corresponding UV-vis spectra of each HPLC peaks in (i) PPC alone, (ii) PPC+ caspase-3 and (iii) PPC+ caspase-3 +inhibitor; C) ESI-MS spectra of the HPLC peaks in PPC +caspase-3 with retention times (i) 14.72 min, (ii) 7.64 min and (iii) 11.95 min.

Figure 4. Photophysical characteristics of different samples:1) total  $^1\text{O}_2$  luminescence counts (A) and lifetime (B) for PP, PPC, PPC+caspase-3, PPC+caspase-3+inhibitor and PP+free CAR; 2) fluorescence emission (C), total  $^1\text{O}_2$  luminescence counts (D), singlet oxygen lifetime (E) and Pyro triplet state lifetime (F) for PP and PP+ free CAR at different molar ratios.

Figure 5. Photodynamic cytotoxicity determined by MTT assay as a function of PS and light doses, compared with untreated cells. means  $\pm$  standard errors for 20 times experiments.

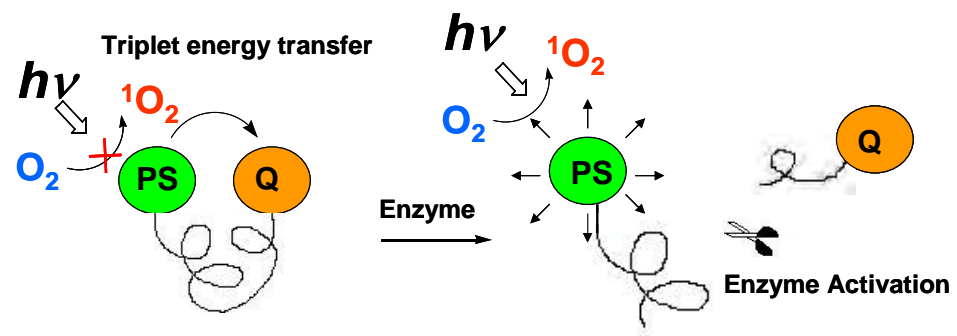


Figure 1

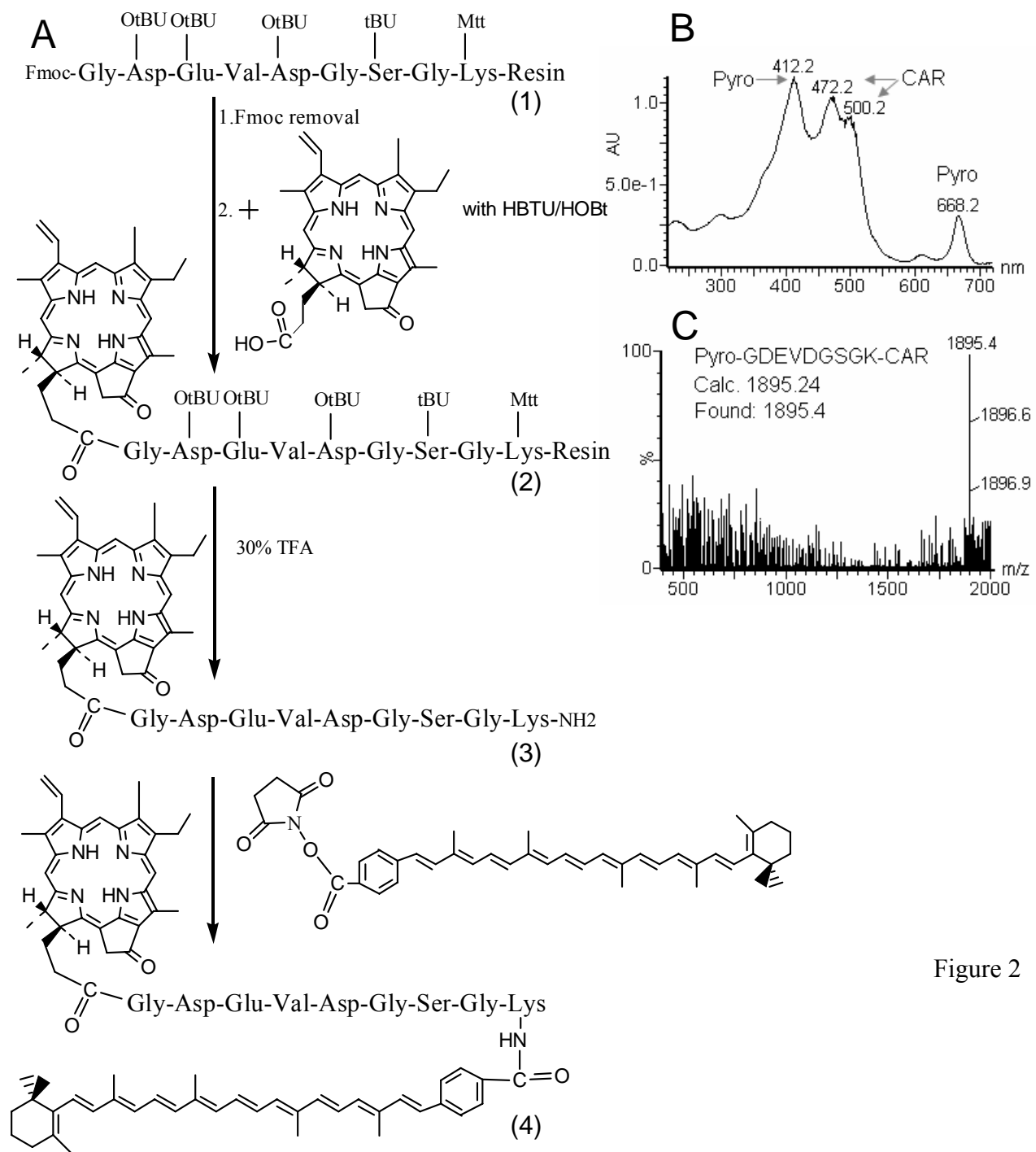


Figure 2

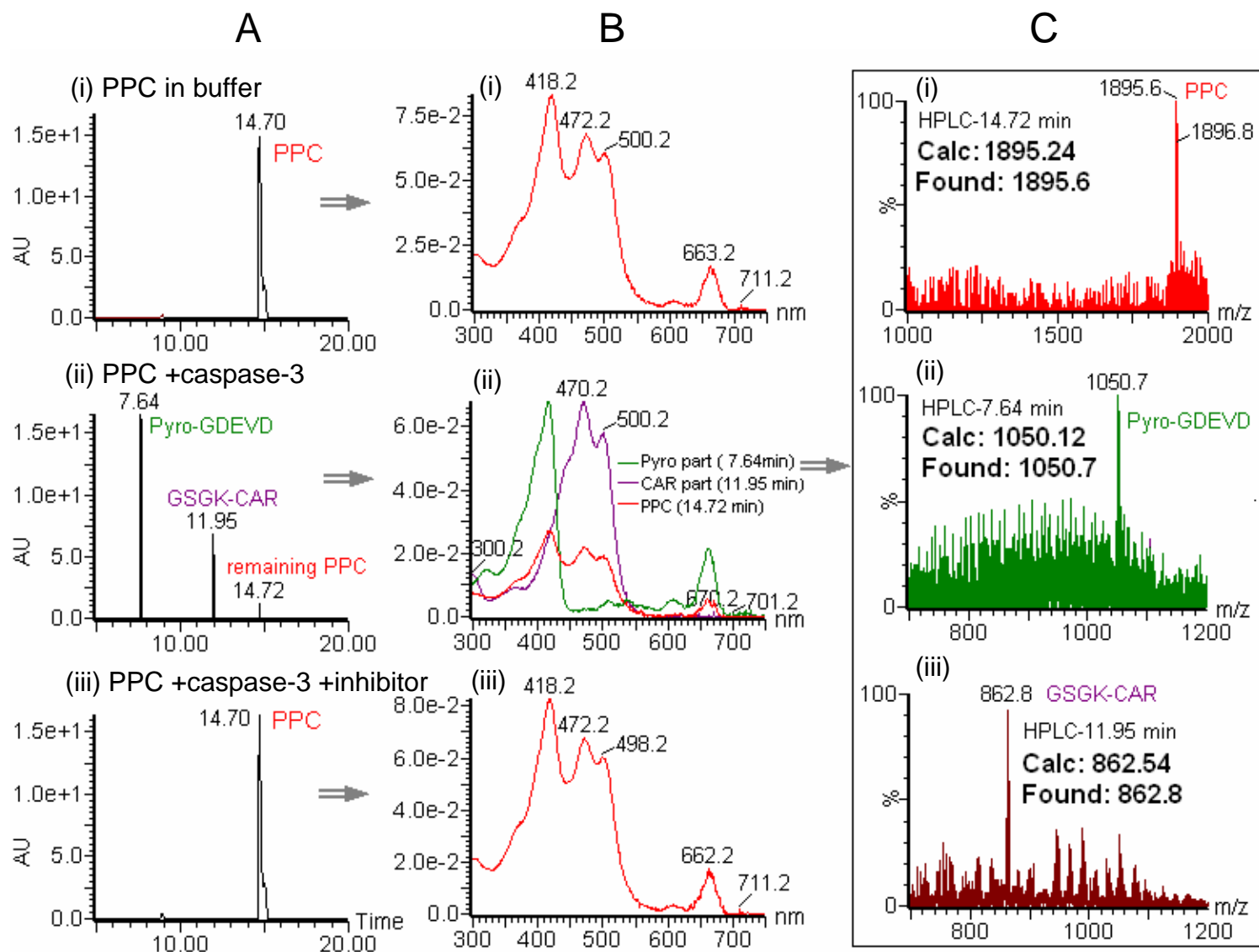


Figure 3

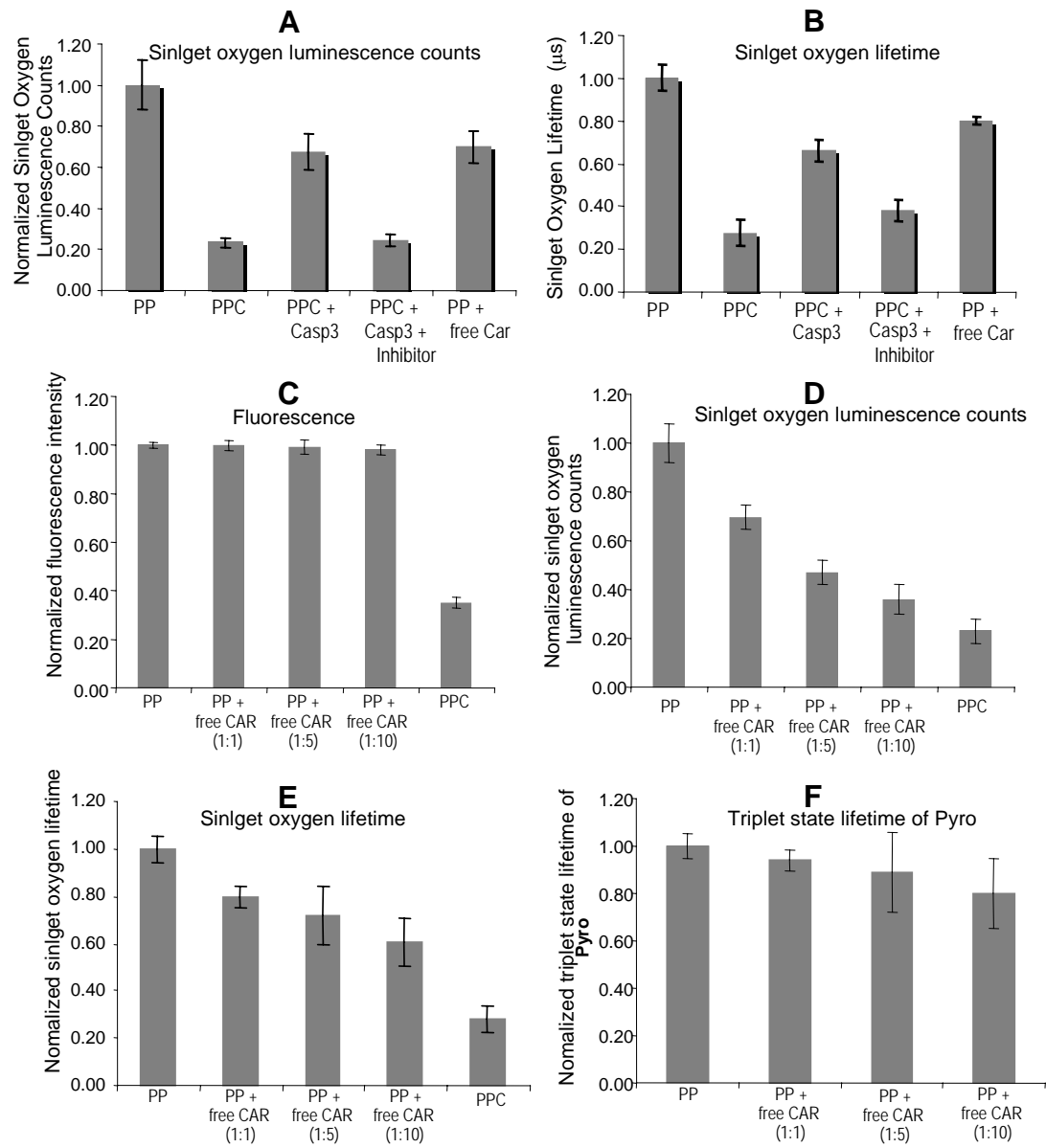


Figure 4

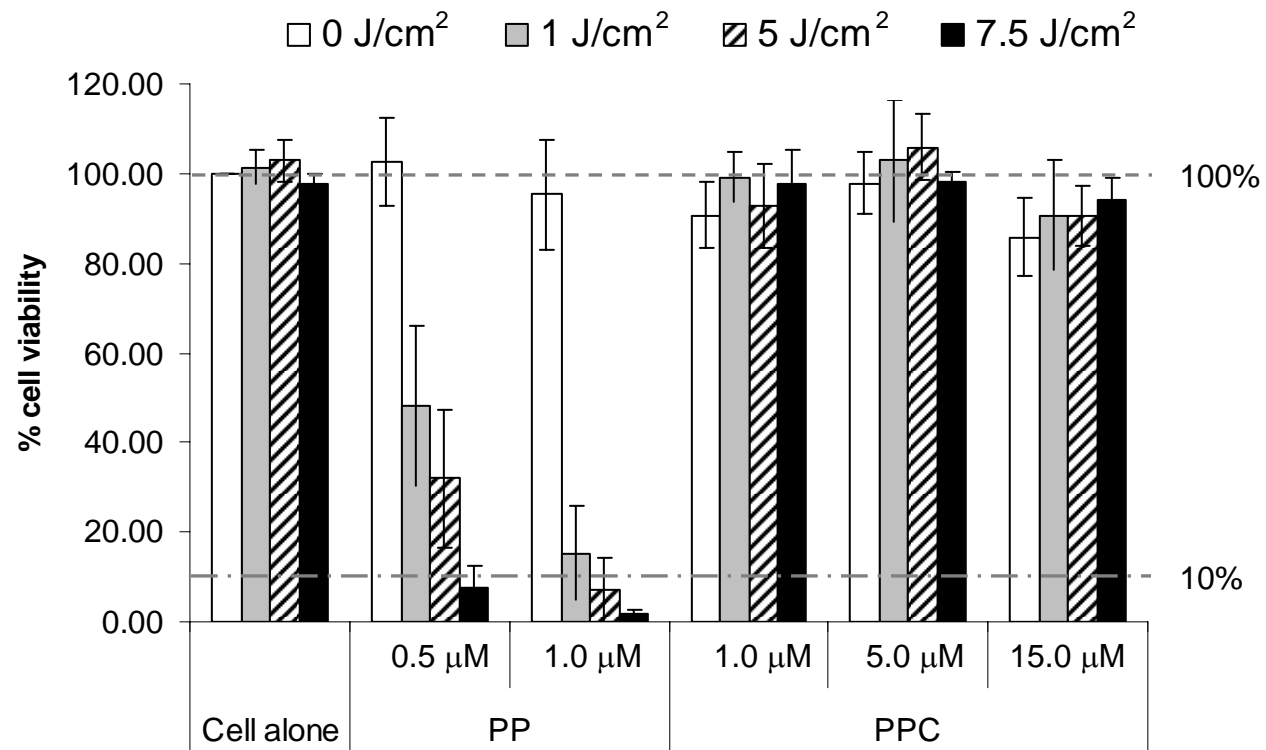


Figure 5

## Photodynamic Therapy Agent with a Built-In Apoptosis Sensor for Evaluating Its Own Therapeutic Outcome in Situ

Klara Stefflova,<sup>†</sup> Juan Chen,<sup>‡</sup> Diane Marotta,<sup>‡</sup> Hui Li,<sup>‡</sup> and Gang Zheng<sup>\*‡</sup>

Departments of Chemistry and Radiology, University of Pennsylvania, Philadelphia, Pennsylvania 19104

Received February 8, 2006

Identifying the extent of apoptosis in cells or tissues after cancer therapy in real time would be a powerful firsthand tool for assessing therapeutic outcome. We combined therapeutic and imaging functions in one agent, choosing photodynamic therapy (PDT) as an appropriate cancer treatment modality. This agent induces photodamage in irradiated cells and simultaneously identifies apoptotic cells by near-infrared fluorescence. This photodynamic therapy agent with a built-in apoptosis sensor (PDT-BIAS) contains a fluorescent photosensitizer used as an anticancer drug, connected to a fluorescence quencher by a caspase-3 cleavable peptide linker. We demonstrated that cleavage of the peptide linker by caspase-3, one of the executioner caspases involved in apoptosis, results in a detectable increase of fluorescence in solution and in cancer cells after PDT treatment. The apoptosis involvement and drug effectiveness were confirmed by Apoptag and cell viability (MTT) assays supporting the ability of PDT-BIAS to induce and image apoptosis in situ.

### Introduction

Apoptosis is essential for the normal development of a multicellular organism but its dysregulation leads to severe diseases<sup>1</sup> including cancer.<sup>2</sup> Many anticancer drugs act against this malfunction, killing the cells by restoring their programmed cell death. Apoptosis is characterized by the ordered manner in which the damaged or otherwise compromised cells die. This form of active death is very different from necrosis which results in an uncontrolled bursting of cells followed by an inflammatory reaction.<sup>3</sup> Common methods of imaging apoptosis<sup>4,5</sup> focus mainly on the early stages where the differences between apoptosis and necrosis are most pronounced.<sup>6</sup> They use features of controlled cell degradation such as disruption of mitochondrial transmembrane potential, activation of caspases, DNA laddering (e.g. TUNEL/Apoptag assay), redistribution of phospholipids in the plasma membrane (e.g. Annexin V-FITC membrane binding) and formation of apoptotic bodies.<sup>7,8</sup> Independent of the stimuli, most apoptotic pathways reach the activation of caspase-3, an executioner caspase usually indicating the point of no-return.<sup>9</sup> This protease, being a specific indicator of apoptosis, is an attractive, useful, and unambiguous target for apoptosis imaging.

Photodynamic therapy (PDT) is a promising cancer treatment modality<sup>10,11</sup> that involves a photosensitizer (PS), light, and molecular oxygen. The tumor-associated photosensitizer,<sup>12</sup> after activation with light of an appropriate wavelength, produces reactive oxygen species, mainly singlet oxygen.<sup>13</sup> This cytotoxic effector of PDT acts locally due to its short lifetime resulting in an average 20 nm diffusion range from the site of generation.<sup>11,14</sup> Therefore, the localization of PS in the cell is also the scene of organelle damage.<sup>15</sup> The desired outcome of PDT is cell death.<sup>16</sup> The type of cell death caused by PDT (apoptosis vs necrosis) depends on a number of factors<sup>17,18</sup> including the type and size of tumor, PDT treatment conditions, as well as the type of photosensitizer<sup>19</sup> and its site of accumulation.<sup>20</sup> It has been shown that when the photosensitizer targets mitochon-

dria or endoplasmic reticulum (but not plasma membrane) it is primarily the apoptotic response that leads to cell death.<sup>21,22</sup> To noninvasively image PDT-induced early apoptosis in situ would, together with the well-established in vitro and ex vivo assays, help to assess the best PDT conditions for each photosensitizer and tumor type and ultimately enable adjustment of the protocol for each patient (patient-tailored treatment). The in situ imaging is possible since the photosensitizer's fluorescence in the near-infrared (NIR) region<sup>23</sup> corresponds to the therapeutic wavelength range with deep tissue penetration.

We have designed a probe that is both a therapeutic and imaging agent in the sense that it combines its original role in treating cancer with the ability to directly assess its own therapeutic outcome by monitoring PDT-induced apoptosis. It contains a photosensitizer that acts as both a drug and a fluorescent label, and a fluorescence quencher bound to the opposing sites of a caspase-3 cleavable peptide linker which holds the photosensitizer and quencher in close proximity enabling FRET.<sup>a</sup> After this construct enters a cell and is activated by light, the photosensitizer produces singlet oxygen that damages the cell. If the damage is sufficient but not catastrophic, the apoptotic cascade starts and caspase-3 is processed to its active form indicating initiation of irreversible apoptotic death.<sup>9,24</sup> Once activated, this protease cleaves the peptide linker, thus separating the photosensitizer from the fluorescence quencher and restoring its fluorescence (Scheme 1). Therefore, the cells actually dying by apoptosis can be visualized by NIR fluorescence. In this way, PDT-BIAS is capable of visualizing its own therapeutic outcome.

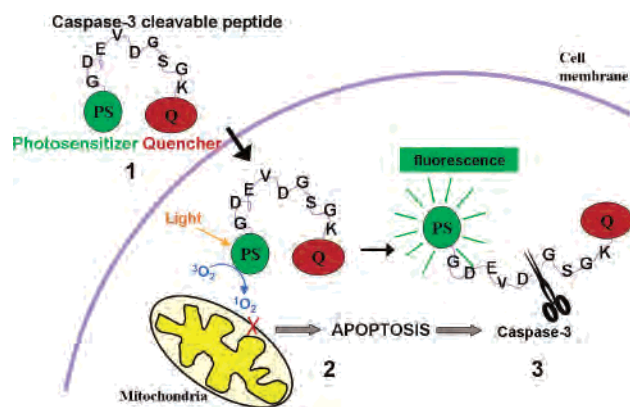
We designed a prototype PDT-BIAS using pyropheophorbide *a* (Pyro), a photosensitizer which localizes near mitochondria<sup>25–27</sup> and induces apoptosis upon irradiation.<sup>26,28</sup> This semisynthetic PS, obtained by three steps from *Spirulina* algae, has a long-wavelength absorption (665 nm) and emission (675 and 720

\* To whom correspondence should be addressed. Phone: 1-215-898-3105. Fax: 1-215-746-8764. E-mail: Gang.Zheng@uphs.upenn.edu.

<sup>†</sup> Department of Chemistry.

<sup>‡</sup> Department of Radiology.

<sup>a</sup> Abbreviations: DCM, dichloromethane; ESI-MS, electrospray ionization mass spectrometry; FRET, fluorescence resonance energy transfer; HPLC, high performance liquid chromatography; MALDI-ToF, matrix assisted laser desorption/ionization–time-of-flight mass spectrometry; MTT, 3-[4,5-dimethylthiazol-2-yl]-2,5-diphenyl tetrazolium bromide; NMP, 1-methyl-2-pyrrolidinone; RT, retention time; TFA, trifluoroacetic acid; TIS, triisopropylsilane; UV–vis, ultraviolet–visible spectroscopy.

Scheme 1. Schematic of PDT-BIAS Function<sup>a</sup>

<sup>a</sup> (1) PDT-BIAS accumulates in tumor cells; fluorescence is quenched in the native state. (2) Singlet oxygen is produced upon light activation and apoptosis is triggered. (3) Activated caspase-3 cleaves the peptide and fluorescence is restored, indicating the apoptotic cells.

nm), good singlet oxygen yield (over 50%), no dark toxicity,<sup>27</sup> and its derivative Photochlor is in phase I/II clinical trial.<sup>29</sup> BHQ-3 (black hole quencher 3, absorption max at 672 nm) was chosen as an appropriate quencher of Pyro's fluorescence via FRET and GDEVDGSGK was used as a previously described caspase-3 cleavable peptide linker<sup>30,31</sup> with the cleavage site between D and G and recognition site in italics.

## Results and Discussion

To validate this concept we needed to determine whether our prototype compound (1) is specifically cleaved by caspase-3, (2) is able to enter cells, (3) causes cell death, (4) is cleavable as a consequence of apoptosis, and (5) can image apoptosis using its restored fluorescence. The substrate specificity was confirmed by HPLC and fluorescence restoration measured after the cleavage with caspase-3 in solution. To prove that our quenched PDT-BIAS, Pyro-GDEVDGSGK-(BHQ-3) (PPB), can enter cells, several fluorescent control molecules substituting the BHQ-3 quencher were synthesized and visualized by laser scanning confocal microscopy in the cancer cell cytoplasm. Cell viability (MTT) assay, in which living cells reduce the colorless MTT to the purple formazan product measurable by UV-vis spectroscopy, was used for assessing the PDT efficacy for different light and drug doses. Using confocal microscopy, we detected an increase of fluorescence inside of the cells incubated with PPB and treated by light. As expected, the increase of fluorescence was a result of *apoptosis*-induced cleavage of the peptide linker as confirmed by the Apoptag method and anticaspase-3 staining. Therefore, by detecting apoptosis in cancer cells using our prototype PDT-BIAS and other well-established methods, we have demonstrated that the photodamage induced by PDT-BIAS causes apoptosis and can be consequently visualized using the same molecule by tracking the NIR fluorescence signal.

**Synthesis of PPB.** The synthesis started by solid-phase peptide synthesis (SPPS), giving Fmoc-GDEVDGSGK on Sieber resin (1). The photosensitizer Pyro acid was then coupled to the N-terminus of the immobilized peptide (Figure 1), giving Pyro-GDEVDGSGK-Sieber resin (2) that was cleaved from the solid phase and deprotected with 50% TFA. The BHQ-3-NHS quencher was coupled in a solution reaction to the C-terminal lysine of Pyro-GDEVDGSGK (PP, 3), and the product Pyro-GDEVDGSGK-(BHQ-3) (PPB, 4) (and a small sample of compound 3) was purified by HPLC and characterized by UV-

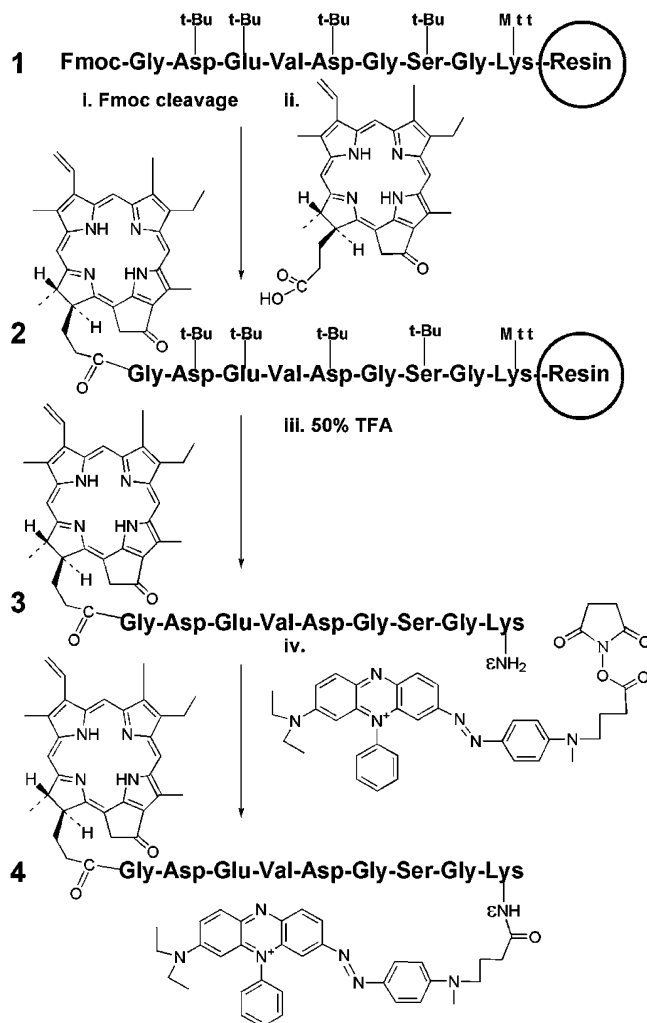
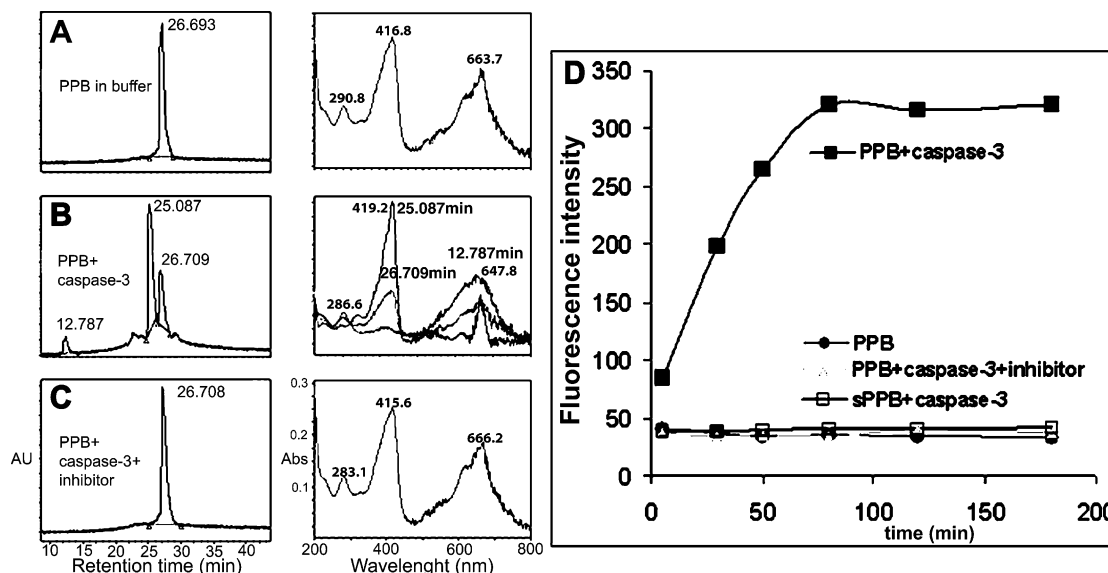


Figure 1. Pyro-GDEVDGSGK-(BHQ-3) (PPB, 4) synthesis.

vis and MALDI-ToF (Supporting Information, Figures 1 and 2).

**Cleavage by Caspase-3 in Solution.** We needed to confirm that (1) PPB is cleavable by caspase-3, (2) the fluorescence of Pyro is effectively quenched by BHQ-3 when restrained by the peptide linker, and (3) this fluorescence is restored after cleavage. We demonstrated this using two solution assays—HPLC for monitoring the cleavage of PPB by purified caspase-3 in solution and fluorescence spectroscopy for detecting the consequent fluorescence restoration. The HPLC chromatogram shows that PPB (RT 26.693 min) is stable in the cleavage buffer (Figure 2A), but two fragments (RT 12.787 and 25.087 min) were generated from an intact molecule (RT 26.709 min) when incubated with caspase-3 for 50 min (Figure 2B). The cleavage is prevented (RT 26.708 min) when caspase-3 specific inhibitor (Ac-DEVD-CHO) is added to the solution of PPB and caspase-3 (Figure 2C). An immediate increase of fluorescence which plateaus at 90 min was monitored by fluorescence spectroscopy (Figure 2D) for PPB incubated with caspase-3 (■). This increase was not observed for PPB alone in buffer (●) or PPB incubated with caspase-3 and caspase-3-specific inhibitor (▲) or for a scrambled sequence sPPB (□, Pyro-GPLGLARK-(BHQ-3)) incubated with caspase-3 (HPLC in Supporting Information, Figure 3), indicating that this cleavage is caspase-3 specific. These assays demonstrate that PPB can be specifically cleaved by caspase-3 in solution, and as a result, there is an 8-fold increase of fluorescence.



**Figure 2.** Cleavage of Pyro-GDEVDGSGK-(BHQ-3) (PPB, **4**) by caspase-3 in solution results in the formation of two fragments and a fluorescence increase that was monitored by HPLC and fluorescence spectroscopy assays. HPLC assay (A–C): HPLC chromatogram at 410 nm (left column), UV–vis spectra of corresponding peak (right column). Single peak of PPB alone incubated in the buffer for 50 min (A), supports its chemical stability. Incubation of PPB (RT 26.709 min) with caspase-3 for 50 min (B) results in formation of two fragments with RT 12.787 min and 25.087 min. This is prevented when PPB is incubated with caspase-3 and caspase-3 inhibitor for 50 min (C). Fluorescence assay (D): Fluorescence intensity increases when PPB is incubated with caspase-3 (■) compared to the stable background fluorescence of PPB alone (●), PPB incubated with caspase-3 and caspase-3 inhibitor (▲), and sPPB (□) (scrambled sequence Pyro-GPLGLARK-(BHQ-3)) incubated with caspase-3, all monitored for 3 h, confirming PPB’s stability and caspase-3 specificity.

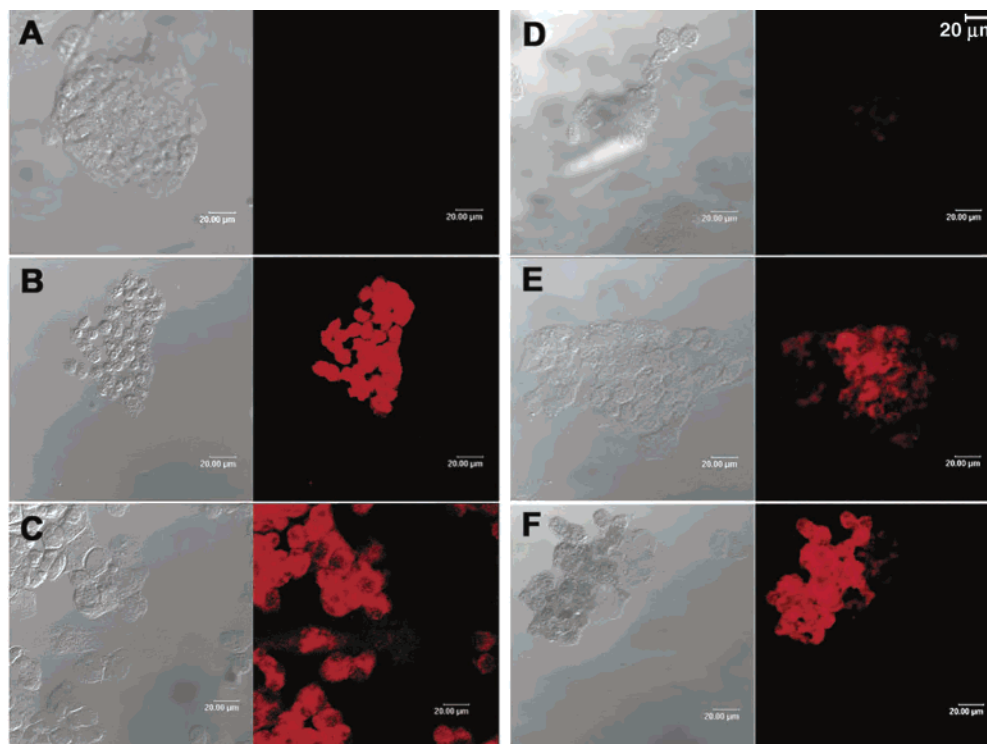


**Figure 3.** Accumulation and cleavage of Pyro-GDEVDGSGK-(BHQ-3) (PPB) inside the hepatoblastoma G<sub>2</sub> cells. Confocal images of (A) HepG<sub>2</sub> cells alone, (B) HepG<sub>2</sub> cells incubated for 24 h with Pyro-GDEVDGSGK (PP, **3**, 200 μM), and (C) HepG<sub>2</sub> cells incubated for 24 h with Pyro-GDEVDGSGK-Fluorescein (PPFI, 200 μM), showing that both PP and PPF1 (used as PPB analogues) accumulate in the cytoplasm; (D) HepG<sub>2</sub> cells incubated for 24 h with PPB (200 μM) show minimal fluorescence increase, excluding apoptosis-independent PPB decomposition; (E) HepG<sub>2</sub> cells incubated for 30 min with PPB (200 μM) and treated with 5 J/cm<sup>2</sup> light dose and (F) HepG<sub>2</sub> cells incubated for 24 h with PPB (200 μM) and treated with 5 J/cm<sup>2</sup> light dose, both showing significant increase of fluorescence from PDT-triggered apoptosis-induced PPB cleavage. In each case, the left image is DIC and the right image is Pyro fluorescence (scale bar (upper right corner) represents 20 μm).

**Accumulation and Cleavage of PPB in Cancer Cells.** Given PPB’s large size, it is important to determine if it can enter cells. We synthesized two model fluorescent molecules whose size and properties are similar to those of PPB: Pyro-GDEVDGSGK (PP, **3**, no quencher) and Pyro-GDEVDGSGK-

Fluorescein (PPFI). Unlike the quenched PPB, these analogues can be visualized by confocal microscopy. A strong fluorescence signal is localized in the cytoplasm of the cells incubated for 24 h with PP (Figure 3B) and PPF1 (Figure 3C) when compared with untreated cells (Figure 3A). Taking advantage of PPB’s

weak intrinsic fluorescence, we were able to visualize even the intact molecule inside living cells using a more sensitive fluorescence microscope (Supporting Information, Figure 4). This confirmed that Pyro can serve as a nonspecific cell delivery vehicle even for molecules with a mass around 2000 Da.

The ability of PPB to be cleaved as a consequence of PDT-induced apoptosis was also monitored using confocal microscopy. Hepatoblastoma G<sub>2</sub> cells (HepG<sub>2</sub>) were incubated with PPB (200  $\mu$ M) for either 30 min or 24 h and subsequently treated with a 5 J/cm<sup>2</sup> light dose using a 670 nm laser (parts E and F of Figure 3, respectively). The PDT-treated cells (Figure 3E,F) show a significant increase of fluorescence intensity. In contrast, the control cells (Figure 3D) incubated with PPB for 24 h without exposure to light showed a minimal fluorescence increase. We have also performed a control experiment showing that the increase of fluorescence for PDT-treated cells previously incubated with Pyro-GDEVDGSGK-(BHQ-3) (**4**) is greater than for those PDT-treated cells incubated with scrambled sequence Pyro-GHSSK(BHQ-3)LQL (Supporting Information, Figure 5). These results confirmed that the peptide linker in the PDT-BIAS can be cleaved inside the PDT-treated cells and that the significant increase of Pyro's fluorescence is induced by apoptosis-specific cleavage. This increase is not simply due to PPB decomposition over a period of 24 h (Figure 3D) or nonspecific proteolytic degradation (Supporting Information, Figure 5). This cleavage was also monitored by Flow cytometry in KB cells (human epidermoid carcinoma cells) incubated with 15  $\mu$ M PPB, showing that the cells treated with light (10 J/cm<sup>2</sup> light dose) display 1.7–2.4-fold fluorescence increase compared to those kept in the dark.

**Confirmation of Apoptosis Involvement.** To ensure that PDT-BIAS is indeed reporting apoptosis, an independent evaluation of apoptosis is required. One of the hallmarks of apoptosis is DNA laddering. This specific DNA cleavage indicates a point of no return in cell death that critically depends on caspase-3 activity and can be detected by an Apoptag (TUNEL) assay. We used this well-established method to visualize apoptotic cells by monitoring Fluorescein fluorescence from the Apoptag assay using confocal microscopy. The HepG<sub>2</sub> cells that were incubated with PPB, treated with PDT, and then stained with Apoptag (Figure 4D) show a clear increase of fluorescence in both the Fluorescein (488 nm) and Pyro (633 nm) fluorescence channels compared to cells alone (Figure 4A) and cells incubated with both PPB and Apoptag but not treated with PDT (Figure 4B). The coexistence of fluorescence from both Pyro (as a result of the caspase-3-dependent cleavage of PDT-BIAS) and Fluorescein (arising from labeling of the apoptosis-induced DNA cleavage in the Apoptag assay) in the PDT- and Apoptag-treated cells (Figure 4D) demonstrates that PDT-BIAS can induce and image apoptosis *in vitro*. The simultaneous appearance of both signals is not due to the Pyro fluorescence leaking into the Fluorescein channel, as shown in Figure 4C.

Also, staining the cells with fluorescently labeled antibody against activated caspase-3 supported this Apoptag data. Using flow cytometry, the KB cells incubated with 15  $\mu$ M PPB and treated with PDT showed a significant (1.5–2.9-fold) increase in anticaspase-3 staining compared to those incubated with drug but kept in dark.

**PDT-Induced Cell Death.** Apoptosis induction correlates with PDT-BIAS cleavage in single cells (Figure 4), but for quantitation of overall cell death in the whole population for variable drug and light doses, we used an MTT assay. This is a standard method of determining the PDT efficacy of a drug

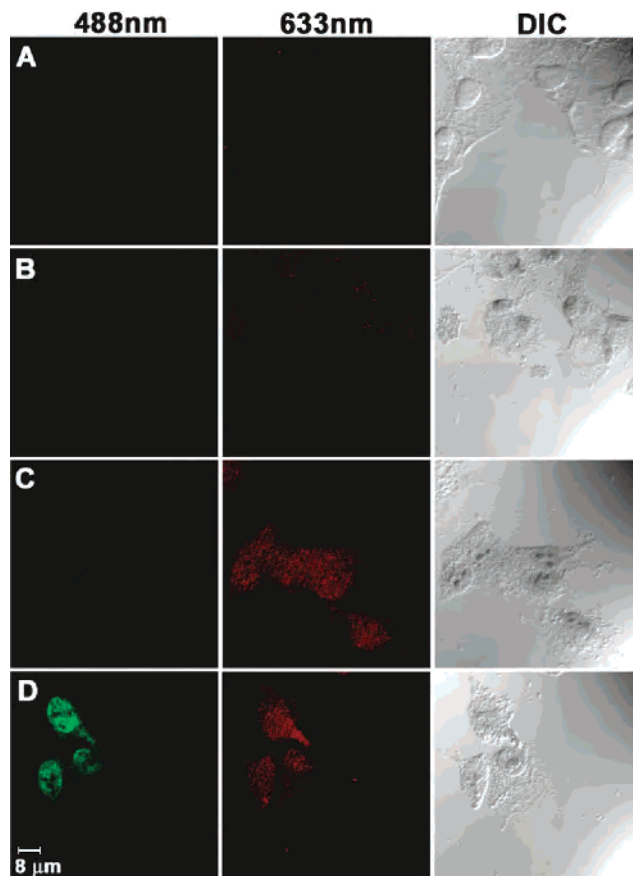


**Figure 4.** Detection of PDT-induced apoptosis in HepG<sub>2</sub> cells by both PDT-BIAS prototype Pyro-GDEVDGSGK-(BHQ-3) (PPB, 200  $\mu$ M) and an Apoptag assay using confocal microscopy. From left to right: fluorescent image at 488 nm (Fluorescein), 633 nm (Pyro), and DIC image. (A) Cells alone. (B) Cells incubated with PPB, kept in dark and stained with Apoptag show minimal fluorescence increase in both channels ruling out the dark toxicity of PPB. (C) Cells incubated with PPB and treated with 5 J/cm<sup>2</sup> but not stained with Apoptag show increased Pyro fluorescence resulting from PDT-dependent cleavage that does not extensively leak into the 488 nm (Apoptag) channel. (D) In cells incubated with PPB, treated with 5 J/cm<sup>2</sup>, and then stained with Apoptag, both Fluorescein and Pyro fluorescence coexist. This confirms that it is the apoptosis causing the PDT-BIAS cleavage.

by correlating the viability of cells before and after PDT treatment, where cells not treated with light and drug serve as a relative reference (100% viable). We have confirmed (as shown in Figure 5) that (1) Pyro has a minimal dark toxicity since the viability of cells incubated with even the highest PPB dose (30  $\mu$ M) but not treated with light (white column, 0 J/cm<sup>2</sup>) is similar to that of the control cells, (2) increased drug or light doses led to decreased cell viability (ANOVA test included in Supporting Information), and (3) cells treated with 7.5 J/cm<sup>2</sup> (the highest light dose) have reduced viability below 10% of that of control cells when incubated with even the lowest PPB dose (1  $\mu$ M).

**Discussion.** PDT-BIAS is a dual function molecule able to assess its own therapeutic outcome by imaging the extent of apoptosis *in situ* after PDT treatment. The therapeutic component of PDT-BIAS is pyropheophorbide *a* (a photosensitizer) that has been shown<sup>26</sup> to trigger apoptosis by light-dependent production of singlet oxygen that disrupts the mitochondrial membrane. The critical imaging component is a caspase-3 cleavable sequence since active caspase-3, a crucial executioner protease involved in the progression of controlled cell death, is indicative of apoptosis induction and is frequently used as a

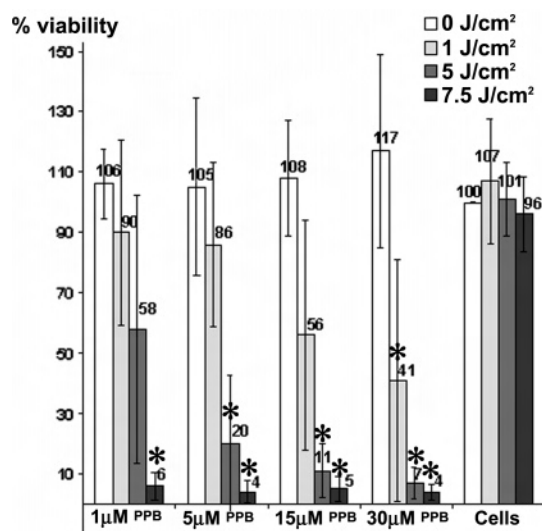


**Figure 5.** PDT efficacy of Pyro-GDEVDGSGK-(BHQ-3) (PPB) determined by cell viability (MTT) assay. Viability of HepG<sub>2</sub> cells after treatment with PPB at four different concentrations (1, 5, 15, and 30 μM) and with three different PDT light doses (1, 5, 7.5 J/cm<sup>2</sup>) compared with cells alone that serve as the 100% viable reference. PPB has minimal dark toxicity even for the highest concentration (30 μM, 0 J/cm<sup>2</sup>) and good PDT efficacy (1 μM, 7.5 J/cm<sup>2</sup>). Comparisons were made to corresponding cell controls by ANOVA (\**P* < 0.05).

target enzyme for apoptosis imaging.<sup>32</sup> We have shown that PDT-BIAS enters the cytoplasm where it triggers apoptotic events after light treatment. As a consequence, the caspase-3 specific sequence which connects the fluorescent photosensitizer with the quencher in PDT-BIAS is cleaved in vitro after light sensitization. The significant increase of the photosensitizer's fluorescence detected in the light-treated area upon caspase-3 specific cleavage is indicative of PDT-triggered apoptosis.

In our study, PDT-BIAS was cleaved in solution by purified caspase-3 enzyme, and the PDT-induced cleavage was also observed in vitro (cancer cells) by confocal microscopy and flow cytometry. To further demonstrate apoptosis involvement in this cleavage we have used an Apoptag assay and fluorescently labeled antibody to visualize apoptosis-specific DNA cleavage and activated caspase-3, respectively, in PDT-BIAS-treated cancer cells. We observed the coexistence of increased signals from both the cleavage of PDT-BIAS and Apoptag assay/anticaspase-3 labeling for cells treated with drug and PDT compared to those cells treated only with drug. We monitored apoptosis using both PDT-BIAS and commercially available apoptosis sensors and can therefore assert that our PDT-BIAS can be used, unlike most current commercial sensors, as a tool for monitoring PDT-triggered apoptosis in situ. We have also made the first attempt to image PDT-triggered apoptosis in vivo, using an intratumor drug injection (Supporting Information, Figure 6).

**Prototype and Targeted PDT-BIAS.** In this proof-of-principle study, we introduced a prototype PDT-BIAS comprised of multiple functional modules featuring a photosensitizer for PDT (Pyro), an apoptosis sensing peptide sequence (caspase-3 specific substrate), an apoptosis reporter (fluorescence of photosensitizer generated upon caspase-3 activation), and a quencher to reduce the background fluorescence thus enhancing the sensitivity. All of these components can be exchanged or modified and their properties fine-tuned, for example, by attaching a delivery vehicle for more discriminate in vivo delivery.

**Apoptosis Detection.** Distinguishing apoptosis from necrosis after PDT treatment is a useful evaluation of new PDT drugs and can be used for optimization of treatment approaches (for example, altering the drug and light dose according to different cancer types). PDT-BIAS can also be used as a membrane-permeant NIR apoptosis sensor for in situ evaluation of other cell-death-causing drugs. Since caspase-3 is exclusively part of the apoptotic machinery, this may be achieved by combining information gained from caspase-3 sensitive probes such as our PDT-BIAS with monitoring the overall cell death marked by Annexin V which is already used as an in situ reporter of cell death, but cannot distinguish apoptosis<sup>5</sup> and necrosis.<sup>33</sup>

**Therapy and Detection.** PDT-BIAS combines therapy with detection. In order for this study to progress from its preliminary phase, we need to circumvent a few problems such as (1) the low cancer-specificity of our nontargeted probe for better in vivo discrimination, (2) the partial singlet oxygen quenching by the BHQ-3 resulting in slightly lower PDT efficacy, and (3) the light-dependent photobleaching of the photosensitizer's fluorescence (although this photobleaching is minimized by the relatively low light doses required for PDT-induced apoptosis). These problems can be solved by attaching a cancer-specific homing molecule and changing the core components of the PDT-BIAS scaffold to adjust its properties. In conclusion, we have shown that membrane-permeable PDT-BIAS can effectively trigger and image apoptosis upon light exposure in situ.

## Experimental Section

The HPLC was run on a Waters 600 controller with a 2996 photodiode array detector and 2475 multi λ fluorescence detector that is used for the analytical HPLC. The eluents are as follows: A = 0.1 M TEAA (pH 7), B = acetonitrile. The method used for all injections is as follows: 90% of A and 10% of B to 100% of B in 45 min, flow: 1.5 mL/min (used for purification) or 1 mL/min (for analysis) on column Zorbax 300SB-C18. The coupling reagents 1-hydroxybenzotriazole (HOBt) and *O*-(benzotriazol-1-yl)-*N,N,N',N'*-tetramethyluronium hexafluorophosphate (HBTU) were purchased from ACROS and Fluka, respectively. MALDI-ToF was obtained from an Applied Biosystems Voyager DE mass spectrometer, and fluorescence was measured on Perkin-Elmer LS50B luminescence spectrometer. We acquired confocal images using a Leica TCS SP2 confocal microscope. The flow cytometry was run on BD LSRII machine for Pyro (exc. 633 nm, em. 695/40) and Alexa Fluor (exc. 488 nm, em. 530/30) at the Flow Cytometry Resource Laboratory, Abramson Cancer Center, at UPENN. Human hepatoblastoma G<sub>2</sub> (HepG<sub>2</sub>) cells were obtained from van Berkel's laboratory from University of Leiden in The Netherlands, and KB cells (human epidermoid carcinoma cells) were purchased from ATCC. We used the following buffers for HepG<sub>2</sub> cells: complete DMEM (87% DMEM—Dulbecco's modified eagle medium, 10% fetal bovine serum, 1% of 200 mM L-glutamine, 1% of 10000 U pen-strep, 1% of 1 M HEPES) and DMEM containing 0.8% BSA (97% DMEM, 8 g/L of bovine serum albumine, 1% of 200 mM L-glutamine, 1% of 10000 U pen-strep, 1% of 1 M HEPES). The buffers used for KB cells were the following: complete MEM (85% MEM—minimum essential medium, 10% fetal bovine serum, 2% of 1.5 g/L sodium bicarbonate, 1% of 200 mM L-glutamine, 1% of 0.1 mM nonessential amino acids and 1% of 1 mM sodium pyruvate) and MEM containing 0.8% BSA (MEM supplemented with 8 g/L of bovine serum albumine). The Apoptag assay (ApopTag plus Fluorescein in situ apoptosis detection kit S7111) was purchased from Chemicon International. The cleaved caspase-3 antibody (Alexa Fluor 488 Conjugate) for flow cytometry was purchased from Cell Signaling Technology. All compounds prepared for in vitro experiments were first dissolved in DMSO (no more than 1% of total volume) then diluted with 0.1% Tween-80 in DNA—water, filtered through a 0.22

$\mu\text{m}$  filter, and further diluted with an appropriate buffer. The laser for PDT treatment was tuned to 670 nm with fluence rate of 20  $\text{mW}/\text{cm}^2$ .

**PPB Synthesis.** For synthesis of immobilized peptide (**1**) see Supporting Information.

**Pyro-GD(Boc)E(Boc)VD(Boc)GS(Boc)GK(Mtt)-Sieber Resin (**2**).** After the last Fmoc group cleavage, the resin was washed and Pyro-acid was coupled to the  $\alpha\text{-NH}_2$  group of N-terminal Gly. The molar ratio of Pyro/HOBt/HBTU to the peptide on resin was 3:1, the coupling time was 17 h, and the reaction was done in the shake flask in dry NMP. The resin was washed afterward by NMP, capped by 0.3 M acetylimidazol in NMP for 15 min, and washed again by excess of NMP, DCM, and dry methanol. The mixture was transferred from the shake flask and dried under high vacuum.

**Pyro-GDEVDGSGK( $\epsilon\text{-NH}_2$ ) (**3**).** Compound **2** was cleaved from resin (33 mg, 8.5  $\mu\text{mol}$ ) and deprotected in one step by 50% TFA/5% TIS/DCM for 2 h to yield Pyro-GDEVDGSGK (**3**, PP) with the  $\epsilon\text{-NH}_2$  group of C-terminal Lys exposed. The compound was precipitated from the cleavage solution by dry ether and prepurified by a few cycles of ether precipitation–DMSO dissolving. Compound **3** (9.6 mg, 7  $\mu\text{mol}$ ) was dried under high vacuum and, without further purification, used in the next reaction. Just a small sample was purified by HPLC and the structure confirmed by MALDI-ToF (mass calculated: 1377.64, found: 1377.95).

**Pyro-GDEVDGSGK( $\epsilon\text{-BHQ-3}$ ) (**4**).** Crude Pyro-GDEVDGSGK (**3**) (6.8 mg, 4.9  $\mu\text{mol}$ ) was dissolved in 50  $\mu\text{L}$  of dry 0.5% DIPEA/DMSO and reacted for 2 h with BHQ-3-NHS (4 mg, 5.1  $\mu\text{mol}$ , purchased from Biosearch Technologies, dissolved in 50  $\mu\text{L}$  of dry DMSO) to give Pyro-GDEVDGSGK-(BHQ-3) (**4**, PPB). The reaction was quenched by precipitation with ether that separates it partially from the redundant BHQ-3-NHS. This final compound was purified by HPLC (the same method as **3**) and dried on speed-vac to obtain 6.5 mg (3.4  $\mu\text{mol}$ ) of pure final product **4** that was stored at  $-20^\circ\text{C}$ . The purity was checked by analytical HPLC coupled with fluorescence and a UV–vis detector ( $\lambda_{\text{max}} = 410\text{ nm}$ ,  $\epsilon \sim 120000$ ) as well as by MALDI-ToF (mass calculated: 1906.91, found: 1906.21).

**Cleavage by Caspase-3 in Solution.** The caspase-3 kit (containing the active form of caspase-3 enzyme, caspase-3 inhibitor Ac-DEVD-CHO,<sup>34</sup> and caspase-3 fluorogenic substrate Z-DEVD-AMC) used for fluorescence and HPLC measurements of PPB cleavage was purchased from BD Pharmagen. The buffer used in all measurements contains 20 mM PIPES, 100 mM NaCl, 10 mM DTT, 1 mM EDTA, 0.1% (w/v) CHAPS, 10% sucrose, 0.3% Tween-80, pH 7.2. The molar ratio of caspase-3:PPB-3:inhibitor is 1:200:3000; the incubation time is 3 h. The activity of caspase-3 was checked before every measurement by its ability to cleave the fluorogenic substrate Z-DEVD-AMC. The PPB sample was prepared as a stock solution of 0.25 mM in DMSO and then diluted to the 6.3  $\mu\text{M}$  solution, while 1 mg of inhibitor was diluted by 1 mL of DMSO to generate a 1 mg/mL stock solution. The composition of each sample is as follows: (1) **PPB alone:** 5  $\mu\text{L}$  of PPB stock solution (0.25 mM) was dissolved in 45  $\mu\text{L}$  of DMSO and 150  $\mu\text{L}$  of buffer to yield 6.3  $\mu\text{M}$  PPB solution. (2) **PPB with caspase-3:** 5  $\mu\text{L}$  of PPB stock solution (0.25 mM) was dissolved in 45  $\mu\text{L}$  of DMSO and 150  $\mu\text{L}$  of buffer (6.3  $\mu\text{M}$  PPB solution), and 0.2  $\mu\text{g}$  of caspase-3 was added. (3) **PPB with caspase-3 and inhibitor:** 5  $\mu\text{L}$  of PPB stock solution (0.25 mM) was dissolved in 35  $\mu\text{L}$  of DMSO, then 10  $\mu\text{L}$  of inhibitor (10  $\mu\text{g}$ ) was added and diluted with 150  $\mu\text{L}$  of buffer (to yield 6.3  $\mu\text{M}$  PPB and 100  $\mu\text{M}$  inhibitor solution) and finally 0.2  $\mu\text{g}$  of caspase-3 was added. All three solutions were incubated for 3 h at  $37^\circ\text{C}$ , and fluorescence was measured using an excitation wavelength of 410 nm and emission at 674 nm after diluting the samples 60-fold by DMSO. After 50 min, 40  $\mu\text{L}$  of each solution was injected into the HPLC.

**Accumulation and Cleavage of PPB in HepG<sub>2</sub> Cells.** HepG<sub>2</sub> cells were grown in 4-well Lab-Tek chamber slides (Naperville, IL) at a density of 50000 cells/well and grown for 24 h in complete DMEM, then rinsed with HBSS (Hank's balanced salt solution) and incubated with 200  $\mu\text{M}$  of the drug in 300  $\mu\text{L}$  of DMEM containing 0.8% BSA at  $37^\circ\text{C}$  for 24 h (except Figure 3E, which

is incubated for 30 min). Cells were repeatedly rinsed with HBSS after the incubation, and 300  $\mu\text{L}$  of complete DMEM was added. PDT-treated cells were illuminated by a laser tuned to 670 nm with a 5  $\text{J}/\text{cm}^2$  light dose and a 20  $\text{mW}/\text{cm}^2$  fluence rate. All cells were fixed 1 hr after PDT by 1% formaldehyde in PBS for 20 min prior to scanning or staining with the Apoptag assay which was performed in accordance with the Chemicon Intl. protocol.

**Settings for Confocal Microscopy.** Detector slits used: 640–800 nm for detection of Pyro and 497–580 nm for Fluorescein (of Apoptag), with zoom = 2, expander = 3, and resolution 1024  $\times$  1024. The settings (objective; power, gain, and offset for each wavelength respectively) for Figure 3: 40  $\times$  objective, 633 nm: 81%, 861.4,  $-19.7$ . For Figure 4: 100  $\times$  objective, 488 nm: 100%, 757.3, 5; 633 nm: 100%, 753.2,  $-21.9$ .

**Flow Cytometry Experiment.** KB cells ( $1 \times 10^6$ ) were seeded in T25 flasks and grown for 1 day in complete MEM. The cells were incubated for 12 h with 15  $\mu\text{M}$  PPB in MEM containing 0.8% BSA (1.5 mL/flask), and at the end of incubation the medium was aspirated and cells washed 3 times with 3 mL of PBS and complete MEM was added. Cells intended for PDT were immediately treated with 10  $\text{J}/\text{cm}^2$ . The cells were carefully harvested 20 h after PDT or drug aspiration by repeated washing first with PBS (most of the PDT-treated cells were already floating) and later with 0.01% Trypsine-EDTA or 0.5 mM EDTA. The cells were fixed with 2% methanol-free formaldehyde in PBS and stained with cleaved caspase-3 antibody (Alexa Fluor 488 conjugate) according to Cell Signaling Technology protocol. Flow cytometry detected FSC/SSC parameters, Pyro (633 nm laser) (cleaved PPB), and Alexa Fluor (488 nm laser) (Antibody staining).

**Cell Viability Assay (MTT Assay).** HepG<sub>2</sub> cells were seeded in clear 96-well plates at a density of 50000 cells/well in 250  $\mu\text{L}$  of complete DMEM and grown overnight at  $37^\circ\text{C}$ . Cells were subsequently rinsed with HBSS and incubated with no or 1, 5, 15, or 30  $\mu\text{M}$  drug in DMEM containing 0.8% BSA (12 wells/concentration) for 20 h. Cells were then rinsed with HBSS, 100  $\mu\text{L}$  of complete DMEM was added, and the cells were treated with three different light doses (by 670 nm laser with 20  $\text{mW}/\text{cm}^2$  fluence rate): 3 wells/concentration/light dose with 3 wells/light dose for “light only control” and 3 wells/concentration kept in dark as “drug only control”. After incubation for 24 h at  $37^\circ\text{C}$ , the cells were incubated for 2 h with a 0.5 mg/mL solution of MTT in complete DMEM, which was disposed afterward and replaced with 100  $\mu\text{L}$  of 70% 2-propanol in 0.1 M HCl. Absorbance at 570 nm was measured. Data shown in Figure 5 were based on 3–8 different experiments, and the results were expressed as mean  $\pm$  standard error. Analysis of variance (ANOVA) with Tukey's multiple comparison post hoc testing was used for evaluation of differences between groups. Differences with *P* value less than 0.05 will be deemed significant.

**Acknowledgment.** We thank Ponzy Lu and Brian C. Wilson for helpful discussions and André E. X. Brown and Cara Bertozzi for critical comments and suggestions on the manuscript. We also thank William F. DeGrado for access to the MALDI-ToF. This work was supported by the DOD Breast Cancer Research Program DAMD17-03-1-0373 and the NIH Grant U54 CA105008.

**Supporting Information Available:** Figure 1 showing purity, UV–vis, and MALDI-ToF of PP (**3**); Figure 2 showing purity, UV–vis, and MALDI-ToF of PPB (**4**); Figure 3 showing HPLC of scrambled sequence Pyro-GPLGLARK-(BHQ-3) (sPPB) incubated with caspase-3 for 180 min; Figure 4 showing accumulation of PPB (**4**) inside KB cells monitored by fluorescence microscopy; Figure 5 showing HepG<sub>2</sub> cells incubated with scrambled sequence Pyro-GHSSK(BHQ-3)LQL and Pyro-GDEVDGSGK-(BHQ-3) (**4**) and activated by light monitored by confocal microscopy; ANOVA test for MTT study; Figure 6 showing preliminary *in vivo* experiment; synthesis of Fmoc-GD(Boc)E(Boc)VD(Boc)GS(Boc)-

GK(Mt)-Sieber (1). This material is available free of charge via the Internet at <http://pubs.acs.org>.

## References

- Thompson, C. B. Apoptosis in the pathogenesis and treatment of disease. *Science* **1995**, *267*, 1456–1462.
- Kaufmann, S. H.; Gores, G. J. Apoptosis in cancer: cause and cure. *Bioessays* **2000**, *22*, 1007–1017.
- Van Cruchten, S.; Van Den Broeck, W. Morphological and biochemical aspects of apoptosis, oncosis and necrosis. *Anat., Histol., Embryol.* **2002**, *31*, 214–223.
- Vermes, I.; Haanen, C.; Reutelingsperger, C. Flow cytometry of apoptotic cell death. *J. Immunol. Methods* **2000**, *243*, 167–190.
- Petrovsky, A.; Schellenberger, E.; Josephson, L.; Weissleder, R.; Bogdanov, A., Jr. Near-infrared fluorescent imaging of tumor apoptosis. *Cancer Res.* **2003**, *63*, 1936–1942.
- Bohm, I.; Schild, H. Apoptosis: the complex scenario for a silent cell death. *Mol. Imaging Biol.* **2003**, *5*, 2–14.
- Walsh, G. M.; Dewson, G.; Wardlaw, A. J.; Levi-Schaffer, F.; Moqbel, R. A comparative study of different methods for the assessment of apoptosis and necrosis in human eosinophils. *J. Immunol. Methods* **1998**, *217*, 153–163.
- Gujral, J. S.; Knight, T. R.; Farhood, A.; Bajt, M. L.; Jaeschke, H. Mode of cell death after acetaminophen overdose in mice: apoptosis or oncotic necrosis? *Toxicol. Sci.* **2002**, *67*, 322–328.
- Thornberry, N. A.; Lazebnik, Y. Caspases: enemies within. *Science* **1998**, *281*, 1312–1316.
- Dougherty, T. J.; Kaufman, J. E.; Goldfarb, A.; Weishaupt, K. R.; Boyle, D.; et al. Photoradiation therapy for the treatment of malignant tumors. *Cancer Res.* **1978**, *38*, 2628–2635.
- Dougherty, T. J.; Gomer, C. J.; Henderson, B. W.; Jori, G.; Kessel, D. et al. Photodynamic therapy. *J. Natl. Cancer I* **1998**, *90*, 889–905.
- Rosenkranz, A. A.; Jans, D. A.; Sobolev, A. S. Targeted intracellular delivery of photosensitizers to enhance photodynamic efficiency. *Immunol. Cell Biol.* **2000**, *78*, 452–464.
- Wilson, B. C.; Patterson, M. S. The physics of photodynamic therapy. *Phys. Med. Biol.* **1986**, *31*, 327–360.
- Niedre, M.; Patterson, M. S.; Wilson, B. C. Direct near-infrared luminescence detection of singlet oxygen generated by photodynamic therapy in cells in vitro and tissues in vivo. *Photochem. Photobiol.* **2002**, *75*, 382–391.
- Oleinick, N. L.; Evans, H. H. The photobiology of photodynamic therapy: cellular targets and mechanisms. *Radiat. Res.* **1998**, *150*, S146–S156.
- Moor, A. C. Signaling pathways in cell death and survival after photodynamic therapy. *J. Photochem. Photobiol., B* **2000**, *57*, 1–13.
- Oleinick, N. L.; Morris, R. L.; Belichenko, I. The role of apoptosis in response to photodynamic therapy: what, where, why, and how. *Photochem. Photobiol. Sci.* **2002**, *1*, 1–21.
- Almeida, R. D.; Manadas, B. J.; Carvalho, A. P.; Duarte, C. B. Intracellular signaling mechanisms in photodynamic therapy. *Biochim. Biophys. Acta* **2004**, *2*, 59–86.
- Lavie, G.; Kaplinsky, C.; Toren, A.; Aizman, I.; Meruelo, D.; et al. A photodynamic pathway to apoptosis and necrosis induced by dimethyl tetrahydroxyhelianthone and hypericin in leukaemic cells: possible relevance to photodynamic therapy. *Br. J. Cancer* **1999**, *79*, 423–432.
- Kessel, D.; Luo, Y.; Deng, Y.; Chang, C. K. The role of subcellular localization in initiation of apoptosis by photodynamic therapy. *Photochem. Photobiol.* **1997**, *65*, 422–426.
- Kessel, D.; Luo, Y. Photodynamic therapy: a mitochondrial inducer of apoptosis. *Cell Death Differ.* **1999**, *6*, 28–35.
- Kessel, D. Relocalization of cationic porphyrins during photodynamic therapy. *Photochem. Photobiol. Sci.* **2002**, *1*, 837–840.
- Morris, R. L.; Azizuddin, K.; Lam, M.; Berlin, J.; Nieminen, A. L.; et al. Fluorescence resonance energy transfer reveals a binding site of a photosensitizer for photodynamic therapy. *Cancer Res.* **2003**, *63*, 5194–5197.
- Porter, A. G.; Janicke, R. U. Emerging roles of caspase-3 in apoptosis. *Cell Death Differ.* **1999**, *6*, 99–104.
- MacDonald, I. J.; Morgan, J.; Bellnier, D. A.; Paszkiewicz, G. M.; Whitaker, J. E. et al. Subcellular localization patterns and their relationship to photodynamic activity of pyropheophorbide-a derivatives. *Photochem. Photobiol.* **1999**, *70*, 789–797.
- Sun, X.; Leung, W. N. Photodynamic therapy with pyropheophorbide-a methyl ester in human lung carcinoma cancer cell: efficacy, localization and apoptosis. *Photochem. Photobiol.* **2002**, *75*, 644–651.
- Zhang, M.; Zhang, Z.; Blessington, D.; Li, H.; Busch, T. M.; et al. Pyropheophorbide 2-deoxyglucosamide: a new photosensitizer targeting glucose transporters. *Bioconjugate Chem.* **2003**, *14*, 709–714.
- Chiu, S. M.; Oleinick, N. L. Dissociation of mitochondrial depolarization from cytochrome *c* release during apoptosis induced by photodynamic therapy. *Br. J. Cancer* **2001**, *84*, 1099–1106.
- Bellnier, D. A.; Greco, W. R.; Loewen, G. M.; Nava, H.; Oseroff, A. R.; et al. Population pharmacokinetics of the photodynamic therapy agent 2-[1-hexyloxyethyl]-2-devinyl pyropheophorbide-a in cancer patients. *Cancer Res.* **2003**, *63*, 1806–1813.
- Chen, J.; Stefflova, K.; Niedre, M. J.; Wilson, B. C.; Chance, B.; et al. Protease-triggered photosensitizing beacon based on singlet oxygen quenching and activation. *J. Am. Chem. Soc.* **2004**, *126*, 11450–11451.
- Pham, W.; Weissleder, R.; Tung, C. H. An azulene dimer as a near-infrared quencher. *Angew. Chem., Int. Ed. Engl.* **2002**, *41*, 3659–3662.
- Bullock, K.; Piwnicka-Worms, D. Synthesis and characterization of a small, membrane-permeant, caspase-activatable far-red fluorescent peptide for imaging apoptosis. *J. Med. Chem.* **2005**, *48*, 5404–5407.
- Appelt, U.; Sheriff, A.; Gaipl, U. S.; Kalden, J. R.; Voll, R. E.; et al. Viable, apoptotic and necrotic monocytes expose phosphatidylserine: cooperative binding of the ligand Annexin V to dying but not viable cells and implications for PS-dependent clearance. *Cell Death Differ.* **2005**, *12*, 194–196.
- Garcia-Calvo, M.; Peterson, E. P.; Leiting, B.; Ruel, R.; Nicholson, D. W.; et al. Inhibition of human caspases by peptide-based and macromolecular inhibitors. *J. Biol. Chem.* **1998**, *273*, 32608–32613.

JM060146U

# Targeted Photodynamic Therapy Agent with a Built-In Apoptosis Sensor for In Vivo Near-Infrared Imaging of Tumor Apoptosis Triggered by Its Photosensitization In Situ

Klara Stefflova, Juan Chen, Hui Li, and Gang Zheng

## Abstract

Imaging apoptotic cells or tissues after cancer therapy in situ would be a very useful tool for assessing proper treatment conditions and therapeutic outcome. By combining therapeutic and imaging functions, we have designed a multifunctional, membrane-permeable, and cancer-specific agent that triggers and images apoptosis in targeted cells. We chose photodynamic therapy (PDT) as an appropriate cancer treatment modality and caspase 3 as an apoptosis-specific imaging target. This targeted photodynamic therapy agent with a built-in apoptosis sensor (TaBIAS) induces photodamage only to target cells and simultaneously identifies those that are apoptotic by its near-infrared fluorescence. It contains a fluorescent photosensitizer used as an anticancer drug and a cancer-associated folate receptor homing molecule connected to a caspase 3 cleavable peptide linker that has a fluorescence quencher on the opposing site. We demonstrated that PDT-triggered cleavage of the peptide linker by caspase 3, one of the key executioner caspases, results in a detectable increase in fluorescence in folate receptor-overexpressing cancer cells and tumors. The presence of apoptosis was confirmed in vitro by flow cytometry and ex vivo by Apoptag assay, supporting the ability of TaBIAS to specifically induce and image apoptosis in situ.

**A**POPTOSIS is a natural process for eliminating unwanted cells in a healthy organism, but failure to induce apoptosis in abnormal cells leads to severe diseases, including cancer.<sup>1</sup> Naturally, many drugs target this malfunction by restoring programmed cell death.<sup>2</sup> Imaging apoptosis in situ<sup>3</sup> would, therefore, be crucial for understanding both physiologic or pathologic cases of excessive apoptosis and would also help to locate the affected site and assess the therapeutic outcome of apoptosis-inducing drugs in vivo.

One of the promising cancer treatment modalities is photodynamic therapy (PDT).<sup>4</sup> It uses a light-activated photosensitizer for the production of reactive singlet

oxygen species<sup>5</sup> that damage the cellular targets within a short range from the photosensitizer's site of accumulation. The therapeutic outcome of PDT depends not only on all three actors involved—light, the photosensitizer, and molecular oxygen availability—but also on the tumor and tissue type.<sup>6</sup> Given that PDT-induced cell death via apoptosis is a desirable end point, developing a bifunctional PDT agent that triggers and images apoptosis in situ would be an important advance.

Here we introduce a targeted photodynamic therapy agent with a built-in apoptosis sensor (TaBIAS) that is designed to detect PDT-induced apoptosis triggered only in targeted cancer cells using real-time near-infrared (NIR) fluorescence imaging and thus to serve as the earliest self-evaluation of its therapeutic outcome in vivo. Our prototype construct, folate receptor targeted TaBIAS, consists of four components (Figure 1): (1) a photosensitizer that was shown to localize near mitochondria (pyropheophorbide *a*),<sup>7</sup> (2) a fluorescence quencher that effectively quenches the photosensitizer's fluorescence Black Hole Quencher-3 (BHQ-3), (3) a caspase 3 cleavable sequence (KGDEVDSGSK)<sup>8,9</sup> with a photosensitizer and a quencher attached at opposing ends, and (4) a tumor-homing molecule folate (F) for in vivo specificity, targeting

From the Departments of Chemistry and Radiology, University of Pennsylvania, Philadelphia, PA.

This work was supported by the Department of Defense Breast Cancer Research Program DAMD17-03-1-0373 and National Institutes of Health grant U54 CA105008 (Penn NTROI).

Address reprint requests to: Gang Zheng, PhD, Department of Radiology, Chemistry Building Wing 1958, Room 284, 231 S. 34th Street, Philadelphia, PA 19104; e-mail: Gang.Zheng@uphs.upenn.edu.

DOI 10.2310/7290.2006.00027

© 2006 BC Decker Inc

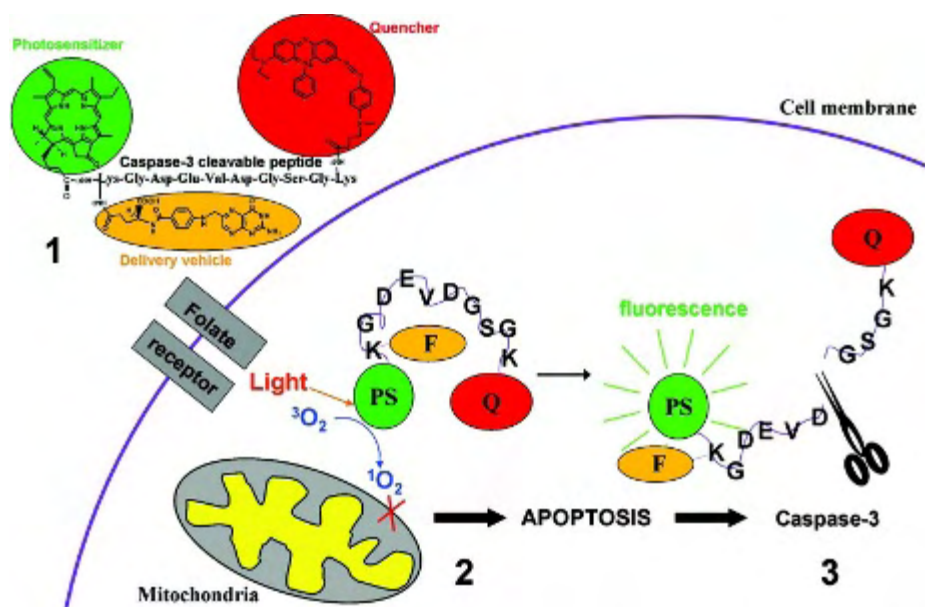


**Figure 1.** Structure and function of a targeted photodynamic therapy agent with a built-in apoptosis sensor (TaBIAS). TaBIAS consists of four parts: the fluorescent photosensitizer (pyro [PS]), caspase 3 cleavable sequence (KGDEVDGSGK), fluorescence quencher (BHQ-3 [Q]), and delivery vehicle (folate [F]) (1). This molecule accumulates preferentially in cells overexpressing folate receptor, and once activated by light, the photosensitizer produces reactive singlet oxygen that destroys the mitochondrial membrane and triggers apoptosis (2). This leads to activation of caspase 3, which cleaves the peptide linker between the PS and the Q, thus restoring the PS's fluorescence and identifying those cells dying by apoptosis by NIR fluorescence imaging (3).

cells that overexpress folate receptor (FR).<sup>10</sup> This construct enters cells via a folate delivery pathway, and when activated by light, the photosensitizer produces singlet oxygen that damages mitochondria,<sup>11</sup> causing apoptosis.<sup>12</sup> This consequently leads to activation of caspase 3,<sup>13</sup> indicating the irreversible point in apoptotic death. Activated caspase 3 promptly cleaves the peptide linker between the photosensitizer and the quencher, restoring the photosensitizer's intrinsic fluorescence and indicating those cells dying by apoptosis. Therefore, TaBIAS induces apoptosis and visualizes it using its own NIR fluorescence.

In a previous study, we designed a nontargeted photodynamic therapy agent with a built-in apoptosis sensor (PDT-BIAS) and demonstrated that this construct is indeed an effective PDT agent and that cleavage of the peptide linker by caspase 3 results in a detectable increase in fluorescence in solution and in cancer cells after PDT treatment (data to be published elsewhere). We therefore confirmed at the cellular level that imaging of tumor cell apoptosis that is triggered by its photosensitization in situ is indeed feasible. However, since PDT-BIAS is nontargeted, it would be a significant challenge to prove this new concept in vivo using intravenous injection and thus enable practical use. Here we report the first targeted PDT-BIAS (TaBIAS) with the ultimate goal of providing a clinically useful strategy for enhancing the specificity and efficacy of PDT in cancer treatment.

We have synthesized TaBIAS and shown that it is cleaved by caspase 3 in solution, in cells, and in animals. We have

confirmed that TaBIAS selectively discriminates between KB cells (overexpressing folate receptor) and HT 1080 cells (lacking folate receptor expression) both in vitro and in vivo. We have also shown that TaBIAS is specifically cleaved by caspase 3 in solution and as a consequence of PDT-triggered apoptosis in cells and animals. The folate receptor-overexpressing KB cells treated with TaBIAS and light display (1) a greater increase in fluorescence from TaBIAS cleavage compared with both the HT 1080 cells under the same conditions (owing to lower accumulation of TaBIAS in HT 1080 cells) and the KB cells treated only with TaBIAS (apoptosis was not triggered without light treatment), (2) shrunken or hypergranular apoptotic morphology monitored by flow cytometry, and (3) decreasing viability with increasing light and drug dose monitored by 3-(4,5-dimethylthiazol-2-yl)-2,5-diphenyltetrazolium bromide (MTT) assay.

Using a double-tumor mouse bearing both a folate receptor-positive (KB; FR+) and a folate receptor-negative (HT 1080; FR-) tumor, we have shown that TaBIAS discriminates between these two tumors, induces apoptosis, and images activated caspase 3 as a marker of this cell death in situ. We proved that the folate receptor-overexpressing KB tumor that was treated with both TaBIAS and PDT is highly apoptotic by ex vivo staining of the dissected tumors with Apoptag assay, an accepted apoptosis-detecting method. Therefore, by detecting both fluorescence from cleaved TaBIAS and apoptosis in vitro, in vivo, and ex vivo, we have demonstrated that the photodamage induced by TaBIAS-based PDT causes apoptosis and can be

consequently visualized using the same molecule by tracking the NIR fluorescence signal by in situ imaging.

## Materials and Methods

The final compound 6 (and intermediates 3, 4, and 5 for obtaining matrix-assisted laser desorption–ionization time of flight mass spectrometry [MALDI-ToF]) was purified by high-performance liquid chromatography (HPLC) (Waters 600 controller with a 2996 photodiode array detector, Waters Corporation, Milford, CT). The eluents were A = 0.1 M TEAA (triethyl amine + acetic acid) (pH 7) and B = acetonitrile, and the method used for all injections was 90% of A and 10% of B to 100% of B in 45 minutes with flow 1.5 mL/min on column Zorbax 300SB-C3 (Agilent, West Chester, PA). The coupling reagents 1-hydroxybenzotriazole (HOBt) and *O*-(benzotriazol-1-yl)-*N,N,N',N'*-tetramethyluronium hexafluorophosphate (HBTU) were purchased from ACROS and Fluka, respectively. MALDI-ToF was obtained from an Applied Biosystems (Foster City, CA) Voyager DE Mass Spectrometer, and fluorescence was measured on a Perkin Elmer (Fremont, CA) LS50B Luminescence Spectrometer. We acquired confocal images using a Leica (Exton, PA) TCS SP2 Confocal Microscope and Xenogen images at the Bioluminescence Molecular Imaging Core facility at the University of Pennsylvania on an IVIS Xenogen Imager. KB cells (human epidermal cancer cells; folate receptor positive) and HT 1080 cells (human fibrosarcoma cells; folate receptor negative) were both purchased from the American Type Culture Collection. “Complete MEM” consists of 85% Minimum Essential Medium (MEM), 10% fetal bovine serum, 2% 1.5 g/L sodium bicarbonate, 1% of 200 mM L-glutamine, 1% 0.1 mM nonessential amino acids, and 1% 1 mM sodium pyruvate, and “MEM containing 0.8% BSA” consists of MEM supplemented with 8 g/L of bovine serum albumin (BSA). The Apoptag assay (ApopTag Plus Fluorescein In Situ Apoptosis Detection Kit S7111) was purchased from Chemicon International. The compound prepared for in vitro and in vivo experiments was first dissolved in dimethylsulfoxide (DMSO) (no more than 0.5% of total volume) and then diluted with 0.1% Tween 80 in DNA-water, filtered through a 0.22 μm filter, and further diluted with MEM containing 0.8% BSA (for the cells) or saline (for the animal). The laser for PDT treatment was tuned to 670 nm with a fluence rate of 20 mW/cm<sup>2</sup> for in vitro studies and 75 mW/cm<sup>2</sup> for in vivo experiments. Mice were euthanized according to guidelines established by the Institutional Animal Care and Use Committee of the University of Pennsylvania.

## pyro-K(Folate)GDEVDSGSK(BHQ-3) (PFPB) Synthesis

*Fmoc-K(Boc)GD(O-2-PhiPr)E(O-2-PhiPr)VD(O-2-PhiPr)GS(Trt)GK(Mtt)-Sieber Resin*

The peptide was synthesized by manual solid-phase peptide synthesis (SPPS) using commercially available Fmoc amine protected amino acids as building blocks and Sieber resin (cleavable by 1% trifluoroacetic acid [TFA]) as a solid phase, all purchased from Novabiochem.

*Pyro-K(Boc)GD(O-2-PhiPr)E(O-2-PhiPr)VD(O-2-PhiPr)GS(Trt)GK(Mtt)-Sieber Resin*

After the last Fmoc group cleavage, the resin was washed with 1-methyl-2-pyrrolidinone (NMP) and pyro-acid was coupled to the α-NH<sub>2</sub> group of the N-terminal lysine. The molar ratio of pyro/HOBt/HBTU to the peptide on resin was 3/3/3:1, and the reaction was done in a shake flask with a 12-hour coupling time using dry NMP as a solvent. The resin was then washed with NMP, capped by 0.3 M acetylimidazole in NMP for 15 minutes, and washed again by an excess of NMP, dichloromethane (DCM), and dry methanol, transferred from the shake flask and dried.

*Pyro-K(Boc)GDEVDSGSK(NH<sub>2</sub>)*

Compound 2 (37.7 mg, 11.5 μmol) was cleaved from the resin and carefully deprotected (from Trt, Mtt, and O-2-PhiPr protecting groups with retaining Boc on N-terminal Lys) in one step by 3% TFA, 5% triisopropylsilane, and DCM for 1 hour to yield pyro-K(Boc)-GDEVDSGSK(NH<sub>2</sub>) (3, PK(Boc)P) with the ε-NH<sub>2</sub> group of the C-terminal lysine exposed. The compound was precipitated from the cleavage solution by dry ether and prepurified by a few cycles of ether precipitation-DMSO dissolving. Compound 3 (10.9 mg, 6.8 μmol) was dried under a high vacuum and, without further purification, used in the next reaction. Only a small sample was purified by HPLC, and the structure was confirmed by MALDI-ToF (mass calculated 1,605.78; found 1,605.61).

*Pyro-K(Boc)GDEVDSGSK(BHQ-3)*

Crude pyro-K(Boc)GDEVDSGSK(NH<sub>2</sub>) (3) (9.3 mg, 5.8 μmol) was dissolved in 100 μL of dry 1% *N,N*-diisopropylethylamine (DIPEA) and DMSO and reacted for 2 hours with BHQ-3-NHS (4.7 mg, 6 μmol; BHQ-3, purchased from Biosearch Technologies) dissolved in 100 μL of dry DMSO to give pyro-K(Boc)GDEVDSGSK(BHQ-3) (4, PK(Boc)PB). The reaction was quenched by precipitation with ether that separates it partially from the

redundant BHQ-3-NHS. Compound 4 (11.7 mg, 5.5  $\mu\text{mol}$ ) was dried under a high vacuum and, without further purification, used in the next reaction. Just a small sample was purified by HPLC, and the structure was confirmed by MALDI-ToF (mass calculated 2,135.05; found: 2,134.64).

#### *Pyro-K(NH<sub>2</sub>)GDEVDGSGK(BHQ-3)*

The Boc protecting group was cleaved from pyro-K(Boc)GDEVDGSGK(BHQ-3) (3) (11.5 mg, 5.4  $\mu\text{mol}$ ) by treating it with 50% TFA, 5% TIS, and DCM for 2 hours to give pyro-K(NH<sub>2</sub>)GDEVDGSGK(BHQ-3) (5, PK(NH<sub>2</sub>)PB). The DCM and TFA were evaporated. Compound 5 (10.6 mg, 5.2  $\mu\text{mol}$ ) was dried on a high vacuum and used in the final reaction without further purification. A small sample was purified by HPLC, and the structure was confirmed by MALDI-ToF (mass calculated 2,035.00; found 2,034.83).

#### *Pyro-K(Folate)GDEVDGSGK(BHQ-3)*

Pyro-K(NH<sub>2</sub>)GDEVDGSGK(BHQ-3) (5) (10.4 mg, 5.1  $\mu\text{mol}$ ) was dissolved in 100  $\mu\text{L}$  of dry 0.5% DIPEA-DMSO and reacted for 3 hours with folate-NHS (4.3 mg, 8  $\mu\text{mol}$ ) dissolved in 100  $\mu\text{L}$  of dry DMSO to give pyro-K(folate)GDEVDGSGK(BHQ-3) (6, PFPB). The reaction was concentrated by precipitation with ether and directly separated by HPLC. Purified compound 6 (7.4 mg, 3  $\mu\text{mol}$ ) was dried under a high vacuum and stored at  $-20^\circ\text{C}$ . The purity was checked by HPLC and MALDI-ToF (mass calculated 2,458.13; found 2,457.10).

#### **PFPB Activation by Caspase 3 in Solution**

The caspase 3 kit (containing the active form of caspase 3 enzyme [molecular weight (MW) = 32,000], caspase 3 inhibitor Ac-DEVD-CHO<sup>14</sup> [MW = 502], and caspase 3 fluorogenic substrate Z-DEVD-AMC) was purchased from BD Pharmagen. The buffer used for cleavage contains 20 mM PIPES, 100 mM NaCl, 10 mM DTT, 1 mM ethylenediaminetetraacetic acid (EDTA), 0.1% (w/v) CHAPS, 10% sucrose, and 0.3% Tween 80 and has a pH of 7.2. The molar ratio of caspase 3 to PFPB to inhibitor is 1:80:2,000, and the incubation time is 2.5 hours. The activity of caspase 3 was checked before every measurement by its ability to cleave the fluorogenic substrate Z-DEVD-AMC. The PFPB sample was prepared as a stock solution of 15.5  $\mu\text{M}$  in 0.1% DMSO-buffer, and 1 mg of inhibitor was diluted by 1 mL of DMSO to generate a 1 mg/mL stock solution. The composition of each sample (each 12.5  $\mu\text{M}$

PFPB) is as follows: (1) PFPB alone: 100  $\mu\text{L}$  of PFPB stock solution with 20  $\mu\text{L}$  of DMSO and 3  $\mu\text{L}$  of buffer; (2) PFPB with caspase 3: 100  $\mu\text{L}$  of PFPB stock solution with 20  $\mu\text{L}$  of DMSO and 3  $\mu\text{L}$  caspase 3 solution (0.2  $\mu\text{g}/\mu\text{L}$ ); and (3) PFPB with caspase 3 and inhibitor: 100  $\mu\text{L}$  of PFPB stock solution with 20  $\mu\text{L}$  of inhibitor (1 mg/mL) and 3  $\mu\text{L}$  of caspase 3 solution (0.2  $\mu\text{g}/\mu\text{L}$ ). All three solutions were incubated for 2.5 hours at  $37^\circ\text{C}$ , and fluorescence was measured using an excitation wavelength of 650 nm and emission at 674 nm after diluting the samples 60-fold by DMSO. Formation of two fragments was confirmed by HPLC.

#### **Accumulation and Cleavage of PFPB in KB and HT 1080 Cells**

KB and HT 1080 cells were grown in four-well Lab-Tek chamber slides (Naperville, IL) at a density of 50,000 cells/well, grown for 24 hours in complete MEM, and then rinsed with Hank's Balanced Salt Solution (HBSS) and incubated with 40 and 20  $\mu\text{M}$  drug in 300  $\mu\text{L}$  of folate-free medium at  $37^\circ\text{C}$  for 4.5 hours. Cells were repeatedly rinsed with HBSS after the incubation, and 300  $\mu\text{L}$  of complete MEM was added. PDT-treated cells were illuminated by a laser tuned to 670 nm with a 1.5  $\text{J}/\text{cm}^2$  light dose and a 20  $\text{mW}/\text{cm}^2$  fluence rate. All cells were fixed 4 hours after PDT or drug aspiration by 1% formaldehyde in PBS for 20 minutes prior to scanning with confocal microscopy. The settings for confocal microscopy are as follows: 640 to 800 nm detector slit for detection of pyro fluorescence, with zoom = 2, expander = 3, resolution  $512 \times 512$ , 633 nm excitation wavelength, 40  $\times$  objective, 100% power, 851.1 gain, and  $-28.5$  offset.

#### **Flow Cytometry Experiment**

KB cells ( $1 \times 10^6$ ) were seeded in T25 flasks and grown for 1 day in complete MEM. The cells were incubated for 12 hours with 3  $\mu\text{M}$  PFPB in MEM containing 0.8% BSA (1.3 mL/flask), and at the end of incubation, the medium was aspirated, cells were washed three times with 2 mL of PBS, and a 1.5 mL/flask of complete MEM was added. Cells intended for PDT were immediately treated with 10  $\text{J}/\text{cm}^2$ . All cells were carefully harvested 4.5 hours after PDT (5 hours after drug aspiration) by repeated washing first with PBS and then with 0.5 mM EDTA-PBS and in the end with 0.01% trypsin-0.5 mM EDTA-PBS. The cells were resuspended in 1 mL of PBS and immediately analyzed on a BD LSRII machine at the Flow Cytometry Laboratory, Abramson Cancer Center at the University of Pennsylvania, focusing on forward scatter, side scatter

(FSC-SSC) parameters and pyro fluorescence (excitation 633 nm, emission 695 nm). To assess the fraction of necrotic cells, the cells were either stained with trypan blue and counted or labeled with 4',6-diamidino-2-phenylindole (DAPI) (3  $\mu$ M, 500,000 cells) and analyzed by flow cytometry immediately after harvesting. For antibody staining, the cells were permeabilized by methanol and stained with cleaved caspase 3 (Alexa Fluor488 Conjugate) antibody for 1 hour as described in the Cell Signaling Technology protocol.

### Cell (MTT) Viability Assay

KB cells were seeded in clear 96-well plates at a density of 50,000 cells/well in 250  $\mu$ L of complete MEM and grown for 24 hours at 37°C. Cells were subsequently rinsed with HBSS and incubated with no or 1, 5, or 10  $\mu$ M PFPB in MEM containing 0.8% BSA for 24 hours. Cells were then rinsed with HBSS, 100  $\mu$ L of complete MEM was added, and the cells were treated with three different light doses (by 670 nm laser with 20 mW/cm<sup>2</sup> fluence rate). After incubation for 24 hours at 37°C, the cells were incubated for 2 hours with a 0.5 mg/mL solution of MTT (3-(4,5-dimethylthiazol-2-yl)-2,5-diphenyltetrazolium bromide) in complete MEM that was disposed afterward and replaced with 100  $\mu$ L of 1:1 DMSO to 70% isopropanol in 0.1 M HCl. Absorbance at 570 nm was measured. The data are based on three different experiments. The results are expressed as mean  $\pm$  standard error, and statistically significant differences between neighboring light doses within each drug concentration are indicated as  $p < .05$ .

### In Vivo Imaging

To obtain an appropriate mouse model, nude mice were inoculated subcutaneously with 10<sup>7</sup> KB cells above the right leg and 10<sup>7</sup> HT 1080 cells above the left leg, and the tumors were grown for about 7 days. In the first case, 100  $\mu$ L of 80 nmol of PFPB was injected intravenously into the tail vein of each of the two mice. Both KB and HT 1080 tumors of one mouse were treated by PDT with a light dose of 90 J/cm<sup>2</sup> per tumor 18 hours after injection and monitored by a Xenogen IVIS imager with a Cy 5.5 filter ( $\lambda_{exc}$  = 615–665 nm,  $\lambda_{em}$  = 695–770 nm) until 23 hours after PDT (41 hours after injection), when the mouse was sacrificed. The control mouse was sacrificed 25 hours after injection. In the second case, one double-tumor bearing mouse was intravenously injected with 25 nmol of PFPB, and both tumors were treated with a 90 J/cm<sup>2</sup> light dose per tumor 3 hours after

injection and monitored by Xenogen. This mouse was sacrificed 24 hours after injection.

### Histology

Histology slides were obtained from three mice in total: (1) KB and HT 1080 tumor tissue dissected from the first mouse injected with 80 nmol of PFPB and treated with light (41 hours after injection); (2) KB and HT 1080 tumor tissue dissected from the control mouse injected with 80 nmol of the drug and kept in the dark (25 hours after injection); and (3) KB tumor and HT 1080 tissue dissected from the mouse injected with 25 nmol of PFPB and treated with light (24 hours after the injection). Both HT 1080 and KB tumors from the first two mice were fixed with 1% formaldehyde in PBS immediately after dissection, whereas both tumors of the third mouse were frozen in liquid nitrogen immediately after dissection. Cryosections were made from all of these samples and an Apoptag assay was performed according to the manufacturer's procedure for all histology tissue samples using the same protocol except for the sections from the mouse injected with 25 nmol of PFPB, which were fixed with 1% formaldehyde prior to processing. Slides were scanned 24 hours after fixation by confocal microscopy with the following setting: 40  $\times$  objective, fluorescein channel: excitation 488 nm, 84% gain, gain 714.8; offset-4.2.

### Results

#### Synthesis of PFPB

The synthesis started with an SPPS, giving Fmoc-K-(Boc)GD(O-2-PhiPr)E(O-2-PhiPr)VD(O-2-PhiPr)GS(Trt)-GK(Mtt) on Sieber resin (1). After the last Fmoc group was cleaved to expose the  $\alpha$ -NH<sub>2</sub> of N-terminal lysine, pyroacid, activated by HOBt/HBTU, was coupled to the N-terminus of this immobilized peptide (Figure 2). In one step, immobilized pyro-K(Boc)GD(O-2-PhiPr)E(O-2-PhiPr)VD(O-2-PhiPr)GS(Trt)GK(Mtt) (2) was cleaved from the solid phase and partially deprotected (retaining the Boc protecting group) with 3% TFA, giving a pyro-K(Boc)GDEVDSGK(NH<sub>2</sub>) (3, PK(Boc)P) with an unprotected  $\epsilon$ -NH<sub>2</sub> group on the C-terminal lysine. This compound was precipitated from TFA by dry ether, and the quencher BHQ-3-NHS was coupled in a solution reaction to the C-terminal lysine under mild basic and anhydrous conditions. The product was then precipitated with ether and dried to give pyro-K(Boc)GDEVDSGK(BHQ-3) (4, PK(Boc)PB). Compound 4 was immediately deprotected using 50% TFA, exposing the  $\epsilon$ -NH<sub>2</sub> group on

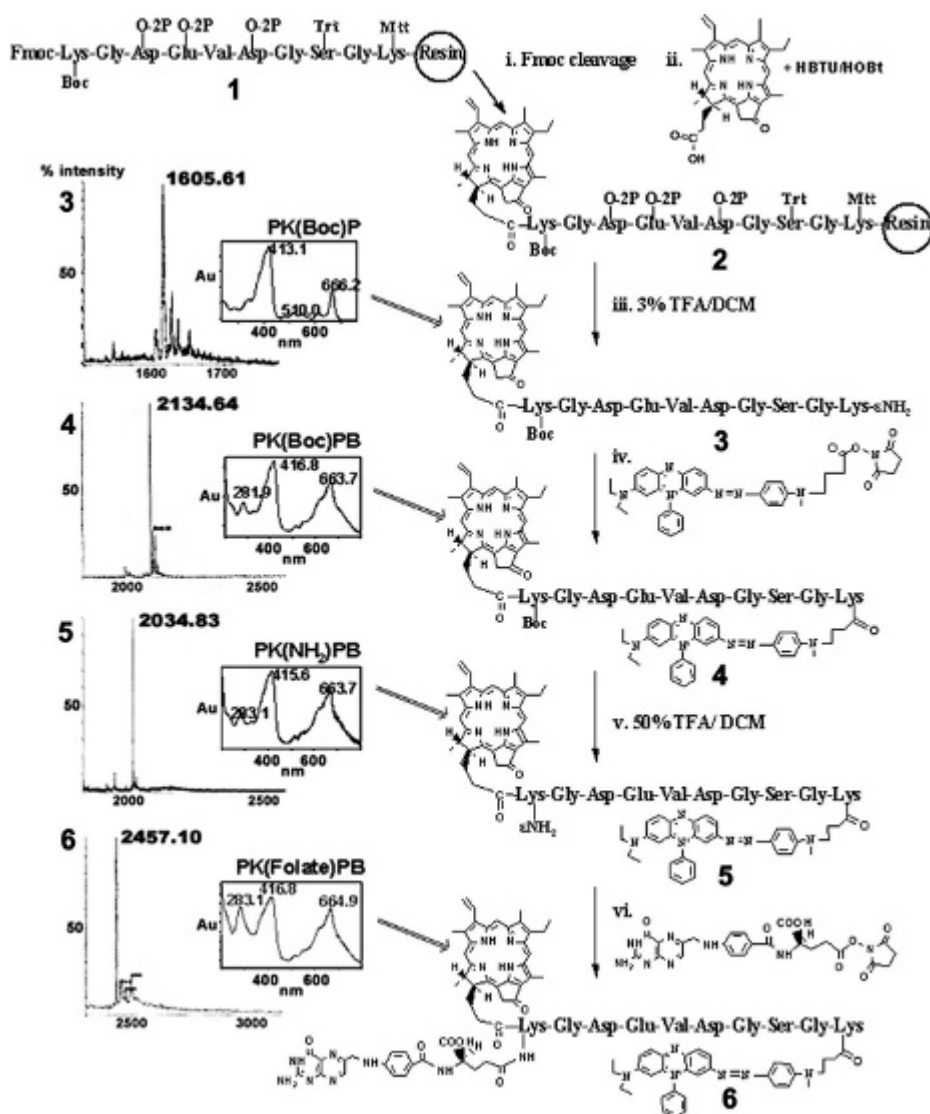


**Figure 2.** Synthesis of pyro-K(folate)GDEVDGSGK (BHQ-3) (PFPB, **6**) (right) and MALDI-ToF combined with UV-Vis of intermediates **3**, **4**, and **5** and of the final product **6** after high-performance liquid chromatographic purification (left).

the N-terminal lysine in pyro-K(NH<sub>2</sub>)GDEVDGSGK(BHQ-3) (**5**, PK(NH<sub>2</sub>)PB). This compound was dried under a high vacuum, and the folate-NHS was coupled to the N-terminal lysine using very mild basic and anhydrous conditions. The final product pyro-K(folate)GDEVDGSGK(BHQ-3) (PFPB, **6**) and a small sample of compounds **3**, **4**, and **5** were purified by HPLC and characterized by ultraviolet-visible spectroscopy (UV-Vis) and MALDI-ToF (see Figure 2).

#### PFPB Activation by Caspase 3 in Solution

To confirm that PFPB is cleavable by caspase 3 and that pyro's fluorescence (quenched in the intact molecule by BHQ-3) is restored after cleavage, we monitored the

fluorescence increase upon the cleavage of PFPB by purified active caspase 3 in solution using fluorescence spectroscopy. An immediate increase in fluorescence that plateaus at 40 minutes was monitored by fluorescence spectroscopy (Figure 3) for PFPB incubated with caspase 3 (▲). This increase was not observed for PFPB alone in buffer (●) or PFPB incubated with caspase 3 enzyme and caspase 3-specific inhibitor (■) (with the ratio 1:80:2,000 for caspase 3 to PFPB to inhibitor). This, together with HPLC monitoring that shows the generation of two fragments on caspase 3 cleavage (data not shown), demonstrated that PFPB is specifically cleaved by caspase 3 in solution, and as a result, there is a ninefold increase in fluorescence.

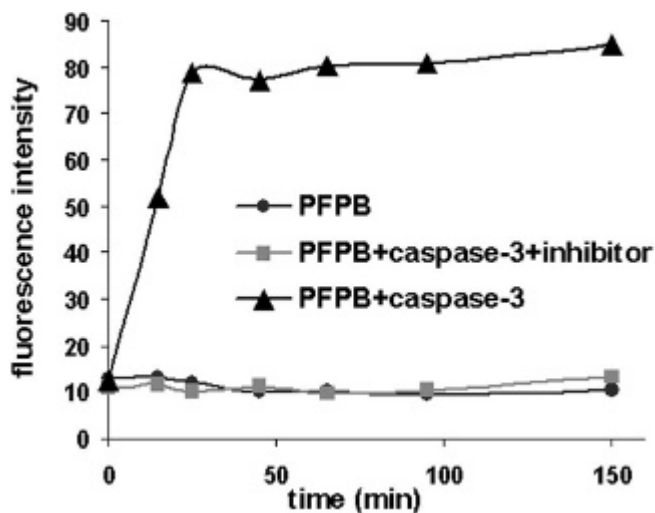


**Figure 3.** Cleavage of pyro-K(folate)GDEVDGSGK(BHQ-3) (PFPB, 6) by caspase 3 in solution results in a fluorescence increase monitored by fluorescence spectroscopy. Fluorescence intensity (monitored for 2.5 hours) increases when PFPB is incubated with caspase 3 (▲) compared with the stable background fluorescence of PFPB alone (●) and PFPB incubated with caspase 3 in the presence of caspase 3 inhibitor (■), which completely prevents the cleavage.

### Accumulation and Cleavage of PFPB in KB and HT 1080 Cells

The ability of PFPB to preferentially enter folate receptor-overexpressing cells and be cleaved as a consequence of PDT-induced apoptosis was monitored using confocal microscopy. We have used two cancer cell lines: KB cells (human epidermoid carcinoma cells; folate receptor positive) and HT 1080 cells (human fibrosarcoma cells; folate receptor negative). KB cells (Figure 4, A–D) and HT 1080 (Figure 4, E–H) cells were incubated with two different PFPB concentrations: 40  $\mu\text{M}$  (Figure 4, B, C, F, and G) and 20  $\mu\text{M}$  (Figure 4, D and H) for 4.5 hours and subsequently treated with a 1.5  $\text{J}/\text{cm}^2$  light dose using a 670 nm laser (Figure 4, C, D, G, and H). There is a strong fluorescence signal increase in the cytoplasm of the KB cells incubated with 40  $\mu\text{M}$  PFPB and treated by light (Figure 4C) when compared with the untreated cell alone control (Figure 4A) or cells incubated with 40  $\mu\text{M}$  PFPB and kept in the dark (Figure 4B). The fluorescence signal is somewhat lower in the case of PDT-treated KB cells

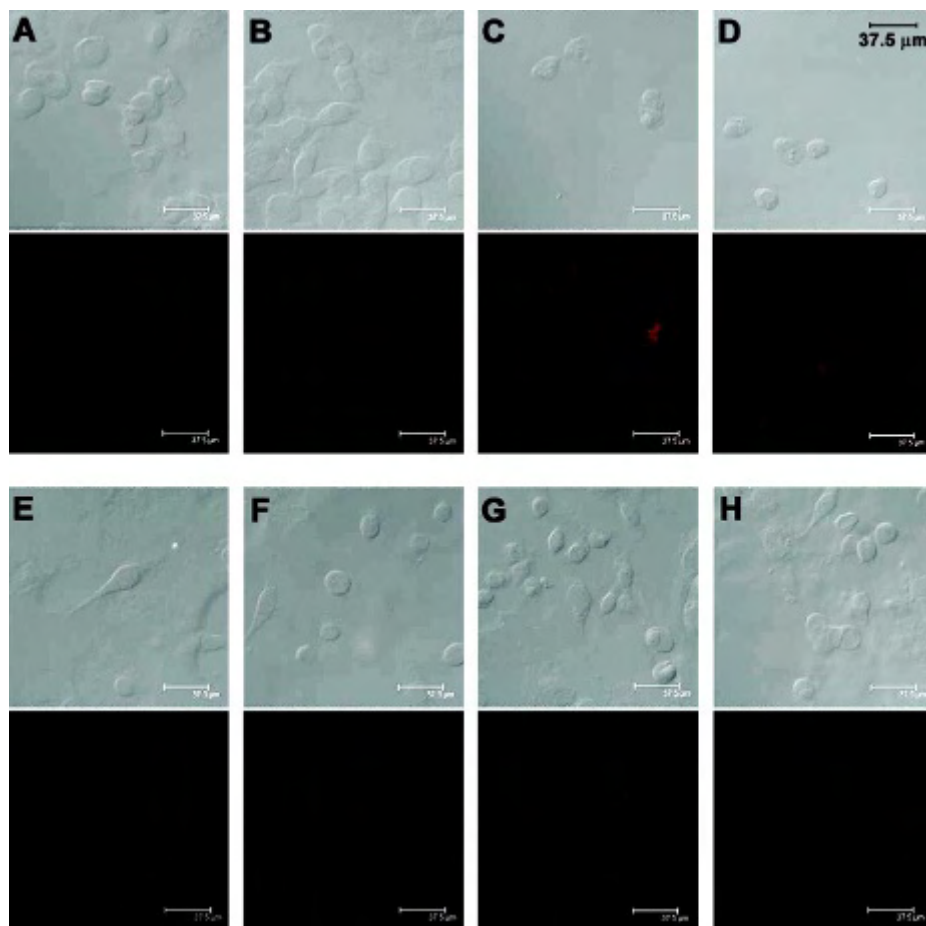


**Figure 4.** Different increase in fluorescence on light-triggered cleavage of pyro-K(folate)GDEVDGSGK(BHQ-3) (PFPB) in KB (A–D) and HT 1080 (E–H) cells monitored by confocal microscopy. Confocal images of (A) KB cells alone; (B) KB cells incubated for 4.5 hours with 40  $\mu\text{M}$  PFPB and kept in the dark; (C) KB cells incubated for 4.5 hours with 40  $\mu\text{M}$  PFPB and treated with 1.5  $\text{J}/\text{cm}^2$ ; (D) KB cells incubated for 4.5 hours with 20  $\mu\text{M}$  PFPB and treated with 1.5  $\text{J}/\text{cm}^2$ ; (E) HT 1080 cells alone; (F) HT 1080 cells incubated for 4.5 hours with 40  $\mu\text{M}$  PFPB and kept in the dark; (G) HT 1080 cells incubated for 4.5 hours with 40  $\mu\text{M}$  PFPB and treated with 1.5  $\text{J}/\text{cm}^2$ ; (H) HT 1080 cells incubated for 4.5 hours with 20  $\mu\text{M}$  PFPB and treated with 1.5  $\text{J}/\text{cm}^2$ . Both KB (B) and HT 1080 (F) cells incubated with 40  $\mu\text{M}$  PFPB but not treated with light show a minimal fluorescence increase, excluding apoptosis-independent PFPB decomposition. The cells treated with drug and light show a concentration-dependent fluorescence increase that is significantly higher in KB cells (C and D) than in HT 1080 cells (G and H) owing to a lower PFPB accumulation in HT 1080 cells than in KB cells. In each case, the upper image is differential interference contrast (DIC) and the lower image is pyro fluorescence.

incubated with a lower drug dose (20  $\mu\text{M}$  PFPB; Figure 4D). HT 1080 cells treated with light, on the other hand, show a comparably lower fluorescence increase than KB cells for both 40 and 20  $\mu\text{M}$  concentrations (Figure 4, G and H). This confirmed that PFPB accumulates less in folate receptor-deficient cells (HT 1080) than in folate-overexpressing cells (KB), thus suggesting that folate receptor-mediated uptake is the primary delivery pathway for PFPB. In contrast, the control cells (both KB and HT 1080) incubated with 40  $\mu\text{M}$  PFPB but not exposed to light showed a minimal fluorescence increase (Figure 4, B and F), excluding apoptosis-independent decomposition of PFPB. In summary, these results confirmed that (1) PFPB preferentially accumulates in KB cells, (2) the peptide linker in TaBIAS can be cleaved inside PDT-treated cells, (3) the significant increase in pyro's fluorescence is caused by apoptosis-specific cleavage and is not simply due to PFPB decomposition, and (4) based on our control experiments (data not shown), we assume that PFPB is taken into the HT 1080 cells by pyro itself, serving as a nonspecific cell delivery vehicle.

### Apoptosis Monitored by Flow Cytometry

Additional evidence for apoptosis triggering was obtained from flow cytometry analysis<sup>15,16</sup> of living KB cells incubated with 3  $\mu\text{M}$  PFPB and treated with a 10  $\text{J}/\text{cm}^2$  light dose using FSC-SSC fluorescence-activated cell sorter (FACS) parameters defining shrunken or hypergranular cells. The fraction of cells with higher SSC and lower FSC (upper left) increased from  $\approx 4\%$  for KB cells either treated with 10  $\text{J}/\text{cm}^2$  (Figure 5A) or with 3  $\mu\text{M}$  PFPB and kept in the dark (Figure 5B) to 58% for KB cells incubated with 3  $\mu\text{M}$  PFPB and treated with 10  $\text{J}/\text{cm}^2$  (Figure 5C). We have identified, using DAPI for flow cytometry and trypan blue for microscopy, less than 2% of these cells as necrotic. The shrunken or hypergranular cells (green, 58%) also have approximately three times higher pyro fluorescence coming from the PDT-induced apoptosis-triggered cleavage of PFPB inside the living cells (Figure 5E compared with Figure 5D). This fluorescence increase is not detected in cells 2 hours after heat-induced necrosis. Also, the whole population of PFPB- and PDT-treated cells (see Figure 5C) has a 1.7 times higher signal from staining with the antibody against activated caspase 3. The correlation of apoptotic shape defined by FSC-SSC and increased fluorescence from cleaved PFPB in more than half of the cells after light treatment supports the function of TaBIAS as an apoptotic trigger and reporter *in vitro*.

### PDT-Induced Cell Death Quantified by Cell Viability (MTT) Assay

We have shown that apoptosis induction correlates with PFPB cleavage using flow cytometry, but for quantitation of overall cell death in the whole population for variable drug and light doses, we used a cell viability (MTT) assay. This assay determines the PDT efficacy of a drug by correlating the viability of cells before and after PDT treatment, in which cells not treated with light and drug serve as a relative reference (100% viable). Despite the decreased potency that is a by-product of the fluorescence quenching (the presence of BHQ-3 reduces singlet oxygen production three to four times by quenching pyro's singlet excited state), we have confirmed (as shown in Figure 6) that PFPB is an effective PDT agent.

### In Vivo Data

Given that PFPB preferentially accumulates in KB cells overexpressing folate receptor compared with HT 1080 cells lacking folate receptor expression, the post-PDT increase in fluorescence was expected to be much higher in a KB tumor than in an HT 1080 tumor. Two double-tumor mice bearing an HT 1080 tumor on the left side and a KB tumor on the right side were injected intravenously with 80 nmol of PFPB. One mouse received a 90  $\text{J}/\text{cm}^2$  whole-tumor PDT treatment with a 670 nm laser for both HT 1080 and KB tumors 18 hours after intravenous injection and was scanned by a Xenogen IVIS imager (see Figure 6A, prescan; Figure 6B, 23 hours after PDT and 41 hours after intravenous injection of PFPB); the other mouse served as a control and was kept in the dark. The Xenogen image of the mouse treated by PDT shows a distinctly higher post-PDT increase in pyro fluorescence in the KB tumor compared with the HT 1080 tumor (see Figure 6B), thus confirming the targeted apoptosis-reporting function of PFPB. This function was independently evaluated using an Apoptag assay that labels the cells that have reached the point of DNA laddering during apoptosis (critically dependent on caspase 3 activation), specifically labeling this DNA cleavage by fluorescein conjugates.

Therefore, after the mice were sacrificed, cryosections from both the KB and HT 1080 tumors of the PDT-treated and control mouse were stained with the Apoptag assay and examined by confocal microscopy (see Figure 6, C–F). As expected, only the KB tumor of the mouse treated by PDT shows a significant increase in both pyro fluorescence (Xenogen images; see Figure 6B) and apoptosis (histology

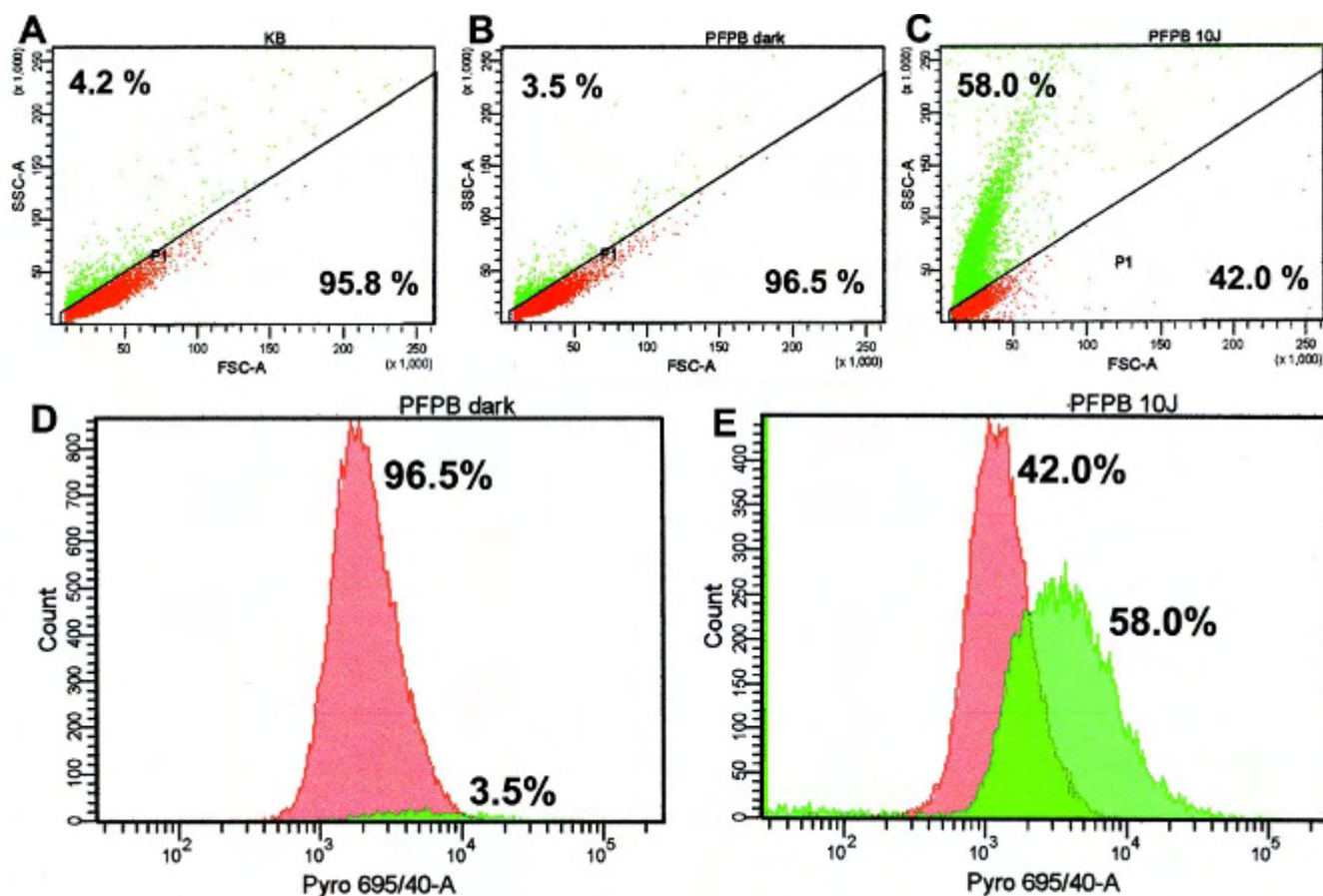


**Figure 5.** Fluorescence-activated cell sorter (FACS) analysis of shrunken or hypergranular cells using forward scatter, side scatter (FSC-SSC) parameters and pyro fluorescence on living KB cells alone or incubated with 3  $\mu\text{M}$  pyro-K(folate)GDEVDGSGK(BHQ-3) (PFPB) and/or treated with light harvested 5 hours after drug aspiration or photodynamic therapy treatment. The same gate (P1) was set between apoptotic and live cells, and the proportion of apoptotic and living cells is shown in the upper left and lower right corners, respectively. It is clear that cells treated with 10  $\text{J}/\text{cm}^2$  (A) or incubated with 3  $\mu\text{M}$  PFPB in the dark (B) are significantly less apoptotic ( $\approx 4\%$ ) than cells incubated with 3  $\mu\text{M}$  PFPB and treated with a 10  $\text{J}/\text{cm}^2$  light dose (58%; C). These apoptotic cells (outside P1 gate) have approximately three times higher pyro fluorescence than those within the P1 gate (comparing D and E), correlating apoptosis with PFPB cleavage in living cells. The profile of log pyro fluorescence versus cell count for P1 (red) and non-P1 (green) populations from Figure 5, B and C, is shown in Figure 5, D and E, respectively.

slides; see Figure 6E) when compared with the HT 1080 tumor from the same mouse (see Figure 6F) or with both tumors from the control mouse that was not subjected to PDT (see Figure 6, C and D).

To further confirm the results from the previous animal experiment and improve the signal to noise ratio, we intravenously injected another double-tumor-bearing mouse with a lower drug dose (25 nmol of PFPB, 100  $\mu\text{L}$ ) and treated both KB and HT 1080 tumors with the same light dose (90  $\text{J}/\text{cm}^2$ ) only 3 hours after the injection. The Xenogen images show an increase in fluorescence in the KB tumor compared with the prescan (Figure 7A: prescan) and a decreasing background with increasing time interval after PDT (Figure 7B: 30 minutes, 7C: 2 hours, Figure 7D: 3 hours after PDT). The organ adjacent to the tumor sites

exhibiting high signal from peptide degradation is probably the kidney, based on the biodistribution of the unquenched folate receptor-targeted probe (data not shown). Histology slides (Figure 7, E and F) of both tumors from this mouse sacrificed 24 hours after injection again show higher Apoptag staining in the KB tumor (see Figure 7F) than in the HT 1080 tumor (see Figure 7E), with an overall better signal to background ratio.

The results from these animal experiments suggest that (1) PFPB accumulates preferentially in folate-overexpressing KB tumors in vivo, (2) there is an increase in pyro fluorescence in the area of PFPB accumulation and PDT treatment as a consequence of in vivo cleavage of the caspase 3-specific peptide linker, and (3) this area is highly apoptotic, as shown in ex vivo analysis.

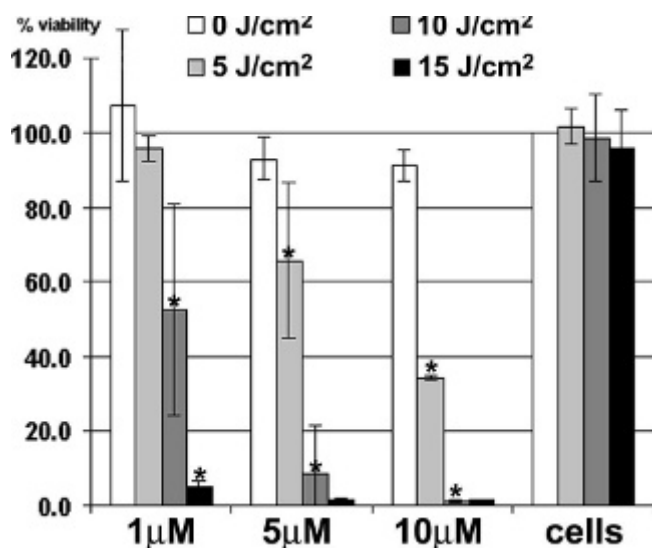


**Figure 6.** Photodynamic therapy (PDT) efficacy of pyro-K(folate)GDEVDSGSK(BHQ-3) (PFPB) determined by cell viability (MTT) assay. Viability of KB cells after treatment with PFPB at three different concentrations (1, 5, and 10  $\mu\text{M}$ ) and with three different PDT light doses (5, 10, and 15  $\text{J}/\text{cm}^2$ ) compared with cells alone that serve as 100% viable reference. PFPB has minimal dark toxicity and good PDT efficacy. Comparisons for increasing light doses within each concentration were made by *t*-test ( $*p < .05$ ); for example, cells incubated with 5  $\mu\text{M}$  PFPB and treated with 5  $\text{J}/\text{cm}^2$  have significantly different viability than those incubated with the same concentration and kept in the dark (0  $\text{J}/\text{cm}^2$ ).

## Discussion

We have designed a molecule with various features: it is multifunctional but small and soluble, specific but versatile, and, most importantly, it is both a therapeutic and an imaging agent. This feature allows TaBIAS to evaluate its own therapeutic outcome by imaging the extent of apoptosis in situ after PDT treatment.

### Multifunctional but Small and Soluble

TaBIAS comprises four principal components. First, the therapeutic component of TaBIAS is a pyropheophorbide *a* (pyro)—a photosensitizer that was shown to trigger apoptosis<sup>7</sup> by light-dependent production of singlet oxygen<sup>17</sup> that disrupts the mitochondrial membrane.<sup>18–20</sup> Second, the imaging component is the fluorescence of pyro<sup>21,22</sup> together with a caspase 3 cleavable sequence.<sup>23</sup> The fluorescence allows tracking of the signal by real-time in vivo NIR imaging, and the caspase 3 cleavable sequence serves as an apoptosis-sensitive switch<sup>24</sup> of the photosensitizer fluorescence. The third component, a background-eliminating fluorescence quencher BHQ-3, is responsible for turning this switch off in living cells. Caspase 3 was

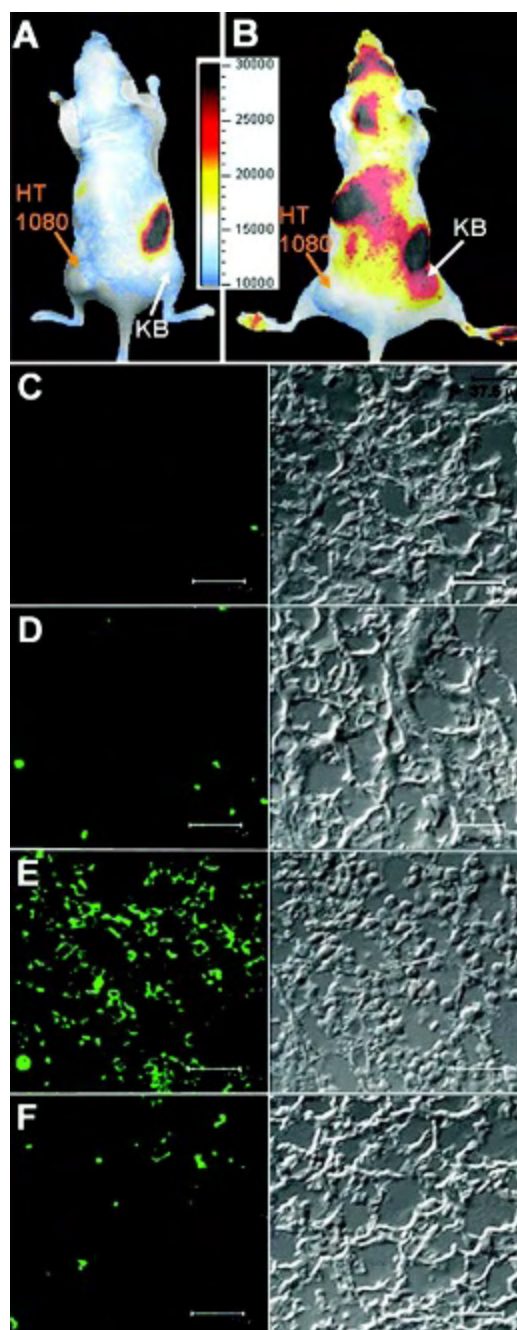


**Figure 7.** In vivo induction and detection of apoptosis in a mouse bearing KB and HT 1080 tumors after photodynamic therapy (PDT) ( $90 \text{ J}/\text{cm}^2$ ) by intravenously injected pyro-K(folate)GDEVDSGSK(BHQ-3) (PFPB, 80 nmol). (A + B): Xenogen images of a mouse bearing an HT 1080 tumor (folate receptor negative) on the left side and a KB tumor (folate receptor positive) on the right side: (A) before injection of PFPB and (B) after PDT (23 hours after PDT and 41 hours after intravenous injection of PFPB). (C–F): Histology tissue slides stained with Apoptag and scanned by confocal microscopy: left, fluorescence of Apoptag (488 nm); right, differential interference contrast (DIC) image; (C) KB tumor from the control mouse; (D) HT 1080 tumor from the control mouse; (E) KB tumor from the PDT-treated mouse; (F) HT 1080 tumor from the PDT-treated mouse. The scale bar is 37.5  $\mu\text{m}$ . Increased apoptosis in the folate-overexpressing tumor (KB) of the PDT-treated mouse was confirmed by ex vivo Apoptag staining.

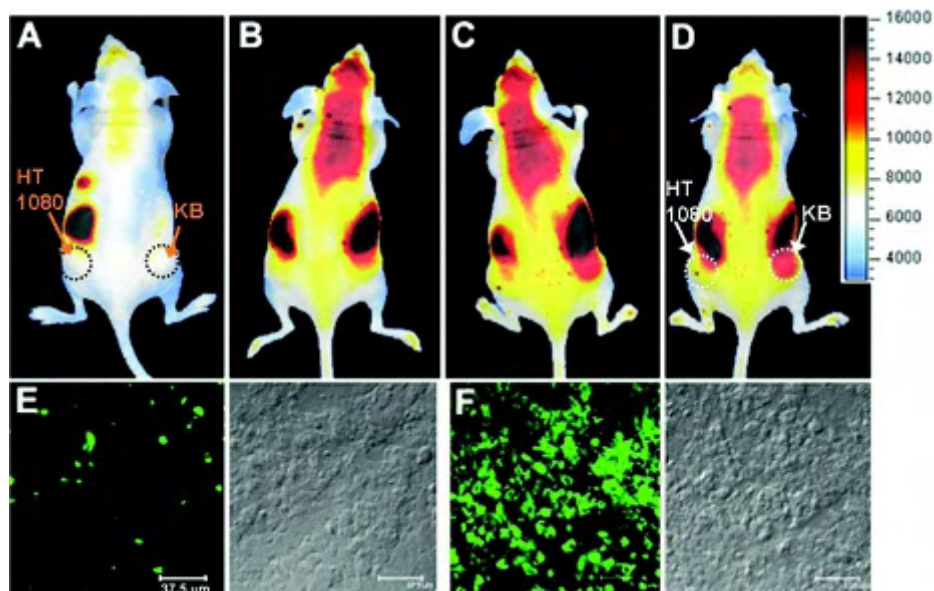


**Figure 8.** *In vivo* induction and detection of apoptosis in a mouse bearing KB and HT 1080 tumors after photodynamic therapy (PDT) ( $90 \text{ J/cm}^2$ ) using a lower dose of intravenously administered pyro-K(folate)GDEVDSGSK (BHQ-3) (PFPB, 25 nmol) and a shorter postinjection delay before PDT. (A–D): Xenogen images of a mouse bearing an HT 1080 tumor (folate receptor negative) on the left side and a KB tumor (folate receptor positive) on the right side: A, before injection of PFPB; B, 30 minutes after PDT (4 hours after intravenous injection of PFPB); C, 2 hours after PDT (5.5 hours after intravenous injection); and D, 3 hours after PDT (6.5 hours after intravenous injection), showing a gradual increase in fluorescence in the KB tumor and a reduced background. (E + F): Histology tissue slides stained with Apoptag and scanned by confocal microscopy; the scale bar is  $37.5 \mu\text{m}$ : left, fluorescence signal of Apoptag (488 nm, fluorescein); right, differential interference contrast (DIC) image; (E) HT 1080 tumor; and (F) KB tumor. This *ex vivo* Apoptag staining confirmed increased PDT-induced apoptosis in the folate-overexpressing tumor (KB).

chosen as the target enzyme because it is a crucial executioner protease involved in the progression of controlled cell death,<sup>25,26</sup> which is indicative of apoptosis induction<sup>27</sup> and is frequently used as a target enzyme for apoptosis imaging.<sup>23,28,29</sup> The fourth component introduces the cancer specificity into our concept by attaching a folate delivery component targeting folate receptor–overexpressing cancer cells. Unlike many multifunctional agents, this molecule has an MW below 2,500 Da, is soluble in water, and has minimal dark toxicity.

### Specific but Versatile

Introduction of a folate delivery vehicle allowed us to distinguish between cells (see Figure 4) and tumors (Figures 7 and 8) with different levels of folate receptor. This specificity was needed to prove the TaBIAS concept *in vivo*, but the delivery vehicle can be exchanged for alternative vehicles or another apoptosis-inducing drug. Our basic construct (containing only the first three components) attached to another drug would be useful for intracellular delivery and for *in vitro* evaluation of a drug's apoptosis-inducing properties since pyropheophor-

bide *a* can serve as both a very efficient (but not specific) delivery vehicle and a fluorescence marker.<sup>17,21</sup>

### Therapeutic and Imaging Agent

TaBIAS enters the cell via a folate delivery pathway, and upon the light treatment, it produces cytotoxic singlet oxygen near mitochondria, triggering apoptosis with caspase 3 activation.<sup>13,24</sup> As a consequence, the caspase 3–specific sequence that connects the fluorescent photosensitizer with the quencher is cleaved. We have demonstrated this cleavage in solution, *in vitro*, and *in vivo*.

The apoptosis involvement in this cleavage was confirmed: (1) *in vitro* by flow cytometry correlating FSC–SSC parameters<sup>16</sup> with pyro's fluorescence and anticaspase 3 staining and (2) *ex vivo* by staining the TaBIAS-treated tumors with Apoptag assay that labels apoptosis-specific DNA cleavage. Flow cytometry of living cells showed that more than half (58%) of the cells treated with  $3 \mu\text{M}$  PFPB and light display shrunken or hypergranular morphology together with triple the pyro fluorescence signal compared with the minimal amount of these cells (4%) in the sample treated with PFPB but kept in the dark. Using an Apoptag

assay performed on tumor tissues treated with drug and/or PDT for both types of tumors, we observed increased apoptosis (signal from Apoptag assay) for PDT- and TaBIAS-treated specimens of folate-overexpressing KB tumors. Monitoring apoptosis using TaBIAS, morphologic assessment, and a commercially available apoptosis sensor confirmed that the significant increase in the photosensitizer's fluorescence detected in the light-treated area is indicative of PDT-triggered apoptosis. We can therefore conclude that TaBIAS triggers apoptosis and can be used, unlike most current commercial sensors, as a tool for monitoring a self-triggered apoptosis *in situ*.

### Future Prospects

Most of the *in vivo* apoptosis imaging methods, using either annexin V<sup>30</sup> or Fluorescence Resonance Energy Transfer (FRET) probes,<sup>23</sup> are used strictly for detection of already existing apoptosis. Also, many of the *in vitro* methods currently used for apoptosis detection struggle with poor intracellular delivery, low specificity toward apoptosis,<sup>31,32</sup> or a lack of feasibility for *in situ* apoptosis assessment. Our TaBIAS can be used as both a built-in evaluation of already existing fluorescent PDT agents or a membrane permeable, a soluble carrier, and an apoptosis sensor for evaluating the properties and efficacy of many small apoptosis-inducing drugs.

Although this study supported all discussed features of TaBIAS, obstacles remain regarding partial (three to four times) singlet oxygen quenching, photobleaching, and *in vivo* peptide degradation. Until these issues are resolved, the current TaBIAS design will be qualitative rather than quantitative in terms of reporting apoptosis response. We anticipate improving our TaBIAS design by changing the core components of the TaBIAS scaffold (eg, shorten the caspase 3 cleavable sequence, use a more suitable quencher and photosensitizer) to fine-tune its properties.

In conclusion, we have shown that TaBIAS can effectively trigger and image apoptosis upon the light exposure *in situ* and can potentially be used as a new *in situ* cancer treatment evaluation for a variety of drugs and cancers. This will be possible by simply substituting the delivery vehicle with an anticancer drug and using pyro as a fluorescent reporter and cell-internalizing molecule.

### Acknowledgments

We thank André E. X. Brown for critical comments and suggestions on the manuscript. We also thank Dr. Wafik El-Deiry for access to the Xenogen imager.

### References

1. Lyons SK, Clarke AR. Apoptosis and carcinogenesis. *Br Med Bull* 1997;53:554–69.
2. Fischer U, Schulze-Osthoff K. New approaches and therapeutics targeting apoptosis in disease. *Pharmacol Rev* 2005;57:187–215.
3. Hakumaki JM, Liimatainen T. Molecular imaging of apoptosis in cancer. *Eur J Radiol* 2005;56:143–53.
4. Dougherty TJ, Gomer CJ, Henderson BW, et al. Photodynamic therapy. *J Natl Cancer Inst* 1998;90:889–905.
5. Wilson BC, Patterson MS. The physics of photodynamic therapy. *Phys Med Biol* 1986;31:327–60.
6. Oleinick NL, Morris RL, Belichenko I. The role of apoptosis in response to photodynamic therapy: what, where, why, and how. *Photochem Photobiol Sci* 2002;1:1–21.
7. Sun X, Leung WN. Photodynamic therapy with pyropheophorbide-a methyl ester in human lung carcinoma cancer cell: efficacy, localization and apoptosis. *Photochem Photobiol* 2002;75:644–51.
8. Stennicke HR, Renatus M, Meldal M, Salvesen GS. Internally quenched fluorescent peptide substrates disclose the substrate preferences of human caspases 1, 3, 6, 7 and 8. *Biochem J* 2000;350:563–8.
9. Pham W, Weissleder R, Tung CH. An azulene dimer as a near-infrared quencher. *Angew Chem Int Ed Engl* 2002;41:3659–62.
10. Hilgenbrink AR, Low PS. Folate receptor-mediated drug targeting: from therapeutics to diagnostics. *J Pharm Sci* 2005;94:2135–46.
11. Moor AC. Signaling pathways in cell death and survival after photodynamic therapy. *J Photochem Photobiol B* 2000;57:1–13.
12. Chiu SM, Oleinick NL. Dissociation of mitochondrial depolarization from cytochrome c release during apoptosis induced by photodynamic therapy. *Br J Cancer* 2001;84:1099–106.
13. Kessel D, Luo Y. Photodynamic therapy: a mitochondrial inducer of apoptosis. *Cell Death Differ* 1999;6:28–35.
14. Garcia-Calvo M, Peterson EP, Leiting B, et al. Inhibition of human caspases by peptide-based and macromolecular inhibitors. *J Biol Chem* 1998;273:32608–13.
15. Vermees I, Haanen C, Reutelingsperger C. Flow cytometry of apoptotic cell death. *J Immunol Methods* 2000;243:167–90.
16. Dive C, Gregory CD, Phipps DJ, et al. Analysis and discrimination of necrosis and apoptosis (programmed cell death) by multi-parameter flow cytometry. *Biochim Biophys Acta* 1992;1133:275–85.
17. Chen J, Stefflova K, Niedre MJ, et al. Protease-triggered photosensitizing beacon based on singlet oxygen quenching and activation. *J Am Chem Soc* 2004;126:11450–1.
18. MacDonald IJ, Morgan J, Bellnier DA, et al. Subcellular localization patterns and their relationship to photodynamic activity of pyropheophorbide-a derivatives. *Photochem Photobiol* 1999;70:789–97.
19. Kessel D, Luo Y, Deng Y, Chang CK. The role of subcellular localization in initiation of apoptosis by photodynamic therapy. *Photochem Photobiol* 1997;65:422–6.
20. Green DR, Reed JC. Mitochondria and apoptosis. *Science* 1998;281:1309–12.
21. Chen Y, Zheng X, Dobhal MP, et al. Methyl pyropheophorbide-a analogues: potential fluorescent probes for the peripheral-type

- benzodiazepine receptor. Effect of central metal in photosensitizing efficacy. *J Med Chem* 2005;48:3692–5.
22. Zhang M, Zhang Z, Blessington D, et al. Pyropheophorbide 2-deoxyglucosamide: a new photosensitizer targeting glucose transporters. *Bioconjugate Chem* 2003;14:709–14.
  23. Bullok K, Piwnica-Worms D. Synthesis and characterization of a small, membrane-permeant, caspase-activatable far-red fluorescent peptide for imaging apoptosis. *J Med Chem* 2005;48:5404–7.
  24. Mancini M, Nicholson DW, Roy S, et al. The caspase-3 precursor has a cytosolic and mitochondrial distribution: implications for apoptotic signaling. *J Cell Biol* 1998;140:1485–95.
  25. Thornberry NA. Caspases: key mediators of apoptosis. *Chem Biol* 1998;5:R97–103.
  26. Thornberry NA, Lazebnik Y. Caspases: enemies within. *Science* 1998;281:1312–6.
  27. Hirata H, Takahashi A, Kobayashi S, et al. Caspases are activated in a branched protease cascade and control distinct downstream processes in Fas-induced apoptosis. *J Exp Med* 1998;187:587–600.
  28. Shah K, Tung CH, Breakefield XO, Weissleder R. In vivo imaging of S-TRAIL-mediated tumor regression and apoptosis. *Mol Ther* 2005;11:926–31.
  29. Mizukami S, Kikuchi K, Higuchi T, et al. Imaging of caspase-3 activation in HeLa cells stimulated with etoposide using a novel fluorescent probe. *FEBS Lett* 1999;453:356–60.
  30. Petrovsky A, Schellenberger E, Josephson L, et al. Near-infrared fluorescent imaging of tumor apoptosis. *Cancer Res* 2003;63:1936–42.
  31. Appelt U, Sheriff A, Gaipf US, et al. Viable, apoptotic and necrotic monocytes expose phosphatidylserine: cooperative binding of the ligand annexin V to dying but not viable cells and implications for PS-dependent clearance. *Cell Death Differ* 2005;12:194–6.
  32. Brauer M. In vivo monitoring of apoptosis. *Prog Neuro-psychopharmacol* 2003;27:323–31.

# Peptide-Based Pharmacomodulation of a Cancer-Targeted Optical Imaging and Photodynamic Therapy Agent

Klara Stefflova,<sup>†</sup> Hui Li,<sup>‡</sup> Juan Chen,<sup>‡,§</sup> and Gang Zheng<sup>\*,‡,§,||</sup>

Departments of Chemistry and Radiology, University of Pennsylvania, Philadelphia, Pennsylvania 19104, and Ontario Cancer Institute, University of Toronto, MaRS Center, TMDT 5-363, 101 College Street, Toronto, Ontario M5G 1L7, Canada. Received August 18, 2006; Revised Manuscript Received November 20, 2006

We designed and synthesized a folate receptor-targeted, water-soluble, and pharmacomodulated photodynamic therapy (PDT) agent that selectively detects and destroys the targeted cancer cells while sparing normal tissue. This was achieved by minimizing the normal organ uptake (e.g., liver and spleen) and by discriminating between tumors with different levels of folate receptor (FR) expression. This construct (Pyro-peptide-Folate, PPF) is composed of three components: (1) pyropheophorbide a (Pyro) as an imaging and therapeutic agent, (2) peptide sequence as a stable linker and modulator improving the delivery efficiency, and (3) Folate as a homing molecule targeting FR-expressing cancer cells. We observed an enhanced accumulation of PPF in KB cancer cells (FR+) compared to HT 1080 cancer cells (FR-), resulting in a more effective post-PDT killing of KB cells over HT 1080 or normal CHO cells. The accumulation of PPF in KB cells can be up to 70% inhibited by an excess of free folic acid. The effect of Folate on preferential accumulation of PPF in KB tumors (KB vs HT 1080 tumors 2.5:1) was also confirmed *in vivo*. In contrast to that, no significant difference between the KB and HT 1080 tumor was observed in case of the untargeted probe (Pyro-peptide, PP), eliminating the potential influence of Pyro's own nonspecific affinity to cancer cells. More importantly, we found that incorporating a short peptide sequence considerably improved the delivery efficiency of the probe—a process we attributed to a possible peptide-based pharmacomodulation—as was demonstrated by a 50-fold reduction in PPF accumulation in liver and spleen when compared to a peptide-lacking probe (Pyro-K-Folate, PKF). This approach could potentially be generalized to improve the delivery efficiency of other targeted molecular imaging and photodynamic therapy agents.

## INTRODUCTION

When a porphyrin-like molecule is activated by light, it relaxes to its ground state in three ways: through nonradiative decay, by emitting a photon, or transferring the energy, producing reactive oxygen species, mainly singlet oxygen (*I*). The detectable outcomes are fluorescence (2) and phototoxicity (3), making the porphyrin-based photosensitizer (PS<sup>1</sup>) a perfect candidate for image-guided therapy.

Curing cancer is a complicated goal, and the success of treatment is often short-term owing to the difficulty in clearing out all the cancer cells. Being able to clearly identify the cancer cells shortly before or during the treatment would most likely increase the success of the therapy, making imaging and therapy a beneficial union (4–7). We have utilized the natural connection of near-infrared (NIR) fluorescence imaging, a sensitive and accessible means of *in vivo* cancer detection (2, 8, 9), with

photodynamic therapy (PDT), a promising cancer therapy using a laser to excite a tumor-associated photosensitizer that produces short-lived cytotoxic singlet oxygen (10, 11). Although many target-specific NIR imaging and PDT agents are being developed, the common limit remains: these agents are mostly lost in organs involved in drug clearance, generating an unwanted toxicity and elevated background (12). Here, we propose a novel construct designed for improving the delivery efficiency of NIR imaging and PDT agents to the desired cancer cell targets with reduced normal tissue retention. It is composed of three functional modules (Scheme 1). The first is a fluorescent photosensitizer pyropheophorbide a (Pyro) for NIR imaging (with a long-wavelength absorption at 665 nm and emission at 675 and 720 nm) and PDT (over 50% singlet oxygen yield) (13, 14). This semisynthetic photosensitizer, obtained by three steps from *Spirulina* algae, has minimal dark toxicity, and its derivative Photochlor is in phase I/II clinical trial (15).

The second component is a folate moiety, serving as a tumor-homing molecule that guides the photosensitizer into folate receptor (FR)-overexpressing cancer cells (16, 17) via receptor-mediated endocytosis (18). FRs are mainly overexpressed on ovary, breast, colon, lung, nose, prostate, and brain cancer cells and activated macrophages (19) but have limited expression on normal cells (e.g., kidney, intestine, lung) with restricted accessibility for blood-circulating drugs (20).

The third component is a short peptide sequence GDEVDSGK inserted between the photosensitizer and folate. It serves multiple purposes: (A) it is a stable and hydrophilic linker that prevents the separation of folate and Pyro and enhances water solubility, (B) it separates the Pyro from the Folate to avoid the hindrance of FR-targeting (20), (C) it serves as a pharmacomodulator for better delivery efficiency and decreased normal

\* To whom correspondence should be addressed. E-mail: gang.zheng@uhnres.utoronto.ca. Phone: 1-416-581-7666. Fax: 1-416-581-7667.

<sup>†</sup> Department of Chemistry and, University of Pennsylvania.

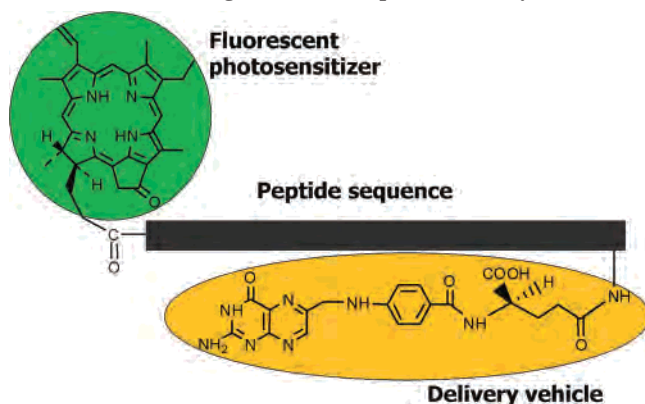
<sup>‡</sup> Department of Radiology, University of Pennsylvania.

<sup>§</sup> Ontario Cancer Institute.

<sup>||</sup> Joey and Toby Tanenbaum/Brazilian Ball Chair in Prostate Cancer Research.

<sup>1</sup> Abbreviations: BSA, bovine serum albumin; DCM, dichloromethane; DIPEA, diisopropylethylamine; DMSO, dimethylsulfoxide; EDTA, ethylenediaminetetraacetic acid; MALDI-ToF, matrix assisted laser desorption/ionization - time of flight mass spectrometry; MTT, 3-[4,5-dimethylthiazol-2-yl]-2,5-diphenyl tetrazolium bromide; NHS, *N*-hydroxysuccinimide; NIR, near-infrared; NMP, 1-methyl-2-pyrrolidinone; PBS, phosphate-buffered saline; PDT, photodynamic therapy; PS, photosensitizer; TEAA, triethyl amine and acetic acid; TFA, trifluoroacetic acid; TIS, triisopropylsilane.

**Scheme 1. Pyro-GDEVDSGSK-Folate Comprises Three Principal Components: (1) Fluorescent Photosensitizer Pyropheophorbide a, an Imaging and Therapeutic Agent; (2) Peptide Sequence Is a Stable and Pharmacomodulating Linker That Can Be Exchanged with Any Organelle-Targeting Sequence; and (3) Folate, Serving as a Cancer-Specific Delivery Vehicle**



tissue toxicity, and (D) it is possible to exchange it with other peptide sequences for targeting subcellular organelles (21–23).

There have been many attempts to enhance the photosensitizer's efficacy by targeting "cancer fingerprints" (24) through association with various vehicles (25, 26) like proteins (e.g., BSA targeting scavenger receptors on macrophages (27), transferrin (28), or LDL (29)), tumor-selective monoclonal antibodies (30), saccharides (31), aptamers (32), or other small molecule ligands (e.g., short peptides or peptidomimetics) (22, 33–35). By attaching Pyro to Folate, an easy-to-conjugate, small, soluble, and nonimmunogenic tumor homing molecule (20) targeting cancer cells overexpressing FR (9, 36, 37), we expected to enhance the cancer specificity of Pyro. To potentiate this specificity, we have inserted a short peptide sequence to serve as a spacer, a solubilizer, and a pharmacomodulator (38). As a spacer, it makes the Folate more accessible to FR and, being small and hydrophilic, it decreases its retention in the excretion organs, making it more suitable for in vivo applications.

In this paper, we describe the synthesis and characterization of such agent, Pyro-GDEVDSGSK-Folate (PPF, Figure 1). We have demonstrated, both in vitro and in vivo, that all three functional modules act in synergy and thus significantly improve the delivery efficiency, reducing the potential toxicity of the probe.

## MATERIALS AND METHODS

The coupling reagents HOBt (1-hydroxybenzotriazole) and HBTU (*O*-(benzotriazol-1-yl)-*N,N,N',N'*-tetramethyluronium hexafluorophosphate) were purchased from ACROS and Fluka, respectively. KB cells (human epidermal cancer cells; folate receptor positive), HT 1080 cells (human fibrosarcoma cells; folate receptor negative), and CHO (chinese hamster ovary cells; folate receptor negative) were purchased from ATCC. "Complete MEM" (for HT 1080 and KB cells) consists of 85% Minimum Essential Medium (MEM), 10% fetal bovine serum, 2% of 1.5 g/L sodium bicarbonate, 1% of 200 mM L-glutamine, 1% of 0.1 mM nonessential amino acids, and 1% of 1 mM sodium pyruvate; and "MEM containing 0.8% BSA" consists of MEM supplemented with 8 g/L of bovine serum albumin. "Complete F12K" (for CHO cells) consists of 85% Ham's F12K medium (F12K), 10% fetal bovine serum, 2% of 1.5 g/L sodium bicarbonate, and 1% of 200 mM L-glutamine; and "F12K containing 0.8% BSA" consists of F12K supplemented with 8 g/L of bovine serum albumin. Compounds 3 (PP), 4 (PPF), and Pyro-K-Folate (PKF) prepared for in vivo experiments were

dissolved in 1  $\mu$ L DMSO and 20  $\mu$ L PBS, filtered through a 0.22  $\mu$ m filter and further diluted with saline to the 120–150  $\mu$ L volume. For the in vitro experiments, compound 4 (PPF) and Pyro-K-Folate (PKF) were first dissolved in DMSO (no more than 0.5% of total volume), then diluted with 0.1% Tween-80 in DNA-water, filtered through a 0.22  $\mu$ m filter, and further diluted with MEM containing 0.8% BSA (HT 1080 and KB cells) or F12K containing 0.8% BSA (CHO cells).

All compounds were purified by HPLC (Waters 600 controller with a 2996 photodiode array detector). The eluents were A = 0.1 M TEAA (pH 7) and B = acetonitrile, and the method used for all injections was 90% of A and 10% of B to 100% of B in 45 min with flow 1.5 mL/min on a Zorbax 300SB-C3 column. MALDI-ToF was measured on an Applied Biosystems Voyager DE mass spectrometer, and fluorescence was measured on a Perkin-Elmer LS50B luminescence spectrometer. We acquired confocal images using a Leica TCS SP2 confocal microscope and Xenogen images at the Bioluminescence Molecular Imaging Core facility at UPenn on an IVIS Xenogen Imager. The laser for PDT treatment was tuned to 670 nm with a fluence rate of 20 mW/cm<sup>2</sup>. Mice were euthanized according to guidelines established by the Institutional Animal Care and Use Committee of the University of Pennsylvania.

**Synthesis of PPF.** The peptide Fmoc-GD(O-2-PhiPr)E(O-2-PhiPr)VD(O-2-PhiPr)GS(Trt)GK(Mtt) (1) was synthesized by manual SPPS using commercially available Fmoc amine-protected amino acids as building blocks and Sieber resin (cleavable by 2% TFA) as a solid phase, all purchased from Novabiochem. After the last Fmoc group cleavage, the resin was washed with NMP, and Pyro acid was coupled to the N-terminal glycine to give Pyro-GD(O-2-PhiPr)E(O-2-PhiPr)VD(O-2-PhiPr)GS(Trt)GK(Mtt)-Sieber resin (2). The molar ratio of Pyro/HOBt/HBTU to the peptide (1) was 3/3/3:1, and the reaction was done in a shaker flask with a 12 h coupling time using dry NMP as a solvent. The resin was then washed with NMP, capped by 0.3 M acetylimidazol in NMP for 15 min, and washed again by an excess of NMP, DCM, and dry methanol, transferred from the shaker flask, and dried. Compound 2 (37.7 mg, 11.5  $\mu$ mol) was cleaved from the resin and deprotected in one step by 2% TFA/5% TIS/DCM for 1 h to yield Pyro-GDEVDSGSK(NH<sub>2</sub>) (3) with the  $\epsilon$ -NH<sub>2</sub> group of the C-terminal lysine exposed. The compound was precipitated from the cleavage solution by dry ether and prepurified by a few cycles of ether precipitation–DMSO dissolving. Compound 3 (10.9 mg, 6.8  $\mu$ mol) was dried under high vacuum and, without further purification, used in the next reaction. For in vivo experiments, compound 3 (PP) was purified by HPLC. The structure was confirmed by MALDI-ToF (Supporting information Figure 1A; mass calculated 1377.64, found 1377.95). Crude PP (9.3 mg, 5.8  $\mu$ mol) was dissolved in 100  $\mu$ L of dry 1% DIPEA/DMSO and reacted for 2 h with Folate-NHS (4.7 mg, 6  $\mu$ mol) dissolved in 100  $\mu$ L of dry DMSO to give Pyro-GDEVDSGSK-Folate (4, PPF). The reaction was concentrated by precipitation with ether and directly separated by HPLC. Purified compound 4 (11.7 mg, 5.5  $\mu$ mol) was dried under high vacuum and stored at –20 °C. The purity was checked by HPLC and MALDI-ToF (mass calculated 1800.76, found 1799.79).

**Synthesis of PKF.** The Fmoc-Lys was coupled to the Sieber resin after activation with HOBt/HBTU in the ratio 1/1/1:3 (Fmoc-Lys/HOBt/HBTU:Sieber resin) in NMP. After the Fmoc group cleavage, the resin was washed with NMP, and Pyro acid was coupled to the N-terminus to give Pyro-K(Mtt)-Sieber resin. The molar ratio of Pyro/HOBt/HBTU to the NH<sub>2</sub>-K(Mtt)-Sieber resin was 3/3/3:1, and the reaction was done in a shaker flask with a 12 h coupling time using dry NMP as a solvent. The resin was then washed with NMP, capped by 0.3 M acetylimidazol in NMP for 15 min, and washed again

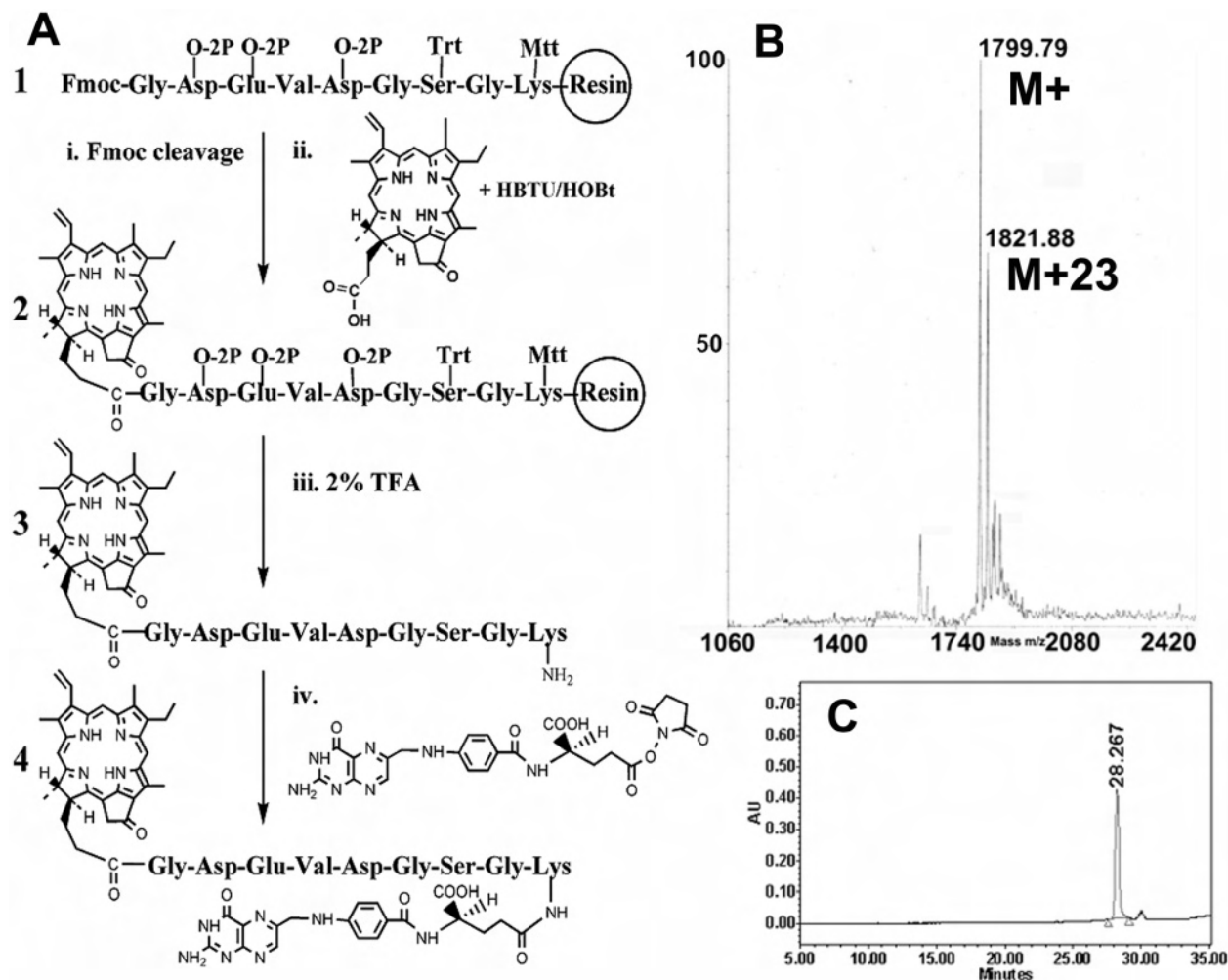


**Figure 1.** Synthesis (A), MALDI-ToF (B, mass calculated 1800.76, found 1799.79) and HPLC (C, absorbance at 410 nm) of Pyro-GDEVDGSGK-Folate.

by an excess of NMP, DCM, and dry methanol, transferred from the shaker flask, and dried. Pyro-K(Mtt)-Sieber resin was cleaved from the resin and the Mtt group deprotected in one step by 2% TFA/5% TIS/DCM for 1 h to yield Pyro-K- $\epsilon$ NH<sub>2</sub>. The compound was precipitated from the cleavage solution by dry ether and dried under high vacuum. This crude compound (21 mg, 31.7  $\mu$ mol) was dissolved in 300  $\mu$ L of dry 1% DIPEA/DMSO and reacted for 2 h with Folate-NHS (31.3 mg, 40  $\mu$ mol) dissolved in 200  $\mu$ L of dry DMSO to give Pyro-K-Folate (PKF). The reaction was concentrated and directly separated by HPLC. Purified PKF (29.8 mg, 27.5  $\mu$ mol) was dried, and the purity was checked by HPLC and MALDI-ToF (Supporting information Figure 1B; mass calculated 1084.50, found 1084.18).

**Confocal Microscopy.** KB and HT 1080 cells were grown in 4-well Lab-Tek chamber slides (Naperville, Illinois) at a density of 50 000 cells/well and grown for 24 h in complete MEM, then rinsed with HBSS (Hank's balanced salt solution) and incubated with 50  $\mu$ M PPF in 300  $\mu$ L of MEM containing 0.8% BSA at 37  $^{\circ}$ C for 5 h. Cells were repeatedly rinsed with HBSS after the incubation and fixed by 1% formaldehyde in PBS for 20 min prior to scanning with confocal microscopy. The settings for confocal microscopy were as follows: 640–800 nm detector slit for detection of Pyro fluorescence, with zoom = 2, expander = 3, resolution 512  $\times$  512, 633 nm excitation wavelength, 40 $\times$  objective, 100% power, 851.1 gain, and –28.5 offset.

**Flow Cytometry Experiments.** KB, HT 1080, and CHO cells were seeded in T25 flasks (each flask 10<sup>6</sup> cells) and grown for

1 day in complete MEM (KB cells and HT 1080 cells) or complete F12K (CHO cells) medium. The cells were incubated for 12 h with 5  $\mu$ M PPF or PKF in MEM containing 0.8% BSA (KB and HT 1080 cells) or F12K containing 0.8% BSA (CHO cells) 1.3 mL/flask alone or with 5 mM folic acid added, and at the end of incubation, the medium was aspirated and cells washed 3 times with 2 mL of PBS. The cells were detached by 0.25% trypsin-EDTA, fixed by 1% formaldehyde (methanol-free) in PBS, resuspended in 1 mL of PBS, and immediately analyzed on a BD LSRII machine at the Flow Cytometry Laboratory, Abramson Cancer Center, at the University of Pennsylvania focusing on Pyro fluorescence (exc. 633 nm, em. 695 nm). The gain was constant for all three samples and set so that the control cells had a fluorescent intensity between 1 and 100 AU.

**Cell Viability (MTT) Assay.** KB, HT 1080, and CHO cells were seeded in clear 96-well plates at a density of 50 000 cells/well in 250  $\mu$ L of complete MEM (KB and HT 1080 cells) or complete F12K (CHO cells) and grown for 24 h at 37  $^{\circ}$ C. Cells were subsequently rinsed with HBSS and incubated with no or 0.5, 5, or 15  $\mu$ M PPF in MEM containing 0.8% BSA (KB and HT 1080 cells) or F12K containing 0.8% BSA (CHO cells) for 24 h. Cells were then rinsed with HBSS, 100  $\mu$ L/well of complete MEM was added, and the cells were either kept in the dark or treated with different light doses (5 or 10 J/cm<sup>2</sup>) by a 670 nm laser with a 20 mW/cm<sup>2</sup> fluence rate. After incubation for 24 h at 37  $^{\circ}$ C, the cells were incubated for 2 h with a 0.5 mg/mL solution of MTT in complete MEM/complete F12K, that was disposed afterward and replaced with 100  $\mu$ L of equal

parts of DMSO and 70% isopropanol in 0.1 M HCl. Absorbance at 570 nm was measured. Data shown are based on three different experiments, and the results were expressed as mean  $\pm$  standard error.

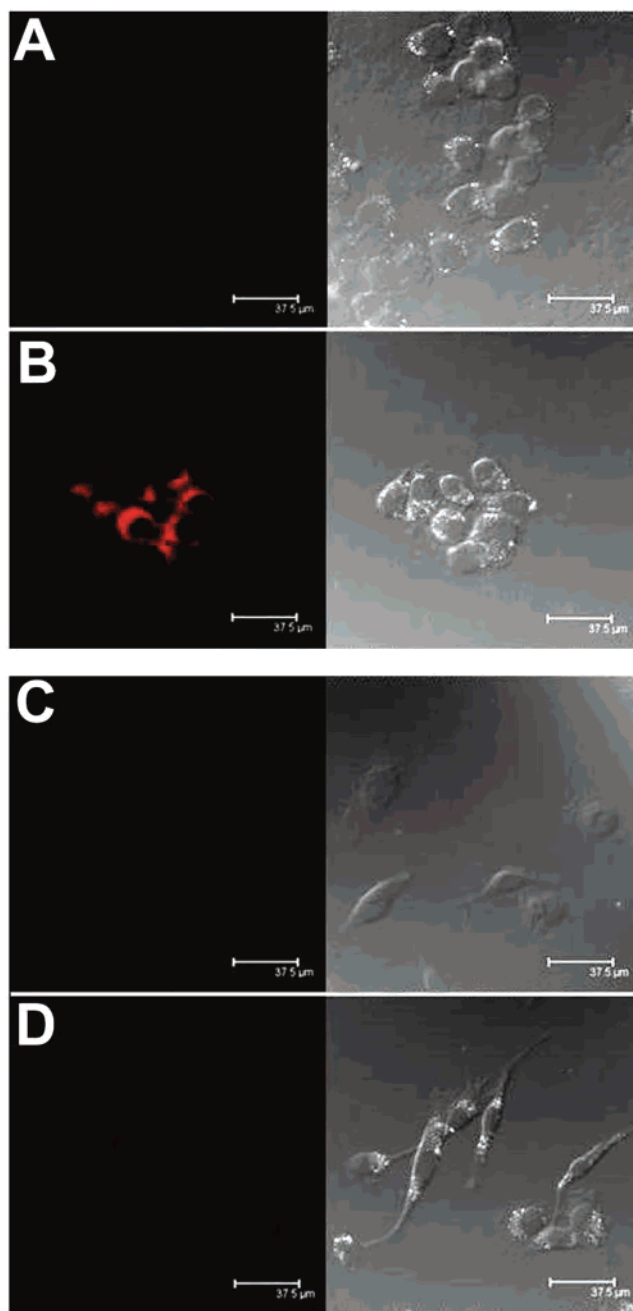
**In Vivo Imaging.** Nude mice were inoculated subcutaneously with  $10^7$  KB cells above the right leg and  $10^7$  HT 1080 cells above the left leg, and the tumors were grown for about 7 days. First, three mice were initially scanned with a Xenogen IVIS imager with a Cy 5.5 filter ( $\lambda_{exc} = 615\text{--}665$  nm,  $\lambda_{em} = 695\text{--}770$  nm) and then intravenously injected with 50 nmol (left), 100 nmol (middle), and 150 nmol (right mouse) of PPF 60–180  $\mu\text{L}/\text{mouse}$  into the tail vein. The mice were imaged 5 min, 6 h, and 24 h after injection. In order to compare the biodistribution of PP and PPF, two double tumor mice were intravenously injected with 30 nmol of PPF or 30 nmol of PP and imaged. These mice were sacrificed 26–30 h after the injection, and the organs (KB tumor, HT 1080 tumor, muscle, heart, adrenal, kidney, spleen, and liver) were imaged directly after dissection and used for biodistribution. In order to compare the biodistribution of PP, PPF, and PKF, the first mouse was injected with 30 nmol of PPF, the second with 30 nmol of PP, and the third with 15 nmol of PKF in two different experiments. The Xenogen images were obtained with the same settings (small binning, 2 s exposure time) and were compared using max = 20 000, min = 3000 for PPF and PP and max = 10 000, min = 1500 for PKF. The mice were sacrificed 26–30 h after iv, the organs were scanned by Xenogen and used for biodistribution.

**Semiquantitative ex Vivo Organ Biodistribution.** The mice were euthanized 26–30 h after drug injection, and the dissected organs were washed in PBS and scanned by Xenogen in a clear 24-well plate. The organs were weighed and disintegrated in DMSO/MeOH (2/3). After settling, the fluorescence was measured (excitation 650 nm, emission 670 nm) and divided by weight for each organ. This ratio of fluorescence vs weight was normalized with respect to muscle, and these semiquantitative values plotted in graphs comparing either PP and PPF (these data are based on three different experiments and the results expressed as mean  $\pm$  standard error) or PP, PPF, and PKF. Statistically significant differences between KB tumor and other organs of PPF mouse are indicated with an asterisk ( $P < 0.05$ ).

## RESULTS AND DISCUSSION

**Synthesis and Characterization of Pyro–GDEVDGSGK–Folate (PPF).** First, Fmoc–GDEVDGSGK was synthesized according the standard solid-phase peptide synthesis (SPPS) protocol using a Sieber resin as a solid phase (1). The photosensitizer Pyro acid was then coupled to the N-terminus of the immobilized peptide (Figure 1A) to give Pyro–GDEVDGSGK–Sieber resin (2), which was cleaved from the solid phase and deprotected with 2% TFA. The folate–NHS was then coupled in a solution reaction to the  $\epsilon\text{-NH}_2$  group of C-terminal lysine of Pyro–GDEVDGSGK (PP, 3), and the product Pyro–GDEVDGSGK–(Folate) (PPF, 4) was characterized by MALDI-ToF (mass calculated 1800.76, found 1799.79; Figure 1B) after purification by HPLC (Figure 1C, absorbance at 410 nm).

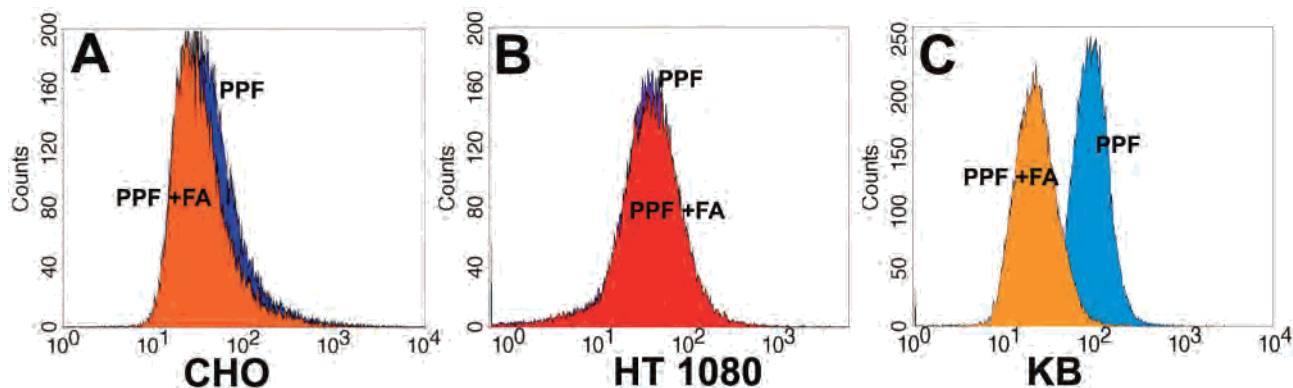
**Accumulation of Pyro–GDEVDGSGK–Folate (PPF) inside FR-Positive and -Negative Cells Monitored by Confocal Microscopy and Flow Cytometry.** To confirm the preferential uptake of PPF by folate receptor-overexpressing tumor cells, KB cells (human epidermal cancer cells; folate receptor positive, FR+) and HT 1080 cells (human fibrosarcoma cells; folate receptor negative, FR–) were incubated with 50  $\mu\text{M}$  PPF for 5 h, and the fluorescence of fixed cells was then monitored by confocal microscopy (Figure 2). By comparing



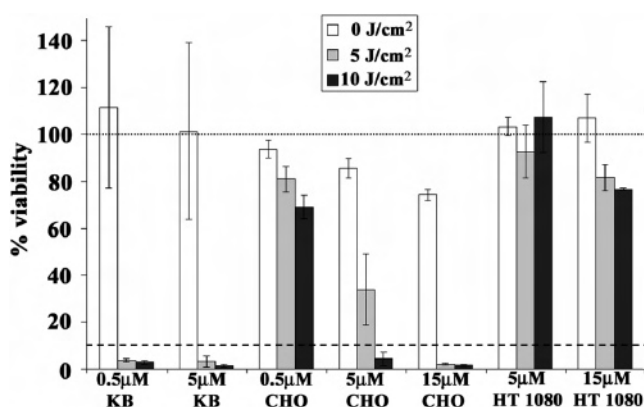
**Figure 2.** Accumulation of Pyro–GDEVDGSGK–Folate (PPF) in KB (FR+) vs HT 1080 (FR–) cells. (A) KB cells alone, (B) KB cells incubated with 50  $\mu\text{M}$  PPF for 5 h, (C) HT 1080 cells alone, (D) HT 1080 cells incubated with 50  $\mu\text{M}$  PPF for 5 h. PPF accumulates preferentially in KB cells. The scale bar represents 37.5  $\mu\text{m}$ .

Figure 2B and D, it is clear that PPF accumulates more in KB cells (FR+) (Figure 2B) than in HT 1080 cells (FR–) (Figure 2D).

In order to establish the FR delivery pathway as the main uptake mechanism for PPF, the inhibition of PPF uptake was monitored by flow cytometry using an excess of free folic acid in KB, HT 1080, and CHO (chinese hamster ovary) cells. As expected, there is a minimal influence of folic acid on the uptake of PPF into HT 1080 and CHO cells (both FR–) in contrast to KB cells, where the uptake was inhibited up to 70% (Figure 3). These results suggest that (A) the main delivery pathway for PPF into the FR+ cells is via folate receptor-mediated endocytosis, (B) PPF's uptake can be inhibited up to 70% by folic acid in the case of KB cells (FR+), and (C) the remaining



**Figure 3.** Monitoring the accumulation of PPF (Pyro-GDEVGDGSGK-Folate) in CHO (FR<sup>-</sup>), HT 1080 (FR<sup>-</sup>), and KB (FR<sup>+</sup>) cells using flow cytometry and inhibition of this uptake with free folic acid. CHO cells (A) and HT 1080 cells (B) incubated with 5  $\mu$ M PPF (blue) or 5  $\mu$ M PPF and 5 mM folic acid (orange/red) show very similar uptake of PPF (695 nm fluorescence) with or without inhibition (PPF + FA vs PPF). Only KB cells (C) show significant (70%) reduction in PPF uptake when incubated with 5  $\mu$ M PPF and 5 mM Folic acid (PPF, blue; vs PPF + FA, orange), suggesting that folate receptor-mediated endocytosis is the main delivery pathway for KB, but not for CHO and HT 1080 cells.



**Figure 4.** Viability of KB cells (FR<sup>+</sup>, cancer cells), HT 1080 cells (FR<sup>-</sup>, cancer cells), and CHO cells (FR<sup>-</sup>, normal cells) incubated with 0.5, 5, and 15  $\mu$ M PPF and treated with light (5 or 10  $J/cm^2$ ) or kept in the dark (0  $J/cm^2$ ). KB cells have viability reduced below 10% when incubated with the lowest drug dose (0.5  $\mu$ M) and treated with 5  $J/cm^2$ . CHO cells reach this level of cell death for the same concentration (5  $\mu$ M) only when treated with the highest light dose (10  $J/cm^2$ ), and in case of HT 1080, even the highest drug dose (15  $\mu$ M) and light dose (10  $J/cm^2$ ) did not reduce their viability below 10%.

uptake of PPF to KB cells and the lower uptake of PPF to the HT 1080 and CHO cells can be attributed to the nonspecific tumor affinity of the Pyro moiety.

**Selective PDT-Induced Cell Killing as a Result of FR Targeting.** To compare the post-PDT viability reduction for cell lines with different levels of FR expression, KB tumor cells (FR<sup>+</sup>), HT 1080 tumor cells (FR<sup>-</sup>), and normal CHO cells (FR<sup>-</sup>) were incubated with 0.5, 5, and 15  $\mu$ M PPF for 24 h and were then either kept in the dark or treated by PDT with 5 or 10  $J/cm^2$  light doses using a 670 nm tunable laser with a fluence rate of 20  $mW/cm^2$ . The MTT study (Figure 4) shows that the viability of KB cells drops below 10% when incubated with 0.5  $\mu$ M PPF and treated with a 5  $J/cm^2$  light dose. Achieving the same cell viability reduction in CHO cells requires both a 10-fold concentration (5  $\mu$ M) in combination with a 2-fold light dose (10  $J/cm^2$ ). Interestingly, using the combination of the highest drug dose (15  $\mu$ M) and light dose (10  $J/cm^2$ ) does not effectively kill the HT 1080 cells, suggesting an even lower accumulation of PPF or a possible PDT resistance of the HT1080 cells. This study further supports the FR-mediated PDT activity of PPF toward FR<sup>+</sup> cancer cells.

**In Vivo Discrimination between KB (FR<sup>+</sup>) and HT 1080 (FR<sup>-</sup>) Tumors.** To validate the FR-targeting specificity of PPF in vivo, nude mice bearing an HT 1080 tumor (FR<sup>-</sup>) on the left flank and a KB tumor (FR<sup>+</sup>) on the right flank were used

for in vivo imaging studies. Three double tumor mice were intravenously injected with 50, 100, and 150 nmol of PPF and scanned by Xenogen imager (Figure 5, using a Cy 5.5 filter) before the drug injection (prescan, Figure 5A) and after the drug injection at three different time points (5 min, 6 h, and 24 h). Five minutes after injection (Figure 5B), PPF is distributed rapidly throughout the body, carried by the blood stream. At 6 h postinjection (Figure 5C), KB tumor accumulates significantly more PPF than HT 1080, and accumulation in normal organs is considerably reduced. At 24 h postinjection (Figure 5D), the uptake of PPF in normal organs as well as the HT1080 (FR<sup>-</sup>) tumor for “50 nmol” and “100 nmol” mouse drops almost to the prescan level in contrast to a high fluorescent signal that remains in the KB tumor. These in vivo imaging studies clearly show that (A) PPF accumulates preferentially in KB tumor with respect to HT1080 tumor and other normal organs, (B) it is clear from the saturated image of the “150 nmol” mouse (Figure 5D) that PPF also accumulates in HT 1080 tumor, and (C) PPF is not toxic at the 150 nmol drug dose and is cleared quickly out of normal tissues.

**The Role of Folate and Peptide Modules in Targeted Delivery of PPF.** In order to examine the impact of each module on delivery efficiency and target specificity, two analogues of PPF were synthesized. One is Pyro-GDEVGDGSGK (PP) that lacks the folate moiety; the other is Pyro-K-Folate (PKF) with one lysine residue replacing the short peptide sequence (Figure 6).

**A. The Role of Folate Attachment for Target-Specific Delivery of PPF in Vivo.** Since Pyro itself can serve as a delivery molecule (albeit with poor specificity), the in vivo imaging and biodistribution of the nontargeting Pyro-GDEVGDGSGK (PP) can help to assess the true influence of folate as a tumor homing molecule. Thus, two double tumor-bearing mice in each experiment were injected with 30 nmol of PPF or with 30 nmol of PP ( $n = 3$ ). The image in Figure 7 (upper left) shows that, around 6.5 h after injection of PPF (left) and PP (right), PPF accumulates significantly more in KB tumors than in HT1080 tumors, whereas PP accumulates comparably in both KB and HT 1080 tumors (see also Figure 8). The animals were sacrificed 26–30 h after injection, and the dissected organs were first imaged (Figure 7, lower left) and then homogenized. The images of the organs showed stronger fluorescence in the KB tumor from the PPF mouse, a weaker signal coming mainly from kidneys and livers of both the PPF and the PP mouse, and almost no signal from other organs.

The uptake of PPF and PP was determined by extracting the homogenized organs with DMSO/MeOH, measuring the fluorescence at 670 nm, and correcting the signal for weight (Figure

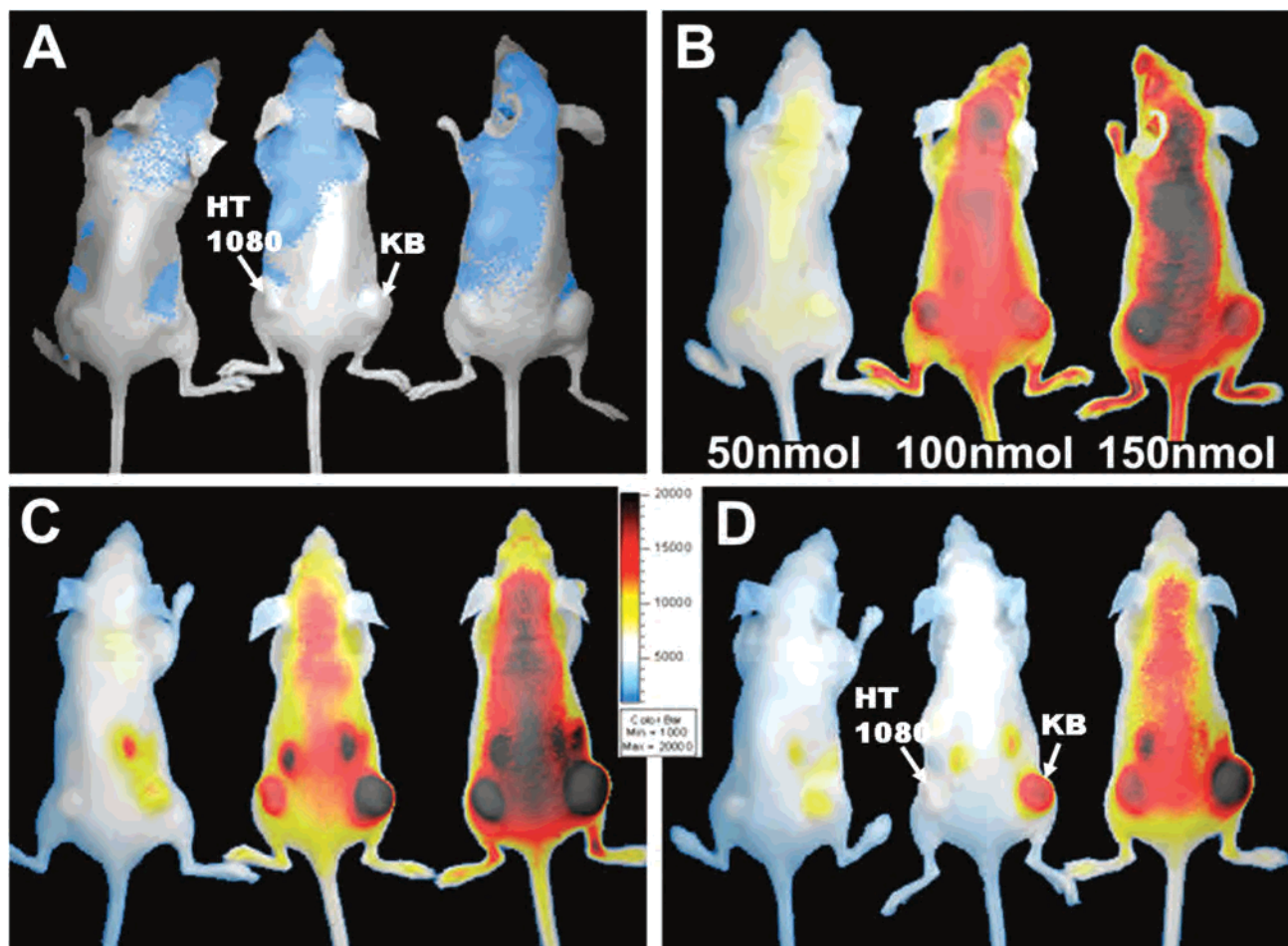


**Figure 5.** Monitoring fluorescence signal distribution after intravenous injection of three different doses of PPF to double tumor-bearing mice that have a KB tumor (FR+) on the right side and an HT 1080 tumor (FR-) on the left side, using a Xenogen imager. (A) Prescan, (B) 5 min after injection of 50 nmol (left mouse), 100 nmol (middle mouse) and 150 nmol (right mouse) of PPF, (C) 6 h after injection, and (D) 24 h after injection. At this point, it is clear that PPF preferentially accumulates in the KB tumor.

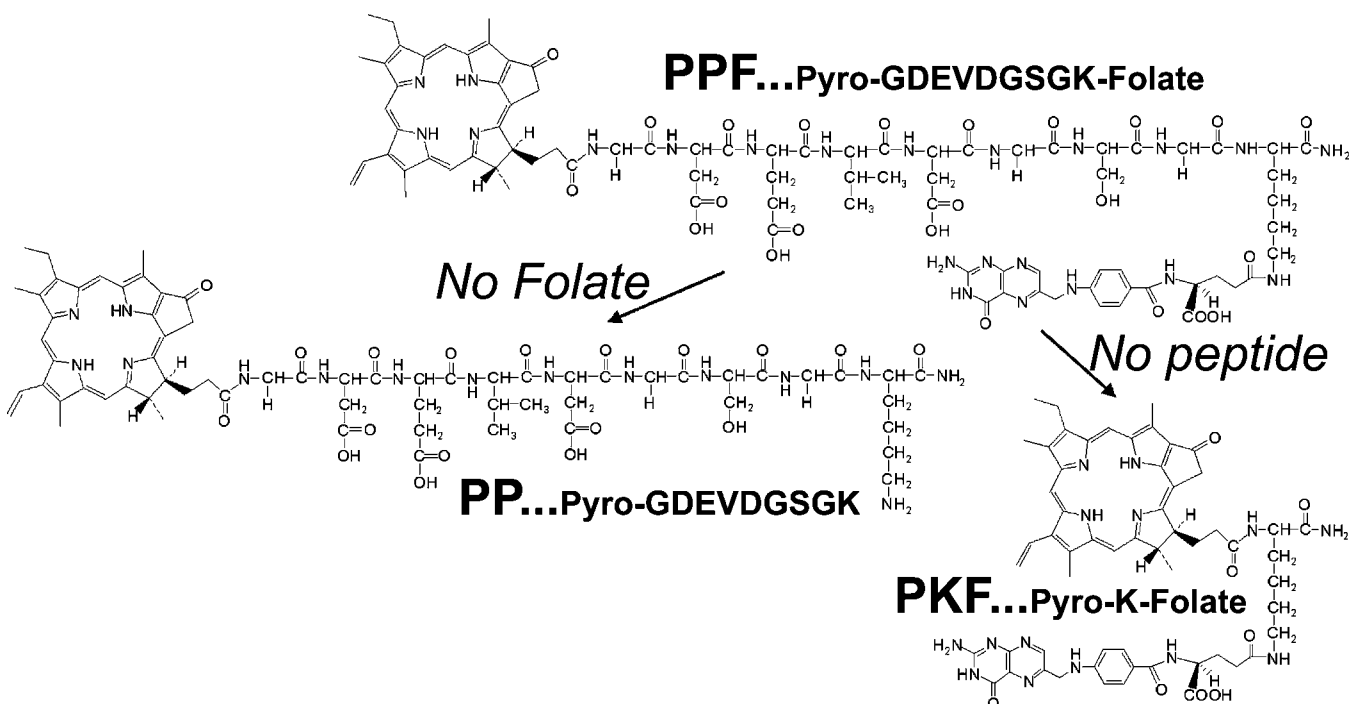


**Figure 6.** Structure of PPF (both peptide and folate modulation), PP (lacking the folate), and PKF (lacking the peptide module).

7, right). By examining the biodistribution of PPF after normalizing with respect to muscle, the highest fluorescence

signal was found in the KB tumor. This signal is only comparable to the signal from kidney, which is known as the

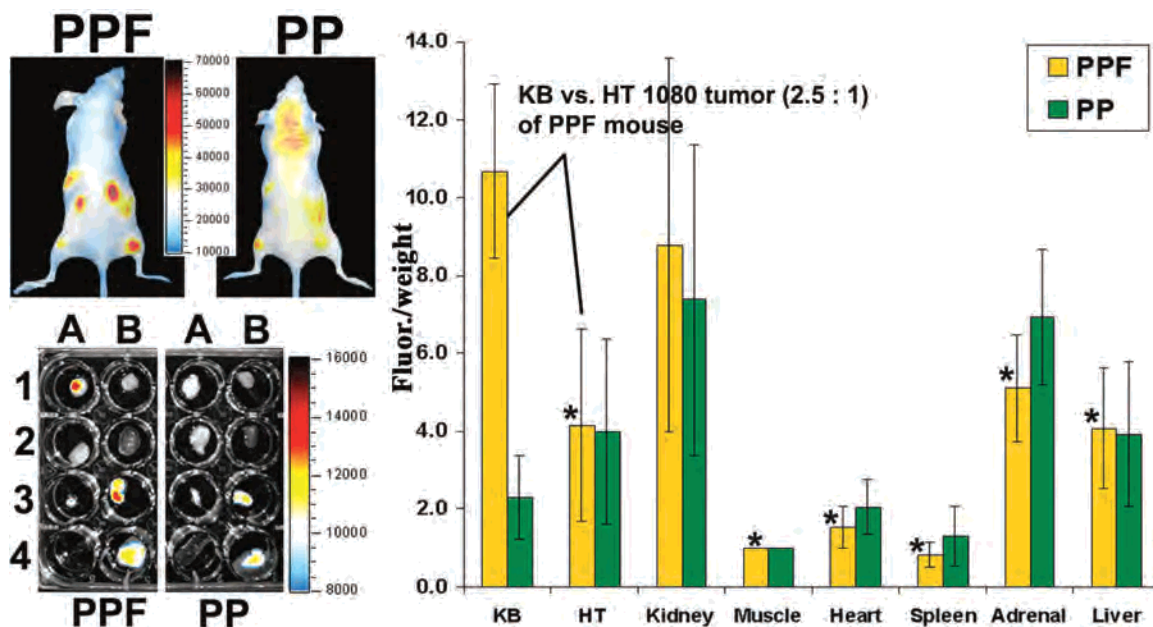


**Figure 7.** In vivo and ex vivo distribution of iv injected Pyro-GDEVDSGSK-Folate (PPF, targeting FR+ KB tumor) and Pyro-GDEVDSGSK (PP, no targeting). Xenogen images of double tumor mice (HT 1080 tumor left, KB tumor right) injected with PPF (left) or PP (right) at 6.5 h after injection (upper left corner) shows higher accumulation of PPF in the KB tumor. This was confirmed by images of the dissected organs (lower left corner): 1A, KB tumor; 1B, HT 1080 tumor; 2A, muscle; 2B, heart; 3A, adrenal; 3B, kidney; 4A, spleen; 4B, liver (left, PPF; and right, PP). Fluorescence from homogenized organs (right: PPF, orange; PP, green), corrected for weight and expressed as a ratio of the signal of muscle (=1), shows a significantly higher accumulation of PPF in the KB tumor than in the HT 1080 tumor but a similar distribution of nontargeting PP in both tumors. The asterisk identifies those organs of the PPF mouse whose relative fluorescence is significantly ( $P < 0.05$ ,  $n = 3$ ) different from that of the KB tumor, showing that the KB tumor has the highest accumulation of PPF, comparable only with kidney, while the HT 1080 tumor has an average signal that is 2.5 times lower.

major clearance pathway for folate bioconjugates. Moreover, the fluorescence signals in HT 1080 and other normal organs (adrenal, liver, heart, and spleen) were significantly lower ( $*P < 0.05$ ) with the ratio of KB to HT 1080 on average 2.5:1. In contrast, the biodistribution of PP shows no significant difference between the HT 1080 tumors and KB tumors (or the rest of the organs), confirming the minimal role of Pyro on the PPF tumor selectivity and thus validating the importance of folate as a tumor homing molecule.

**B. The Role of Peptide Modulation in Targeted Delivery of PPF.** In order to clarify the role of peptide in the targeted delivery of PPF, Pyro-K-Folate (PKF) was synthesized by replacing the nine amino acid peptide sequence in PPF with a single lysine residue. The following investigations revealed the consequences of removing the peptide module. First, PKF showed the increased hydrophobicity and decreased water solubility when compared to PPF (HPLC, Supporting information Figure 2). Next, the accessibility of the folate moiety to FR in PKF vs PPF was also investigated in vitro using flow cytometry. KB, HT 1080, and CHO cells were incubated with the same concentration ( $5 \mu\text{M}$ ) of PKF or PPF. It was observed that both PPF and PKF accumulate in HT 1080 and CHO cells (both FR-) with similar efficiency, whereas in KB cells (FR+), the efficiency of PKF uptake drops almost to 50% compared to that of PPF (Supporting information Figure 3). This indicates that the nine amino acid linker in PPF increases the efficiency of the FR-mediated uptake probably by making the folate more accessible (Supporting information Figure 4).

Perhaps the most profound effect of peptide modulation on the targeted delivery of PPF was its role in the biodistribution pattern of PPF as depicted in Figure 8 and Supporting information Figure 5. As expected, when we compare the in vivo biodistribution of PPF with that of PP, the difference in KB and HT 1080 tumor accumulation of PPF is visible at 1.5 h (Figure 8, column C) and is much more distinguishable at 6.5 h (Figure 8, column D) postinjection. This is clearly due to

the effect of FR targeting by the folate moiety, which facilitates the preferential accumulation of PPF in the KB tumor (FR+), since folate-lacking PP does not distinguish between the FR+ and FR- tumors. However, what is notable is the common biodistribution pattern showing a low retention in the organs responsible for drug clearance for both PPF and PP. We attribute this finding to the peptide-based pharmacomodulation, meaning that the presence of a short peptide sequence significantly alters the pharmacokinetics and pharmacodynamics of the parent molecule. Such modulation becomes more obvious when we compare the biodistribution pattern of PPF with that of PKF (Figure 8, row 3, and Supporting information Figure 5). Even though PKF immediately after the injection (Figure 8, 3B) displays a distribution pattern very similar to that of PPF and PP (Figure 8, 1B and 2B), this pattern is drastically changed only 1.5 h postinjection (Figure 8, column C). At 6.5 h, it is clear that most PKF is retained by the excretion organs and exhibits extremely low tumor accumulation (Figure 8, 3D). In contrast, both PPF and PP are delivered to the tumors with much higher efficiency even though there is a difference in FR-targeting specificity.

The ex vivo organ biodistribution corrected for weight and normalized for muscle (Supporting information Figure 5) further confirmed this accumulation pattern. It identifies liver and spleen (followed by adrenal and kidney) as the organs accumulating most of the PKF, and when comparing the relative fluorescence intensity with both that of PPF and PP, this accumulation is approximately 50-fold higher for PKF. This pharmacomodulation highlights the positive impact of the peptide sequence on the targeted delivery of PPF by minimizing the nonspecific uptake by liver, spleen, and other organs.

**Future Perspective.** In principle, the target-specific, peptide-based pharmacomodulation approach described here could be applicable for improving the delivery efficiency of other cancer diagnostics and therapeutics. The versatility of this approach lies in its modular design in which any module could be easily

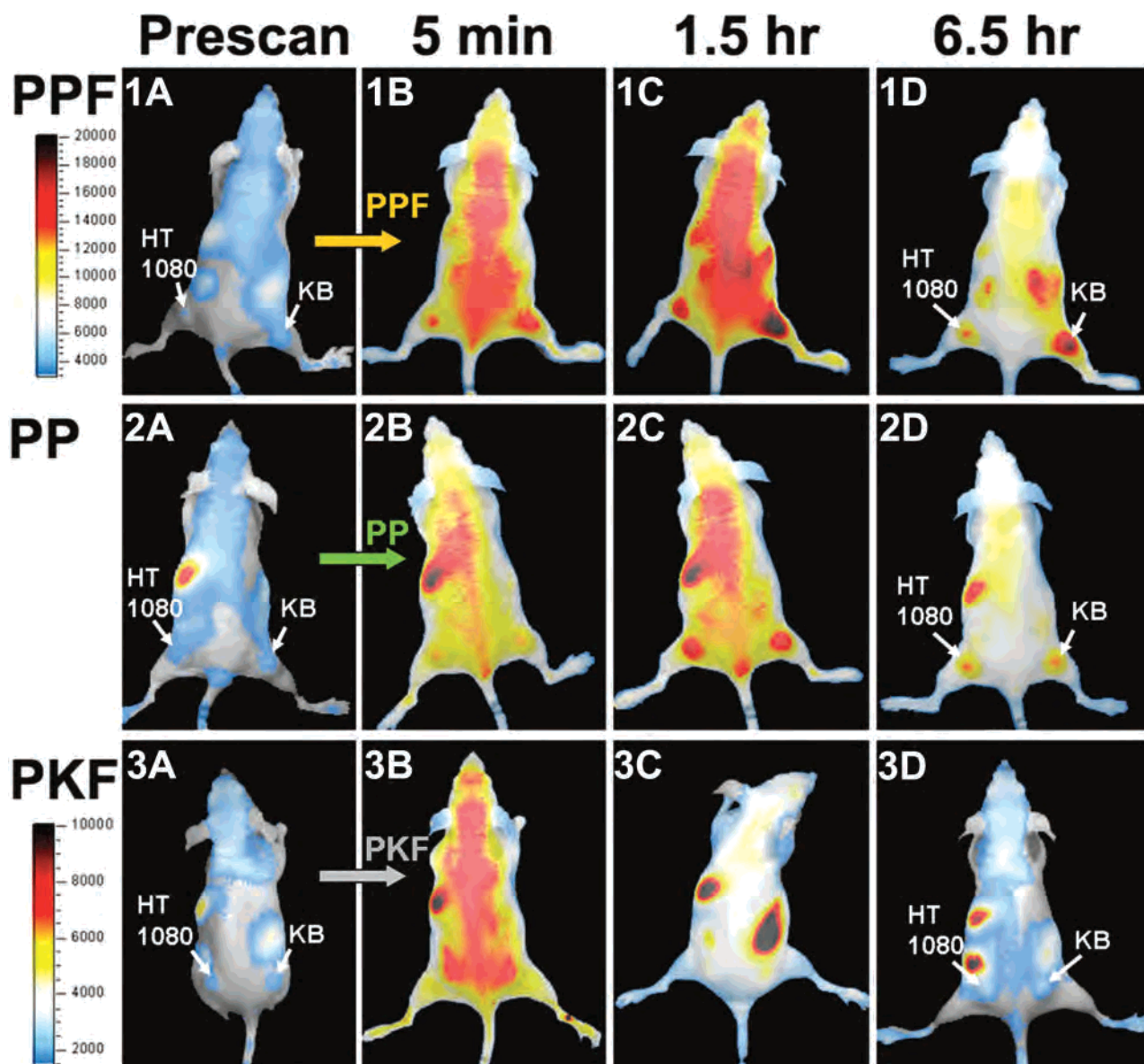


**Figure 8.** Double tumor mice (HT 1080 tumor, left; KB tumor, right) injected with Pyro–GDEVDGSGK–Folate (PPF, row 1), Pyro–GDEVDGSGK (PP, row 2), or Pyro–K–Folate (PKF, row 3) and imaged before the injection (Prescan, A) and 5 min (B), 1.5 h (C), and 6.5 h (D) after the drug injection. It is clear that 6.5 h after the injection PPF accumulates mostly in the KB tumor (1D) and PP equally in both tumors (2D), demonstrating the folate-introduced cancer specificity. This is in contrast to PKF (3D) that has minimal tumor accumulation and is retained in organs responsible for drug clearance, clearly identifying the peptide as the pharmacomodulating component.

replaced for a different purpose. For example, the Pyro moiety could be replaced with another photosensitizer that is active at a longer-wavelength absorption (e.g., bacteriochlorophylls (39) or naphthalocyanines (40)) or even a chemotherapeutic agent (e.g., docetaxel, etc.). The target specificity can also be modulated by exchanging the folate moiety for any small molecule ligand targeting other cancer signatures. Finally, the length and the sequence of the peptide linker could be fine-tuned to optimize the pharmacomodulation, improving not only the solubility and the target accessibility, but most importantly, also the delivery efficiency. In the future, the peptide linker could also serve as an subcellular organelle specific delivery vehicle when exchanged for different sequences.

#### SUMMARY

We synthesized, characterized, and evaluated a target-specific NIR imaging and PDT agent with improved target specificity and delivery efficiency. This agent is composed of three modules: a fluorescent photosensitizer Pyro for NIR imaging

and PDT, folate for selective delivery, and a short peptide linker for pharmacomodulation. Although there were several previous attempts to link a dye (9) or a photosensitizer (9, 37) to a folate moiety in order to specifically deliver the agent to cancer cells overexpressing FR, they were limited either to use in vitro or only to the imaging purposes. Here, we report a novel, modular approach using the combination of a folate-mediated targeting and a peptide-based pharmacomodulation to improve the efficiency of targeted delivery of NIR imaging and PDT agents. This study created a fluorescent photosensitizer with an excellent biodistribution pattern (folate receptor-specific tumor uptake and low accumulation in normal tissues), a crucial step toward lowering the toxicity and background signal, thus making it potentially applicable for detecting and treating cancers in patients.

#### ACKNOWLEDGMENT

We thank André E. X. Brown for critical comments and suggestions on the manuscript. This work was supported by the

DOD Breast Cancer Research Program DAMD17-03-1-0373 and the NIH grant U54 CA105008 (Penn NTROI).

**Supporting Information Available:** MALDI-ToF of PP and PKF; HPLC and UV-vis of PPF (4), PP (3), and PKF; flow cytometry of CHO, HT 1080, and KB cells incubated with 5  $\mu$ M PKF or PPF; the 3D structure of PPF; ex vivo biodistribution of PPF, PP, and PKF. This material is available free of charge via the Internet at <http://pubs.acs.org>.

## LITERATURE CITED

- (1) Berg, K., Selbo, P. K., Weyergang, A., Dietze, A., Prasmickaite, L., Bonsted, A., Engesaeter, B. O., Angell-Petersen, E., Warloe, T., Frandsen, N., and Hogset, A. (2005) Porphyrin-related photosensitizers for cancer imaging and therapeutic applications. *J. Microsc.* 218, 133–147.
- (2) Licha, K. (2002) Contrast agents for optical imaging. *Top. Curr. Chem.* 222, 1–29.
- (3) Oleinick, N. L., and Evans, H. H. (1998) The photobiology of photodynamic therapy: cellular targets and mechanisms. *Radiat. Res.* 150, S146–156.
- (4) Bogaards, A., Varma, A., Collens, S. P., Lin, A., Giles, A., Yang, V. X., Bilbao, J. M., Lilge, L. D., Muller, P. J., and Wilson, B. C. (2004) Increased brain tumor resection using fluorescence image guidance in a preclinical model. *Lasers Surg. Med.* 35, 181–190.
- (5) Coleman, C. N. (2003) Linking radiation oncology and imaging through molecular biology (or now that therapy and diagnosis have separated, it's time to get together again!) *Radiology* 228, 29–35.
- (6) Huang, X., El-Sayed, I. H., Qian, W., and El-Sayed, M. A. (2006) Cancer cell imaging and photothermal therapy in the near-infrared region by using gold nanorods. *J. Am. Chem. Soc.* 128, 2115–2120.
- (7) Dougherty, T. J. (1987) Photosensitizers: therapy and detection of malignant tumors. *Photochem. Photobiol.* 45, 879–889.
- (8) Gurfinkel, M., Thompson, A. B., Ralston, W., Troy, T. L., Moore, A. L., Moore, T. A., Gust, J. D., Tatman, D., Reynolds, J. S., Muggenburg, B., Nikula, K., Pandey, R., Mayer, R. H., Hawrysz, D. J., and Sevcik-Muraca, E. M. (2000) Pharmacokinetics of ICG and HPPH-car for the detection of normal and tumor tissue using fluorescence, near-infrared reflectance imaging: a case study. *Photochem. Photobiol.* 72, 94–102.
- (9) Moon, W. K., Lin, Y., O'Loughlin, T., Tang, Y., Kim, D. E., Weissleder, R., and Tung, C. H. (2003) Enhanced tumor detection using a folate receptor-targeted near-infrared fluorochrome conjugate. *Bioconjugate Chem.* 14, 539–545.
- (10) Dougherty, T. J., Gomer, C. J., Henderson, B. W., Jori, G., Kessel, D., Korbelik, M., Moan, J., and Peng, Q. (1998) Photodynamic therapy. *J. Natl. Cancer Inst.* 90, 889–905.
- (11) Niedre, M. J., Secord, A. J., Patterson, M. S., and Wilson, B. C. (2003) In vitro tests of the validity of singlet oxygen luminescence measurements as a dose metric in photodynamic therapy. *Cancer Res.* 63, 7986–7994.
- (12) Jori, G. (1996) Tumour photosensitizers: approaches to enhance the selectivity and efficiency of photodynamic therapy. *J. Photochem. Photobiol., B* 36, 87–93.
- (13) Chen, J., Stefflova, K., Neidre, M., Wilson, B., Chance, B., Glickson, J. D., and Zheng, G. (2004) Protease-triggered photosensitizing beacon based on singlet oxygen quenching and activation. *J. Am. Chem. Soc.* 126, 11450–11451.
- (14) Sun, X., and Leung, W. N. (2002) Photodynamic therapy with pyropheophorbide-a methyl ester in human lung carcinoma cancer cell: efficacy, localization and apoptosis. *Photochem. Photobiol.* 75, 644–651.
- (15) Bellnier, D. A., Greco, W. R., Loewen, G. M., Nava, H., Oseroff, A. R., Pandey, R. K., Tsuchida, T., and Dougherty, T. J. (2003) Population pharmacokinetics of the photodynamic therapy agent 2-[1-hexyloxyethyl]-2-devinyl pyropheophorbide-a in cancer patients. *Cancer Res.* 63, 1806–1813.
- (16) Reddy, J. A., Allagadda, V. M., and Leamon, C. P. (2005) Targeting therapeutic and imaging agents to folate receptor positive tumors. *Curr. Pharm. Biotechnol.* 6, 131–150.
- (17) Lu, Y., and Low, P. S. (2002) Folate-mediated delivery of macromolecular anticancer therapeutic agents. *Adv. Drug Delivery Rev.* 54, 675–693.
- (18) Sabharanjak, S., and Mayor, S. (2004) Folate receptor endocytosis and trafficking. *Adv. Drug Delivery Rev.* 56, 1099–1109.
- (19) Paulos, C. M., Turk, M. J., Breur, G. J., and Low, P. S. (2004) Folate receptor-mediated targeting of therapeutic and imaging agents to activated macrophages in rheumatoid arthritis. *Adv. Drug Delivery Rev.* 56, 1205–1217.
- (20) Hilgenbrink, A. R., and Low, P. S. (2005) Folate receptor-mediated drug targeting: from therapeutics to diagnostics. *J. Pharm. Sci.* 94, 2135–2146.
- (21) Sibrian-Vazquez, M., Jensen, T. J., Hammer, R. P., and Vicente, M. G. (2006) Peptide-mediated cell transport of water soluble porphyrin conjugates. *J. Med. Chem.* 49, 1364–1372.
- (22) Rosenkranz, A. A., Jans, D. A., and Sobolev, A. S. (2000) Targeted intracellular delivery of photosensitizers to enhance photodynamic efficiency. *Immunol. Cell Biol.* 78, 452–464.
- (23) Dozzo, P., Koo, M. S., Berger, S., Forte, T. M., and Kahl, S. B. (2005) Synthesis, characterization, and plasma lipoprotein association of a nucleus-targeted boronated porphyrin. *J. Med. Chem.* 48, 357–359.
- (24) Hanahan, D., and Weinberg, R. A. (2000) The hallmarks of cancer. *Cell* 100, 57–70.
- (25) Sharman, W. M., van Lier, J. E., and Allen, C. M. (2004) Targeted photodynamic therapy via receptor mediated delivery systems. *Adv. Drug Delivery Rev.* 56, 53–76.
- (26) Konan, Y. N., Gurny, R., and Allemann, E. (2002) State of the art in the delivery of photosensitizers for photodynamic therapy. *J. Photochem. Photobiol., B* 66, 89–106.
- (27) Hamblin, M. R., Miller, J. L., and Ortel, B. (2000) Scavenger-receptor targeted photodynamic therapy. *Photochem. Photobiol.* 72, 533–540.
- (28) Derycke, A. S., Kamuhabwa, A., Gijssens, A., Roskams, T., De Vos, D., Kasran, A., Huwyler, J., Missiaen, L., and de Witte, P. A. (2004) Transferrin-conjugated liposome targeting of photosensitizer ALPcS4 to rat bladder carcinoma cells. *J. Natl. Cancer Inst.* 96, 1620–1630.
- (29) Zheng, G., Chen, J., Li, H., and Glickson, J. D. (2005) Rerouting lipoprotein nanoparticles to selected alternate receptors for the targeted delivery of cancer diagnostic and therapeutic agents. *Proc. Natl. Acad. Sci. U.S.A.* 102, 17757–17762.
- (30) Morgan, J., Gray, A. G., and Huehns, E. R. (1989) Specific targeting and toxicity of sulphonated aluminium phthalocyanine photosensitized liposomes directed to cells by monoclonal antibody in vitro. *Br. J. Cancer* 59, 366–370.
- (31) Chen, X., Hui, L., Foster, D. A., and Drain, C. M. (2004) Efficient synthesis and photodynamic activity of porphyrin-saccharide conjugates: targeting and incapacitating cancer cells. *Biochemistry* 43, 10918–10929.
- (32) Farokhzad, O. C., Karp, J. M., and Langer, R. (2006) Nanoparticle-aptamer bioconjugates for cancer targeting. *Expert Opin. Drug Delivery* 3, 311–324.
- (33) Ichikawa, K., Hikita, T., Maeda, N., Yonezawa, S., Takeuchi, Y., Asai, T., Namba, Y., and Oku, N. (2005) Antiangiogenic photodynamic therapy (PDT) by using long-circulating liposomes modified with peptide specific to angiogenic vessels. *Biochim. Biophys. Acta* 1669, 69–74.
- (34) Renno, R. Z., Terada, Y., Haddadin, M. J., Michaud, N. A., Gragoudas, E. S., and Miller, J. W. (2004) Selective photodynamic therapy by targeted verteporfin delivery to experimental choroidal neovascularization mediated by a homing peptide to vascular endothelial growth factor receptor-2. *Arch. Ophthalmol.* 122, 1002–1011.
- (35) Bisland, S. K., Singh, D., and Garipey, J. (1999) Potentiation of chlorin e6 photodynamic activity in vitro with peptide-based intracellular vehicles. *Bioconjugate Chem.* 10, 982–992.
- (36) Kukowska-Latallo, J. F., Candido, K. A., Cao, Z., Nigavekar, S. S., Majoros, I. J., Thomas, T. P., Balogh, L. P., Khan, M. K., and Baker, J. R., Jr. (2005) Nanoparticle targeting of anticancer drug improves therapeutic response in animal model of human epithelial cancer. *Cancer Res.* 65, 5317–5324.
- (37) Schneider, R., Schmitt, F., Frochet, C., Fort, Y., Lourette, N., Guillemin, F., Muller, J. F., and Barberi-Heyob, M. (2005) Design, synthesis, and biological evaluation of folic acid targeted tetraphenylporphyrin as novel photosensitizers for selective photodynamic therapy. *Bioorg. Med. Chem.* 13, 2799–2808.

- (38) Schottelius, M., Rau, F., Reubi, J. C., Schwaiger, M., and Wester, H. J. (2005) Modulation of pharmacokinetics of radioiodinated sugar-conjugated somatostatin analogues by variation of peptide net charge and carbohydrate chemistry. *Bioconjugate Chem.* *16*, 429–437.
- (39) Zheng, G., Chen, Y., Intes, X., Chance, B., and Glickson, J. D. (2004) Contrast-enhanced near-infrared (NIR) optical imaging for subsurface cancer detection. *J. Porphyrins Phthalocyanines* *8*, 1106–1117.
- (40) Li, H., Marotta, D. E., Kim, S., Busch, T. M., Wileyto, E. P., and Zheng, G. (2005) High payload delivery of optical imaging and photodynamic therapy agents to tumors using phthalocyanine-reconstituted low-density lipoprotein nanoparticles. *J. Biomed. Opt.* *10*, 41203.

BC0602578

# Killer Beacons for Combined Near-Infrared Fluorescence Imaging and Photodynamic Therapy of Cancer

Klara Stefflova<sup>1</sup>, Juan Chen<sup>b,c,d</sup> and Gang Zheng<sup>\*b,c,d\*</sup>

Department of <sup>1</sup>Chemistry, <sup>2</sup>Radiology, University of Pennsylvania, Philadelphia, PA 19104, USA; <sup>3</sup>Department of Medical Biophysics, University of Toronto and <sup>4</sup>Division of Biophysics and Bioimaging, Ontario Cancer Institute, Toronto, ON M5G 1L7, Canada

**Abstract:** Precisely localizing therapeutic agents in neoplastic areas would greatly improve their efficacy for killing tumor cells and reduce their toxicity to normal cells. Photodynamic therapy (PDT) is a promising cancer treatment modality, and near-infrared fluorescence imaging (NIRF-I) is a sensitive and noninvasive approach for *in vivo* cancer detection. This review focuses on the current efforts to engineer single molecule constructs that allow these two modalities to be combined to achieve a high level of selectivity for cancer treatment. The primary component of these so called killer beacons is a fluorescent photosensitizer responsible for both imaging and therapy. By attaching other components, e.g. various DNA- or peptide-based linkers, quenchers or cancer cell-specific delivery vehicles, their primary diagnostic and therapeutic functions as well as their target specificity and pharmacological properties can be modulated. This modular design makes these agents customizable, offering the ability to assemble a few simple and often interchangeable functional modules into beacons with totally different functions. This review will summarize following three types of killer beacons: photodynamic molecular beacons, traceable beacons and beacons with built-in apoptosis sensor. Despite the rapid progress in killer beacon development, numerous challenges remain before these beacons can be translated into clinics, such as photobleaching, delivery efficiency and cancer-specificity. In this review we outline the basic principles of killer beacons, the current achievements and future directions, including possible cancer targets and different therapeutic applications.

**Keywords:** Near-infrared fluorescence imaging (NIRF-I), photodynamic therapy (PDT), apoptosis imaging, singlet oxygen, quenching, activation, image-guided therapy, delivery.

## INTRODUCTION

According to the International Agency for Research on Cancer, in 2002 there were 10.9 million people diagnosed with cancer and over 6.7 million people died as a result of cancer [1]. In the United States, these numbers were estimated to be 1.4 million and 0.6 million respectively in 2006 [2]. Cancer most often strikes the lungs and gastrointestinal tract (over 45%), followed by the breast, prostate, and skin [1]. Curing cancer is a difficult goal and often includes a variety of treatments such as surgery and chemotherapy. Despite the rapid improvement of both surgical methods and drugs, conventional therapies still suffer from a lack of necessary cancer selectivity resulting in cancer recurrence and treatment toxicity. To address these issues, there have been extensive efforts to both understand and identify possible cancer-specific triggering mechanisms and targets, as well as to use this knowledge in the design of new drugs. This research is accompanied by the equally important development of novel treatment approaches exploring new techniques or combining already well explored imaging techniques and existing therapies.

## Combined Cancer Imaging and Therapy

Currently, nobody doubts that early cancer detection is a very important step towards successful treatment. Imaging is crucial for diagnosing the disease in the first place and also plays an important role as a follow up to the treatment to assess the success of the therapy and to identify any possible recurring lesions. With increasing demand on treatment selectivity, a less toxic and more efficient treatment modality, image-guided therapy, is now recognized as an excellent method both for localizing cancer targets during treatment and for monitoring the treatment outcome noninvasively [3, 4]. Image-guided therapy is already being explored in radiotherapy, but out of the vast array of possible imaging-therapy combinations, the synergy of near-infrared fluorescence imaging (NIRF-I) and photodynamic therapy (PDT) is extremely compelling for several

reasons. First, it is possible to use a single molecule for both purposes, since most porphyrin-like compounds can both emit fluorescence (for NIRF-I) and produce cytotoxic reactive oxygen species (for PDT) when activated by light [5, 6]. Second, the concentrations required for killing and imaging cells are in the same range and third, both of the techniques are promising *in vivo* cancer imaging and treatment modalities [7, 8].

## Photodynamic Therapy (PDT)

PDT is a promising treatment modality mainly for skin, esophagus and lung cancers [9] and many noncancerous conditions such as atherosclerosis, macular degeneration and rheumatoid arthritis [10, 11]. Recently, it has also been used for blood sterilization [12] and as antimicrobial agent [13]. Intravenously or topically applied photosensitizer (PS) is retained selectively by cancer cells [14], creating a difference in concentration of PS in normal vs. cancerous tissue. The PS absorbs light delivered by a laser that is typically from the near-infrared (NIR) part of the spectrum, minimizing the absorption of tissue chromophores such as oxy- and deoxy-hemoglobin, melanin, and fat [15]. When photoactivated, the PS enters a short-lived excited singlet state and from there, by intersystem crossing, to a long-lived excited triplet state. In the case of PDT, the PS transfers this energy from the triplet state to a ground state triplet oxygen, generating the cytotoxic actor of PDT—singlet oxygen (<sup>1</sup>O<sub>2</sub>) (Fig. 1) [16].

Since the recognition of <sup>1</sup>O<sub>2</sub> as the major cytotoxic agent in 1976 [17], there has been great interest in the physics and chemistry of this reactive form of oxygen. <sup>1</sup>O<sub>2</sub> has a very short lifetime (<200 ns *in vitro* and *in vivo* [18]) resulting in an average diffusion range of 20 nm from the site of generation [19]. Therefore, the site of the PS accumulation in the cell is also the site of organelle damage. The damage on a tissue level can be either *via* a direct destruction of malignant cells or changes in the tissue vasculature. The latter is the reason why PDT is also used in treatment of macular degeneration and atherosclerosis [10]. On a subcellular level, the targets—mainly cytoskeletal tubulins, lysosomes, mitochondria, plasma membrane, and nucleus—are very PS-sensitive. Of these organelles, the damage caused to tubulins and lysosomes [20] is either reversible or not very effective. In the case of lysosomes, this could be due to a PDT-associated destruction of lysosomal enzymes that would otherwise

\*Address correspondence to this author at the Ontario Cancer Institute/University of Toronto, MaRS Center, TMDT 5-363, 101 College Street, Toronto, ON M5G 1L7, Canada; Tel: +1-416-581-7666; Fax: +1-416-581-7667; Email: gang.zheng@uhnres.utoronto.ca

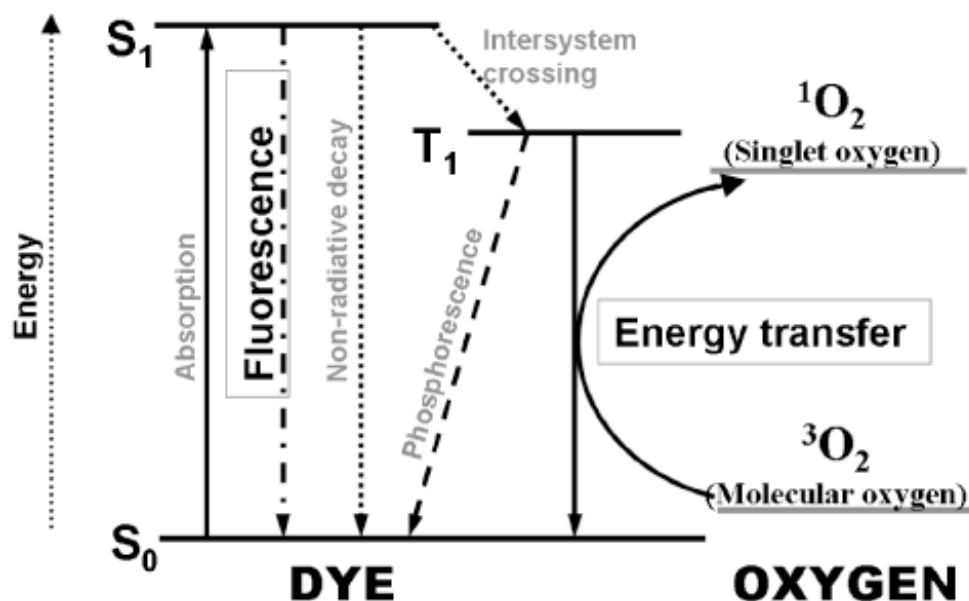


Fig. (1). Modified Jablonsky diagram of photosensitization processes during PDT (used with permission from Figure 1 of *Front. Biosci.* 2007, 12:4709-21).

be involved in triggering the post-treatment apoptosis [21]. Although most PSs localize mainly in membranes and thus do not enter the nucleus, some damage to nuclear DNA has been reported [22]. This is an unwanted site of damage since chromosome aberrations and mutations may produce even more complications, owing to their critical role in the primary tumorigenesis. The damage to mitochondria and plasma membrane is more important and plays a role in the decision between two “death mechanisms”: apoptosis and necrosis [23]. The response to PDT depends on all three components involved—the type of PS, oxygen level and light dose. The choice of PS is very important, since the localization of PS also determines the site of primary damage [24]. Generally, using high light doses, targeting tissues with low levels of oxygen, and using PSs that localize in plasma membrane (mostly hydrophobic PSs) leads to necrosis while low light doses to well oxygenated tissue using a PSs that localize near mitochondria leads to apoptosis [25]. But, since different tumor cell lines respond differently to the same treatment conditions, most tumor tissues are heterogeneous, and many PSs accumulate near more than one organelle, the precise prediction of apoptosis *vs.* necrosis for each case could be challenging. To summarize, there is no single factor that leads exclusively to apoptosis or necrosis although their relative amounts can be somewhat controlled by altering the treatment conditions. Therefore, the increasing number of PDT studies that focus on improving the existing FDA approved drugs in terms of toxicity and selectivity [26] leads to its greater clinical relevance.

### Near-Infrared Fluorescence Imaging (NIRF-I)

NIRF-I is a noninvasive and sensitive method of both monitoring a drug's fate [6] and for *in vivo* cancer imaging [15] and is recognized as a promising match to PDT since many PDT drugs are intrinsically fluorescent [7]. A focus on the near-infrared (NIR) region (650-900 nm) for absorption and emission is especially useful for *in vivo* imaging because the major tissues absorbers, since oxy-/deoxyhemoglobin and water absorb strongly in the visible and IR respectively but not in the NIR. As a consequence, NIR light can penetrate deeper into and out of the tissue than visible and IR light.

NIRF-I can be used for a variety of applications. Simple dyes can usually only show the nonspecific differences in permeability and are therefore mostly used in the mapping of vasculature and tissue perfusion (e.g. in an eye or a brain tissue) [27]. In order to

image specific cellular targets, dyes need to be conjugated to target-homing molecules. NIR dyes were shown to acquire the necessary specificity by association with lipoproteins or serum albumins [28, 29] or by conjugation to macromolecules, namely Annexin V which indicates cell death [30] or proteins such as epidermal growth factor (EGF) which are overexpressed on cancer cells [31]. Small molecule ligands, represented by ligands (e.g. prostate-specific antigen (PSA)-binding ligand [32]), short peptides (e.g. RGD peptides binding  $\alpha_v\beta_3$  integrins [33]), peptidomimetics, and small delivery vehicles (e.g. folate [34]) can also enhance the target delivery of NIRF-I probes to cancer cells. These approaches for selective imaging of specific, target cell-associated biomarkers, laid down the necessary precedent for selective targeting or activation used in the killer beacon design.

### Killer Beacons for Combined NIRF-I and PDT

Killer beacons are therapeutic constructs that consist of several modular components, assembled to create a multifunctional probe that will target cancer signatures as well as image and treat. This modular design is crucial because it not only makes the beacons flexible, since a similar layout can be used for different purposes, but also makes them specific since the target of each module can be changed. The beacon design also allows for the successful combination of imaging and therapy without compromising the compound's biodistribution by creating a large and insoluble construct.

## 1. BASIC COMPONENTS OF KILLER BEACONS

Killer beacons can be comprised of up to four modules whose properties can be fine-tuned, altered, or combined to serve different purposes. These four modules are: a fluorescent photosensitizer, a quencher, a linker, and a delivery vehicle. In this review, progress on the following three types of beacons is summarized: a) photodynamic molecular beacons (PMB), b) traceable beacons, c) beacons with built-in apoptosis sensor.

### 1.1. Photosensitizer (PS)

The most important characteristics that make a PS good PDT drug are: high yield of  $^1O_2$  production, no dark toxicity (low absorption between 450-600nm), low prolonged accumulation in normal tissue, and high target (tumor) to normal tissue ratio [35].

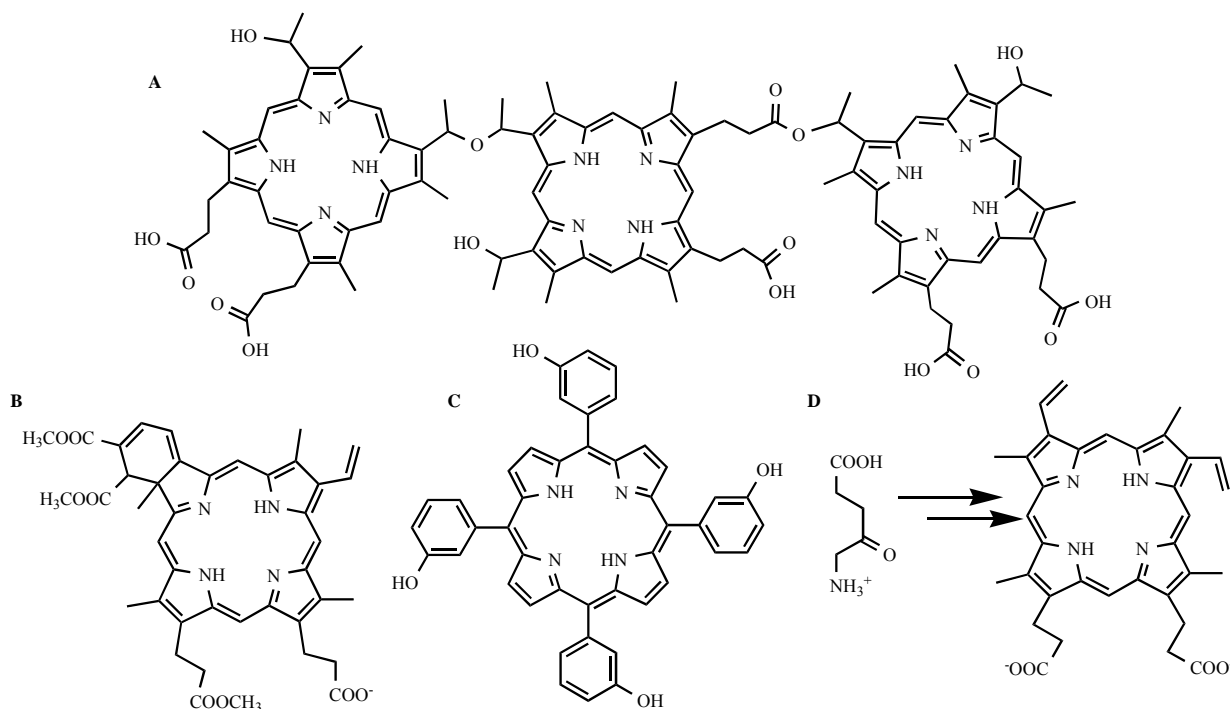


**Fig. (2). Structures of FDA approved photosensitizers.** A) The active component of hematoporphyrin (HpD, Photofrin®), B) benzoporphyrin derivative-monoacid (BPD-MA or Verteporfin), C) *meso*-tetrahydroxyphenyl-chlorin (m-THPC), and D) ALA ( $\delta$ -aminolevulinic acid) processed to Protoporphyrin IX.

The requirements for a NIR dye to be a good imaging tool are similar. In particular, a low level of photobleaching and a high quantum yield that make it stable and bright long enough to reach the target, as well as high target to background ratio, are desirable [27]. Currently, there is no ideal PS or NIR dye, only compromises between these ultimate goals. Low molecular weight and multi-modular constructs like killer beacons could partially compensate for some of the intrinsic deficiencies of PSs and dyes alone, combining the imaging and therapeutic roles and introducing target specificity.

The first approved PS in clinical PDT was Photofrin. Photofrin is obtained by partial purification of a porphyrin mixture called "hematoporphyrin derivative" (HPD, Fig. 2A) used first in the 1950s to visualize tumors during surgery [36] and recognized by Dougherty in the 1970s as a PS useful in cancer treatment [37]. The active component of Photofrin has some selectivity towards tumor cells although this may simply be due to the inability of tumors to excrete the PS aggregate as a result of their poor lymphatic system. There are several issues with Photofrin: 1) it is a mixture rather than a single molecule and the composition of the mixture varies, 2) it absorbs weakly and only on the edge of the NIR spectrum (630 nm,  $\epsilon \sim 10^3 \text{ cm}^{-1} \text{ mol}^{-1} \text{ l}^{-1}$ )—for deeper tissue penetration this needs to be shifted to longer wavelengths and to have a stronger overall absorp-

tion ( $>650 \text{ nm}$ ,  $\epsilon > 10^4 \text{ cm}^{-1} \text{ mol}^{-1} \text{ l}^{-1}$ ); 3) it is extensively photobleached (degraded) during the treatment; and also 4) normal tissues, particularly skin, significantly accumulate Photofrin, generating an unwanted phototoxicity [9]. Later, three other photosensitizers (benzoporphyrin derivative-monoacid (BPD-MA), *meso*-tetrahydroxyphenyl-chlorin (mTHPC), and endogenous protoporphyrin IX, synthesized *in situ* from topically administered  $\delta$ -aminolevulinic acid (ALA) (Fig. 2B-D)) were approved and are currently used for treatment of various cancerous conditions or vascular abnormalities (characteristics are summarized in Table 1) [38]. These drugs improve upon many of Photofrin's drawbacks but are still not ideal.

Further improvements were made with a second generation of PSs. From the synthetic perspective, there have been three main goals: 1) pushing the absorption maximum over 650nm while keeping it below the upper limit of  $\sim 850\text{nm}$  where tissue-bound water begins to absorb more strongly and the photons no longer have sufficient energy to generate  $^1\text{O}_2$ , 2) using readily available starting materials for easy synthesis, and 3) lowering self-aggregation [26]. The PSs currently undergoing clinical trials are mainly from the group of naphthalo- and phthalocyanines, expanded porphyrins (e.g., texaphyrin), bacteriochlorins and other derivatives of chlorins

**Table 1. Photosensitizers Approved for Clinical Use**

Photosensitizer or prodrug	$\lambda_{\text{MAX}}$ (nm) / $\epsilon$ ( $\text{cm}^{-1} \text{ mol}^{-1} \text{ l}^{-1}$ )	Indications	Administration	Drug-light interval
HpD (Photofrin)	630 / 1,170	Cancer of: endobronchus, cervix, esophagus, stomach, bladder, Barrett's HGD	iv	48-72 hrs
mTHPC (Foscan)	652 / 22,400	Cancer of head and neck	iv, topical	96 hrs
ALA (Levulan)	635 / 5,000	Actinic keratosis, basal cell carcinoma	Topical	3-6 hrs
BDP (Verteporfin)	650 / 18,000	Macular degeneration	iv, liposomes	15 min*

**Abbreviations:** ALA,  $\delta$ -aminolevulinic acid; BDP, benzoporphyrin derivative-monoacid; HGD, high-grade dysplasia; HpD, hematoporphyrin derivative; iv, intravenous; mTHPC, *meso*-tetrahydroxyphenyl-chlorin.

\*Since the primary target of BDP are veins, only a short interval between the drug administration and light treatment is desirable.

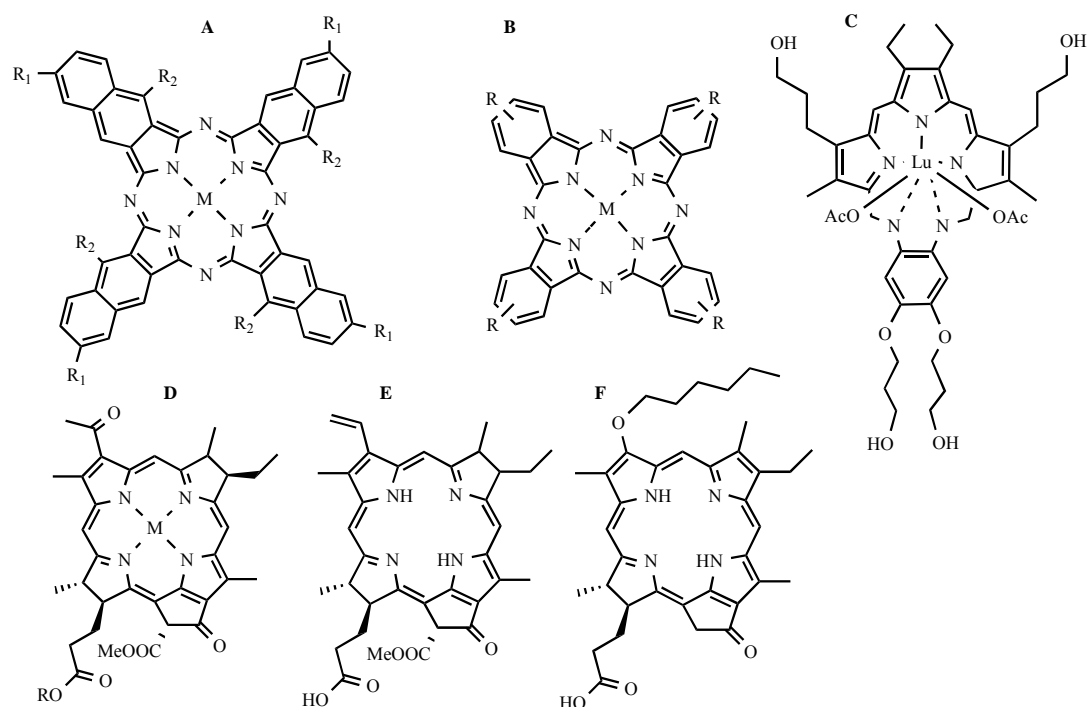


**Fig. (3).** The structure of 2<sup>nd</sup> generation photosensitizers: A) Naphthalocyanine, B) Phthalocyanine, C) Lutetium texaphyrin, D) Palladium bacteriopheophorbide, E) Chlorin e<sub>6</sub>, and F) HPPH (2-(1-hexyloxyethyl)-2-devinyl pyropheophorbide-*a*, Photochlor).

(Fig. 3) [35]. Out of this group, palladium bacteriopheophorbide (Tookad) [39] or chlorins like Chlorin e<sub>6</sub> (already approved in Japan) [40, 41] and HPPH (Photochlor, 2-(1-hexyloxyethyl)-2-devinyl pyropheophorbide-*a*, [42]) (Fig. 3D, 3E, and 3F, respectively) have a lot of potential for future *in vivo* studies since they satisfy most of the universal demands for good semisynthetic PSs and are currently in promising clinical trials [43, 44]. Phthal- and naphthalocyanines, on the other hand, are fully synthetic, but have the advantage of being powerful NIR dyes [45] (see Table 2 for the list of extinction coefficients).

**Table 2.** Absorption Maximum and Extinction Coefficient of 2<sup>nd</sup> Generation Photosensitizers

Photosensitizer	$\lambda_{\text{MAX}}$ (nm)	$\epsilon$ (cm <sup>-1</sup> mol <sup>-1</sup> l <sup>-1</sup> )
Naphthalocyanines	780	350,000
Phthalocyanines	700	200,000
Texaphyrin Lu	732	42,000
Bacteriochlorins	780	100,000
Chlorins	680	40,000

From the perspective of clinical applications, the efforts are directed towards increasing the target specificity of the already approved or second generation photosensitizers. This is a complex problem, since good behavior in solution does not often correlate with preferential cellular uptake and damage, and sufficient damage to cancer cells observed *in vitro* does not guarantee success *in vivo*, suggesting that there are often conflicting results from different experimental levels [46, 47]. Starting from the first level, a PS or its formulation needs to be soluble in water in order to be intravenously administered (with the exception of topically applied PSs) [48]. On the cellular level, the site of PS's accumulation is an important (but not the sole) factor in predicting the degree and mode of cellular death, since the site of generation of the short-lived <sup>1</sup>O<sub>2</sub> is also the site of subcellular damage (the drug and light dose and

cell type also play an important role) [49]. PSs that do not accumulate inside cells are less effective than those that diffuse into/through the plasma membrane. Moreover, PSs that end up in lysosomes are often less effective than those that can effectively escape endosomes and target mitochondria, endoplasmic reticulum, and Golgi apparatus [50]. The nucleus is a rather unwanted site of damage, since DNA damage can cause undesirable further mutagenesis. Often more hydrophobic PSs tend to accumulate "in bulk" in cells, but are not generally more effective (possibly because they fail to escape the endosomes or accumulate in lysosomes). Amphiphilic PSs are not only easier to formulate for better water solubility, they are also more successful when it comes to overall cellular damage [23]. The death decision between apoptosis and necrosis as a response to PDT is also a significant factor worth considering when choosing PS and treatment conditions, since the inflammatory response following necrosis can complicate effective healing [25]. On the other hand, it can also be an important factor in initiation of patient antitumor immune response. The factors privileging one over the other will be discussed in detail in Section 2.3.

The main problem of clinically applied PDT is the prolonged phototoxicity and poor tumor-to-normal tissue ratio of most PDT agents. Strategies for improving this insufficient selectivity are mostly adopted from the well-explored approaches of targeting indiscriminative NIR dyes. They mainly focus on attaching various biologically active molecules to existing PSs that silence the photoactivity in normal cells (Section 1.2) and restore it specifically in the target cells (Section 1.3), deliver the PSs to specific target-associated sites (Section 1.4) or help to avoid the organs responsible for drug clearance (Section 2.2).

## 1.2. Quencher (Q)

Learning from NIRF-I, there are two basic ways to improve the signal to noise ratio. The first one is to direct the dye towards the target by attaching a selective delivery vehicle (Section 1.4). The second way is to silence the dye in the absence of the target and restore its fluorescence only after the target is present. To achieve that, the dye must be conjugated to a quencher molecule (Q) *via* a

suitable linker, which can keep the dye and quencher close enough to enable fluorescence resonance energy transfer (FRET). FRET is a process of nonradiative energy transfer from the dye to the quencher *via* intermolecular long-range dipole-dipole coupling that is efficient if they are positioned within the Förster radius (typically 3-6nm), determining the dye-sensitive distance in which 50% of the energy is transferred [51]. Once the target is present, the Q is separated in space from the dye, restoring the fluorescence and identifying the target. FRET is not supposed to provide any structural distance information in this case—it is more of a “yes or no” situation, reporting the intact or separated states.

#### Quenching Method 1: Inactivated Dye

One of the first beacons for detection of various proteases in solution and *in vitro* featured a peptide-bound fluorochrome (e.g. 7-amino-4-methylcoumarin, AMC) emitting enhanced fluorescence at 380nm after the peptide linker was cleaved with proteases that recognized its peptide sequence (Fig. 4A) [52, 53]. This simple protease-sensing dye, using UV-excitabile fluorochromes, is not very applicable for the beacon design.

ase-sensing dye, using UV-excitabile fluorochromes, is not very applicable for the beacon design.

#### Quenching Method 2: Dye-Dye Quenching

A dye can often serve as its own quencher if held closely to another molecule, making the process of labeling easier at the expense of weaker quenching. Dyes can be held together in a variety of ways—they can be either entrapped in the limited space of liposomes (e.g. in the case of fluorophore-loaded liposomes monitoring membrane fusion [54]), conjugated to opposite sides of a short peptide linker [55] or evenly distributed on a larger platform [56] (protein substrate or poly-L-lysine) (Fig. 4B, 4C, and 4D, respectively). The fluorophores are released only after encountering the target, i.e. upon membrane fusion or cleavage by target proteases, and this results in selective fluorescence restoration [57]. Naturally, solution applications mainly use fluorophores like fluorescein (excitation 490nm, emission 514nm), while *in vitro* and *in vivo* applications favor genetically engineered GFP (green fluores-

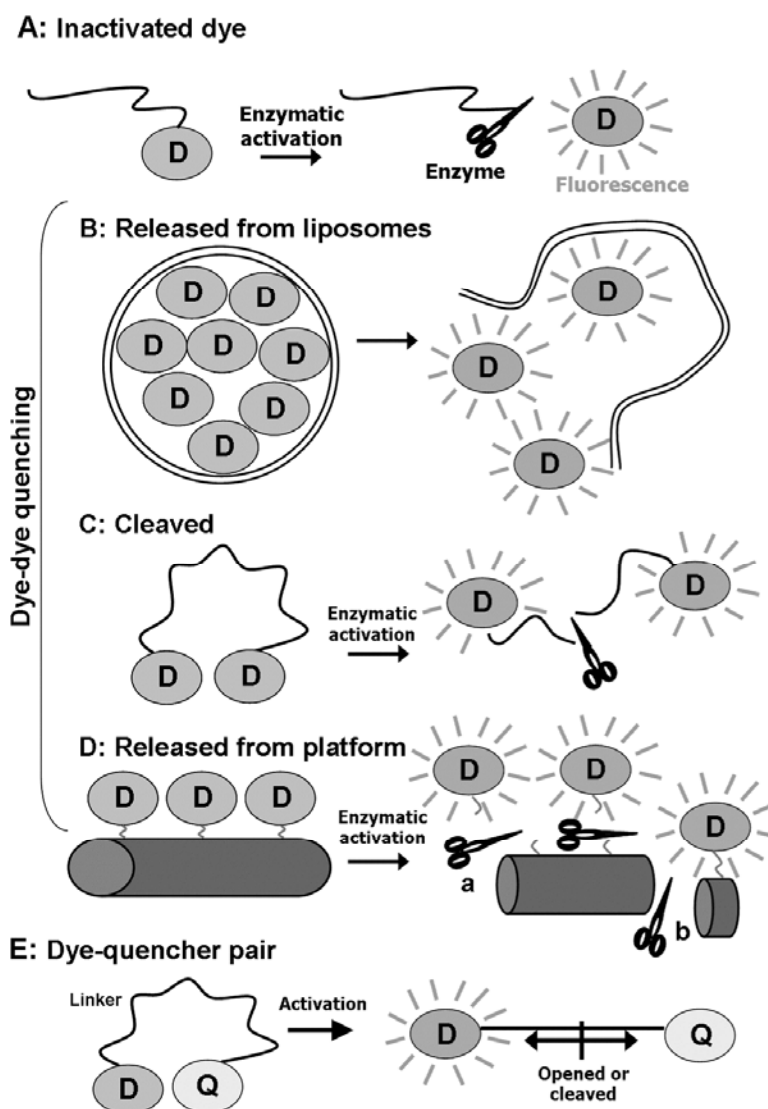


**Fig. (4). Means of quenching.** Quenching can be achieved either by inactivating the dye (A), coupling to another dye (B-D) or by coupling to a quencher (E). A) Dyes like AMC restore their fluorescence once cleaved from the peptide linker [52], B) encapsulated dyes are quenched by mutual close proximity and activated upon release [54], C) two dyes linked to opposing sides of peptide linker are quenched until released by enzyme cleavage [55], D) multiple dyes are coupled to a poly-L-lysine (a) or a protein platform (b) and their fluorescence is restored by the cleavage of the linker between the dye and poly-L-lysine or the platform's enzymatic degradation [56], and E) the activity of a dye is quenched by close proximity of a quencher and restored by stabilizing the linker in the open conformation or by enzymatic cleavage.

cent protein) and its variants [58] or NIR dyes from di-/tricyanin [59] or the Alexa Fluor family [60].

### Quenching Method 3: Dye-Quencher Pair

Using a quencher that differs from the dye has the advantage of higher quenching efficiency, although it often complicates the synthesis of the beacon by requiring sophisticated chemistry for conjugation of the dye and quencher. This usually limits the design to one dye conjugated to one quencher through a well-defined linker that holds them in close proximity, enabling FRET (Fig. 4E). Ideally, the choice of a dye-quencher combination should account for the detailed photophysics of the pair [61]. But in the absence of this information, ensuring significant overlap of the dye's emission spectrum with the quencher's absorption spectrum is often sufficient. This consideration places the absorption maximum of a quencher suitable for quenching the fluorescence of existing photosensitizers over 650nm. Examples of such quenchers come from the family of quenchers that are characterized by a lack of native fluorescence—black hole quencher 3 (BHQ-3) that has its  $\lambda_{MAX}$  at 672 nm or QSY-21 with  $\lambda_{MAX}$  at 661 nm with an optimal quenching range of 620-730 nm. Unlike for conventional dyes, the intimate proximity of the PS-linker-Q design can be used for quenching more than just the PS's fluorescence.

### $^1O_2$ Quenching

Production of  $^1O_2$  is central to a PS's PDT-induced toxicity, so lowering the production of  $^1O_2$  would protect cells from damage [18]. Therefore, exploring the possibility of selective quenching and restoration of  $^1O_2$  production in normal versus diseased cells respectively would make the PS a highly selective drug and PDT significantly less toxic.

Since  $^1O_2$  is produced by energy transfer from the excited triplet state of a PS, generated by an intersystem crossing from the PS's excited singlet state,  $^1O_2$  quenching can be potentially achieved by: 1) direct  $^1O_2$  scavenging, 2) quenching a PS's excited triplet state, or 3) quenching a PS's excited singlet state. The third type of quenching is a side product of good fluorescence quenching but can be efficiently used in some types of beacon design, as discussed in Section 2.1. When the  $^1O_2$  is generated, it can react with surrounding molecules ("chemical quenching", [62]) or return to its ground triplet state *via* physical quenching. Chemical quenching in biological systems, in which  $^1O_2$  reacts with proteins (mainly with Cys, Met, Trp, Tyr, and His), lipid membranes (unsaturated fatty acids and cholesterol [63, 64]), DNA (mainly guanine) or carbohydrates, is the main reason for singlet oxygen's cytotoxicity. Regarding physical quenching, there are two major types: energy transfer and charge transfer [65]. Energy transfer is the reverse of the reaction by which  $^1O_2$  was formed:



This mechanism was first described in the 1970s in an attempt to explain the role of carotenoid in the prevention of damage in biological systems [66] and is possible for quenchers that have their triplet state very near or below the energy of  $^1O_2$  (22kcal/mol). In charge transfer quenching, the electron-poor  $^1O_2$  interacts with electron donors (mostly easily oxidized compounds) to form a charge-transfer complex where the restrictions of intersystem crossing are relaxed followed by dissociation of donor and triplet oxygen:



Some compounds not only quench  $^1O_2$  *via* charge transfer physical quenching, but also react with  $^1O_2$ . Non-destructive energy transfer is preferred as a means of  $^1O_2$  quenching in the beacon design.

Therefore, the following characteristics make a compound an ideal quencher of  $^1O_2$  production: 1) the Q should quench the excited states (triplet or singlet state) of PS (Fig. 1), 2) the Q should

not react with  $^1O_2$  ("chemical quenching") since this leads to fast deactivation of the quenching ability, and 3) the energy of the triplet state ( $\Delta E_{T1}$ ) of the Q should be close to or below 22kcal/mol ( $\Delta E_{T1}$  of  $^1O_2$ ) to allow an efficient deactivation of the  $^1O_2$  generated by possible incomplete quenching of the PS's excited states. In summary, the best  $^1O_2$  quencher prevents the  $^1O_2$  from being generated by quenching the excited states of PS. This will also diminish the need for Q's ultimate chemical stability—the most difficult requirement to fulfil since many quenchers are highly conjugated molecules prone to destruction by oxidation or photochemical reactions.

### Quenchers of $^1O_2$

Carotenoids were among the first  $^1O_2$  quenchers to be described. They play an important role as a pro-vitamin A and an antioxidant in animals, and as a pigment and photoprotective agent in the photosynthetic system of plants [67]. These important bio-functions stem from the ability of carotenoids to: A) quench chlorophyll's (Chl) (or other porphyrin-based molecule's) triplet state, inhibiting the production of harmful  $^1O_2$ , B) directly scavenge  $^1O_2$ , protecting the photosynthetic apparatus [66, 68], C) either absorb light around 500 nm and transfer this excitation energy to the Chl as part of light harvesting or vice-versa quench the Chl fluorescence (depending on the energy of the singlet states of Chl and that particular carotenoid) [69], and D) act as antioxidants, quenching radical species that could potentially react with various biomolecules [67]. Both the number of conjugated double bonds in carotenoids [70] and the PS-carotenoid distance dictate the ability of carotenoid to quench the triplet state of the PS, scavenge  $^1O_2$ , and quench PS fluorescence [66, 69] and can therefore be fine-tuned for different purposes (see Section 2.1). Carotenoids are therefore perfect candidates for a biocompatible and efficient quencher of PS's  $^1O_2$  production and this concept was already explored using a carotenoid analogue covalently bound to *meso*-tetraphenyl-substituted porphyrins [71].

Other compounds suitable for  $^1O_2$  quenching are either from families of naturally occurring antioxidants (e.g. tocopherols [72], thioredoxin [73]), synthetic antioxidants [65] (e.g. highly conjugated stilbene quinones, azomethine dyes, amines like DABCO (1,4-diazabicyclo[2.2.2]octane) or lidocaine [74]) or metal complexes (out of which the Ni (II) chelates are the best quenchers, but they are not biocompatible [75]). Also, some PSs can alter their production of  $^1O_2$  by covalent attachment of a molecule with quenching abilities that depend on the surrounding physical conditions like pH [76].

### 1.3. Linker

The linker design is crucial for killer beacons since it not only plays a pivotal role in keeping the beacon inactive in non-targeted cells, but also dictates the ultimate activity of the beacon towards a particular target. Two basic linkers have been designed so far to make the beacon switchable. One is an "openable" linker and the other is a "cleavable" linker. Both of these linkers could hold a dye and a quencher in close proximity initially to achieve effective fluorescence or  $^1O_2$  quenching. Upon meeting a target, the linkers could be either opened or cleaved to force the quencher to move away from the close proximity of the dye, making the dye active.

#### Openable Linker

The most famous example of the "openable" linkers is the nucleic acid-based molecular beacons that are widely used in nucleic acid research and real-time PCR (Fig. 5A). These molecular probes are able to report the presence of specific nucleic acid strands by monitoring the fluorescence increase upon unquenching [77, 78]. They are composed of a dye and a quencher conjugated to opposing sides of a short nucleic acid strand. This strand usually includes 4-6 nucleic acid bases at both of the strand's ends that are complementary to each other, forming a short stem that keeps the dye and Q in

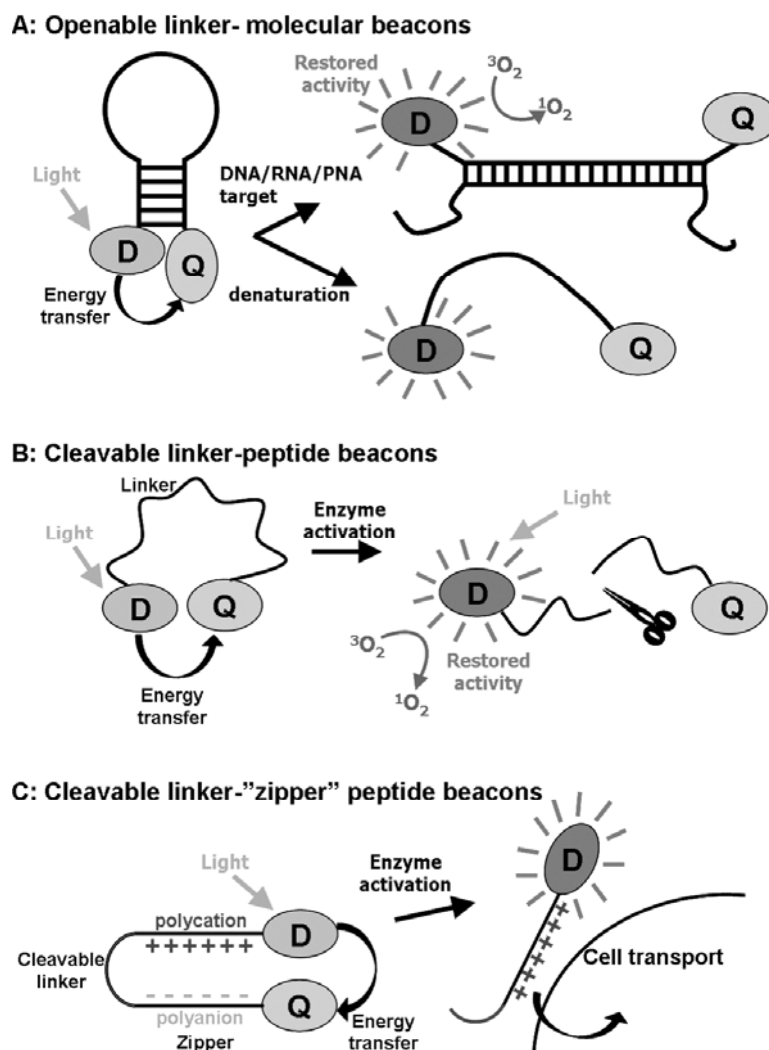


**Fig. (5). Types of activatable linkers.** Two basic types of linker: openable (A) or cleavable (B and C). A) Molecular beacons (MBs) are composed of a dye (D) and quencher (Q), conjugated to opposing sides of a short DNA/RNA strand containing the stem that holds D and Q together in the native state. MBs can be opened and therefore activated either by hybridization to the DNA or RNA complementary target sequence or by denaturation with temperature, pH or denaturing agents. B) Peptide beacons contain a D conjugated through a short peptide sequence to a Q molecule. The peptide presents a restriction that can be released by protease cleavage, restoring the D's activity. C) A special type of cleavable peptide beacon contains a string of polycation (Arg) and polyanion (Glu) that forms a "zipper", keeping D and Q together. After the cleavage of the internal peptide linker sequence, the strands are separated and activity is restored. Fully functional dye is consequently delivered inside the cells secreting the target protease by the freed polyanion.

close proximity in the native state. The middle part of this nucleic acid strand (the loop, containing 15-20 bases) is complementary to the nucleic acid strand that is to be reported/visualized. Therefore the FRET between dye and Q can be disrupted upon the hybridization of the loop to a DNA or RNA target that outcompetes the stem's hydrogen bonds, or by denaturation of the beacon's stem with temperature, pH or denaturing reagents [79]. To successfully visualize only the DNA/RNA target, excluding a target with only one mismatch, special care needs to be taken when designing the beacon. The stem needs to be strong enough for keeping the beacon in the "closed" state at experimental temperature (the "melting temperature" factor) or for outcompeting a one mismatched target. On the other hand, it also needs to be weak enough to allow successful hybridization to the complementary target. This can be achieved by altering the number (and, in the case of the stem, also the character) of bases in the stem and loop, customizing it to the target [80], although recent work suggests that even stemless beacons can provide the necessary signal-to-noise ratios [81].

Featuring these openable linkers, nucleic acid-based molecular beacons have been explored for imaging disease-unique or overexpressed mRNAs. For the beacon design, there are two sources of potential mRNA targets: 1) the secure one is from the pool of antisense therapeutics currently in clinical trials—secure in the sense that it is a well established antisense oligonucleotide (AS-ON) sequence with a known accessible target mRNA sequence, and 2) the pool of mRNAs that have a cancer-specific mutation (or deletion, insertion). Most of the AS-ONs target the transcripts coding for proteins involved in tumor progression or apoptosis suppression, i.e. protein kinase c (responsible for signal transduction and implicated in cell growth and tumor development), Bcl-2 family (blocking the release of cytochrome C that would initiate apoptosis) or C-raf kinase [82], BRAF-1 (most specific for melanoma) [83], or EGFRvIII (type III epidermal growth factor receptor) [84].

Using hybridization to activate a beacon is an ideal approach for selective PDT—it keeps the PS and either fluorescence or  $^1O_2$  quencher in close proximity until it finds a disease-specific mRNA

target. Only after finding its unique target while distinguishing between the targets with only 1-mismatch, it restores its activity, identifying and/or killing the cell. However, challenges of *in vitro* and *in vivo* applications are plentiful, starting with the rapid degradation of DNA probes in cells (partially circumventable by the use of phosphorothioate, 2'-O-Me-RNA nucleotide analogues [85, 86] or peptide nucleic acids [87], etc.), followed by difficulties in finding unique and accessible sequences on the target mRNA, and ending with problems of delivering the probes into cells or tumors. Despite all these drawbacks, this approach is, with increasing knowledge about the human genome and disease-associated targets, definitely worth exploring.

The mRNA-based openable linker can also be applied to DNA sequence-controlled on-and-off switchable beacons [88], in which a PS and a  $^1\text{O}_2$  quencher are kept in close contact in the "off-state" by DNA-programmed assembly and the PS will be activated after being released from the quencher through a process of competitive DNA hybridization.

Another group of "openable" linkers are the membrane-encapsulated formulation of PSs (Fig. 4B). It is known that both fluorescence and phototoxicity is reduced if the PS fails to escape the confined space of liposomes, endosomes or lysosomes, and monomerize [89, 90].

#### Cleavable Linker

The most well known cleavable linkers are short peptides specifically recognized and cleaved by certain disease-specific proteases (Fig. 5B). These proteases are ideal targets for the beacon design. The pioneering work on synthetic probes using resonance energy transfer for measurement of hydrolase activity was done in 1972 by Latt et al. [91] and was followed by Wang et al. [92], significantly improving the donor-acceptor pair from Tryptophan-Dansyl to the nowadays well known EDANS-DABCYL pair. They focused initially on retroviral proteases that are useful in rapid detection of HIV virus protease activity [93] and later on the synthesis of fluorogenic substrates resembling part of the normal and altered amyloid precursor protein, in an attempt to discover the proteases responsible for this lethal "molecular switch" in Alzheimer's disease [94].

There are hundreds (over 500) of proteases inside normal and diseased cells, but only a few are characteristic of or overexpressed in diseased cells. Focusing on cancer, these are proteases involved in tissue remodeling, protein catabolism, metastasis, or other proteases that help tumors to alter the normal environment to better supply nutrients, grow, and spread [95]. Some examples of such proteases are: cathepsin D, B, and H, overexpressed in breast cancers [96, 97], matrix metalloproteinases (MMP), mainly MMP-2 (gelatinase), MMP-7, and MMP-9 [98] that are extracellular proteases involved in degradation of the extracellular matrix [99, 100]; or fibroblast activation protein (FAP), overexpressed by tumor stromal fibroblasts in tumor epithelium [101, 102].

One of the first whole body animal imaging studies of protease activity using dye-dye quenching was done by Weissleder and colleagues. They conjugated Cy 5.5 dyes densely to the methoxypolyethylen-glycol-derivatized poly-L-lysine backbone either directly [56] (cleavable by tumor-associated cathepsin B and H) or through short peptide substrates that direct the selectivity towards other proteases [96, 103].

Activation by cleavage of a short peptide is an excellent strategy to be applied to the killer beacon design. The advantages are the following: 1) short peptide linker improves the beacon's bioavailability, 2) keeping PS and Q in close proximity provides efficient fluorescence and  $^1\text{O}_2$  quenching, and 3) short peptide linkers can also easily accommodate additional functional module, such as delivery module [104]. Another interesting module that can be integrated into the beacon design is a "zipper" beacon, valuable for

both quenching and delivery. The "zipper" can be composed of two strands of polycation (arginines) and polyanion (aspartic acids) connected by a protease-cleavable linker. The dye and quencher are located at the ends of these strands and held closely by the electrostatic interactions of the polycation and polyanion strands. Once the internal peptide sequence is cleaved, the dye coupled to polycation is released and the polycation can deliver it into the cell (Fig. 5C, for details on delivery see Section 1.4) [105].

Other cleavable linkers for the beacon design include nucleic acid-based molecular beacons cleavable by DNases or RNases [106, 107]. Alternatively, it could be applied to a phospholipase-activated optical probe, in which a tumor-associated phospholipase is used as the triggering device [108].

#### 1.4. Delivery Vehicle

The function of the delivery vehicle is to transport any attached molecule to the site of interest—either to organs or tissues, specific cells (e.g. cancer cells) or particular organelles. The choice of delivery vehicle is subject to many factors, varying with the selected target or potential toxicity of the carried molecule. In choosing a delivery vehicle, one should consider the following issues: 1) Where is the target located? (e.g. blood vessels or cells, on the surface or inside the cells); 2) Can the vehicle carrying beacons be taken up by endocytosis? 3) Is the beacon able to escape the organs responsible for drug clearance? One must also keep in mind that neither the delivery vehicle nor the beacon that is delivered determines the final biodistribution independently. Rather, each module and their interaction can both play important roles (Section 2.2).

#### PS's Self-Delivery

Most porphyrin-like PSs can enter cells by themselves. This is crucial since the PDT efficacy of most of these PSs depends on their ability to enter cells and accumulate near the most PDT-susceptible organelles. However, the relationship between the PDT efficacy and the PS properties (e.g., hydrophobicity/amphiphilicity of the PSs, their uptake into cells and sites of intracellular accumulation) is a very complex one [14]. It was reported that hydrophobicity helps the PSs to be retained by tumor cells, but it also increases their aggregation [89]. Since excessively hydrophilic PSs are often retained in circulation and excreted before reaching the tumor, the most interesting class is the amphiphilic PSs. These can be taken up by endocytosis in large amounts, escape the endosome, and then easily monomerize, or simply pass through similarly amphiphilic membranes. Therefore, they have a chance to localize near mitochondria at the benzodiazepine receptors—an ideal site for PDT damage [109].

Of course, even though amphiphilic PSs can enter cells, a successful *in vivo* application additionally requires the ability to escape the organs responsible for drug clearance and specifically target certain cells. Even though PDT possesses an intrinsic spatial targeting in the form of pointing the laser to specific sites, accumulation of PS in normal tissue still increases the patient's light sensitivity and decreases the amount of compound that actually reaches the tumor. To increase the amount of compound that reaches tumor cells, PSs can be associated with other delivery systems.

#### Targeted Delivery Systems for PSs

Photosensitizers' efficacy can be enhanced by associating them with other molecules that can deliver the whole construct inside cancer cells either nonspecifically [48] or specifically, by targeting "cancer fingerprints" [110]. For example, PSs associated with liposomes, oil dispersions, or hydrophilic polymers (PEG) are delivered by passive diffusion or phagocytosis selectively to cancer cells. Although nonspecific, these vehicles help solubilize the PS in water (for intravenous injection) and also to increase the selective uptake and retention by tumor (this is simply a result of their leaky vasculature and poor lymphatic system).

A similar formulation, but with specific targeting, is offered by low density lipoprotein (LDL), which could accommodate multiple PSs that can be improved by attaching hydrophobic anchors [111, 112]. Tumor accumulation is enhanced by a targeted active endocytosis mediated by LDL receptors (LDLR), which are overexpressed on certain types of cancer cells to satisfy their need for cholesterol to build more membrane [113]. LDL, with a long circulation time in plasma and no immunogenicity, can store the PSs in its apolar core and release them selectively in cancer cells [114]. Although LDL has a high capacity to carry many PS molecules inside one core and thus partially quench their activity until released (see Fig. 4B), it still suffers from low tumor selectivity as liver, adrenal, and reproductive organs all express high levels of LDLR. Another limitation of using LDL particles as carriers for PS is the narrow purview of LDLR-positive tumor types. Our lab has recently introduced a simple and versatile strategy to reroute LDL away from LDLR to selected alternate receptors that drastically expands the range and improves the accuracy of using LDL for PS delivery [45]. The same strategy can be applied to the high-density lipoprotein (HDL) that is the smallest lipoprotein (<10 nm) and thus has superior pharmacokinetic properties.

Another strategy to actively deliver PSs inside cancer cells involves connecting them to monoclonal antibodies (Ab) [115]. These antibodies are directed against specific antigens of malignant cells and were designed with the idea of selectively curing particular tumor types. Although having promising *in vitro* results, there are still many problems that prevent the full use of Ab-PS conjugates *in vivo*. These are associated with the Ab's big size impairing biodistribution, low carrying capability, and immunogenicity (many antibodies are of murine origin) as well as tumor heterogeneity accompanied by a low density of specific antigens. There are other proteins used in PS delivery, for example a serum albumin or a transferrin, which is normally involved in iron transportation into rapidly growing cancer cells [116].

In contrast to large proteins, small delivery vehicles have a better chance of *in vivo* success. One of the vehicles is the small and easy-to-conjugate folate, shown to facilitate the uptake of cargos of various physical properties to cells overexpressing folate receptor (FR) *via* receptor-mediated endocytosis. FRs are mainly overexpressed on ovary, breast, colon, lung, nose, prostate, and brain can-

cer cells and activated macrophages [117] but have limited expression on normal cells (e.g. kidney, intestine, lung) with restricted accessibility for blood-circulating drugs [118]. It was shown that a PS-Folate conjugate has enhanced *in vitro* PDT efficacy [119, 120] and a dye-folate conjugate accumulated selectively in FR overexpressing tumors *in vivo* [34, 120] when compared with FR negative tumors. This makes folate a good candidate for an efficient and cancer-selective drug delivery system. Another class of small delivery vehicles are short peptides or peptidomimetics that target cancer-overexpressed receptors like somatostatin receptor, bombesin [121], and  $\alpha_v\beta_3$  integrin (RGD peptide). Although they have a more limited number of targets, these peptides have very promising biodistribution profiles and are good candidates for extending the work done on the delivery of NIR dyes to the delivery of PSs. The drawback is obvious—neither folate nor receptor-targeting peptidomimetics are universal delivery vehicles since not every cancer cell overexpresses the target receptors. To address this issue, a class of glucose transporter-targeted PSs and NIR dyes were developed [122, 123] since enhanced tumor glycolysis is one of the biochemical hallmarks of malignancy and glucose transporters are overexpressed in most cancer cells regardless of cancer types. Another interesting class of universal delivery vehicles are short peptides like Tat [124], antenapedia [125], transportan [126] or poly-arginine [127], which can facilitate the uptake of PSs to cells nonspecifically mostly by spontaneous cell permeation. These universal delivery vehicles can be combined with other methods of selective delivery or activation (for example the “zipper” peptide beacons using poly-arginine for improving the overall performance, see Fig. 5C) [128, 129].

## 2. BASIC TYPES OF KILLER BEACONS

### 2.1. Photodynamic Molecular Beacon (PMB)

We have recently introduced the PMB concept featuring the precise control of the ability of PS to produce  $^1O_2$  in responses to specific cancer-associated biomarkers [130, 131]. PMBs are designed to silence the PS's phototoxicity in normal cells/tissues. Once they encounter a cancer cell-specific target, they are activated and able to kill these target cells. PMBs integrate a  $^1O_2$  quencher held in close proximity to a PS by a disease associated linker and

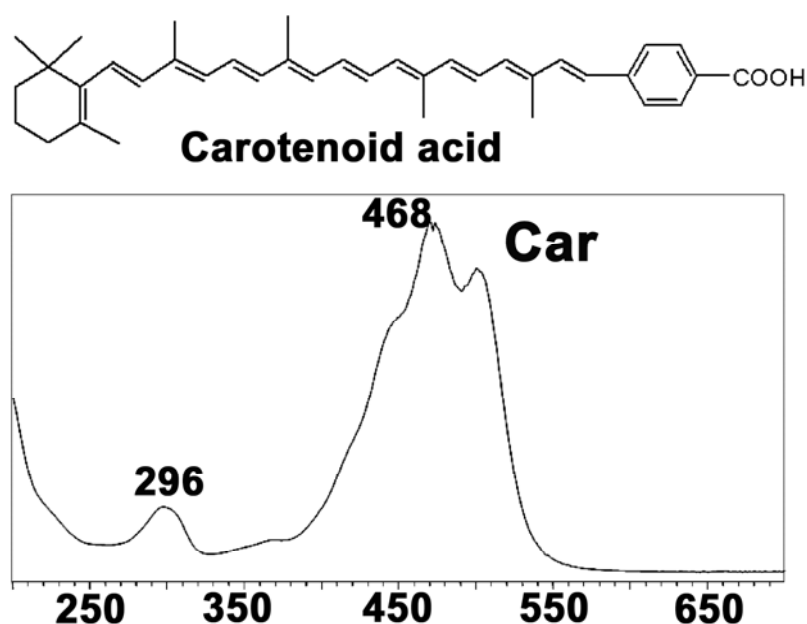


Fig. (6). Structure of a synthetic analogue of carotenoid and its UV-Vis absorption spectrum.

therefore precisely control the PS's ability to produce  $^1\text{O}_2$  by responding to the chosen cancer cell-specific biomarkers. Thus, the selectivity of PDT is highly enhanced, since it not only depends on the two levels of control—the preferential accumulation of PS in tumor mass and laser focusing on affected sites—but most importantly, it depends on the selectivity of the biomarker to cancer cells and the beacon-biomarker interaction.

Production of  $^1\text{O}_2$  can be inhibited either by transferring the triplet state energy of the PS to the quencher (see also Section 1.2), or by directly scavenging  $^1\text{O}_2$ . Also, quenching the excited singlet state of the PS (i.e. quenching the fluorescence) will reduce the population in the triplet state (since the electron follows the (simplified)  $S_0 \rightarrow S_1 \rightarrow T_1$  pathway), thus ultimately leading to lower  $^1\text{O}_2$  production. The overall quenching efficiency of PMB is dictated by the choice of PS-quencher and the linker design. Focusing on these two points, by altering the character and composition of each module, PMB's design is versatile and customizable depending on the purpose and target.

### 2.1.1. PMB Featuring Carotenoid as $^1\text{O}_2$ Quencher

Carotenoid (Car) analogues were shown to have different quenching abilities depending on the relative spatial position of the porphyrin, type of attachment, and the number of conjugated double bonds. The number of conjugated double bonds for triplet energy transfer should be  $>5$ , for efficient  $^1\text{O}_2$  scavenging  $>8$ , and for decent fluorescence quenching  $>10$  [66, 67, 69]. In contrast to porphyrins most carotenoids display a very low yield of ( $S_1 \rightarrow T_1$ ) intersystem crossing. This, together with the lack of reverse transfer from the Car  $\rightarrow$  porphyrin triplet state makes it an effective triplet energy quencher. This one-way transfer does not apply for singlet state energy transfer, as demonstrated by both the light harvesting (Car  $\rightarrow$  porphyrin transfer) and fluorescence quenching (porphyrin  $\rightarrow$  Car transfer) abilities of Car. Furthermore, the partial mobility of Car (or any type of quencher) with respect to porphyrin will more likely reduce the quenching of the PS's short-lived  $S_1$  ( $\sim 10$  nsec in  $\text{CCl}_4$  for chlorins) than the long-lived  $T_1$  [132].

#### Directly Linked Carotenoporphyrins (Non-Activatable)

Car-porphyrin interactions were widely studied because of the important role of Car in photoprotection and antenna function in

photosynthetic systems. Extensive work was done on carotenoporphyrins, where the Car analogue (Fig. 6) was directly conjugated to either *meso*-tetraphenyl porphyrins [71, 132], pheophorbide [6, 133] or hematoporphyrin [134]. Carotenoporphyrins were found to also be useful as diagnostic agents for tumors, taking advantage of their low toxicity, attributed to the ability of Car to efficiently quench the porphyrin triplet state. However, the fluorescence imaging capability of carotenoporphyrins is somewhat limited because Car also partially quenches porphyrin fluorescence [6, 134]. More importantly, the nonactivatable nature of these directly-linked carotenoporphyrins renders it inapplicable for PMB design.

#### Protease-Triggered PMB Featuring Car Quencher.

The first PMB utilizing  $^1\text{O}_2$  quenching and activation was designed to comprise a Car conjugated to a pyropheophorbide-based PS (Pyro) through a peptide linker (GDEVDGSGK) that is cleavable by the protease caspase-3 (Fig. 5B). Using this model PMB, Pyro-peptide-Car (PPC), we have demonstrated in a proof-of-principle study that the  $^1\text{O}_2$  generation of Pyro is effectively inhibited by the Car quencher and that caspase-3-induced separation of the quencher and the PS molecules allows the sequence-specific photoactivation of the latter [130].

As shown in Fig. (7A), PPC itself has 8-fold less  $^1\text{O}_2$  production than PP (Pyro-peptide as a positive control, lacking Car) and caspase-3 and its inhibitor have no effect on the  $^1\text{O}_2$  production of PP. Thus,  $^1\text{O}_2$  quenching in PPC is due to the presence of Car. Moreover, addition of caspase-3 to PPC resulted in a 4-fold increase in  $^1\text{O}_2$  signal, an effect that was completely prevented by coinubation with the caspase-3 inhibitor. The 2-fold difference in  $^1\text{O}_2$  luminescence as well as  $^1\text{O}_2$  lifetime between the PP and PPC + caspase-3 is due to the presence of free Car scavenger in solution after cleavage. The difference in  $^1\text{O}_2$  luminescence between PPC alone and PPC + caspase-3 is likely due to both PS excited states quenching and  $^1\text{O}_2$  scavenging by Car. The ratio of the PPC : PPC + caspase-3 (intact molecule vs. the cleaved molecule) in total  $^1\text{O}_2$  counts is 1:4 (Fig. 7A), compared to the  $^1\text{O}_2$  lifetime that is 3:4 (Fig. 7B). Knowing that  $^1\text{O}_2$  luminescence is directly proportional to  $^1\text{O}_2$  lifetime, we can conclude that quenching of the excited states of Pyro by Car seems to be more important for the intact PPC

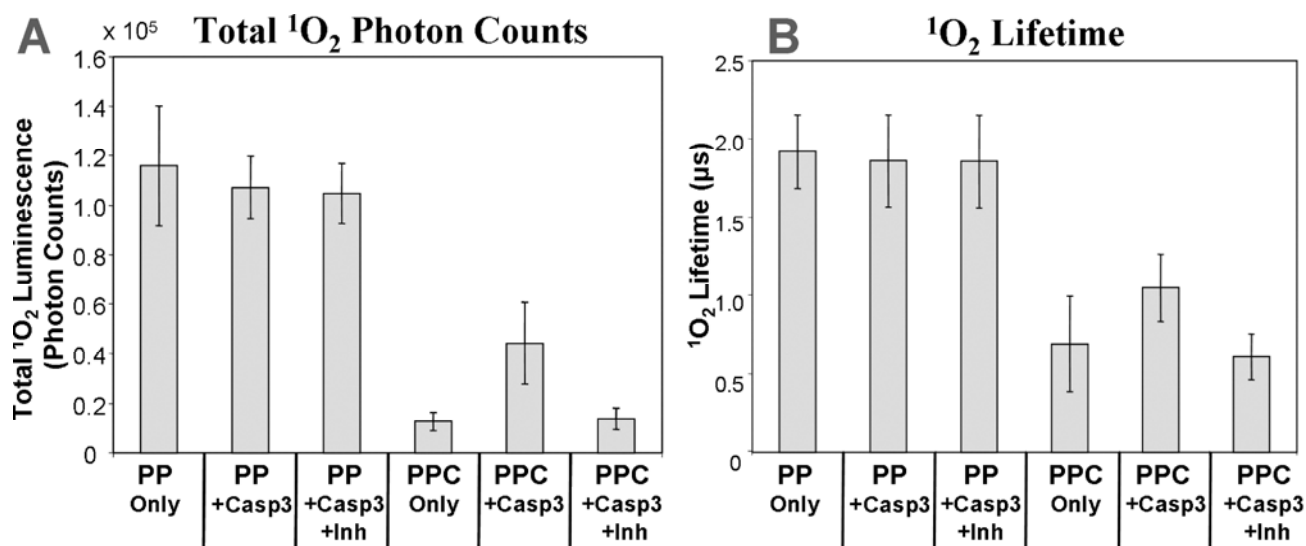


**Fig. (7).** Singlet oxygen production measured as 1270 nm luminescence (modified with permission from Figure 3 of ref. 130). A) Total  $^1\text{O}_2$  luminescence counts for PP, PP + caspase-3, PP + caspase-3 + inhibitor, PPC, PPC + caspase-3, PPC + caspase-3 + inhibitor shows a 10-fold  $^1\text{O}_2$  quenching in PPC when compared to PP and a 4-fold  $^1\text{O}_2$  restoration after incubation of PPC with caspase-3. This restoration was not observed for both PPC incubated with caspase-3 and inhibitor or PP incubated with caspase-3. B) The corresponding  $^1\text{O}_2$  lifetime shows decreased lifetime of  $^1\text{O}_2$  in the solution of PPC + caspase-3, probably due to the presence of free Car, explaining the 2.5-fold difference between the activated (cleaved) PPC and PP.

molecule than  $^1\text{O}_2$  scavenging (since only ~25% of the generated  $^1\text{O}_2$  was scavenged in the intact PPC). This is consistent with the fact that the requirement for efficient triplet state quenching is less rigid than for direct  $^1\text{O}_2$  quenching (five double bonds in Car are required for the former but nine are required for the latter, Section 1.2). In summary, this study demonstrates that Car turns off the  $^1\text{O}_2$  production of Pyro by both quenching the Pyro excited states (singlet/triplet) and directly scavenging  $^1\text{O}_2$ . If this cleaved Car cannot diffuse after cleavage, it could lose some PDT potency of PPC toward targeted cells, although this could be compensated for by increased concentration of PPC. On the other hand, Car-mediated  $^1\text{O}_2$  scavenging could add an additional photoprotective role in non-targeted (normal) cells, scavenging the residual  $^1\text{O}_2$  production and therefore minimizing the potential photodamage. Thus, Car-based PMB could potentially improve the PDT selectivity.

It should be noted that caspase-3, used in the above design, is a well-known cell apoptosis marker and is not expressed in viable tumor cells. Therefore this PMB was utilized for evaluating the photoprotection role of the Car in PMB towards non-targeted cells. We demonstrated that Car-mediated  $^1\text{O}_2$  quenching in PPC fully protects the non-targeted viable cells (no caspase-3 expression) from the harmful toxic effects of  $^1\text{O}_2$ . On the contrary, Pyro-peptide (PP) without the Car moiety readily kills these cells even at a 30-fold lower concentration. These data clearly show the photoprotective role of Car when conjugated to Pyro through this flexible peptide linker and suggest that the PDT selectivity is protease sequence-dependent [135].

#### mRNA-Triggered PMB Featuring Car Quencher

mRNA-triggered beacons are analogous to the protease-triggered beacons. They are the novel variations of the original molecular beacons (Section 1.3), in which DNA-RNA double helix formation is featured in the control of  $^1\text{O}_2$  production. In this case, the “closed” conformation of this beacon allows for the formation of a stem (Fig. 5A) that keeps Pyro and Car locked in close proximity. The loop part of the beacon should be designed to be complementary to the cancer-specific or overexpressed mRNA so that it opens and restores its activity only after hybridizing to the target mRNA. These beacons have great potential, since the preliminary experiments showed that Pyro can facilitate the rapid uptake of the

whole beacon into cells—an important prerequisite for all DNA/RNA-based therapeutics [135].

Carotenoid is not the only option for the  $^1\text{O}_2$  quencher and cleavage of the peptide linker or opening of the molecular beacon is not the only method of activation (Section 1.2). For example quenchers that are sensitive to physical differences like pH gradients can also be used [76]. These beacons have a very promising future, but more targets, quenchers, and activation strategies must be explored in order to translate this research into the clinical phase.

#### 2.1.2. Protease-Triggered PMB Featuring Black Hole Quencher for Image-Guided Therapy

As mentioned in Section 1.2,  $^1\text{O}_2$  quenching can be achieved by quenching the PS excited singlet state. This type of quenching is a side product of good fluorescence quenching since the deactivation of PS's excited singlet state also inevitably reduces the production of Pyro's excited triplet state and ultimately leads to lower  $^1\text{O}_2$  production, see Fig. (1). The extent of such quenching depends on the flexibility and tightness of the PS-quencher association. A fluorescence quencher, unlike carotenoids, does not have the capacity to quench the long-lived triplet state or scavenge the  $^1\text{O}_2$  that has already been generated; therefore the  $^1\text{O}_2$  quenching capabilities are limited by the requirements for good fluorescence quenching.

Black hole quencher 3 (BHQ3) was previously reported to efficiently quench both Pyro fluorescence [136] and Pyro  $^1\text{O}_2$  production [88]. Using this BHQ3 as a quencher, we hypothesized that upon protease-triggered activation, the PMB will both identify (by emitting fluorescence) and destroy (by producing  $^1\text{O}_2$ ) the cancer cells, while leaving normal cells undetected and unharmed. Thus, it has the potential to generate a clinically useful strategy for a controlled image-guided therapy.

The first protease target of this BHQ3-based PMB was matrix metalloproteinase 7 (MMP7) which is overexpressed in pancreatic [137], colon, breast [138] and non-small cell lung cancers [139]. This beacon, so-called ‘PP<sub>MMP7</sub>B’, contains a MMP7-cleavable peptide sequence GPLGLARK that allows for a tight conformation of Pyro and a BHQ3, conjugated to each end of this sequence. As shown in Fig. (8), this is reflected in both good fluorescence quenching (15-fold) and effective  $^1\text{O}_2$  quenching (18-fold).

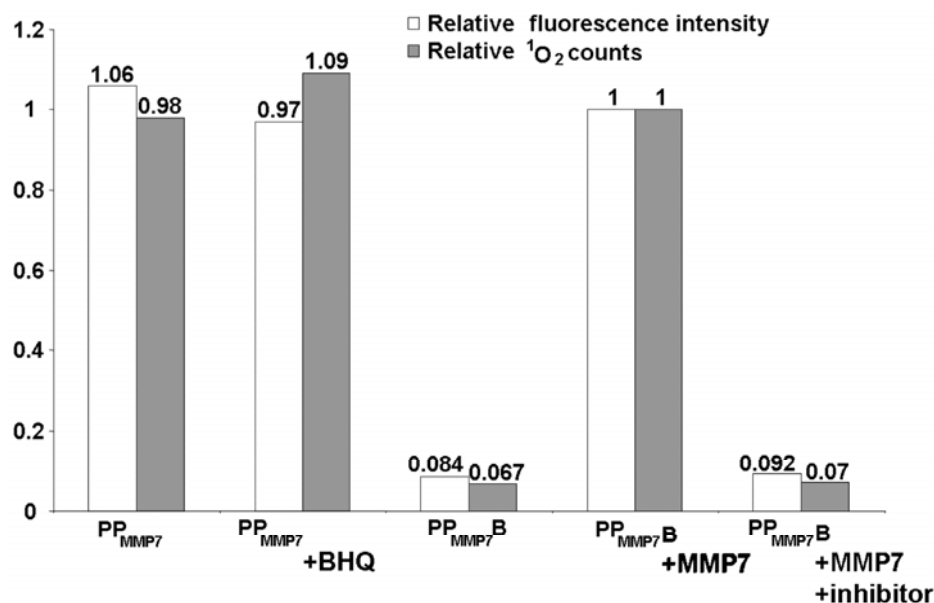


**Fig. (8). Relative fluorescence intensity and relative  $^1\text{O}_2$  counts** (modified with permission from Figure 2C of ref. 131). From left to right: PP<sub>MMP7</sub>, PP<sub>MMP7</sub> combined with free BHQ3, PP<sub>MMP7</sub>B, PP<sub>MMP7</sub>B incubated with MMP7 and PP<sub>MMP7</sub>B incubated with MMP7 and MMP7-specific inhibitor. Both the fluorescence and the  $^1\text{O}_2$  production was fully restored to the level of PP<sub>MMP7</sub> upon the sequence-specific cleavage of PP<sub>MMP7</sub>B by MMP7 enzyme.

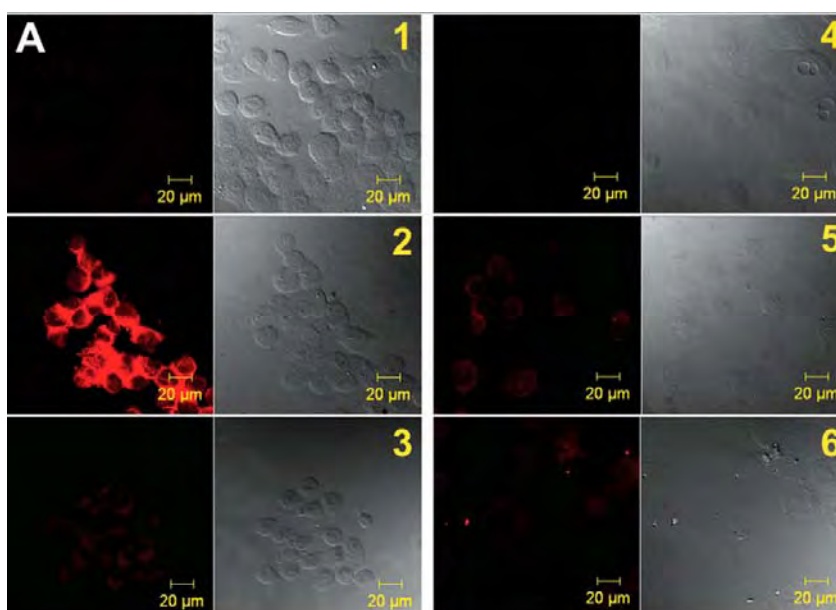


**Fig. (9).** Confocal images of  $PP_{MMP7B}$  and control C-PPB in KB ( $MMP7^+$ ) and BT20 ( $MMP7^-$ ) cells showing fluorescence (left) and bright field (right) in each case. 1) KB cells alone, 2) KB cells+60 $\mu$ M  $PP_{MMP7B}$ , 3) KB cells+60 $\mu$ M C-PPB, 4) BT20 cells alone, 5) BT20 cells+60 $\mu$ M  $PP_{MMP7B}$  and 6) BT20 cells+60 $\mu$ M C-PPB (used with permission from Figure 3A of ref. 131).

Using this  $PP_{MMP7B}$  [131], cells with different expression levels of MMP7 can be distinguished by their restored fluorescence (Fig. 9). Cells that overexpress MMP7 (in this case KB cells,  $MMP7^+$ ), are identified by increased fluorescence from the extracellular cleavage of  $PP_{MMP7B}$ , which is consequently delivered inside these cells. The MMP7 negative cells (BT20 cells,  $MMP7^-$ ) can accumulate but cannot cleave this compound and therefore remain dark. As a consequence, the  $MMP7^+$  cells were readily killed following the PDT treatment whereas using the same concentration of  $PP_{MMP7B}$  showed no phototoxicity for  $MMP7^-$  cells (Fig. 10). These data confirmed that the PDT activity of this  $PP_{MMP7B}$  toward cancer cells is peptide sequence-specific. Furthermore, *in vivo* study showed that the tumor overexpressing MMP7 can be identified by

the restored fluorescence. Following PDT, fast tumor disappearance without recurrence over a span of 30 days was observed.

The ability to quench both fluorescence and  $^1O_2$  makes the BHQ3-based PMBs uniquely suited for a controlled image-guided therapy mainly for two reasons. First, the biomarker-triggered photodynamic activation ( $^1O_2$  production) directs the PDT selectivity towards the targeted cells and second, the ability to control fluorescence emission in response to cancer biomarkers maximizes the tumor *vs.* normal tissue contrast, offering the ultimate control for image-guided therapy.

An alternative approach, using the dye-dye quenching strategy, was also described. Here the Chlorins  $e_6$ , conjugated to the poly-L-

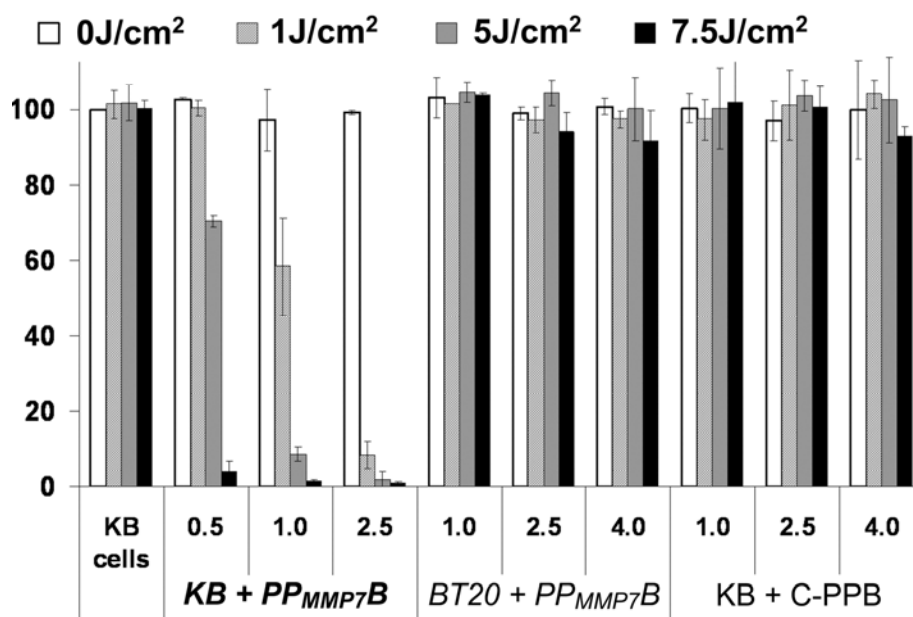


**Fig. (10).** Photodynamic cytotoxicity determined by MTT assay (used with permission from Figure 4 of ref. 131). The cytotoxicity is a function of PS and light doses, compared with untreated cells: means  $\pm$  standard errors for triplicate experiments.

lysine backbone, have both fluorescence and  $^1\text{O}_2$  production partially quenched until the release by Cathepsin B [140]. However, the utility of this approach for the activatable PDT beacon design is limited by the coupling ratio of PS to the polymer backbone. While a high degree of PS substitution leads to higher quenching efficiency, inversely, it also lowers the  $^1\text{O}_2$  activation efficiency since it decreases the availability of Cathepsin B cleavage sites.

## 2.2. Traceable Beacons

Traceable beacons are unquenched beacons that are able to selectively accumulate in the target cells and consequently be used for imaging and killing those cells. Although many PSs have a preferential accumulation in cancer cells, we have decided to omit them from this section since we have already touched on this topic in Section 1.4: “PS’s self-delivery” and many other useful reviews have dealt with this broad field [26, 48]. We have also already summarized the possible delivery vehicles of PSs (Section 1.4: “Delivery systems for photosensitizers”). Therefore, this section on traceable beacons is narrowed to a few promising new studies that use novel methods for delivery and activation.

One of the novel approaches is the protease-triggered delivery of “zipper” beacons (Section 1.3) utilizing matrix metalloproteinase (MMP) 2 and 9 [105] as well as prostate-specific antigen (PSA) [141]. Briefly, this type of beacons comprises of a polyanion arm and a polycation arm linked together with a MMP-2/MMP-9 or PSA-cleavable peptide sequence. The cargo or molecule-of-interest is attached to the other end of polycation. In the absence of the target, the beacon adopts a “zipper” conformation by electrostatic interaction thus neutralizing the polycation’s ability to deliver the cargo. Once the linker is cleaved by the protease, this cargo can be selectively delivered in cancer cells by the released polycation arm (Fig. 5C). Although such “zipper” beacons have not been explored for PS delivery, it is a very promising site-specific beacon delivery approach.

In the traceable beacon development, short peptide sequences are commonly used for increasing the probe’s solubility, selective activation, receptor-mediated uptake [121] or intracellular delivery [124], depending on the sequence’s length, hydrophilicity, basicity and amino acid composition. In this review, we will discuss a rather new and promising role of peptide in pharmacomodulation of the traceable beacons. A recent report shows that when a hydrophilic 9-amino acid sequence GDEVDGSGK (originally intended to be

cleavable by apoptosis-activated caspase-3) was conjugated to a PS (Pyro), it positively influenced the Pyro’s biodistribution by avoiding its accumulation in the liver and spleen [120]. This beacon (Pyro-peptide-Folate, PPF) is composed of three components: (1) Pyro as a fluorescent PS, (2) peptide sequence as a stable linker and modulator for improving the delivery efficiency, and (3) folate as a homing molecule targeting folate receptor (FR)-expressing cancer cells (Fig. 11). The synergy of all three components leads to an unusually good biodistribution, where the beacon selectively accumulates inside the FR-overexpressed tumor, and only very little of the probe ends up in the FR negative tumor or other organs (only the kidneys, known to express FR, are visible).

Comparison with two controls—one that lacks the folate (Pyro-peptide) and the other that lacks the peptide (Pyro-K-folate)—clearly identifies the function of each module. The control without folate (Pyro-peptide) accumulates equally in tumors with different levels of FR expression while having low accumulation in liver and spleen. On the other hand, the control without peptide shows a ~200-fold increase in liver and spleen accumulation. Thus, the peptide appears to play a role in pharmacomodulation in these beacons. An extensive study is still needed to identify the molecular mechanism underlying this positive effect and to select for peptides that could be useful in this respect. If this strategy can be generalized, it could be used to improve the biodistribution profiles of the conventional drugs and imaging probes.

## 2.3. Beacons with Built-in Apoptosis Sensor

Designing a killer beacon in which a PS is conjugated to a fluorescence quencher (Q) through a peptide sequence specifically cleavable only by the target enzyme, can be potentially used for imaging or identifying PDT-induced treatment response. For example, PDT treatment can result in a variety of conditions depending on the drug/light dose, PS and cell type. These can be divided into three extreme cases: survival, apoptosis, or necrosis. Apoptosis is characterized by the ordered manner in which the damaged cells die and this cell death mode is very different from the inflammatory reaction that follows the bursting of necrotic cells [142]. Since cell death *via* apoptosis is a desirable endpoint of PDT, developing a beacon that would trigger and consequently image apoptosis *in situ* could help to understand and evaluate the conditions that lead preferentially to this type of cell death. Currently, the methods of *in situ* apoptosis imaging are scarce [143] (for example *in vivo* imaging of caspase-1 utilizing the poly-L-lysine backbone [144]) and many

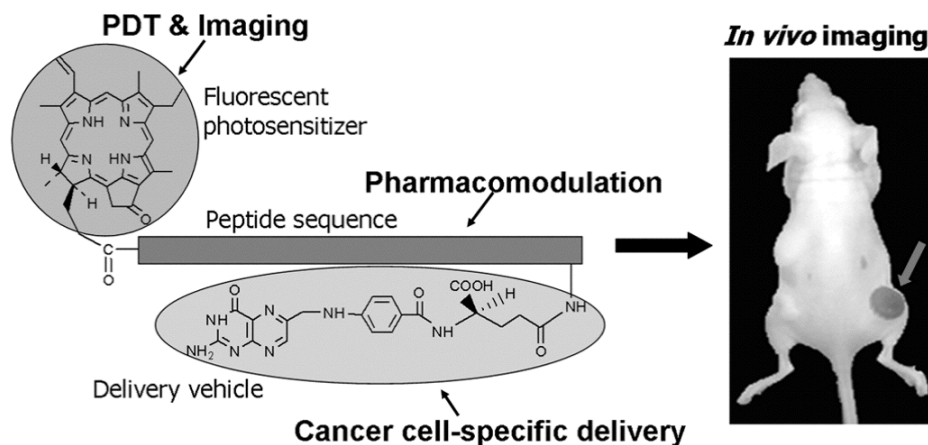


**Fig. (11). Pharmacomodulating effect of peptide in FR-targeted traceable beacon** (modified with permission from ref. 120). This beacon is composed of the fluorescent photosensitizer Pyropheophorbide *a* for PDT and NIR imaging; a short peptide sequence for pharmacomodulation, and a delivery vehicle folate for cancer cell-specific delivery to folate receptor-overexpressing cells (FR<sup>+</sup>). 24 hours after injecting this beacon into a double-tumor bearing mouse, the *in vivo* imaging demonstrates preferential accumulation of this beacon in the FR<sup>+</sup> tumor (red arrow) with lower accumulation in kidney and minimal retention by liver and spleen, as confirmed by *ex vivo* biodistribution.

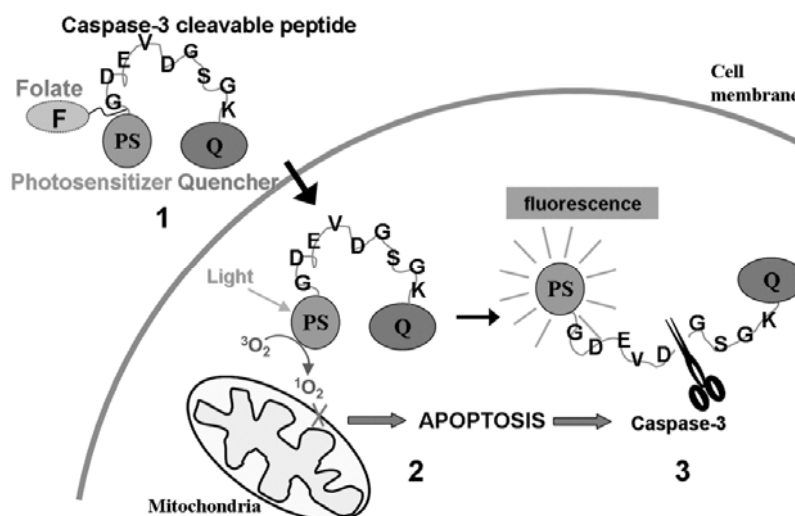


**Fig. (12). Beacon for post-PDT imaging of apoptosis** (modified with permission from Figure 1 of ref. 148). This beacon consists of three main parts (1): a fluorescent photosensitizer (Pyro, PS), a caspase-3 cleavable sequence (KGDEVDGSGK), a fluorescence quencher (BHQ3, Q) and an optional delivery vehicle (folate, F). This construct accumulates in cells (preferentially in FR<sup>+</sup> cells if folate is attached) and once activated by light, the photosensitizer produces  $^1\text{O}_2$  that destroys the mitochondrial membrane and triggers apoptosis (2) together with activation of caspase-3. Caspase-3 then cleaves the peptide linker between the PS and the Q, restoring the PS's fluorescence and identifying those cells dying by apoptosis by NIRF-I (3).

have poor intracellular delivery or low specificity towards apoptosis (e.g. Annexin V, [145, 146]). One of the examples successfully dealing with both issues is the recently published study of a NIR peptide beacon activatable by caspase-3 that uses the Tat-peptide-based permeation peptide sequence for cellular delivery [104]. Caspase-3 is an attractive and unambiguous target for apoptosis imaging, since most of the apoptotic pathways involve the activation of this executioner protease [147].

This review will focus on the development of beacons with built-in apoptosis sensor designed to both trigger cell death by PDT and report apoptosis *in situ* in a real time. This beacon has three fixed components: a PS (Pyro), a fluorescence quencher (BHQ-3), a caspase-3 cleavable peptide sequence (GDEVDGSGK), and one optional folate component as a delivery vehicle [148] (Fig. 12). Pyro was previously shown to accumulate inside cells in various intracellular membrane systems associated with apoptosis [149], most importantly the peripheral benzodiazepine receptors of mitochondria [150]. Therefore, even without the folate, this beacon [136] can accumulate inside cells, led by Pyro.

The crucial part of this beacon is to maintain the PS' ability to generate  $^1\text{O}_2$  production while completely inhibit its ability to emit fluorescence. Experiments confirmed this is possible with the use of caspase-3-specific peptide sequence (GDEVDGSGK) as the linker [136, 148].

Briefly, once activated by PDT, Pyro moiety of such beacons compromises the mitochondrial membrane and if a sufficient number of mitochondria are destroyed to the point where the cell cannot compensate for this loss, the cell will die. If this damage is not drastic enough to lead to cell disintegration *via* necrosis, the release of cytochrome c from the mitochondrial membrane triggers an apoptotic cascade, which ultimately leads to caspase-3 activation. Once activated, caspase-3 cleaves the GDEVDGSGK peptide linker between Pyro and BHQ-3 and restores the fluorescence, identifying those cells dying by apoptosis. This fluorescence increase is not observed for light-only or drug-only control cells (i.e. when the cells are not killed) or in the case of cells incubated with a beacon containing a scrambled sequence (not cleavable by caspase-3) and treated with light.

Attachment of folate increases the specificity of the probe necessary for *in vivo* applications [148] and also shows that incorpora-

tion of delivery component does not impair the beacon's function. Triggering and reporting apoptosis was demonstrated *in vitro* and *in vivo*, although the main obstacle in widely applying this approach remains the partial  $^1\text{O}_2$  quenching. Nevertheless, this beacon can be used as a tool for elucidating the true PDT mechanism of selective toxicity. In addition, since the beacon can penetrate cancer cells without entering the nucleus (unlike Tat peptide) and specifically reporting apoptosis, it could potentially be used for evaluating existing apoptosis-inducing chemotherapeutics [148].

## CONCLUSION

We have summarized the important points that underlie the function of killer beacons that are designed to combine PDT and NIRF-I. Adopting the modular design principle, these beacons are built on a single fluorescent photosensitizer base unit with the integration of other functional modules (e.g., quencher, linker and delivery vehicle). Versatile and customizable in nature, these beacons are useful tools for a wide range of cancer applications. This review is a guide through the design of three killer beacons including photodynamic molecular beacons, traceable beacons and beacons with built-in apoptosis sensor.

## ACKNOWLEDGMENTS

We thank André E. X. Brown and Brian Wilson for critical comments and suggestions on the manuscript. This work was supported by grants from DOD DAMD17-03-1-0373, NIH R21-CA95330, the Oncologic Foundation of Buffalo and the Joey and Toby Tanenbaum/Brazilian Ball Chair in Prostate Cancer Research, Princess Margaret Hospital (GZ).

## ABBREVIATIONS

$^1\text{O}_2$	=	singlet oxygen
Ab	=	Antibody
ALA	=	$\delta$ -aminolevulinic acid
AMC	=	7-amino-4-methylcoumarin
AS-ON	=	antisense oligonucleotide

BDP	=	benzoporphyrin derivative-monoacid
Cy	=	cypate
D	=	dye
DABCO	=	1,4-diazabicyclo[2.2.2]octane
DNA	=	deoxyribonucleic acid
$\epsilon$	=	extinction coefficient
EGF	=	epidermal growth factor
FR	=	Folate receptor
FRET	=	fluorescence resonance energy transfer
GFP	=	green fluorescent protein
HGD	=	high-grade dysplasia
HpD	=	hematoporphyrin derivative
HPPH	=	2-(1-hexyloxyethyl)-2-devinyl pyropheophorbide-a
IR	=	infrared
iv	=	intravenously administered
LDL	=	low density lipoprotein
MB	=	molecular beacons
mTHPC	=	meso-tetrahydroxyphenyl-chlorin
NIRF-I	=	Near-infrared fluorescence imaging
PCR	=	polymerase chain reaction
PDT	=	photodynamic therapy
PMB	=	photodynamic molecular beacon
PNA	=	peptide nucleic acid
PS	=	photosensitizer
PSA	=	prostate-specific antigen
Q	=	quencher
RNA	=	ribonucleic acid

## REFERENCES

- [1] Parkin, D. M.; Bray, F.; Ferlay, J.; Pisani, P. *CA: Cancer J. Clin.*, **2005**, *55*, 74-108.
- [2] Jemal, A.; Siegel, R.; Ward, E.; Murray, T.; Xu, J.; Smigal, C.; Thun, M. J. *Cancer J. Clin.*, **2006**, *56*, 106-30.
- [3] Bogaards, A.; Varma, A.; Collens, S. P.; Lin, A.; Giles, A.; Yang, V. X.; Bilbao, J. M.; Lilge, L. D.; Muller, P. J.; Wilson, B. C. *Lasers Surg. Med.*, **2004**, *35*, 181-90.
- [4] Coleman, C. N. *Radiology*, **2003**, *228*, 29-35.
- [5] Dougherty, T. J. *Photochem. Photobiol.*, **1987**, *45*, 879-89.
- [6] Gurfinkel, M.; Thompson, A. B.; Ralston, W.; Troy, T. L.; Moore, A. L.; Moore, T. A.; Gust, J. D.; Tatman, D.; Reynolds, J. S.; Muggenburg, B.; Nikula, K.; Pandey, R.; Mayer, R. H.; Hawrysz, D. J.; Sevick-Muraca, E. M. *Photochem. Photobiol.*, **2000**, *72*, 94-102.
- [7] Wagnieres, G. A.; Star, W. M.; Wilson, B. C. *Photochem. Photobiol.*, **1998**, *68*, 603-32.
- [8] Salva, K. A. *Clinics Dermat.*, **2002**, *20*, 571-81.
- [9] McCaughan, J. S., Jr. *Drugs Aging*, **1999**, *15*, 49-68.
- [10] Levy, J. G.; Obochi, M. *Photochem. Photobiol.*, **1996**, *64*, 737-9.
- [11] Trauner, K. B.; Hasan, T. *Photochem. Photobiol.*, **1996**, *64*, 740-50.
- [12] Ben-Hur, E.; Horowitz, B. *Photochem. Photobiol.*, **1995**, *62*, 383-8.
- [13] Jori, G.; Fabris, C.; Soncin, M.; Ferro, S.; Coppellotti, O.; Dei, D.; Fantetti, L.; Chiti, G.; Roncucci, G. *Lasers Surg. Med.*, **2006**, *38*, 468-81.
- [14] Oleinick, N. L.; Evans, H. H. *Radiation Res.*, **1998**, *150*, S146-56.
- [15] Sevick-Muraca, E. M.; Houston, J. P.; Gurfinkel, M. *Curr. Opin. Chem. Biol.*, **2002**, *6*, 642-50.
- [16] Wilson, B. C.; Patterson, M. S. *Physics in Med. Biol.*, **1986**, *31*, 327-60.
- [17] Weishaupt, K. R.; Gomer, C. J.; Dougherty, T. J. *Cancer Res.*, **1976**, *36*, 2326-9.
- [18] Niedre, M. J.; Secord, A. J.; Patterson, M. S.; Wilson, B. C. *Cancer Res.*, **2003**, *63*, 7986-94.
- [19] Peng, Q.; Moan, J.; Warloe, T.; Iani, V.; Steen, H. B.; Bjorseth, A.; Nesland, J. M. *J. Photochem. Photobiol. B*, **1996**, *34*, 95-6.
- [20] Berg, K.; Moan, J. *Photochem. Photobiol.*, **1997**, *65*, 403-9.
- [21] Berg, K.; Moan, J. *Int. J. Cancer*, **1994**, *59*, 814-22.
- [22] Evensen, J. F.; Moan, J. *Br. J. Cancer*, **1982**, *45*, 456-65.
- [23] Kessel, D. *Photochem. Photobiol. Sci.*, **2002**, *1*, 837-40.
- [24] Moor, A. C. *J. Photochem. Photobiol. B*, **2000**, *57*, 1-13.
- [25] Oleinick, N. L.; Morris, R. L.; Belichenko, I. *Photochem. Photobiol. Sci.*, **2002**, *1*, 1-21.
- [26] Jori, G. *J. Photochem. Photobiol. B*, **1996**, *36*, 87-93.
- [27] Frangioni, J. V. *Curr. Opin. Chem. Biol.*, **2003**, *7*, 626-34.
- [28] Zheng, G.; Li, H.; Yang, K.; Blessington, D.; Licha, K.; Lund-Katz, S.; Chance, B.; Glickson, J. D. *Bioorg. Med. Chem. Lett.*, **2002**, *12*, 1485-8.
- [29] Tanaka, E.; Choi, H. S.; Fujii, H.; Bawendi, M. G.; Frangioni, J. V. *Ann. Surg. Oncol.*, **2006**, *13*, 1671-81.
- [30] Petrovsky, A.; Schellenberger, E.; Josephson, L.; Weissleder, R.; Bogdanov, A., Jr. *Cancer Res.*, **2003**, *63*, 1936-42.
- [31] Ke, S.; Wen, X.; Gurfinkel, M.; Charnsangavej, C.; Wallace, S.; Sevick-Muraca, E. M.; Li, C. *Cancer Res.*, **2003**, *63*, 7870-5.
- [32] Humblet, V.; Lapidus, R.; Williams, L. R.; Tsukamoto, T.; Rojas, C.; Majer, P.; Hin, B.; Ohnishi, S.; De Grand, A. M.; Zaheer, A.; Renze, J. T.; Nakayama, A.; Slusher, B. S.; Frangioni, J. V. *Mol. Imaging*, **2005**, *4*, 448-62.
- [33] Chen, X.; Conti, P. S.; Moats, R. A. *Cancer Res.*, **2004**, *64*, 8009-14.
- [34] Moon, W. K.; Lin, Y.; O'Loughlin, T.; Tang, Y.; Kim, D. E.; Weissleder, R.; Tung, C. H. *Bioconjug. Chem.*, **2003**, *14*, 539-45.
- [35] Nyman, E. S.; Hynninen, P. H. *J. Photochem. Photobiol. B*, **2004**, *73*, 1-28.
- [36] Rassmussen-Taxdal, D. S.; Ward, G. E.; Figge, F. H. *Cancer*, **1955**, *8*, 78-81.
- [37] Dougherty, T. J.; Kaufman, J. E.; Goldfarb, A.; Weishaupt, K. R.; Boyle, D.; Mittleman, A. *Cancer Res.*, **1978**, *38*, 2628-35.
- [38] Triesscheijn, M.; Baas, P.; Schellens, J. H.; Stewart, F. A. *Oncologist*, **2006**, *11*, 1034-44.
- [39] Woodhams, J. H.; MacRobert, A. J.; Novelli, M.; Bown, S. G. *Int. J. Cancer*, **2006**, *118*, 477-82.
- [40] Chin, W. W.; Lau, W. K.; Heng, P. W.; Bhuvanewari, R.; Olivo, M. J. *Photochem. Photobiol. B*, **2006**, *84*, 103-10.
- [41] Gad, F.; Zahra, T.; Francis, K. P.; Hasan, T.; Hamblin, M. R. *Photochem. Photobiol. Sci.*, **2004**, *3*, 451-8.
- [42] Lobel, J.; MacDonald, I. J.; Ciesielski, M. J.; Barone, T.; Potter, W. R.; Pollina, J.; Plunkett, R. J.; Fenstermaker, R. A.; Dougherty, T. J. *Lasers Surg. Med.*, **2001**, *29*, 397-405.
- [43] Kato, H.; Furukawa, K.; Sato, M.; Okunaka, T.; Kusunoki, Y.; Kawahara, M.; Fukuoka, M.; Miyazawa, T.; Yana, T.; Matsui, K.; Shirashi, T.; Horinouchi, H. *Lung Cancer*, **2003**, *42*, 103-11.
- [44] Bellnier, D. A.; Greco, W. R.; Nava, H.; Loewen, G. M.; Oseroff, A. R.; Dougherty, T. J. *Cancer Chemother. Pharmacol.*, **2006**, *57*, 40-5.
- [45] Zheng, G.; Chen, J.; Li, H.; Glickson, J. D. *Proc. Natl. Acad. Sci. U S A*, **2005**, *102*, 17757-62.
- [46] Peng, Q.; Moan, J.; Nesland, J. M. *Ultrastruct. Pathol.*, **1996**, *20*, 109-129.
- [47] Toledano, H.; Edrei, R.; Kimel, S. J. *Photochem. Photobiol. B*, **1998**, *42*, 20-7.
- [48] Konan, Y. N.; Gurny, R.; Allemann, E. *J. Photochem. Photobiol. B*, **2002**, *66*, 89-106.
- [49] Kessel, D.; Poretz, R. D. *Photochem. Photobiol.*, **2000**, *71*, 94-6.
- [50] Kessel, D.; Luo, Y. *Cell Death Differ.*, **1999**, *6*, 28-35.
- [51] Wu, P.; Brand, L. *Anal. Biochem.*, **1994**, *218*, 1-13.
- [52] Gurtu, V.; Kain, S. R.; Zhang, G. *Anal. Biochem.*, **1997**, *251*, 98-102.
- [53] Kasili, P. M.; Song, J. M.; Vo-Dinh, T. *J. Am. Chem. Soc.*, **2004**, *126*, 2799-806.
- [54] Bowen, M. E.; Weninger, K.; Ernst, J.; Chu, S.; Brunger, A. T. *Biophys. J.*, **2005**, *89*, 690-702.
- [55] Komoriya, A.; Packard, B. Z.; Brown, M. J.; Wu, M. L.; Henkart, P. A. *J. Exp. Med.*, **2000**, *191*, 1819-28.
- [56] Weissleder, R.; Tung, C. H.; Mahmood, U.; Bogdanov, A., Jr. *Nat. Biotechnol.*, **1999**, *17*, 375-8.
- [57] Baruch, A.; Jeffery, D. A.; Bogoy, M. *Trends Cell Biol.*, **2004**, *14*, 29-35.
- [58] Zhang, J.; Campbell, R. E.; Ting, A. Y.; Tsien, R. Y. *Nat. Rev. Mol. Cell Biol.*, **2002**, *3*, 906-18.
- [59] Perlitz, C.; Licha, K.; Scholle, F. D.; Ebert, B.; Bahner, M.; Hauff, P.; Moesta, K. T.; Schirner, M. *J. Fluoresc.*, **2005**, *15*, 443-54.
- [60] Ballou, B.; Ernst, L. A.; Waggoner, A. S. *Curr. Med. Chem.*, **2005**, *12*, 795-805.
- [61] Johansson, M. K. *Methods Mol. Biol.*, **2006**, *335*, 17-29.
- [62] Foote, C. S. *Science*, **1968**, *162*, 963-70.
- [63] Schafer, F. Q.; Buettner, G. R. *Photochem. Photobiol.*, **1999**, *70*, 858-67.
- [64] Girotti, A. W.; Korytowski, W. *Methods Enzymol.*, **2000**, *319*, 85-100.
- [65] Foote, C. S.; Shook, F. C.; Abakerli, R. B. *Methods Enzymol.*, **1984**, *105*, 36-47.
- [66] Foote, C. S.; Chang, Y. C.; Denny, R. W. *J. Am. Chem. Soc.*, **1970**, *92*, 5216-8.
- [67] Edge, R.; McGarvey, D. J.; Truscott, T. G. *J. Photochem. Photobiol. B*, **1997**, *41*, 189-200.
- [68] Telfer, A.; Bishop, S. M.; Phillips, D.; Barber, J. *J. Biol. Chem.*, **1994**, *269*, 13244-53.
- [69] Young, A. J.; Frank, H. A. *J. Photochem. Photobiol. B*, **1996**, *36*, 3-15.
- [70] Di Mascio, P.; Kaiser, S.; Sies, H. *Arch. Biochem. Biophys.*, **1989**, *274*, 532-8.
- [71] Reddi, E.; Segalla, A.; Jori, G.; Kerrigan, P. K.; Liddell, P. A.; Moore, A. L.; Moore, T. A.; Gust, D. *Br. J. Cancer*, **1994**, *69*, 40-5.

- [72] Foote, C. S.; Ching, T. Y.; Geller, G. G. *Photochem. Photobiol.*, **1974**, *20*, 511-3.
- [73] Das, K. C.; Das, C. K. *Biochem. Biophys. Res. Commun.*, **2000**, *277*, 443-7.
- [74] Das, K. C.; Misra, H. P. *Mol. Cell Biochem.*, **1992**, *115*, 179-85.
- [75] Wennersten, G. *Acta Derm. Venereol.*, **1977**, *57*, 519-24.
- [76] McDonnell, S. O.; Hall, M. J.; Allen, L. T.; Byrne, A.; Gallagher, W. M.; O'Shea, D. F. *J. Am. Chem. Soc.*, **2005**, *127*, 16360-1.
- [77] Tyagi, S.; Kramer, F. R. *Nat. Biotechnol.*, **1996**, *14*, 303-8.
- [78] Yang, C. J.; Medley, C. D.; Tan, W. *Curr. Pharm. Biotechnol.*, **2005**, *6*, 445-52.
- [79] Tan, W.; Fang, X.; Li, J.; Liu, X. *Chemistry*, **2000**, *6*, 1107-11.
- [80] Tsourkas, A.; Bao, G. *Brief Funct. Genomic Proteomic*, **2003**, *1*, 372-84.
- [81] Gifford, L. K.; Jordan, D.; Pattanayak, V.; Vernovsky, K.; Do, B. T.; Gewirtz, A. M.; Lu, P. *Anal. Biochem.*, **2005**, *347*, 77-88.
- [82] Stahel, R. A.; Zangemeister-Wittke, U. *Lung Cancer*, **2003**, *41 Suppl 1*, S81-8.
- [83] Davies, H.; Bignell, G. R.; Cox, C.; Stephens, P.; Edkins, S.; Clegg, S.; Teague, J.; Woffendin, H.; Garnett, M. J.; Bottomley, W.; Davis, N.; Dicks, E.; Ewing, R.; Floyd, Y.; Gray, K.; Hall, S.; Hawes, R.; Hughes, J.; Kosmidou, V.; Menzies, A.; Mould, C.; Parker, A.; Stevens, C.; Watt, S.; Hooper, S.; Wilson, R.; Jayatilake, H.; Gusterson, B. A.; Cooper, C.; Shipley, J.; Hargrave, D.; Pritchard-Jones, K.; Maitland, N.; Chenevix-Trench, G.; Riggins, G. J.; Bigner, D. D.; Palmieri, G.; Cossu, A.; Flanagan, A.; Nicholson, A.; Ho, J. W.; Leung, S. Y.; Yuen, S. T.; Weber, B. L.; Seigler, H. F.; Darrow, T. L.; Paterson, H.; Marais, R.; Marshall, C. J.; Wooster, R.; Stratton, M. R.; Futreal, P. A. *Nature*, **2002**, *417*, 949-54.
- [84] Moscatello, D. K.; Holgado-Madruga, M.; Godwin, A. K.; Ramirez, G.; Gunn, G.; Zoltick, P. W.; Biegel, J. A.; Hayes, R. L.; Wong, A. J. *Cancer Res.*, **1995**, *55*, 5536-9.
- [85] Stein, C. A.; Benimetskaya, L.; Mani, S. *Semin. Oncol.*, **2005**, *32*, 563-72.
- [86] Warfield, K. L.; Panchal, R. G.; Aman, M. J.; Bavari, S. *Curr. Opin. Mol. Ther.*, **2006**, *8*, 93-103.
- [87] Lundin, K. E.; Good, L.; Stromberg, R.; Graslund, A.; Smith, C. I. *Adv. Genet.*, **2006**, *56*, 1-51.
- [88] Clo, E.; Snyder, J. W.; Voigt, N. V.; Ogilby, P. R.; Gothelf, K. V. *J. Am. Chem. Soc.*, **2006**, *128*, 4200-1.
- [89] Kelbaskaus, L.; Diemel, W. *Photochem. Photobiol.*, **2002**, *76*, 686-94.
- [90] Berg, K.; Moan, J. *Int. J. Cancer*, **1994**, *59*, 814-22.
- [91] Latt, S. A.; Auld, D. S.; Vallee, B. L. *Analyt. Biochem.*, **1972**, *50*, 56-62.
- [92] Wang, G. T.; Matayoshi, E. D.; Huffaker, H. J.; Krafft, G. A. *Tetrahedr. Lett.*, **1990**, *45*, 6493-6496.
- [93] Matayoshi, E. D.; Wang, G. T.; Krafft, G. A.; Erickson, J. *Science*, **1990**, *247*, 954-8.
- [94] Wang, G. T.; Lador, U. S.; Holzman, T. F.; Klein, W. L.; Krafft, G. A. *Mol. Chem. Neuropathol.*, **1994**, *23*, 191-9.
- [95] Sloane, B. F.; Sameni, M.; Podgorski, I.; Cavallo-Medved, D.; Moin, K. *Annu. Rev. Pharmacol. Toxicol.*, **2006**, *46*, 301-15.
- [96] Tung, C. H.; Bredow, S.; Mahmood, U.; Weissleder, R. *Bioconjug. Chem.*, **1999**, *10*, 892-6.
- [97] Mahmood, U.; Tung, C. H.; Bogdanov, A., Jr.; Weissleder, R. *Radiology*, **1999**, *213*, 866-70.
- [98] Chen, J.; Tung, C. H.; Allport, J. R.; Chen, S.; Weissleder, R.; Huang, P. L. *Circulation*, **2005**, *111*, 1800-5.
- [99] Giambrenardi, T. A.; Grant, G. M.; Taylor, G. P.; Hay, R. J.; Maher, V. M.; McCormick, J. J.; Klebe, R. J. *Matrix Biol.*, **1998**, *16*, 483-96.
- [100] Kline, T.; Torgov, M. Y.; Mendelsohn, B. A.; Cerveny, C. G.; Senter, P. D. *Mol. Pharm.*, **2004**, *1*, 9-22.
- [101] Cheng, J. D.; Dunbrack, R. L., Jr.; Valianou, M.; Rogatko, A.; Alpaugh, R. K.; Weiner, L. M. *Cancer Res.*, **2002**, *62*, 4767-72.
- [102] Lee, K. N.; Jackson, K. W.; Christiansen, V. J.; Lee, C. S.; Chun, J. G.; McKee, P. A. *Blood*, **2006**, *107*, 1397-404.
- [103] Pham, W.; Choi, Y.; Weissleder, R.; Tung, C. H. *Bioconjug. Chem.*, **2004**, *15*, 1403-7.
- [104] Bullock, K.; Piwnicka-Worms, D. *J. Med. Chem.*, **2005**, *48*, 5404-7.
- [105] Jiang, T.; Olson, E. S.; Nguyen, Q. T.; Roy, M.; Jennings, P. A.; Tsien, R. Y. *Proc Natl. Acad. Sci. U S A*, **2004**, *101*, 17867-72.
- [106] Yang, C. J.; Li, J. J.; Tan, W. *Methods Mol. Biol.*, **2006**, *335*, 71-81.
- [107] Li, J. J.; Geyer, R.; Tan, W. *Nucleic Acids Res.*, **2000**, *28*, E52.
- [108] Mawn, T. M.; Popov, A. V.; Milkvitch, M.; Kim, S.; Zheng, G. & Delikatny, E. J. *Mol. Imaging* **2006**, *5*, 315.
- [109] Verma, A.; Nye, J. S.; Snyder, S. H. *Proc. Natl. Acad. Sci. U S A*, **1987**, *84*, 2256-60.
- [110] Hanahan, D.; Weinberg, R. A. *Cell*, **2000**, *100*, 57-70.
- [111] Zheng, G.; Li, H.; Zhang, M.; Lund-Katz, S.; Chance, B.; Glickson, J. D. *Bioconjug. Chem.*, **2002**, *13*, 392-6.
- [112] Li, H.; Marotta, D. E.; Kim, S.; Busch, T. M.; Wileyto, E. P.; Zheng, G. J. *Biomed. Opt.*, **2005**, *10*, 41203.
- [113] Tosi, M. R.; Tugnoli, V. *Clin. Chim. Acta*, **2005**, *359*, 27-45.
- [114] Rensen, P. C.; de Vrueth, R. L.; Kuiper, J.; Bijsterbosch, M. K.; Biessen, E. A.; van Berkel, T. J. *Adv. Drug. Deliv. Rev.*, **2001**, *47*, 251-76.
- [115] Morgan, J.; Gray, A. G.; Huehns, E. R. *Br. J. Cancer*, **1989**, *59*, 366-70.
- [116] Sharman, W. M.; van Lier, J. E.; Allen, C. M. *Adv. Drug Deliv. Rev.*, **2004**, *56*, 53-76.
- [117] Paulos, C. M.; Turk, M. J.; Breur, G. J.; Low, P. S. *Adv. Drug Deliv. Rev.*, **2004**, *56*, 1205-17.
- [118] Hilgenbrink, A. R.; Low, P. S. *J. Pharm. Sci.*, **2005**, *94*, 2135-46.
- [119] Schneider, R.; Schmitt, F.; Frochet, C.; Fort, Y.; Lourette, N.; Guillemin, F.; Muller, J. F.; Barberi-Heyob, M. *Bioorg. Med. Chem.*, **2005**, *13*, 2799-808.
- [120] Stefflova, K.; Li, H.; Chen, J.; Zheng, G. *Bioconjug. Chem.*, **2007**, *18*, 379-88.
- [121] Achilefu, S.; Jimenez, H. N.; Dorshow, R. B.; Bugaj, J. E.; Webb, E. G.; Wilhelm, R. R.; Rajagopalan, R.; Jolner, J.; Erion, J. L. *J. Med. Chem.*, **2002**, *45*, 2003-15.
- [122] Zhang, M.; Zhang, Z.; Blessington, D.; Li, H.; Busch, T. M.; Madrak, V.; Miles, J.; Chance, B.; Glickson, J. D.; Zheng, G. *Bioconjug. Chem.*, **2003**, *14*, 709-14.
- [123] Chen, Y.; Zheng, G.; Zhang, Z. H.; Blessington, D.; Zhang, M.; Li, H.; Liu, Q.; Zhou, L.; Intes, X.; Achilefu, S.; Chance, B. *Opt. Lett.*, **2003**, *28*, 2070-2.
- [124] Vives, E. *J. Mol. Recognit.*, **2003**, *16*, 265-71.
- [125] Derossi, D.; Joliot, A. H.; Chassaing, G.; Prochiantz, A. *J. Biol. Chem.*, **1994**, *269*, 10444-50.
- [126] Pooga, M.; Hallbrink, M.; Zorko, M.; Langel, U. *Faseb J.*, **1998**, *12*, 67-77.
- [127] Mitchell, D. J.; Kim, D. T.; Steinman, L.; Fathman, C. G.; Rothbard, J. B. *J. Pept. Res.*, **2000**, *56*, 318-25.
- [128] Ichikawa, K.; Hikita, T.; Maeda, N.; Yonezawa, S.; Takeuchi, Y.; Asai, T.; Namba, Y.; Oku, N. *Biochim. Biophys. Acta*, **2005**, *1669*, 69-74.
- [129] Bisland, S. K.; Singh, D.; Garipey, J. *Bioconjug. Chem.*, **1999**, *10*, 982-92.
- [130] Chen, J.; Stefflova, K.; Niedre, M. J.; Wilson, B. C.; Chance, B.; Glickson, J. D.; Zheng, G. *J. Am. Chem. Soc.*, **2004**, *126*, 11450-1.
- [131] Zheng, G.; Chen, J.; Stefflova, K.; Jarvi, M.; Li, H.; Wilson, B. C. *Proc. Natl. Acad. Sci. U S A*, **2007**, *104*, 8989-94.
- [132] Moore, A. L.; Joy, A.; Tom, R.; Gust, D.; Moore, T. A.; Bensasson, R. A.; Land, E. J. *Science*, **1982**, *216*, 982-984.
- [133] Wasielewski, M. R.; Liddell, P. A.; Barrett, D.; Moore, T. A.; Gust, D. *Nature*, **1986**, *322*, 570-572.
- [134] Tatman, D.; Liddell, P. A.; Moore, T. A.; Gust, D.; Moore, A. L. *Photochem. Photobiol.*, **1998**, *68*, 459-66.
- [135] Stefflova, K. In *Chemistry*; University of Pennsylvania: Philadelphia, **2006**, pp. 223.
- [136] Stefflova, K.; Chen, J.; Marotta, D.; Li, H.; Zheng, G. *J. Med. Chem.*, **2006**, *49*, 3850-6.
- [137] Crawford, H. C.; Scoggins, C. R.; Washington, M. K.; Matrisian, L. M.; Leach, S. D. *J. Clin. Invest.*, **2002**, *109*, 1437-44.
- [138] Shiomi, T.; Okada, Y. *Cancer Metast. Rev.*, **2003**, *22*, 145-52.
- [139] Zhang, J.; Jin, X.; Fang, S.; Wang, R.; Li, Y.; Wang, N.; Guo, W.; Wang, Y.; Wen, D.; Wei, L.; Dong, Z.; Kuang, G. *Carcinogen*, **2005**, *26*, 1748-53.
- [140] Choi, Y.; Weissleder, R.; Tung, C. H. *Cancer Res.*, **2006**, *66*, 7225-9.
- [141] Goun, E. A.; Shinde, R.; Dehnert, K. W.; Adams-Bond, A.; Wender, P. A.; Contag, C. H.; Franc, B. L. *Bioconjug. Chem.*, **2006**, *17*, 787-96.
- [142] Van Cruchten, S.; Van Den Broeck, W. *Anat., Histol., Embryol. C*, **2002**, *31*, 214-23.
- [143] Vermes, I.; Haanen, C.; Reutelingsperger, C. *J. Immunol. Methods*, **2000**, *243*, 167-90.
- [144] Messerli, S. M.; Prabhakar, S.; Tang, Y.; Shah, K.; Cortes, M. L.; Murthy, V.; Weissleder, R.; Breakefield, X. O.; Tung, C. H. *Neoplasia*, **2004**, *6*, 95-105.
- [145] Brauer, M. *Prog. Neuro-Psychoph.*, **2003**, *27*, 323-31.
- [146] Appelt, U.; Sheriff, A.; Gaip, U. S.; Kalden, J. R.; Voll, R. E.; Herrmann, M. *Cell Death Differ.*, **2005**, *12*, 194-6.
- [147] Thornberry, N. A.; Lazebnik, Y. *Science*, **1998**, *281*, 1312-6.
- [148] Stefflova, K.; Chen, J.; Li, H.; Zheng, G. *Mol. Imaging*, **2006**, *5*, 520-32.
- [149] MacDonald, I. J.; Morgan, J.; Bellnier, D. A.; Paszkiewicz, G. M.; Whitaker, J. E.; Litchfield, D. J.; Dougherty, T. J. *Photochem. Photobiol.*, **1999**, *70*, 789-97.
- [150] Dougherty, T. J.; Sumlin, A. B.; Greco, W. R.; Weishaupt, K. R.; Vaughan, L. A.; Pandey, R. K. *Photochem. Photobiol.*, **2002**, *76*, 91-7.